Optical Communication Through the Turbulent Atmosphere with Transmitter and Receiver Diversity, Wavefront Control, and Coherent Detection

by

Andrew Lee Puryear

B.S., Texas A&M University (2002)
M.S., Stanford University (2003)

Submitted to the Department of Electrical Engineering and Computer Science
in partial fulfillment of the requirements for the degree of

Doctor of Philosophy in Electrical Engineering and Computer Science

at the

MASSACHUSETTS INSTITUTE OF TECHNOLOGY

June 2011

© Massachusetts Institute of Technology 2011. All rights reserved.

Author .....
Department of Electrical Engineering and Computer Science
June 2011

Certified by .....
Vincent W. S. Chan
Joan and Irwin M. Jacobs Professor of Electrical Engineering and Computer Science
Thesis Supervisor

Accepted by .....
Leslie A. Kolodziejski
Chair, Department Committee on Graduate Students

Optical Communication Through the Turbulent Atmosphere with Transmitter and Receiver Diversity, Wavefront Control, and Coherent Detection

by

Andrew Lee Puryear

Submitted to the Department of Electrical Engineering and Computer Science
on June 2011, in partial fulfillment of the
requirements for the degree of
Doctor of Philosophy in Electrical Engineering and Computer Science

Abstract

Free space optical communication through the atmosphere has the potential to provide secure, low-cost, rapidly deployable, dynamic, data transmission at very high rates. However, the deleterious effects of turbulence can severely limit the utility of such a system, causing outages of up to 100 ms. For this thesis, we investigate an architecture that uses multiple transmitters and multiple coherent receivers to overcome these turbulence-induced outages. By controlling the amplitude and phase of the optical field at each transmitter, based on turbulence state information fed back from the receiver, we show that the system performance is greatly increased by exploiting the instantaneous structure of the turbulence. This architecture provides a robust high-capacity free-space optical communication link over multiple spectral bands, from visible to infrared.

We aim to answer questions germane to the design and implementation of the diversity optical communication architecture in a turbulent environment. We analyze several different optical field spatial modulation techniques, each of which is based on a different assumption about the quality of turbulence state information at the transmitter. For example, we explore a diversity optical system with *perfect* turbulence state information at the transmitter and receiver that allocates transmit power into the *spatial modes* with the smallest propagation losses in order to decrease bit errors and mitigate turbulence-induced outages. Another example of a diversity optical system that we examine is a diversity optical system with only a subset of the turbulence state information: this system could allocate all power to the *transmitter* with the smallest attenuation.

We characterize the system performance for the various spatial modulation techniques in terms of average bit error rate (BER), outage probability, and power gain due to diversity. We first characterize the performance of these techniques in the idealized case, where the instantaneous channel state is perfectly known at both the receiver and transmitter. The time evolution of the atmosphere, as wind moves tur-

bules across the propagation path, can limit the ability to have perfect turbulence state knowledge at the transmitter and, thus can limit any improvement realized by optical field spatial modulation techniques. The improvement is especially limited if the latency is large or the feedback rate is short compared to the time it takes for turbules to move across the link. As a result, we make successive generalizations, until we describe the optimal system design and communication techniques for sparse aperture systems for the most general realistic case, one with inhomogeneous turbulence and imperfect (delayed, noisy, and distorted) knowledge of the atmospheric state.

Thesis Supervisor: Vincent W. S. Chan
Title: Joan and Irwin M. Jacobs Professor of Electrical Engineering and Computer Science

Acknowledgments

I would like to express my deepest gratitude to my advisor, Vincent W.S. Chan, for his guidance, support, and patience. He taught me that asking the right question is just as important as the answer. His exceptional engineering intuition has always pushed me to look beyond the equations to understand things at a physical level. Vincent has always led by example, showing integrity and honesty–when it's easy to do so *and* when it's difficult to do so.

I would like to thank Steve Prutzer for his encouragement and unequivocal support. It is because of his mentorship that I arrived at MIT prepared for the research ahead. I thank my thesis committee, Eric Swanson and Jeff Shapiro, for many useful comments and discussions. While both contributed to the thesis as a whole, Eric contributed much to the engineering while Jeff kept me firmly rooted in the physics. The friendship and administrative support offered by Donna Beaudry is much appreciated.

Andrew Puryear

Cambridge, Mass.

The research contained in this thesis was supported, in part, by the Defense Advanced Research Projects Agency (DARPA) and the Office of Naval Research.

Contents

List of Figures

List of Tables

Chapter 1

Introduction

Many applications would benefit from a secure, low-cost, rapidly deployable, dynamic, high data rate communication link [7]. For example, a company may require extra communication capacity to support a short term project. Installing new fiber, with the right-of-way and installation costs, is very expensive. Microwave or radio communication is limited in data rate and available spectrum. Free space optical communication is an attractive solution because it provides license-free long range operation at very high data rates without expensive installation costs. Additionally, free space optical communication is relatively secure due to the high directionality and narrowness of laser beams. The deleterious effects of the atmosphere can severely limit the utility of such a system, however. Factors such as beam dispersion, atmospheric absorption, rain, fog, snow, and scintillation, among other factors, can lead to higher implementation costs [1]. In the clear atmosphere, turbulence can cause severe fading that increases the cost and decreases the reliability of free space optical communication [26, 27, 40]. The reliability of these systems is reduced considerably by deep fades of 20 to 30 dB of typical duration of 1 to 100 ms [45]. Such fades, caused by microscale atmospheric temperature fluctuation, may result in the corruption of 10^9 bits at 10 Gbps. A system engineer typically has four degrees of freedom to mitigate the effects of fading: power, temporal diversity, frequency diversity, and/or spatial diversity. Increasing power to provide 30 dB of margin, or extra power, is prohibitively costly. Similarly, increasing temporal diversity by implementing a space-time code is

not an attractive solution because it requires a gigabit interleaver and long delays. Frequency diversity can provide some additional robustness but is costly because of the broadband components required. These components must be broadband because of the large frequency coherence of atmospheric turbulence. Thus we are motivated to explore architectures with a high degree of spatial diversity.

Specifically, this thesis investigates the use of spatial diversity with wavefront predistortion based on feedback from the receiver and coherent detection to overcome turbulence-induced outages, mitigate interference, and prevent eavesdropping. This architecture provides a robust high-capacity free-space optical communication link over multiple spectral bands, from visible to infrared. We focus on sparse aperture systems: the primary goal of sparse aperture architecture is to increase spatial diversity without the need for large, expensive, monolithic apertures such as deformable mirrors. This requires systems with many transmit and receive apertures. Such systems can be readily implemented due to the relatively short coherence length of the atmosphere at optical wavelengths.

With the successful shift toward net-centric systems, there is a desire to be able to detect anything, from anywhere, at any time with a requirement to globally share this information in real-time with high reliability and security. The desire for net-centric operations and global information dissemination will place an increased burden on existing and future communication systems. To realize the full bandwidth potential of optical communication and provide seamless handoff with radio frequency (RF) technologies, the optical phase and frequency must be preserved and controlled in a manner similar to current RF phase and frequency treatments. This phase and frequency control enables high-capacity communication through a dispersive fading channel with a low probability of detection, intercept and denial of service. The use of this coherent free space optical transmission, coupled with high-speed electronics and real-time digital signal processing (DSP), enables these next generation free space optical system architectures.

1.1 Previous Work

Free space optical communication has been present since antiquity. In 405 BCE the ancient Greeks used polished shields to signal during battle [11]. Circa 35 CE, the Roman emperor Tiberius, by then very unpopular, ruled his vast empire from a villa on the Isle of Capri, an island off the western coast of what is now Italy. It is thought that he used a heliograph to send coded orders every day to the mainland, eight miles away [20]. The ancient Chinese, Egyptians, and Romans all used beacons, large fires stacked on hills or atop high towers, to send early warning messages. A famous example from British history is the line of beacons set up along the southern coast of England in the year 1588 to warn that the Spanish invasion fleet, the Armada, was coming. By the time the fleet appeared on the horizon off Cornwall, the fires on the hillsides were lit — sending the message to London faster than any horseman could ride [38]. Not until April 1, 1880 did the world make its first wireless telephone call: Alexander Graham Bell and his assistant Charles Sumner Tainter used a photophone, a device that used sunlight reflected off a vibrating mirror and a selenium photo cell to send sound and conversations on a beam of light, to place a call from the Franklin School in Washington, D.C. to the window of Bell's laboratory, 213 meters away [4]. The photophone's first practical use came several decades later when the U.S. military used the system for communication. The invention of the laser in the 1960s revolutionized the field, enabling modern optical communication systems. Systems have been developed for ground-to-ground, ground-to-aircraft, ground-to-satellite, satellite-to-satellite, and even satellite-to-submarine applications.

The feasibility of coherent free space optical systems was investigated in the early 1980s as a means to improve a receiver's sensitivity, thereby increasing system performance [5, 6]. In coherent detection, an optical local oscillator field is added to the incoming field and the sum is detected by a square law detector. With a dual-detector coherent receiver, quantum limited performance can be achieved [52]. In addition, in contrast to existing optical direct-detection system technology, because optical coherent detection systems can also detect not only an optical signal's amplitude but phase

and polarization as well, a number of other modulation schemes were also possible, potentially further improving the receiver sensitivity.

1.2 Modern Free Space Optical Systems

As free space optical communication systems proliferate, demands imposed on their performance—higher data rates with increased reliability and security—require advanced techniques to achieve. There are several techniques employed to achieve the required performance and overcome turbulence induced fading. Some current systems use a single transmitter and single detector and simply use extra power to overcome the 20 to 30 dB fades. This approach is prohibitively expensive due to the high cost of 30 dB amplifiers at moderate to high power (> 1 W). Another approach, borrowed from astronomy, is to employ a large deformable mirror to compensate for the turbulence, essentially using spatial diversity to overcome turbulence induced fading [46]. The deformable mirror concept performs well, but is there a way to exploit spatial diversity without using large, expensive deformable mirrors? The answer is a sparse aperture system, which uses many small transmitters and receivers configured to achieve the same spatial diversity as the deformable mirror systems at a fraction of the cost [44]. This thesis will address the efficient utilization of sparse aperture systems and finds that this architecture effectively mitigates the effects of the turbulent atmosphere. In this thesis, we focus on sparse aperture systems that are able to measure the turbulence state at the receiver, feed back some information about the turbulence state to the transmitter, and then use that information to exploit the instantaneous structure of the turbulence by controlling the phase and magnitude of the field of each transmitter. For example, a sparse aperture system with knowledge of the turbulence at the transmitter could select the transmit aperture with the smallest attenuation. Another example is a system that optimally allocates transmit power into the spatial modes with the smallest propagation losses in order to decrease bit errors and mitigate turbulence-induced outages. In addition to fade mitigation, spa-

tial mode modulation and rejection provides robust communication in the presence of interference by other users.

Previous work on sparse aperture coherent detection systems has focused on the case in which the transmitter has no knowledge of the turbulence state. For this case, it is optimal to allocate equal power with identical phase to each transmitter. The average bit error rate (BER) was studied in [39, 21]. Outage probability was studied in [28]. When the transmitter has knowledge of the turbulence state, the optimal performance is achieved by allocating all of the transmit power to the input eigenmode with the best performance [43]. The performance of this scheme when the channel state is known *perfectly* at both the transmitter and receiver is addressed in this thesis. Perfect knowledge of the channel state at both the transmitter and receiver is not possible because, in the optical and infrared wavebands, the atmospheric channel is continually changing because of wind and the evolution of turbulent eddies. The dynamic nature of the atmosphere causes the receiver to necessarily have a delayed estimate of the channel. Further, because of the dynamic nature of the atmosphere and the finite rate feedback link, the transmitter will necessarily have a delayed and distorted description of the turbulence state. For any system employing wavefront predistortion based on turbulence state feedback, the amount of delay and distortion of the turbulence state information must be small: how small should the delay and distortion be? In this thesis, we develop a model of the dynamic atmosphere and use it to find the optimal performance of the system as a function of latencies, both estimation and feedback, feedback link rate, and fundamental system and physical parameters, such as number of apertures, turbulence strength, link range, etc. We also find a feedback scheme that achieves optimal performance. Where possible we analyze data to validate the theory developed.

1.3 Thesis Overview and Outline

For the thesis, we attempt to use the simplest possible model while still capturing the important effects. Most engineering work is, in fact, performed on simplified

models; for example, researchers often model noise as an additive white Gaussian noise (AWGN) random process while understanding that the AWGN model is valid only for sufficiently small bandwidths. Of course, with AWGN we expect the model to be very accurate when used properly. In contrast, statistical models characterizing the optical atmospheric channel are relatively poor, providing only order-of-magnitude guides to system design. The ultimate purpose of simplified models is to provide a basis for comparison of different system approaches while guiding engineering design intuition.

Often in this thesis we perform an asymptotic analysis, assuming the number of transmitters and receivers grows infinite with a given aspect ratio (number of transmitter to number of receivers). This analysis is never strictly exact for any physically realizable system, but does admit a number of powerful and appealing closed form solutions. We quantify the extent to which these asymptotic solutions approximate physical, finite systems and, in the process, we find that these asymptotic solutions are often very good approximations. Of course, there are times when an asymptotic solution is a poor approximation to the finite system. However, just as Shannon's noisy-channel coding theorem (an example of an asymptotic analysis) provided important performance bounds and insight into finite length codes to drive the wireless revolution, we hope to provide performance bounds and insight to drive free space optical communication innovation.

In Chapter 2, we review the background necessary to place the theory presented in this thesis on a solid foundation. We begin with first principles, Maxwell's equations in this case, and derive the system model while emphasizing the assumptions required for the theory to be applicable. First, we outline the derivation of scalar diffraction theory from Maxwell's equations. Next, we review the impact of micro-scale index of refraction on optical beam propagation. Subsequently we discuss system power budget, including the impact of coherent detection and propagation on signal power.

In the next chapter, Chapter 3, we examine the performance of sparse aperture communication systems when the turbulence state is *perfectly* known by the transmitter. We find closed-form performance expressions for various spatial modulation

techniques including optimal wavefront predistortion diversity (allocate power to couple into the mode that propagates the most efficiently), selection diversity (allocate all power to the transmit aperture that gives the best instantaneous performance), and open-loop diversity (allocate equal power and identical phase to each transmitter). For each of these diversity techniques, we find the average performance, outage performance, and power margin. We show that, in the turbulent atmosphere, wavefront predistortion based on receiver-to-transmitter feedback can significantly improve transmit and receive diversity sparse aperture optical communication system performance, both in terms of average performance and outage performance.

The time evolution of the atmosphere, as wind moves turbulent eddies across the propagation path, can limit any improvement realized by wavefront predistortion with feedback. The improvement is especially limited if the latency is large or the feedback rate is small compared to the time it takes for turbulent eddies to move across the link. In Chapter 4, we derive theoretical expressions relating latencies, such as feedback latency and channel state estimate latency, and feedback rate to optimal performance. Specifically, we find the theoretical optimal average BER as a function of fundamental parameters such as wind speed, atmospheric coherence length, feedback rate, feedback latency, and channel state estimate latency. Further, we describe a feedback strategy to achieve the optimal BER. We find that the sufficient feedback rate scales linearly with the inverse of the atmospheric coherence time and sublinearly with number of transmitters. Under typical turbulence conditions, low-rate feedback, on the order of hundreds of bits per second, with associated latencies of less than a few milliseconds is sufficient to achieve most of the gain possible from wavefront predistortion. We use the theory developed to answer design questions important to system implementation and deployment. How much do feedback delay and computational time impact performance? Given a system geometry, what feedback rate is needed to take full advantage of the diversity? Given a feedback link rate, what is the best performance possible? How often does the transmitter need channel state updates? At each update, what information does the transmitter need? In terms of feedback information, we have two degrees of freedom: how often to feed

back an update, and what information is fed back at each update. If we feed back very infrequently with respect to the channel coherence time, we would need to send back a full set of channel state information. If we update the state information more frequently, we may not have to transmit the full set of channel state information. For example, if we update the state information at a tenth of the channel coherence time, we could possibly feed back a state update, or perturbation, instead of the full set of channel state information (CSI). Finally, given a system geometry and performance requirements, what is the trade between increasing transmit power and increasing feedback rate?

In Chapter 5, we analyze data collected by an experimental system with a single laser transmitter located 250 meters from two coherent receivers [28]. We first use the data to validate the use of a two-state continuous time Markov process to model outage statistics of the diversity system. In the two-state channel model, symbols received during an outage are assumed to be lost, and symbols received during a non-outage are assumed to be received correctly. This channel model can be used to analyze the performance of the transport layer. Next, we use statistical and spectral analysis techniques to create a linear prediction model for signal attenuation for both the single-receiver and diversity systems. The prediction model is an optimal estimator that predicts signal attenuation 1 ms into the future to 1.5 dB accuracy for the single-receiver cases and to 1 dB accuracy for the diversity case. The maximum amount of time the estimator can predict into the future with some confidence is about 5 to 10 ms. This channel prediction and adaptation can be used to greatly improve the efficiency of free-space optical communication systems in the atmosphere.

Despite the ability for free space optical technology to transmit a narrow beam of light to a specific destination, it is still possible for an eavesdropper to gather light and decode information intended for another user. Further, it is possible for an interferer to couple light into the intended receiver's aperture, thereby reducing the performance of the communication link. Chapter 6 address security, interference rejection and eavesdropper prevention, for the free space optical communication system. We find

that wavefront predistortion is an effective technique to improve the security of free space optical communication.

Finally, we conclude the thesis with Chapter 7. In this chapter, we highlight some of the important contributions given in the thesis and provide recommendations for future work. Further, we discuss how these contributions can be applied to future communication systems.

Chapter 2

Background and Preliminaries

This chapter reviews the background necessary to place this thesis on solid theoretical footing. First, we outline the derivation of scalar diffraction theory from Maxwell's equations. Next, we review the impact of micro-scale index of refraction on optical beam propagation. Finally we discuss system power budget, including the impact of coherent detection and propagation on signal power.

2.1 From Maxwell's Equations to Scalar Diffraction Theory

This section reviews the derivation of turbulent propagation theory from first principles focusing on the necessary assumptions for the topics of this thesis. By focusing on assumptions of the derivation, we find the limitations of the results, the inaccuracies of approximations, and the regions of applicability of the theory. First, we outline the derivation of the scalar wave equation for laser propagation through free space. Next we show the Green's function formulation of propagation through free space. Finally, we show the Green's function formulation of propagation through atmospheric turbulence. Here we specify a turbulence model and a model for how the interaction of the turbulence affects the propagation of the field.

In general, light is energy propagated through interacting, coupled electric and magnetic fields. The propagation and coupling are fully described by Maxwell's equations in the absence of free charge:

$$\begin{aligned} \nabla \times \vec{\mathcal{E}} &= -\mu \frac{\partial \vec{\mathcal{H}}}{\partial t} \\ \nabla \times \vec{\mathcal{H}} &= \epsilon \frac{\partial \vec{\mathcal{E}}}{\partial t} \\ \nabla \cdot \epsilon \vec{\mathcal{E}} &= 0 \\ \nabla \cdot \mu \vec{\mathcal{H}} &= 0 \end{aligned} \tag{2.1}$$

where $\vec{\cdot}$ denotes a vector quantity, $\vec{\mathcal{E}}$ is the electric field, $\vec{\mathcal{H}}$ is the magnetic field, μ is the permeability of the propagation medium, ϵ is the permittivity of the propagation medium, and t is time. The electric field $\vec{\mathcal{E}}$ and magnetic field $\vec{\mathcal{H}}$ are, in general, a function of both time t and position $\vec{P}$. We assume the atmosphere is nonmagnetic, implying the relative permeability of the propagation medium is uniformly unity regardless of time or position. In contrast, the permittivity of the atmosphere varies with time and position. The primary cause of the spatial and temporal nonuniformity of the permittivity is solar energy: convective mixing, due to heat from the Sun that is transferred from the Earth's surface to the surface air layer, along with wind-shear induced turbulent mixing creates random atmospheric temperature variation, and therefore permittivity variation, in the form of turbulent eddies. Further temporal variation is caused by wind moving the eddies in bulk. Exact models describing the permittivity variation are impractical, due to their sensitivity to local terrain, and not particularly useful for developing a communication channel model. As a result, we turn to a statistical description of the turbulence; this statistical model encapsulates the germane effects of the permittivity variation while neglecting effects due to local topography, etc. We review the statistical model used to describe the random permittivity variation in Section 2.3, and continue now to develop a propagation model with the understanding that the variation causes the propagation medium to be inhomogeneous. For laser communication through the atmosphere, the propagation

medium is approximately linear, isotropic, inhomogeneous, effectively nondispersive, and nonmagnetic dielectric. Thus, Maxwell's equations simplify to [16]:

$$\nabla^2\vec{\mathcal{E}} + 2\nabla\left(\vec{\mathcal{E}}\cdot\nabla \ln n\right) - \frac{n^2}{c^2}\frac{\partial^2\vec{\mathcal{E}}}{\partial t^2} = 0 \tag{2.2}$$

where c is the speed of light in the propagation medium and n is the index of refraction in the medium, given by:

$$n = \sqrt{\frac{\epsilon}{\epsilon_0}} \tag{2.3}$$

where ϵ_0 is the permittivity of free space. The $2\nabla\left(\vec{\mathcal{E}}\cdot\nabla \ln n\right)$ term, which is nonzero whenever the permittivity varies spatially, represents a coupling between the components of the electric field. Because the term causes the wave to change polarization as it propagates, we call it the *polarization term*. Detailed analysis in [45] has shown that the polarization term is negligible for laser communication through the atmosphere. As a result, equation (2.2) simplifies to the familiar wave equation:

$$\nabla^2\vec{\mathcal{E}} - \frac{n^2}{c^2}\frac{\partial^2\vec{\mathcal{E}}}{\partial t^2} = 0 \tag{2.4}$$

Because each component of the electric and magnetic field must satisfy equation (2.4), we replace the vector equation with the scalar wave equation:

$$\nabla^2 u(\vec{P},t) - \frac{n^2}{c^2}\frac{\partial^2 u(\vec{P},t)}{\partial t^2} = 0 \tag{2.5}$$

where $u(\vec{P},t)$ is a function of both position $\vec{P}$ and time t and can represent any component of the electric or magnetic field. Of course, the assumptions of the scalar wave equation do not strictly hold because any field must be launched from a finite aperture; the aperture represents sharp change in the permittivity that causes coupling between the various polarizations, and even between the electric and magnetic fields. The fields couple only in the region near (within several wavelengths of) the boundary; far from the boundary the fields are uncoupled, as in equation (2.5). Thus, as long as the aperture is large compared to a wavelength, $\lambda = 10^{-6}$ m for a typi-

cal optical communication system, the errors introduced by using scalar diffraction theory will be small. [16]

If $u(\vec{P},t)$ is well approximated as a monochromatic wave, it can be written in the following form:

$$u(\vec{P},t) = \Re\left\{U(\vec{P})\exp\left(-j2\pi\frac{ct}{n\lambda}\right)\right\} \tag{2.6}$$

where c is the speed of light in the propagation medium and $U(\vec{P}) = A(\vec{P})\exp(j\phi(\vec{P}))$ is a complex function that contains all of the information about the amplitude $A(\vec{P})$ and phase $\phi(\vec{P})$ of the wave. Substituting the expression for the monochromatic wave into scalar wave equation gives the time-independent Helmholtz wave equation:

$$\left(\nabla^2 + k^2\right)U = 0 \tag{2.7}$$

where $k = 2\pi/\lambda$ is commonly known as the wavenumber and λ is the wavelength in the medium.

2.2 Vacuum Propagation, Scalar Diffraction Theory

The Helmholtz wave equation describes a wave over all of space and time. For the Helmholtz wave equation to be useful, we must be able to use it to calculate a field in the receive plane given a field, or boundary condition, in the transmit field. More formally, referring to figure 2-1 we would like to calculate the field $U_o(\vec{\rho}\,')$ in the $\vec{\rho}\,'$-plane given a monochromatic field $U_i(\vec{\rho})$ in the $\vec{\rho}$-plane. The $\vec{\rho}$-plane and $\vec{\rho}\,'$-plane are separated by a length of L and are perpendicular to the propagation axis. The vectors in the transmit and receive plane are real, two-dimensional vectors: $\vec{\rho} = [\rho_x, \rho_y]^T$ and $\vec{\rho}\,' = [\rho'_x, \rho'_y]^T$. Using Green's theorem along with the proper choice of Green's function, the solution to the Helmholtz wave equation gives the Rayleigh-Sommerfeld

diffraction formula [16]:

$$U_o(\vec{\rho}\,') = \frac{1}{j\lambda}\int_{R_{tx}} U_i(\vec{\rho}\,)\,\frac{\exp(jk|\vec{r}_{tr}|)}{|\vec{r}_{tr}|}\cos(\theta)\,d\vec{\rho} = \frac{L}{j\lambda}\int_{R_{tx}} U_i(\vec{\rho}\,)\,\frac{\exp(jk|\vec{r}_{tr}|)}{|\vec{r}_{tr}|^2}d\vec{\rho} \tag{2.8}$$

where U_o is the propagated field, R_{tx} is the region where the launched field is non-zero, $\vec{r}_{tr}$ is the vector from $\vec{\rho}$ to $\vec{\rho}\,'$ as shown in figure 2-1, θ is the angle between $\vec{r}_{tr}$ and the z-axis and $|\vec{r}_{tr}| = \sqrt{L^2 + (\rho'_x - \rho_x)^2 + (\rho'_y - \rho_y)^2}$ is the length of the vector $\vec{r}_{tr}$.

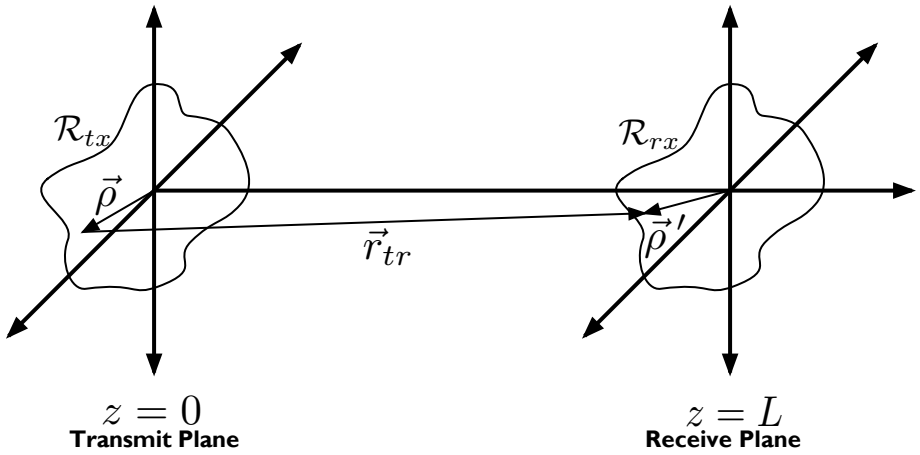

Figure 2-1: Diffraction geometry

There are other solutions to the Helmholtz wave equation, such as Fresnel-Kirchhoff diffraction formula and even another Rayleigh-Sommerfeld diffraction formula. It is easy to show that they are effectively the same provided that the aperture linear dimension is smaller than the propagation distance. This is always true for communication systems addressed in this thesis. A nice physical interpretation of the Rayleigh-Sommerfeld diffraction formula is that each point of the wave in the receive plane may be regarded as the weighted superposition of infinitely many point sources in the transmit plane. Each point source is weighted by the input field $\vec{U}_i$ and the obliquity factor, $\cos(\theta)$.

The Rayleigh-Sommerfeld diffraction formula defined above is the most general diffraction formula; it is valid for very short propagation distances, on the order of a few wavelengths, and at high angles off the optical axis. The Rayleigh-Sommerfeld

diffraction formula is difficult to calculate for many applications, rarely having a closed form solution. This is primarily due to the square-root operation when calculating the length of $\vec{r}_{tr}$ in the exponent and denominator of equation (2.8). Because the term $\exp(jk|\vec{r}_{tr}|)$ is periodic as a function of $|\vec{r}_{tr}|$, the requirement on the approximation error in the length calculation must be much smaller than 2π, regardless of the magnitude of $\vec{r}_{tr}$. As such, we perform a binomial expansion to arrive at the approximation for $|\vec{r}_{tr}|$ in the exponent of equation (2.8) [16]:

$$\begin{aligned} |\vec{r}_{tr}| &= L\sqrt{1+\left(\frac{\rho_x-\rho_x'}{L}\right)^2+\left(\frac{\rho_y-\rho_y'}{L}\right)^2} \\ &\approx L\left[1+\frac{1}{2}\left(\frac{\rho_x-\rho_x'}{L}\right)^2+\frac{1}{2}\left(\frac{\rho_y-\rho_y'}{L}\right)^2\right] \end{aligned} \tag{2.9}$$

The approximation error in the denominator of equation (2.8) must be small compared to the magnitude of $\vec{r}_{tr}$. Thus, $|\vec{r}_{tr}|$ can further be approximated as $|\vec{r}_{tr}| = L$. These two approximations give rise to the Fresnel diffraction equation [16]:

$$U_o\left(\rho_x',\rho_y'\right) = \frac{e^{jkL}}{j\lambda L}\int\int_{R_{tx}} U_i\left(\rho_x,\rho_y\right)\exp\left(j\frac{k}{2L}\left[(\rho_x'-\rho_x)^2+(\rho_y'-\rho_y)^2\right]\right)d\rho_x d\rho_y \tag{2.10}$$

Physically, the Fresnel diffraction equation replaces the infinitely many point sources with spherical wavefront of Rayleigh-Sommerfeld diffraction with infinitely many point sources with a quadratic wavefront. The Fresnel diffraction equation is accurate provided that the length approximation in the exponent is accurate:

$$\begin{aligned} \max_{\vec{\rho}\in R_{tx},\vec{\rho}\,'\in R_{rx}}\left||\vec{r}_{tr}|-L\left[1+\frac{1}{2}\left(\frac{\rho_x-\rho_x'}{L}\right)^2+\frac{1}{2}\left(\frac{\rho_y-\rho_y'}{L}\right)^2\right]\right| &\ll \frac{\pi}{k} \\ \max_{\vec{\rho}\in R_{tx},\vec{\rho}\,'\in R_{rx}}\frac{L}{8}\left[\left(\frac{\rho_x-\rho_x'}{L}\right)^2+\left(\frac{\rho_y-\rho_y'}{L}\right)^2\right]^2+\text{HOT} &\ll \frac{\lambda}{2} \end{aligned} \tag{2.11}$$

where HOT represent higher order terms, which can be ignored. Rearranging the terms provides a minimum propagation distance for the Fresnel approximation to be

valid:

$$L^3 \gg \frac{1}{4\lambda} \max_{\vec{\rho}\in R_{tx}, \vec{\rho}\,'\in R_{rx}} \left[\left(\rho_x - \rho_x'\right)^2 + \left(\rho_y - \rho_y'\right)^2 \right]^2 \tag{2.12}$$

where R_{tx} is the transmitter region and R_{rx} is the receiver region. For a system with the transmit aperture the same size as the receive aperture, each having a largest linear dimension of $2\mathsf{w}$, the condition that a propagation calculation must satisfy for the Fresnel diffraction formula to be valid simplifies to:

$$L^3 \gg \frac{64\mathsf{w}^4}{\lambda} \tag{2.13}$$

A more detailed analysis, such as in [16], shows that this sufficient condition is overly stringent and can be relaxed significantly. We now continue to further simplify the Fresnel diffraction equation. Expanding the quadratic term in the Fresnel diffraction equation, we arrive at:

$$U_o\left(\rho_x', \rho_y'\right) = \cdots$$
$$\frac{e^{jkL}}{j\lambda L} \exp\left(j\frac{k}{2L}\left[\rho_x'^2 + \rho_y'^2\right]\right) \int\int_{R_{tx}} U_i\left(\rho_x, \rho_y\right) \exp\left(j\frac{k}{2L}\left[\rho_x^2 + \rho_y^2 - 2\rho_y\rho_y' - 2\rho_x\rho_x'\right]\right) d\rho_x d\rho_y \tag{2.14}$$

From this expression, the quadratic term inside the integral is approximately unity under the condition that:

$$L \gg \max_{\vec{\rho}\in R_{tx}} \frac{k\left(\rho_x^2 + \rho_y^2\right)}{2} \tag{2.15}$$

Thus simplifying the Fresnel diffraction equation to:

$$U_o\left(\rho_x', \rho_y'\right) = \cdots$$
$$\frac{e^{jkL}}{j\lambda L} \exp\left(j\frac{k}{2L}\left[\rho_x'^2 + \rho_y'^2\right]\right) \int\int_{R_{tx}} U_i\left(\rho_x, \rho_y\right) \exp\left(-j\frac{k}{L}\left[\rho_y\rho_y' + \rho_x\rho_x'\right]\right) d\rho_x d\rho_y \tag{2.16}$$

which is called the Fraunhofer diffraction equation. Before we continue to study the effect of atmospheric turbulence, we provide the Fraunhofer diffraction for a circular

aperture with radius w illuminated by a unit amplitude plane wave:

$$U_o\left(\vec{\rho}\,'\right) = e^{jkL} e^{j\frac{k|\vec{\rho}\,'|^2}{2L}} \frac{\pi \mathsf{w}^2}{j\lambda L}\left[2\frac{J_1(k\mathsf{w}|\vec{\rho}\,'|^2/L)}{k\mathsf{w}|\vec{\rho}\,'|^2/L}\right] \tag{2.17}$$

where $J_1(\cdot)$ is a Bessel function of the first kind of order one. Later in this thesis, we assert that the amplitude across the receive aperture is approximately constant. This assertion is approximately true if the receiver aperture falls within the main lobe of the diffraction pattern:

$$d < \frac{2\lambda L}{\mathsf{w}} \tag{2.18}$$

where d is the maximum extent of the receive aperture. We now continue to present scalar diffraction theory in the presence of atmospheric turbulence.

A wave can only be approximated as a monochromatic provided that:

$$\frac{\Delta\lambda}{\lambda} \ll 1 \text{ and } \frac{\lambda^2}{\Delta\lambda} \gg n|\vec{r}_{tr}| \tag{2.19}$$

where λ is the peak wavelength of the spectrum and $\Delta\lambda$ is the full-width half max of the source spectrum near λ.

For sources not well modeled as a monochromatic wave, we can simply use the set of all monochromatic waves as a complete orthonormal set that spans the space of all physically realizable (i.e., L_2) waveforms. Because we assumed a linear propagation medium, we can calculate the resulting field to any arbitrary wave by: (1) finding the decomposition of the arbitrary wave into monochromatic waves (2) calculating the resulting field due to the monochromatic waves and (3) constructing the output of the arbitrary wave based on a recomposition of the monochromatic waves. Because we can find the field of any arbitrary wave from linear combinations of monochromatic waves, we consider only monochromatic waves in the following sections.

2.3 Atmospheric Propagation, Scalar Diffraction Theory

The refractive index in Earth's atmosphere is a function of pressure, temperature, and wavelength. At optical wavelengths, a good approximation, neglecting water vapor pressure, for the index of refraction is [46]:

$$n_1 = n - 1 = 77.6 \times 10^{-6} \left(1 + 7.52 \times 10^{-3} \lambda^{-2}\right) \frac{P_r}{T} \tag{2.20}$$

where λ, for this equation, is the wavelength in μm, P_r is the atmospheric pressure in millibars and T is the temperature in Kelvin. The term n_1, which represents the *deviation* of the index of refraction from free space, is typically small, on the order of a few parts per thousand. For example, at one atmosphere, approximately $P_r = 1013.25$ millibars, room temperature $T = 300$ K, and typical optical wavelengths on the order of $\lambda = 10^{-6}\mu m$ the deviation from free space is $n_1 = 2.6 \times 10^{-4}$. Therefore, a small change in temperature δT translates to a small change in index of refraction δn according to:

$$\delta n = \left(\frac{-58 \times 10^{-6} P_r}{T^2}\right) \delta T \tag{2.21}$$

where we have assumed a wavelength of $\lambda = 10^{-6}\mu m$. Thus, a one Kelvin change in temperature can cause a 10^{-6} change in index of refraction at room temperature and one atmosphere. As we will see, this one part in a million variation in the index of refraction can substantially impact optical communication performance.

2.3.1 Model for Atmospheric Index of Refraction

Differential heating of the Earth's surface causes wind and convective mixing. The bulk of the turbulent energy is not due to convective mixing, but instead is due to energy injected at large scales by wind shear. The energy of the large scale eddies, parcels of air with characteristic velocity, vorticity, and pressure, cascades to smaller scale structures by an inertial and inviscid mechanism. This process continues to

create smaller and smaller eddies until the eddies are smaller than the inner-scale l_0, where viscous dissipation of energy finally takes place. The inner-scale typically ranges between a few millimeters to a centimeter for optical wavelengths. Figure 2-2 shows the energy cascade through the inertial subrange.

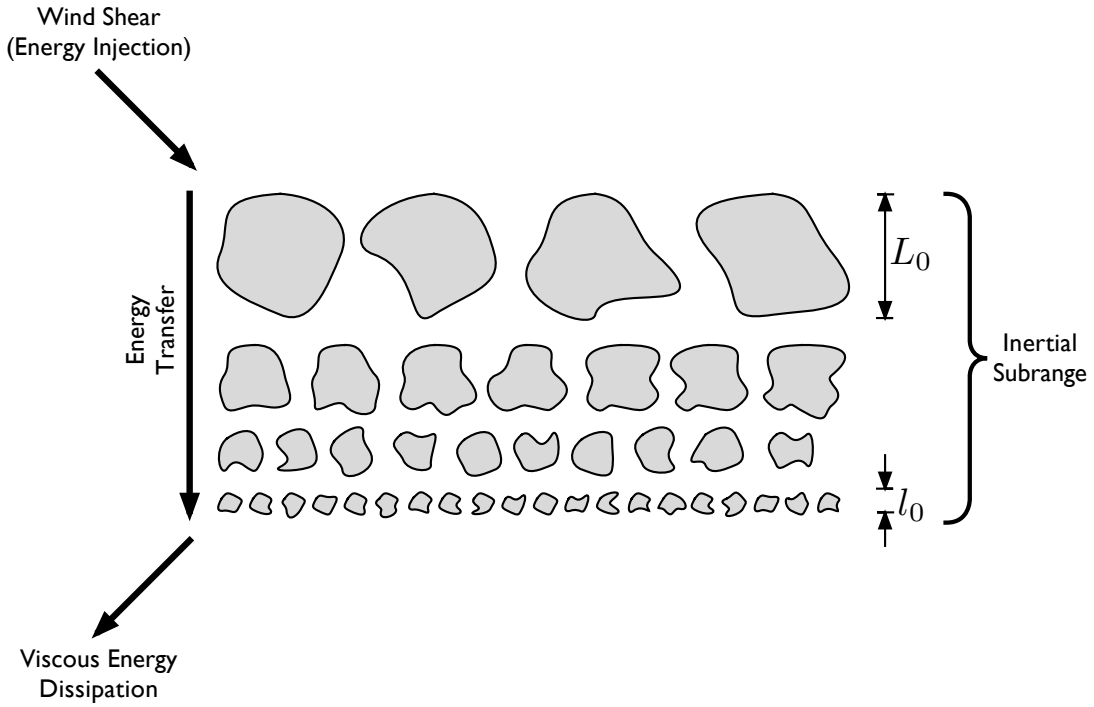

Figure 2-2: Energy cascade through the inertial subrange: energy is injected into large scale eddies by wind shear, the eddies transfer their energy to smaller and smaller eddies, when the eddies become smaller than the inner scale l_0 the energy is dissipated to heat [37].

A statistical characterization of the spatial structure of the turbulence is essential to characterize wave propagation through random media. Specifically, we wish to find the spatial index of refraction autocorrelation function and the power spectral density. Because eddies in the largest range, eddies larger than the outer scale size of L_0, are governed by local geographical and meteorological conditions [17] there is no physics based expression describing eddies of this scale. Typical values of the outer scale size, which varies with height above the ground among other parameters, range from one to one hundred meters for optical wavelengths. Optical communication is not strongly effected by eddies in this range, thus it is not important to find an expression in this

Table 2.1: Structure constant, C_n^2, for various atmospheric conditions.

Weak Turbulence	$10^{-16}\ m^{-2/3}$
Mild Turbulence	$10^{-15}\ m^{-2/3}$
Moderate Turbulence	$10^{-14}\ m^{-2/3}$
Strong Turbulence	$10^{-12}\ m^{-2/3}$

range. Energy in eddies smaller than the outer scaled L_0 but larger than the inner scale l_0, the so called inertial subrange of turbulence scales, is in equilibrium with the net energy cascading to smaller energy where it is dissipated. Within the inertial subrange, Kolmogorov showed that the random fluctuation of index of refraction has a power spectral density of the following form [17]:

$$\Phi_n(\kappa) = 0.033 C_n^2 \kappa^{-11/3}, \qquad 2\pi/L_0 < \kappa < 2\pi/l_0 \tag{2.22}$$

where κ is the spatial wavenumber in units of radians per meter and C_n^2 is the structure constant of refractive index fluctuations. Table 2.1 shows typical structure constant values, which is a measure of the turbulence strength, for various atmospheric conditions.

Energy for eddies smaller than the inner scale dissipates very rapidly, and thus has only a very small effect on optical communication. Others have modified the Kolmogorov spectrum in an attempt to increase its validity outside the inertial subrange (Tatarski, von Karman). For the remainder of this thesis however, we assume Kolmogorov turbulence.

2.3.2 Wave Propagation through Random Media

Similar to free-space propagation, propagation through turbulence is governed by the scalar wave equation:

$$\nabla^2 u(\vec{P}, t) - \frac{n^2}{c^2} \frac{\partial^2 u(\vec{P}, t)}{\partial t^2} = 0 \tag{2.23}$$

Unlike free-space propagation, however, the wave equation cannot be solved for the turbulent atmosphere because the index of refraction varies both spatially and temporally. Because the wave propagates much faster than the turbulence time scale,

the temporal variation is generally ignored. Because the wave equation cannot be solved exactly, the Born and Rytov approximations are widely used for solving the wave equation in turbulence. The wave-fluctuation approximations derived by the Born and Rytov approximations are simply the first terms in perturbation expansions valid for sufficiently weak atmospheric inhomogeneities. Experimental results have shown that the Rytov method yields better results for the region outside of very weak turbulence. Within the region of very weak turbulence, both approximations yield roughly the same result. Consequently, we assume Rytov's approximation throughout this thesis. Without loss of generality, the field in the receive plane is [46]:

$$U_o\left(\vec{\rho}\,'\right) = \frac{e^{jkL}}{j\lambda L}\int_{R_{tx}} U_i\left(\vec{\rho}\,\right)\exp\left(j\frac{k}{2L}|\vec{\rho}\,' - \vec{\rho}\,|^2\right)\times\exp\left(\chi(\vec{\rho},\vec{\rho}\,') + j\phi(\vec{\rho},\vec{\rho}\,')\right)d\vec{\rho} \quad (2.24)$$

where $\chi(\vec{\rho},\vec{\rho}\,')$ is the stochastic turbulence induced log-amplitude fluctuation and $\phi(\vec{\rho}\,',\vec{\rho})$ is the stochastic turbulence induced phase fluctuation. Further, within the region of validity for the Rytov method, the stochastic perturbation terms are jointly Gaussian random processes:

$$\begin{bmatrix}\chi(\vec{\rho},\vec{\rho}\,')\\ \phi(\vec{\rho},\vec{\rho}\,')\end{bmatrix} = \mathcal{N}\left(\begin{bmatrix}\mu_\chi\\ \mu_\phi\end{bmatrix},\begin{bmatrix}C_\chi(\vec{\rho},\vec{\rho}\,') & C_{\chi,\phi}(\vec{\rho},\vec{\rho}\,')\\ C_{\chi,\phi}(\vec{\rho},\vec{\rho}\,') & C_\phi(\vec{\rho},\vec{\rho}\,')\end{bmatrix}\right) \quad (2.25)$$

where μ_χ and μ_ϕ are the log-amplitude mean and phase mean, respectively. C_χ is the log-amplitude autocovariance, C_ϕ is the phase autocovariance, and $C_{\chi,\phi}$ is the cross covariance between the log-amplitude and phase. The quantities are defined as [53, 32]:

$$\begin{aligned}
\mu_\chi &= \langle\chi(\vec{\rho},\vec{\rho}\,')\rangle\\
\mu_\phi &= \langle\phi(\vec{\rho},\vec{\rho}\,')\rangle\\
C_\chi(\vec{\rho},\vec{\rho}\,') &= \langle[\chi(\vec{\rho}_1+\vec{\rho},\vec{\rho}_1'+\vec{\rho}\,') - \mu_\chi]\,[\chi(\vec{\rho}_1,\vec{\rho}_1') - \mu_\chi]\rangle\\
C_\phi(\vec{\rho},\vec{\rho}\,') &= \langle[\phi(\vec{\rho}_1+\vec{\rho},\vec{\rho}_1'+\vec{\rho}\,') - \mu_\phi]\,[\phi(\vec{\rho}_1,\vec{\rho}_1') - \mu_\phi]\rangle\\
C_{\chi,\phi}(\vec{\rho},\vec{\rho}\,') &= \langle[\chi(\vec{\rho}_1+\vec{\rho},\vec{\rho}_1'+\vec{\rho}\,') - \mu_\chi]\,[\phi(\vec{\rho}_1,\vec{\rho}_1') - \mu_\phi]\rangle
\end{aligned} \quad (2.26)$$

where $\vec{\rho}_1$ is a vector in the transmit plane, $\vec{\rho}_1{}'$ is a vector in the receive plane, and $\langle\cdot\rangle$ is the ensemble average over all atmospheric states. Within the weak perturbation regime, the two-source spherical wave auto and cross covariances can be expressed as [46, 27]:

$$\begin{aligned}
C_\chi(\vec{\rho},\vec{\rho}\,') &= 4\pi^2k^2\int_0^L\int_0^\infty uC_n^2(z)\Phi_n(u)J_0\left(\frac{u|\vec{\rho}\,'z+\vec{\rho}(L-z)|}{L}\right)\sin^2\left[\frac{u^2z(L-z)}{2kL}\right]dzdu\\
C_\phi(\vec{\rho},\vec{\rho}\,') &= 4\pi^2k^2\int_0^L\int_0^\infty uC_n^2(z)\Phi_n(u)J_0\left(\frac{u|\vec{\rho}\,'z+\vec{\rho}(L-z)|}{L}\right)\cos^2\left[\frac{u^2z(L-z)}{2kL}\right]dzdu\\
C_{\chi,\phi}(\vec{\rho},\vec{\rho}\,') &= 2\pi^2k^2\int_0^L\int_0^\infty uC_n^2(z)\Phi_n(u)J_0\left(\frac{u|\vec{\rho}\,'z+\vec{\rho}(L-z)|}{L}\right)\sin\left[\frac{u^2z(L-z)}{kL}\right]dzdu
\end{aligned} \tag{2.27}$$

where $J_0(\cdot)$ is a Bessel function of the first kind of order zero and $\Phi_n(\cdot)$ is the refractive index spatial frequency spectrum. And by convention, $\sigma_\chi^2 = C_\chi(\vec{0},\vec{0})$ is the log-amplitude variance and $\sigma_\phi^2 = C_\phi(\vec{0},\vec{0})$ is the phase variance. Evaluating the two-source spherical wave autocovariance at $\vec{\rho} = \vec{\rho}\,' = \vec{0}$ over a horizontal path through the clear atmosphere, the log-amplitude variance is:

$$\sigma_\chi^2 = \min\left\{0.124k^{7/6}C_n^2L^{11/6}, 0.5\right\} \tag{2.28}$$

The variance saturates at approximately 0.5. When the log-amplitude fluctuations are this high, the turbulence is in the strong fluctuation regime where the applicability of the log-normal model becomes questionable. This is because the assumptions used to derive the log-amplitude fluctuations are not strictly valid in the strong fluctuation regime [1].

Figure 2-3 shows the log-amplitude variance as a function of horizontal path length for various turbulence strengths. Without loss of generality for systems studied in this thesis, the phase standard variation is very large with respect to two radians:

$$\sigma_\phi \gg 2\pi \tag{2.29}$$

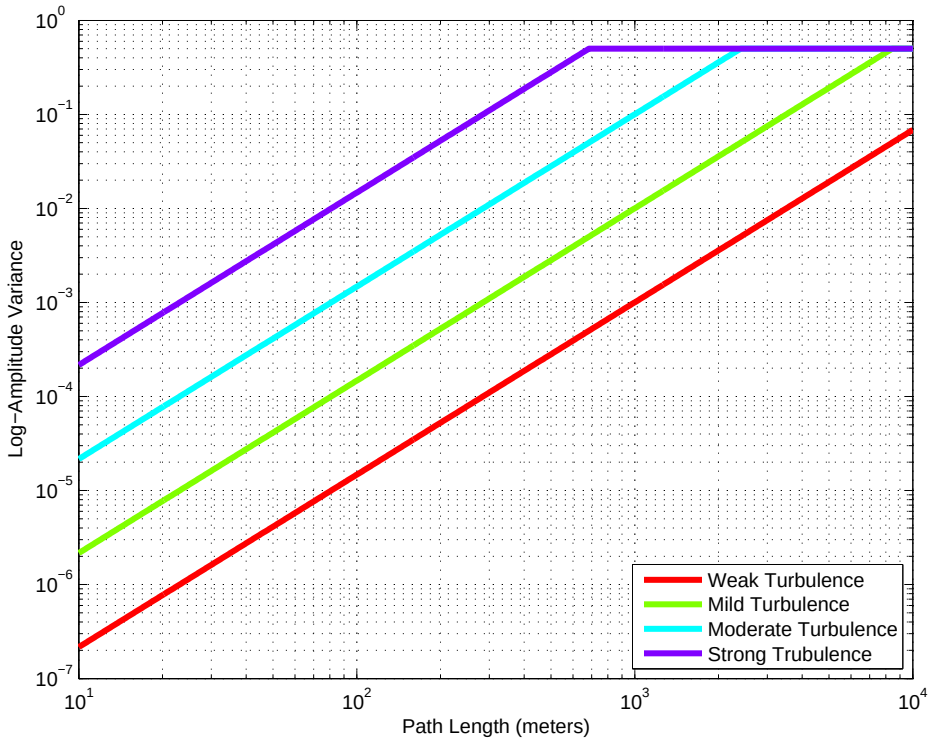

Figure 2-3: Log-amplitude variance, σ_χ^2, over a horizontal path through the clear atmosphere for $\lambda = 10^{-6}$ m. The structure constant for the various turbulence strengths are defined in Table 2.1.

Conservation of energy implies [17]: $\mu_\chi = -\sigma_\chi^2$. Figure 2-4 shows the joint probability density function (pdf) of the real and imaginary part of the multiplicative perturbation $\exp(\chi + \phi)$ for $\sigma_\chi^2 = 0.4$. Notice that the pdf is zero mean, circularly symmetric.

It is the structure function of the turbulence, not the covariance, that influences the performance of communication systems [17]. The structure functions are defined as [27]:

$$\begin{aligned} D_\chi(\vec{\rho}, \vec{\rho}\,') &= 2\left[C_\chi(0,0) - C_\chi(\vec{\rho}, \vec{\rho}\,')\right] \\ D_\phi(\vec{\rho}, \vec{\rho}\,') &= 2\left[C_\phi(0,0) - C_\phi(\vec{\rho}, \vec{\rho}\,')\right] \\ D_{\chi,\phi}(\vec{\rho}_{\chi,\phi}, \vec{\rho}\,') &= 2\left[C_{\chi,\phi}(0,0) - C_{\chi,\phi}(\vec{\rho}, \vec{\rho}\,')\right] \end{aligned} \tag{2.30}$$

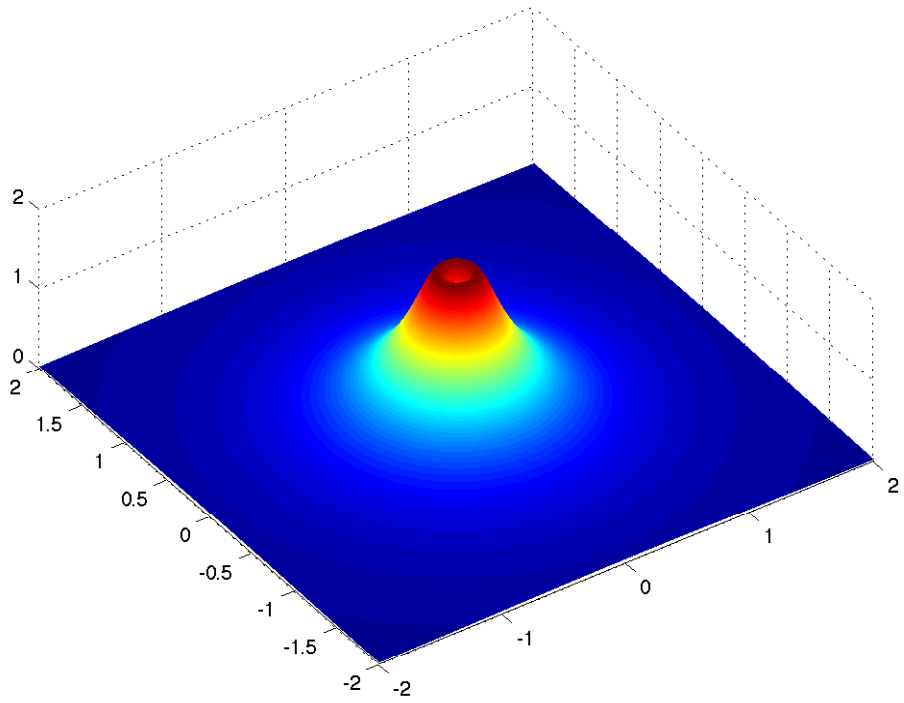

Figure 2-4: Sample probability density function of multiplicative perturbation $\exp(\chi + \phi)$ for $\sigma_\chi^2 = 0.4$.

The two-source wave functions are then given by [27]:

$$
\begin{aligned}
D_\chi(\vec{\rho},\vec{\rho}\,') &= 8\pi^2 k^2 \int_0^L \int_0^\infty uC_n^2(z)\Phi_n(u)\left[1 - J_0\left(\frac{u|\vec{\rho}\,'z + \vec{\rho}(L-z)|}{L}\right)\right]\sin^2\left[\frac{u^2 z(L-z)}{2kL}\right] dzdu \\
D_\phi(\vec{\rho},\vec{\rho}\,') &= 8\pi^2 k^2 \int_0^L \int_0^\infty uC_n^2(z)\Phi_n(u)\left[1 - J_0\left(\frac{u|\vec{\rho}\,'z + \vec{\rho}(L-z)|}{L}\right)\right]\cos^2\left[\frac{u^2 z(L-z)}{2kL}\right] dzdu \\
D_{\chi,\phi}(\vec{\rho},\vec{\rho}\,') &= 4\pi^2 k^2 \int_0^L \int_0^\infty uC_n^2(z)\Phi_n(u)\left[1 - J_0\left(\frac{u|\vec{\rho}\,'z + \vec{\rho}(L-z)|}{L}\right)\right]\sin\left[\frac{u^2 z(L-z)}{kL}\right] dzdu \\
D(\vec{\rho},\vec{\rho}\,') &= 8\pi^2 k^2 \int_0^L \int_0^\infty uC_n^2(z)\Phi_n(u)\left[1 - J_0\left(\frac{u|\vec{\rho}\,'z + \vec{\rho}(L-z)|}{L}\right)\right] dzdu
\end{aligned}
\tag{2.31}
$$

where we have defined the two-source spherical-wave wave structure function as $D(\vec{\rho},\vec{\rho}\,') = D_\chi(\vec{\rho},\vec{\rho}\,') + D_\phi(\vec{\rho},\vec{\rho}\,')$. For the special case where $\vec{\rho} = 0$ and fixed structure

constant along the propagation path:

$$D(0,\vec{\rho}\,') = 1.09k^2 LC_n^2|\vec{\rho}\,'|^{5/3} \tag{2.32}$$

If however, the structure constant varies along the propagation path, the two-source spherical-wave wave structure function is [46]:

$$D(\vec{\rho},\vec{\rho}\,') = 2.91k^2 \int_0^L C_n^2(z)\left[\frac{|\vec{\rho}\,'z + \vec{\rho}(L-z)|}{L}\right]^{5/3} dz \tag{2.33}$$

For any practical communication system, the phase variance is much larger than 2π implying that the Green's function statistical moments are [46]:

$$\mathbb{E}\left[h(\vec{\rho},\vec{\rho}\,')\right] \approx 0 \tag{2.34}$$

$$\mathbb{E}\left[h(\vec{\rho}+\vec{\rho}_1,\vec{\rho}\,'+\vec{\rho}_1')h(\vec{\rho},\vec{\rho}\,')\right] \approx 0 \tag{2.35}$$

where $h(\vec{\rho},\rho\,')$ is the Green's function. This implies that, for any arbitrary input fields, the output field statistical moments are approximately:

$$\mathbb{E}\left[U_o(\vec{\rho}\,')\right] \approx 0 \tag{2.36}$$

$$\mathbb{E}\left[U_o(\vec{\rho}_1')U_o(\vec{\rho}_2')\right] \approx 0 \tag{2.37}$$

By the extended Huygens-Fresnel principle, the mutual coherence function for an arbitrary input field is then given by [46]:

$$\mathbb{E}\left[U_o(\vec{\rho}_1')U_o^\dagger(\vec{\rho}_2')\right] = \int\int U_i\left(\vec{\rho}_1\right) U_i^\dagger\left(\vec{\rho}_2\right) \mathbb{E}\left[h(\vec{\rho}_1,\vec{\rho}_1')h^\dagger(\vec{\rho}_2,\vec{\rho}_2')\right] d\vec{\rho}_1 d\vec{\rho}_2 \tag{2.38}$$

where $(\cdot)^\dagger$ is the conjugate and the field mutual coherence function, $\mathbb{E}\left[h(\vec{\rho}_1,\vec{\rho}_1')h^\dagger(\vec{\rho}_2,\vec{\rho}_2')\right]$, is given by:

$$\begin{aligned}\mathbb{E}\left[h(\vec{\rho}_1,\vec{\rho}_1')h^\dagger(\vec{\rho}_2,\vec{\rho}_2')\right] &= \left(\frac{1}{\lambda L}\right)^2 \mathbb{E}\left[e^{\chi(\vec{\rho}_1,\vec{\rho}_1')+\chi(\vec{\rho}_2,\vec{\rho}_2')+j\phi(\vec{\rho}_1,\vec{\rho}_1')-j\phi(\vec{\rho}_2,\vec{\rho}_2')}\right] e^{\frac{jk}{2L}\left(|\vec{\rho}_1'-\vec{\rho}_1|^2-|\vec{\rho}_2'-\vec{\rho}_2|^2\right)} \\ &= \left(\frac{1}{\lambda L}\right)^2 e^{\frac{jk}{2L}\left(|\vec{\rho}_1'-\vec{\rho}_1|^2-|\vec{\rho}_2'-\vec{\rho}_2|^2\right)-\frac{1}{2}D(\vec{\rho}_1-\vec{\rho}_2,\vec{\rho}_1'-\vec{\rho}_2')}\end{aligned} \tag{2.39}$$

For a spherical wave launched in the transmit plane, the distance required for two points in the receiver plane to be approximately uncorrelated is given by the spherical wave atmospheric coherence length [46]:

$$\rho_0' = \left[2.91k^2\int_0^L C_n^2(z)(z/L)^{5/3}dz\right]^{-3/5} \tag{2.40}$$

Similarly, the atmospheric coherence length in the transmit plane is given by [46]:

$$\rho_0 = \left[2.91k^2\int_0^L C_n^2(z)(1-z/L)^{5/3}dz\right]^{-3/5} \tag{2.41}$$

If the structure constant is uniform along the propagation path, the coherence length is the same in both the transmit and receive plane:

$$\rho_0 = \rho_0' = \left(1.09k^2C_n^2L\right)^{-3/5}$$

Figure 2-5 shows the spatial coherence length for the clear atmosphere at various turbulence strengths.

2.4 Coherent Detection

Optical coherent detection uses a local oscillator to mitigate limitations imposed by avalanche photodiode (APD) excess noise, background noise, and amplifier noise [6]. A typical coherent detection receiver is shown in figure 2-6. In the figure, U_o is the

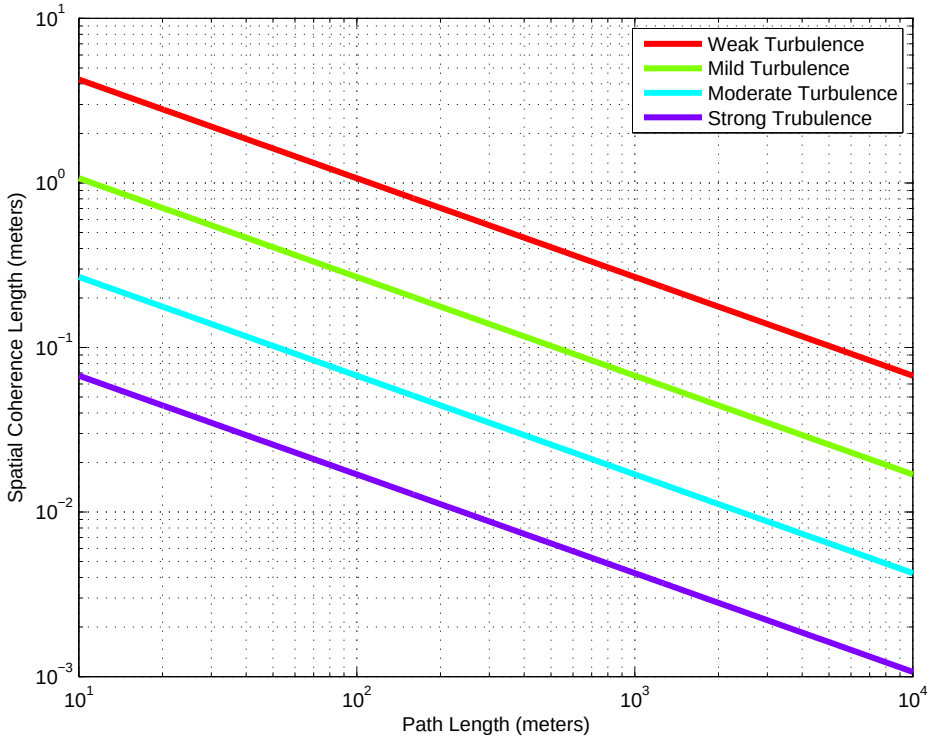

Figure 2-5: Spatial coherence length for the clear atmosphere at various turbulence strengths for $\lambda = 10^{-6}$ m. The structure constant for the various turbulence strengths are defined in Table 2.1.

received field collected over a detector area A_{rx} and U_{lo} is the local oscillator. The two fields are optically added with a mirror and then measured with a square-law detector. Finally, the signal is bandpass filtered and an estimate of the amplitude and phase of the incoming field is given in $y(t)$. Not shown in the figure is the background noise field.

At the detector plane, the optical field is given by:

$$u_D(\vec{\rho}', t) = u_o(\vec{\rho}', t) + u_b(\vec{\rho}', t) + u_{lo}(\vec{\rho}', t) \tag{2.42}$$

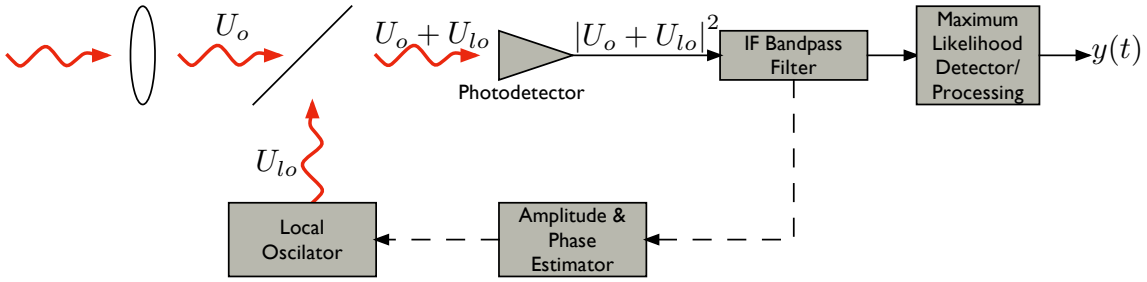

Figure 2-6: Pictorial representation of heterodyne detection. In the figure, we neglect energy lost by the splitter.

The detector produces a conditional Poisson process, with average count rate of:

$$\begin{aligned} n(t) &= \frac{\eta}{hf}\int_{R_{tx}} |u_D(\vec{\rho}',t)|^2\, d\vec{\rho}' \\ &= \frac{\eta}{hf}\int_{R_{tx}} |u_o(\vec{\rho}',t) + u_b(\vec{\rho}',t) + u_{lo}(\vec{\rho}',t)|^2\, d\vec{\rho}' \\ &= \frac{\eta}{hf}\int_{R_{tx}} |u_o(\vec{\rho}',t) + u_b(\vec{\rho}',t)|^2\, d\vec{\rho}' + \frac{\eta}{hf}\int_{R_{tx}} |u_{lo}(\vec{\rho}',t)|^2\, d\vec{\rho}' \\ &\qquad + \frac{2\eta}{hf}\Re\left\{\int_{R_{tx}} (u_o(\vec{\rho}',t) + u_b(\vec{\rho}',t))u_{lo}^{\dagger}(\vec{\rho}',t)d\vec{\rho}'\right\} \end{aligned} \tag{2.43}$$

where η is the detector quantum efficiency, h is Planck's constant, and f is field frequency. The last term in the last line is the information bearing beat term $n_{ib}(t)$. We assume the local oscillator frequency is chosen such that the intensity terms can be filtered out completely while the beat term is left unperturbed. After such filtering, the average count rate is then $n(t) = n_{ib}(t)$. If we assume the information bearing beat term varies much faster than the atmospheric coherence time, we can write the received field as the product of a time varying complex envelope $s(t) = a_s(t)e^{j\theta_s(t)}$ and spatially varying field $U_o(\vec{\rho}')$:

$$u_o(\vec{\rho}',t) = s(t)U_o(\vec{\rho}')e^{j\omega_o t} \tag{2.44}$$

where $\omega_o = 2\pi f$ is the angular frequency of the incoming wave. Similarly, we write the local oscillator as an time invariant amplitude term a_{lo} and a spatially varying field $U_{lo}(\vec{\rho}')$:

$$u_{lo}(\vec{\rho}',t) = a_{lo}U_{lo}(\vec{\rho}')e^{j\omega_{lo}t} \tag{2.45}$$

where ω_{lo} is the angular frequency of the local oscillator. The beat term is then:

$$\begin{aligned} n_{ib}(t) &= \frac{2\eta}{hf}\Re\left\{\int_{R_{tx}}(u_o(\vec{\rho}',t)+u_b(\vec{\rho}',t))u_{lo}^{\dagger}(\vec{\rho}',t)d\vec{\rho}'\right\} \\ &= \frac{2\eta}{hf}\Re\left\{\int_{R_{tx}}s(t)U_o(\vec{\rho}')e^{j\omega_o t}a_{lo}U_{lo}^{\dagger}(\vec{\rho}')e^{-j\omega_{lo}t}d\vec{\rho}'+\int_{R_{tx}}u_b(\vec{\rho}',t)a_{lo}U_{lo}^{\dagger}(\vec{\rho}')e^{-j\omega_{lo}t}d\vec{\rho}'\right\} \end{aligned} \tag{2.46}$$

Assuming the local oscillator is spatially matched to the propagated field, $U_o(\vec{\rho}') = U_{lo}(\vec{\rho}')$, the beat term simplifies to:

$$\begin{aligned} n_{ib}(t) &= \frac{2\eta}{hf}a_s(t)a_{lo}\cos((\omega_{lo}-\omega_o)t-\theta_s(t))\int_{R_{tx}}U_o(\vec{\rho}')U_o^{\dagger}(\vec{\rho}')d\vec{\rho}' \\ &\quad + \frac{2\eta a_{lo}}{hf}\Re\left\{e^{-j\omega_{lo}t}\int_{R_{tx}}u_b(\vec{\rho}',t)U_{lo}^{\dagger}(\vec{\rho}')d\vec{\rho}'\right\} \\ &= \frac{2\eta}{hf}a_s(t)a_{lo}\cos((\omega_{lo}-\omega_o)t-\theta_s(t))P_o+\frac{2\eta a_{lo}}{hf}b(t) \end{aligned} \tag{2.47}$$

where we define the output field power as:

$$P_o = \int_{R_{tx}}U_o(\vec{\rho}')U_o^{\dagger}(\vec{\rho}')d\vec{\rho}' \tag{2.48}$$

and the background noise process as:

$$b(t) = \Re\left\{e^{-j\omega_{lo}t}\int_{R_{tx}}u_b(\vec{\rho}',t)U_{lo}^{\dagger}(\vec{\rho}')d\vec{\rho}'\right\} \tag{2.49}$$

In [12], the background noise process spectral level is $A_{rx}N_o/4$ over the optical bandwidth centered at $(\omega_o - \omega_{lo})$. For blackbody background radiation of temperature T, the noise spectral level is:

$$N_o = \frac{hf}{e^{hf/\kappa T}-1} \tag{2.50}$$

where κ is the Boltzmann constant. Including the effects of shot and thermal noise but excluding the effects of dark current, we arrive at the signal to noise ratio (SNR):

$$\text{SNR} = \frac{2(q\eta/hf)^2 P_{lo}P_o}{[(q^2\eta/hf)P_{lo}+(2q\eta/hf)^2P_{lo}(N_o/4)+N_{oc}]2B_c} \tag{2.51}$$

where P_{lo} is the power in the local oscillator, q is the charge of an electron, B_c is the optical carrier modulated bandwidth and N_{oc} is the thermal noise level given by [12]:

$$N_{oc} = \frac{2\kappa T}{R_L} \tag{2.52}$$

where T in this case is the temperature of the load resistor and R_L is the local equivalent resistance. Within a bit period T_b we define the SNR as:

$$\text{SNR} = \frac{2(q\eta/hf)^2 P_{lo} P_o T_b}{[(q^2\eta/hf)P_{lo} + (q\eta/hf)^2 P_{lo} N_o + N_{oc}]} \tag{2.53}$$

2.5 Problem Formulation

We assume transmitters are arranged in the $\vec{\rho}$-plane and receivers are arranged in $\vec{\rho}\,'$-plane. The $\vec{\rho}$- and $\vec{\rho}\,'$-planes are assumed to be parallel and separated by a length of L, as shown in Fig. 2-7. The vector from the $\vec{\rho}$-plane origin to transmitter k is denoted $\vec{\rho}_{\mathsf{k}}$. Similarly, the distance from the $\vec{\rho}\,'$-plane origin to receiver j is denoted $\vec{\rho}\,'_{\mathsf{j}}$.

We assume a coherent monochromatic scalar field of wavelength λ is transmitted from n_{tx} apertures in the $\vec{\rho}$-plane. Each transmit aperture is denoted by the region $R_{tx,\mathsf{k}}$ in the $\vec{\rho}$-plane. The union of all transmitter regions is denoted:

$$R_{tx} = \cup_{\mathsf{k}=1}^{n_{tx}} R_{tx,\mathsf{k}} \tag{2.54}$$

The area of the k^{th} region, $R_{tx,\mathsf{k}}$, is denoted $A_{tx,\mathsf{k}}$ while the area of R_{tx}, is denoted $A_{tx}^{\cup}$.

The field propagates L meters through a linear, isotropic, statistically homogeneous medium to the $\vec{\rho}\,'$-plane where it is detected with n_{rx} apertures. Each receive aperture is denoted by the region $R_{rx,\mathsf{j}}$ in the $\vec{\rho}\,'$-plane. The union of all receiver regions is denoted:

$$R_{rx} = \cup_{\mathsf{j}=1}^{n_{rx}} R_{rx,\mathsf{j}} \tag{2.55}$$

The area of the j^{th} region, $R_{rx,\mathsf{j}}$, is denoted $A_{rx,\mathsf{j}}/n_{rx}$ while the area of R_{rx}, is denoted $A_{rx}^{\cup}$. The area of the j^{th} region is normalized by n_{rx} so the receive power remains constant as the number of receive apertures is increased.

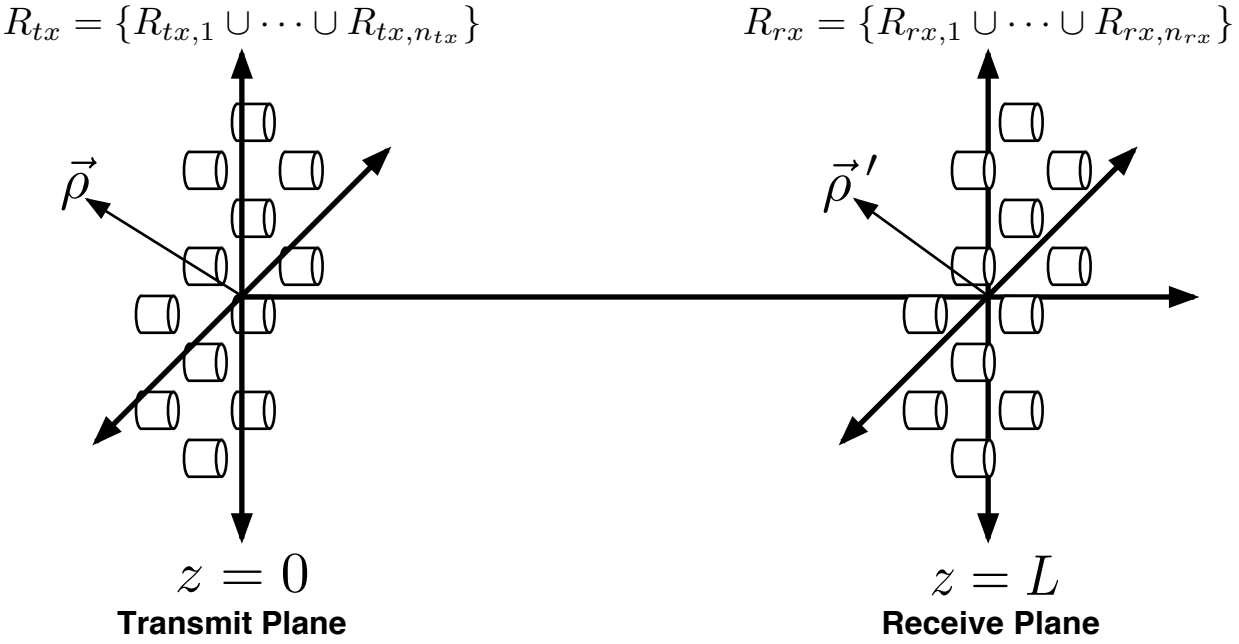

Figure 2-7: Sparse aperture system geometry: A field is transmitted from n_{tx} transmitters in the ρ-plane to n_{rx} receivers the ρ'-plane.

Figure 2-8 shows a drawing of the optical communication system that we are describing. A single laser source, with optical power P_{laser}, couples into a fiber. The power is divided among n_{tx} channels using a variable optical power splitter. A phase modulator adjusts the phase of each channel before optical power is coupled into the atmosphere. After propagating through the turbulence, the optical wave is coherently detected and combined at the receive plane.

As derived in Section 2.3.2, the received field U_o is related to the transmitted field U_i by the Green's function:

$$\begin{aligned} U_o(\vec{\rho}\,') &= \frac{e^{jkL}}{j\lambda L}\int_{R_{tx}} U_i(\vec{\rho}\,)\, e^{j\frac{k}{2L}|\vec{\rho}\,'-\vec{\rho}\,|^2} \times e^{\chi(\vec{\rho},\vec{\rho}\,')+j\phi(\vec{\rho},\vec{\rho}\,')} d\vec{\rho} \\ &= \sum_{\mathsf{k}=1}^{n_{tx}} \frac{e^{jkL}}{j\lambda L}\int_{R_{tx,\mathsf{k}}} U_i(\vec{\rho}\,)\, e^{j\frac{k}{2L}|\vec{\rho}\,'-\vec{\rho}\,|^2} \times e^{\chi(\vec{\rho},\vec{\rho}\,')+j\phi(\vec{\rho},\vec{\rho}\,')} d\vec{\rho} \end{aligned} \tag{2.56}$$

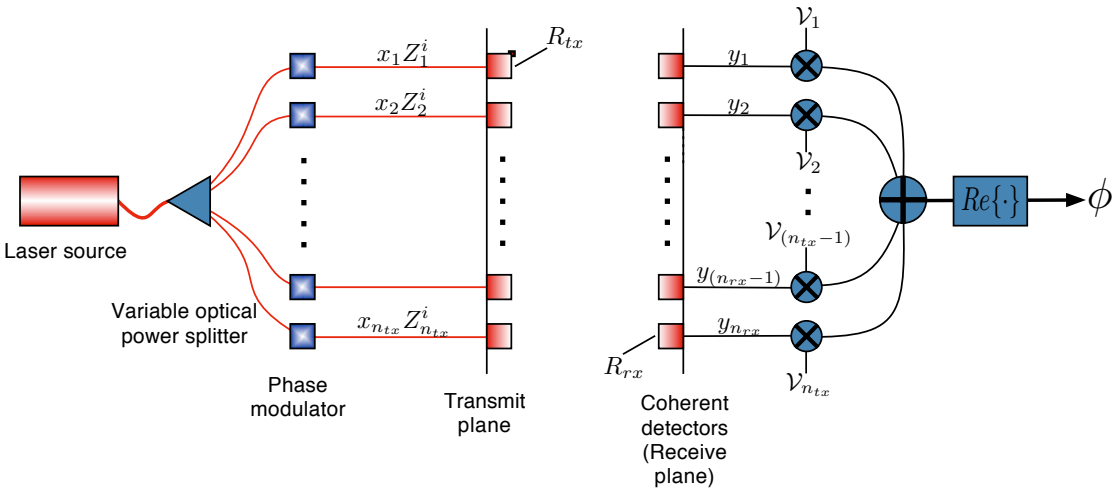

Figure 2-8: Sparse aperture system geometry: A field is transmitted from n_{tx} transmitters in the ρ-plane to n_{rx} receivers the ρ'-plane.

We now further assume that the transmit field is constant over each transmit aperture, with only amplitude and phase varying from one transmitter to the next. This constant field assumption is made for specificity, other transmit field distributions which may not be constant over each transmit aperture are equally valid. Mathematically, this assumption is stated as follows:

$$U_i(\vec{\rho}) = \sum_{\mathsf{k}=1}^{n_{tx}} x_{\mathsf{k}} Z_{\mathsf{k}}^i(\vec{\rho}) \tag{2.57}$$

where $x_{\mathsf{k}} \in \mathbb{C}$ represents the amplitude and phase at the k^{th} transmitter and $Z_{\mathsf{k}}^i(\vec{\rho})$ is a spatially constant field with non-zero values only within $R_{tx,\mathsf{k}}$:

$$Z_{\mathsf{k}}^i(\vec{\rho}) = \begin{cases} \sqrt{\frac{P_{\text{laser}}}{A_{tx}}} & \vec{\rho} \in R_{tx,\mathsf{k}} \\ 0 & \vec{\rho} \notin R_{tx,\mathsf{k}} \end{cases} \tag{2.58}$$

where we have further assumed that each transmit aperture is the same size (i.e., $A_{tx} = A_{tx,\mathsf{k}}, \forall \mathsf{k} = 1 \ldots n_{tx}$ and $A_{rx} = A_{rx,\mathsf{j}}, \forall \mathsf{j} = 1 \ldots n_{rx}$), although the transmit apertures may be a different size from the receiver apertures. The amplitude and

phase can be set arbitrarily provided that the power constraint is met:

$$\sum_{\mathsf{k}=1}^{n_{tx}} \mathbb{E}\left[|x_{\mathsf{k}}|^2\right] = 1 \tag{2.59}$$

where the expectation implies an average power constraint. This normalization ensures that the transmitted optical power remains constant P_{laser} as the number of transmitters is increased. We can see this by examining the transmitted field power:

$$\begin{aligned}
\mathbb{E}\left[\int_{R_{tx}} |U_i(\vec{\rho})|^2 \, d\vec{\rho}\right] &= \mathbb{E}\left[\int_{R_{tx}} \left|\sum_{\mathsf{k}=1}^{n_{tx}} x_{\mathsf{k}} Z_{\mathsf{k}}^i(\vec{\rho})\right|^2 d\vec{\rho}\right] \\
&= \sum_{\mathsf{k}=1}^{n_{tx}} \mathbb{E}\left[|x_{\mathsf{k}}|^2\right] \int_{R_{tx,\mathsf{k}}} \left|Z_{\mathsf{k}}^i(\vec{\rho})\right|^2 d\vec{\rho} \\
&= \sum_{\mathsf{k}=1}^{n_{tx}} \mathbb{E}\left[|x_{\mathsf{k}}|^2\right] P_{\text{laser}} \\
&= P_{\text{laser}}
\end{aligned} \tag{2.60}$$

Combining the propagation equation, equation (2.56), with the constraints gives:

$$\begin{aligned}
U_o\left(\vec{\rho}\,'\right) &= \frac{e^{jkL}}{j\lambda L} \int_{R_{tx}} \left(\sum_{\mathsf{k}=1}^{n_{tx}} x_{\mathsf{k}} Z_{\mathsf{k}}^i(\vec{\rho})\right) e^{j\frac{k}{2L}|\vec{\rho}\,'-\vec{\rho}\,|^2} \times e^{\chi(\vec{\rho},\vec{\rho}\,')+j\phi(\vec{\rho},\vec{\rho}\,')} d\vec{\rho} \\
&= \frac{e^{jkL}}{j\lambda L} \sqrt{\frac{P_{\text{laser}}}{A_{tx}}} \sum_{\mathsf{k}=1}^{n_{tx}} x_{\mathsf{k}} \int_{R_{tx,\mathsf{k}}} e^{j\frac{k}{2L}|\vec{\rho}\,'-\vec{\rho}\,|^2} \times e^{\chi(\vec{\rho},\vec{\rho}\,')+j\phi(\vec{\rho},\vec{\rho}\,')} d\vec{\rho}
\end{aligned} \tag{2.61}$$

If we further assume that each transmitter is smaller than a coherence length in the transmit plane and each receiver is smaller than a coherence length in the receive plane, we can simplify to:

$$Z_{\mathsf{j}}^o\left(\vec{\rho}\,'\right) = \frac{e^{jkL}}{j\lambda L} \sqrt{\frac{P_{\text{laser}}}{A_{tx}}} \sum_{\mathsf{k}=1}^{n_{tx}} x_{\mathsf{k}} e^{\chi(\vec{\rho}_{\mathsf{k}},\vec{\rho}_{\mathsf{j}}\,')+j\phi(\vec{\rho}_{\mathsf{k}},\vec{\rho}_{\mathsf{j}}\,')} \int_{R_{tx,\mathsf{k}}} e^{j\frac{k}{2L}|\vec{\rho}\,'-\vec{\rho}\,|^2} d\vec{\rho} \tag{2.62}$$

where $Z_{\mathsf{j}}^{o}\left(\vec{\rho}\,'\right), \forall \mathsf{j} = 1 \ldots n_{rx}$ is the field in the region of the j^{th} receiver.

$$Z_{\mathsf{j}}^{o}(\vec{\rho}\,') = \begin{cases} U_o(\vec{\rho}\,'), & \vec{\rho}\,' \in R_{rx,\mathsf{j}} \\ 0 & \vec{\rho}\,' \notin R_{rx,\mathsf{j}} \end{cases} \tag{2.63}$$

Assuming Fraunhofer diffraction, $\mathsf{w}_{tx} \ll \sqrt{L\lambda}$, where w_{tx} is the radius of a single transmitter, we find the received field:

$$Z_{\mathsf{j}}^{o}\left(\vec{\rho}\,'\right) = \frac{e^{jkL}}{j\lambda L}\sqrt{\frac{P_{\text{laser}}}{A_{tx}}}\sum_{\mathsf{k}=1}^{n_{tx}} x_{\mathsf{k}} e^{\chi(\vec{\rho}_{\mathsf{k}},\vec{\rho}_{\mathsf{j}}\,')+j\phi(\vec{\rho}_{\mathsf{k}},\vec{\rho}_{\mathsf{j}}\,')} A_{tx} e^{\frac{jkr_{\mathsf{jk}}^2}{2L}} \left[\frac{2J_1(k\mathsf{w}_{tx}|\vec{\rho}\,' - \vec{\rho}_{\mathsf{k}}|/L)}{k\mathsf{w}_{tx}|\vec{\rho}\,' - \vec{\rho}_{\mathsf{k}}|/L}\right] \tag{2.64}$$

The Fraunhofer diffraction assumption is not necessary, but we use it here for simplicity. If we further assume that the receive field is constant over a single receive aperture, which is true if $\mathsf{w}_{rx} \ll L/k\mathsf{w}_{tx}$, where w_{rx} is the radius of a single receiver, then:

$$Z_{\mathsf{j}}^{o}\left(\vec{\rho}\,'\right) = \frac{e^{jkL}}{j\lambda L}\sqrt{\frac{P_{\text{laser}}}{A_{tx}}}\sum_{\mathsf{k}=1}^{n_{tx}} x_{\mathsf{k}} e^{\chi(\vec{\rho}_{\mathsf{k}},\vec{\rho}_{\mathsf{j}}\,')+j\phi(\vec{\rho}_{\mathsf{k}},\vec{\rho}_{\mathsf{j}}\,')} A_{tx} e^{\frac{jkr_{\mathsf{jk}}^2}{2L}} \left[\frac{2J_1(k\mathsf{w}_{tx}|\vec{\rho}_{\mathsf{j}}\,' - \vec{\rho}_{\mathsf{k}}|/L)}{k\mathsf{w}_{tx}|\vec{\rho}_{\mathsf{j}}\,' - \vec{\rho}_{\mathsf{k}}|/L}\right] \tag{2.65}$$

If the field is not constant over a single receive aperture, we simply split up the aperture in multiple apertures each with an approximately constant field. This is tantamount to approximating a continuous function as piecewise constant. However, we will usually assume the minimum distance between each transmitter is at least a coherence length, far enough apart so that the statistics of all $n_{tx}n_{rx}$ links are uncorrelated. We refer to this geometry as a *sparse aperture system*. Finally, if we assume all receivers are uniformly illuminated on average, $\max_{\mathsf{j},\mathsf{k}} |\vec{\rho}_{\mathsf{j}}\,' - \vec{\rho}_{\mathsf{k}}| < L/k\mathsf{w}_{tx}$, the equation describing the output field simplifies to:

$$Z_{\mathsf{j}}^{o} = \sqrt{\frac{A_{tx}P_{\text{laser}}}{(\lambda L)^2}}\sum_{\mathsf{k}=1}^{n_{tx}} x_{\mathsf{k}} e^{\chi(\vec{\rho}_{\mathsf{k}},\vec{\rho}_{\mathsf{j}}\,')+j\phi(\vec{\rho}_{\mathsf{k}},\vec{\rho}_{\mathsf{j}}\,')} e^{\frac{jk|\vec{\rho}_{\mathsf{j}}\,' - \vec{\rho}_{\mathsf{k}}|^2}{2L}} e^{jkL+j\pi/2} \tag{2.66}$$

We assume $\sigma_\phi \gg 2\pi$ so that the phase probability distribution function is approximately uniform from zero to 2π, $\phi \sim U[0, 2\pi]$. This assumption implies that:

$$e^{\chi(\vec{\rho}_\mathsf{k},\vec{\rho}_\mathsf{j}')+j\phi(\vec{\rho}_\mathsf{k},\vec{\rho}_\mathsf{j}')} e^{\frac{jk|\vec{\rho}_\mathsf{j}'-\vec{\rho}_\mathsf{k}|^2}{2L}} e^{jkL+j\pi/2} \stackrel{d}{=} e^{\chi(\vec{\rho}_\mathsf{k},\vec{\rho}_\mathsf{j}')+j\phi(\vec{\rho}_\mathsf{k},\vec{\rho}_\mathsf{j}')} \tag{2.67}$$

where $\stackrel{d}{=}$ denotes equality in distribution. This simplifies the expression for the output field even further to:

$$Z_\mathsf{j}^o = \sqrt{\frac{A_{tx}P_{\text{laser}}}{(\lambda L)^2}} \sum_{\mathsf{k}=1}^{n_{tx}} x_\mathsf{k} e^{\chi(\vec{\rho}_\mathsf{k},\vec{\rho}_\mathsf{j}')+j\phi(\vec{\rho}_\mathsf{k},\vec{\rho}_\mathsf{j}')} \tag{2.68}$$

Finally, after each field Z_j^o is coherently detected as described in Section 2.4, the instantaneous estimated amplitude and phase of the received field, y_j, is given by:

$$y_\mathsf{j} = \sqrt{\frac{2(q\eta/hf)^2 P_{lo} P_{\text{laser}} A_{tx} A_{rx}}{[(q^2\eta/hf)P_{lo} + (2q\eta/hf)^2 P_{lo} N_o/4 + N_{oc}] 2B_c(\lambda L)^2 n_{rx}}} \sum_{\mathsf{k}=1}^{n_{tx}} x_\mathsf{k} e^{\chi(\vec{\rho}_\mathsf{k},\vec{\rho}_\mathsf{j}')+j\phi(\vec{\rho}_\mathsf{k},\vec{\rho}_\mathsf{j}')} + w_\mathsf{j} \tag{2.69}$$

where w_j, which represents background noise, shot noise, and thermal noise, is circularly complex Gaussian noise with unit variance. The area normalization, $1/n_{rx}$, ensures that the received optical power remains constant as the number of receivers is increased. Within a bit period T_b:

$$y_\mathsf{j} = \sqrt{\frac{2(q\eta/hf)^2 P_{lo} P_{\text{laser}} T_b A_{tx} A_{rx}}{[(q^2\eta/hf)P_{lo} + (q\eta/hf)^2 P_{lo} N_o + N_{oc}] (\lambda L)^2 n_{rx}}} \sum_{\mathsf{k}=1}^{n_{tx}} x_\mathsf{k} e^{\chi(\vec{\rho}_\mathsf{k},\vec{\rho}_\mathsf{j}')+j\phi(\vec{\rho}_\mathsf{k},\vec{\rho}_\mathsf{j}')} + w_\mathsf{j} \tag{2.70}$$

where we have assumed that the turbulence is approximately fixed over the period of a bit, $T_b \ll t_o$. Rewriting the previous equation in matrix notation, we have:

$$\vec{y} = \sqrt{\frac{\text{SNR}}{n_{rx}}} \mathbf{H}\vec{x} + \vec{w} \tag{2.71}$$

where $\vec{x} \in \mathbb{C}^{n_{tx}}$ is a vector representing the amplitude and phase of the transmitted field, $\vec{y} \in \mathbb{C}^{n_{rx}}$ is a vector representing amplitude and phase of the received field, $\text{SNR} \in \mathbb{R}$ is the signal-to-noise ratio for a single aperture transmitter (area A_{tx})

and a single-aperture heterodyne receiver (area A_{rx}) in the absence of turbulence when $|x_{\mathsf{k}}|^2 = 1$ for that transmitter, and $\vec{w} \in \mathbb{C}^{n_{tx}}$ represents independent identically distributed additive white circularly symmetric complex Gaussian noise with unit variance. The SNR is given by:

$$\text{SNR} = \frac{2(q\eta/hf)^2 P_{lo} P_{\text{laser}} T_b A_{tx} A_{rx}}{[(q^2\eta/hf)P_{lo} + (q\eta/hf)^2 P_{lo} N_o + N_{oc}](\lambda L)^2} \tag{2.72}$$

Finally, $\mathbf{H} \in \mathbb{C}^{n_{rx} \times n_{tx}}$ represents the turbulence effects on propagation. Entry h_{kj} of $\mathbf{H}$ is the complex-value coupling from the k^{th} transmit aperture to the j^{th} receive aperture:

$$\begin{aligned} \mathbf{H} &= \begin{bmatrix} | & | & & | \\ \vec{h}_1 & \vec{h}_2 & \cdots & \vec{h}_{n_{tx}} \\ | & | & & | \end{bmatrix} = \begin{bmatrix} h_{11} & \dots & h_{n_{tx}1} \\ \vdots & \ddots & \vdots \\ h_{1n_{rx}} & \dots & h_{n_{tx}n_{rx}} \end{bmatrix} \\ &= \begin{bmatrix} e^{\chi(\vec{\rho}_1, \vec{\rho}_1') + j\phi(\vec{\rho}_1, \vec{\rho}_1')} & \dots & e^{\chi(\vec{\rho}_{n_{tx}}, \vec{\rho}_1') + j\phi(\vec{\rho}_{n_{tx}}, \vec{\rho}_1')} \\ \vdots & \ddots & \vdots \\ e^{\chi(\vec{\rho}_1, \vec{\rho}_{n_{rx}}') + j\phi(\vec{\rho}_1, \vec{\rho}_{n_{rx}}')} & \dots & e^{\chi(\vec{\rho}_{n_{tx}}, \vec{\rho}_{n_{rx}}') + j\phi(\vec{\rho}_{n_{tx}}, \vec{\rho}_{n_{rx}}')} \end{bmatrix} \end{aligned} \tag{2.73}$$

Alternative Normalizations

The particular normalization that we have chosen (i.e., where the size of the individual transmit apertures does not depend on the number of transmit apertures) implies that the beam width at the receive plane is larger than the maximum extent of the convex hull of the receive apertures, as shown in figure 2-9. Systems operating in this regime exhibit relatively inefficient power transfer, because of the relatively large beam, but can employ less complex and less expensive tracking systems. This normalization is not symmetric because it treats transmit apertures and receive apertures differently. As a result, careful considerations must be taken to show reciprocity. There are other meaningful normalizations, depending on the constraints of the particular system. Consequently, we present a generalized normalization so that the appropriate

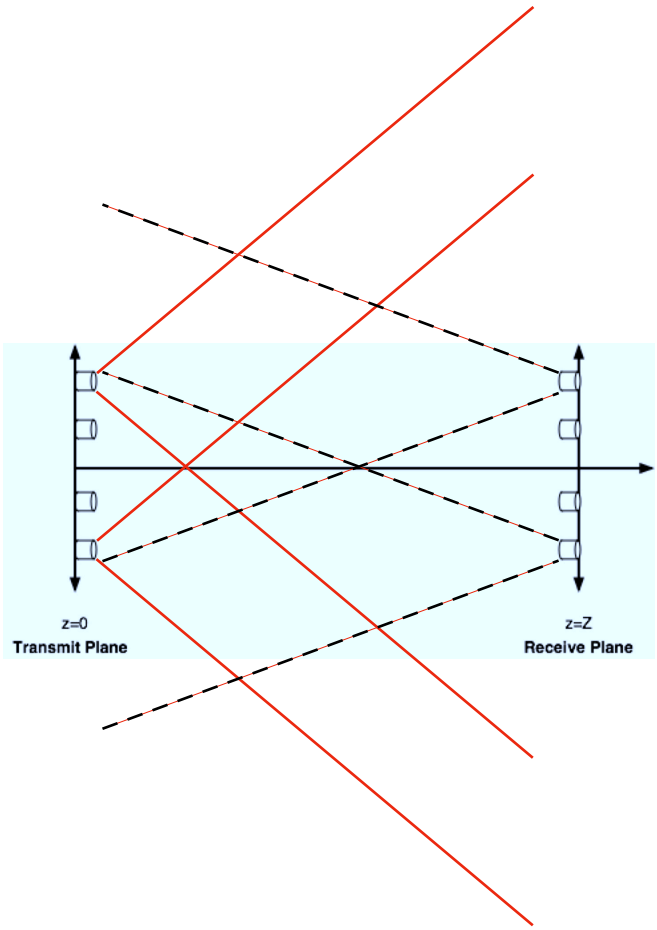

Figure 2-9: Normalization implied by the system model: $\vec{y} = \sqrt{\frac{\text{SNR}}{n_{rx}}}\mathbf{H}\vec{x} + \vec{w}$. The red lines pictorially represent the full width half maximum of a field emitted from a single transmit aperture. The dashed black lines pictorially represent the receiver field of view. Because of the relatively large beam in the receiver plane, this system has relatively inefficient power transfer, but can employ less complex and less expensive tracking systems.

normalization can be used for different systems with different constraints:

$$\vec{y} = \sqrt{\frac{\text{SNR}}{N}}\mathbf{H}\vec{x} + \vec{w} \tag{2.74}$$

where N can be any function of the number of transmit apertures and receive apertures. For systems operating in regimes where power transfer is very important, the beam width at the receive plane should be equal to the maximum extent of the convex hull of the receive apertures. As a result, if the number of transmitters is

increased then, by diffraction theory, the beam width of each transmitter must be increased. The corresponding normalization is $N = n_{tx}n_{rx}$. This normalization is symmetric because it treats transmit apertures and receive apertures the same. For

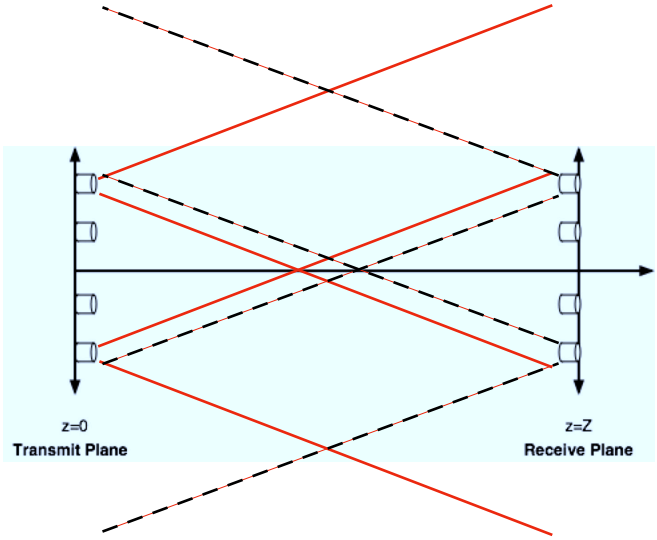

Figure 2-10: Normalization implied by the system model: $\vec{y} = \sqrt{\frac{\text{SNR}}{n_{tx}n_{rx}}}\mathbf{H}\vec{x} + \vec{w}$. The red lines pictorially represent the full width half maximum of a field emitted from a single transmit aperture. The dashed black lines pictorially represent the receiver field of view. Because of the relatively small beam in the receiver plane, this system has relatively efficient power transfer, but must employ more complex and expensive tracking systems.

a systems where the engineer does not have control of the diameter of the transmit and receive apertures (e.g., the engineer is restricted to using commercial off the shelf parts), a normalization of $N = 1$ is appropriate. Other normalizations could included the number of transmitters $N = n_{tx}$ or the number of independent channels $N = \min(n_{tx}, n_{rx})$.

In this thesis we normalize by the number of receive apertures $N = n_{rx}$. We see in the next chapter that this normalization provides a natural normalization for comparing sparse aperture systems *with* and *without* feedback. Put another way, we focus on the question: "What is the value of wavefront predistortion based on receiver to transmitter feedback?" Other questions, such as "How much diversity should a given system have?" or "Is it better to have more transmit apertures or more receive apertures?" require a different normalization. Because other comparisons should use

different normalizations, we provide corollaries for the generalized normalization of key theorems.

2.5.1 Problem Formulation, Atmospheric Dynamics

The model developed in the previous section describes the atmospheric channel at a particular instant. To study time dynamics of the turbulent channel, we must develop a model that describes the way the atmosphere evolves from one state to another. Specifically, to study the time dynamics of communication through turbulence, we must find the atmospheric temporal field autocovariance function $R_{hh}(t)$. We have [32, 53]:

$$\begin{aligned}\left\langle h\left(\vec{\rho}_1\vec{\rho}_1'\right)h^{\dagger}\left(\vec{\rho}_2,\vec{\rho}_2'\right)\right\rangle = \\ \frac{1}{(\lambda L)^2}\exp\left\{\frac{j\pi}{\lambda L}\left(\left|\vec{\rho}_1'-\vec{\rho}_1\right|^2-\left|\vec{\rho}_2'-\vec{\rho}_2\right|^2\right)-\right. \\ \left.\frac{1}{2}D\left(\vec{\rho}_1'-\vec{\rho}_2',\vec{\rho}_1-\vec{\rho}_2\right)\right\}\end{aligned} \tag{2.75}$$

where $\langle\cdot\rangle$ denotes averaging over the turbulence ensemble, $(\cdot)^{\dagger}$ is the conjugate transpose, and $D(\vec{\rho}',\vec{\rho})$ is the two-source spherical-wave structure function given by:

$$D(\vec{\rho}',\vec{\rho}) = 2.91k^2\int_0^L C_n^2(z)\left[\frac{1}{L}|\vec{\rho}'+\vec{\rho}(L-z)|\right]^{5/3}dz \tag{2.76}$$

where $C_n^2(\cdot)$ is the refractive index structure constant along the propagation path and $k=2\pi/\lambda$ is the angular wavenumber. Under the Taylor frozen atmosphere hypothesis [47], we evaluate $\left\langle h\left(\vec{\rho}_1\vec{\rho}_1'\right)h^{\dagger}\left(\vec{\rho}_2,\vec{\rho}_2'\right)\right\rangle$ at $\vec{\rho}_1=\vec{\rho}_1'=\vec{0}$ and $\vec{\rho}_1=\vec{\rho}_1'=[v_{\perp}t,0]$, where $v_{\perp}$ is the wind speed transverse to the optical path, to find the field autocovariance function:

$$\begin{aligned}R_{hh}(t) = (\lambda L)^2\left\langle h\left(0,0\right)h^{\dagger}\left(v_{\perp}t,v_{\perp}t\right)\right\rangle = \\ \exp\left\{-\frac{1}{2}D\left(v_{\perp}t,v_{\perp}t\right)\right\}\end{aligned} \tag{2.77}$$

If the transmit or receive terminal is moving, the transverse wind speed should be the apparent wind speed. The two-source spherical-wave structure function becomes:

$$\begin{aligned} D\left(v_\perp t, v_\perp t\right) &= 2.91k^2 \int_0^L C_n^2 \left[\frac{1}{L}|v_\perp tz + v_\perp t(L-z)|\right]^{5/3} dz \\ &= \frac{2.91k^2 C_n^2}{L^{5/3}} \int_0^L \left(v_\perp tL\right)^{5/3} dz \\ &= 2.91k^2 C_n^2 L \left(v_\perp t\right)^{5/3} \end{aligned} \tag{2.78}$$

where we have assumed homogeneous turbulence so that the refractive index structure constant $C_n^2(z) = C_n^2$. Therefore the atmospheric temporal field auto-covariance function becomes:

$$\begin{aligned} R_{hh}(t) &= \exp\left\{-\frac{2.91k^2 C_n^2 L}{2}\left(v_\perp t\right)^{5/3}\right\} \\ &= \exp\left\{-\frac{1}{2}\left(\frac{v_\perp t}{\rho_0}\right)^{5/3}\right\} \end{aligned} \tag{2.79}$$

where $\tilde{\rho}_0$ is the plane-wave atmospheric correlation length, given by:

$$\tilde{\rho}_0 = \left(\frac{1}{2.91k^2 C_n^2 L}\right)^{3/5} \tag{2.80}$$

We also define the atmospheric coherence time, or the approximate time that it takes for the atmosphere to become uncorrelated, as:

$$t_0 = \frac{\tilde{\rho}_0}{v_\perp} \tag{2.81}$$

We model the atmospheric evolution from some initial state $\mathbf{H}_0$ to some subsequent state $\mathbf{H}_c(t)$ as the weighted combination of some initial state $\mathbf{H}_0$ and some innovations matrix, $\mathbf{H}_1$:

$$\mathbf{H}_c(t) = \sqrt{R_{hh}(t)}\mathbf{H}_0 + \sqrt{1 - R_{hh}(t)}\mathbf{H}_1 \tag{2.82}$$

where the innovations matrix $\mathbf{H}_1$ has the same statistics as the initial state $\mathbf{H}_0$.

This model is appealing because $\mathbf{H}_c(t)$ is distributed approximately circularly symmetric log-normal [41] with the proper mean and variance for any value of t. Further, the subsequent state $\mathbf{H}_c(t)$ has a physically realistic covariance structure relative to the initial state $\mathbf{H}_0$, $\left\langle \mathbf{H}_c(t)\sqrt{R_{hh}(t)}\mathbf{H}_0 \right\rangle = R_{hh}(t)$, which implies that $\mathbf{H}_c(0) = \mathbf{H}_0$ and $\lim_{\tau\to\infty} \mathbf{H}_c(\tau) = \mathbf{H}_1$. Within the regime of weak turbulence, the regime where the Born approximation is valid, this additive time evolution model is the only possible model. For mild turbulence, outside the regime where the Born approximation is valid but within the region where the Rytov approximation is valid, a multiplicative model, as opposed to the additive model, may be more accurate. It is unclear which time evolution model better approximates the atmospheric evolution's impact on communication performance in the mild turbulence regime. Further, there are no closed form solutions for communication performance for a multiplicative model. As such, we continue this thesis assuming the additive model. Physically, the field auto-covariance accounts for the time evolution of turbules with sizes between the inner and outer scale. This model is only appropriate for two atmospheric state analysis, a higher order model would be required for problems that require multiple state analysis. We denote $\mathbf{H}_c(t)$ as $\mathbf{H}_c$ for simplicity when the time dependence is implicit from the context.

2.5.2 Channel Measurement

There are many possible schemes to measure the instantaneous channel state, $\mathbf{H}$. Fundamentally, any scheme must somehow calculate the component of the output due to each of the transmit apertures, thereby filling out the columns of the channel matrix. The conceptually simplest method to decouple the output is to transmit a pilot signal from each transmitter sequentially and recording the time variation of the received field at each receiver. From this measurement, we can build up a channel transfer matrix as a function of time and perform some operation to estimate the appropriate channel matrix. This conceptually simple method however is inefficient: time spent sending pilot symbols is time not spent transmitting data.

Another way to decouple the effect of each transmitter on the field in the receive plane is to superimpose a signal on each transmitter to uniquely identify it at the receiver. Such a signal should be small compared to the information bearing signal, vary quickly compared to the atmospheric coherence time, and preferably each transmitter's identification signal should be orthogonal to every other transmitters identification signal.

The communication system we have described relies on the instantaneous channel state estimate being available to the transmitter via a feedback link. Implied in this assumption is a feedback path from the receiver to the transmitter of sufficient rate and delay to allow for some minimum set of channel information to be received at the transmitter before the atmospheric state has changed. The delay is required to be less than an atmospheric coherence time, on the order of 1 to 100 ms, which is reasonable for communication links on the order of tens of kilometers. Additionally, we invoke the Taylor frozen atmosphere hypothesis [47], assuming the atmosphere will remain approximately constant over the period of a code word. For gigabit communication, this assumption is easily satisfied.

For two way optical communication, systems may exploit reciprocity to get the transmitter-side channel state information. Within regions where a feedback path from the receiver to the transmitter of sufficient rate and delay to allow for some minimum set of channel information to be received at the transmitter before the atmospheric state has changed is not possible, such as a ground to satellite system, reciprocity is an attractive method to measure the channel state.

2.5.3 Performance Metrics

A common metric for system performance is turbulence average bit error rate (BER). While this metric is useful, it is incomplete when the variation about the turbulence average is significant. In this case, we can define an additional metric to characterize the variation's impact on system performance, the outage probability. The outage probability is the average proportion of time that the instantaneous BER, P_i, is

greater than some prescribed BER threshold, P^*:

$$P_{outage}(P^*) = \Pr(P_i > P^*) \tag{2.83}$$

Closely related to the probability of outage is the notion of diversity power margin, which is the multiplicative power factor required to ensure a system experiencing turbulence will perform at least as well a system not experiencing turbulence. In this way, diversity power margin serves as a comparison of the two systems and as a proxy for performance gain.

When an interferer is hampering communication, we again use the notion of average BER. In this case, however, there are two possible interpretations of the average, based on different assumptions about the interaction between the transmitter and the interferer. If the transmitter and interferer use spatial mode hopping to allocate power according to some probability distribution, the average BER is interpreted as being averaged over the turbulence, the transmitter power allocation probability distribution and the interferer power allocation probability distribution. If the transmitter and interferer simply allocate a fixed power to the various spatial modes, the average is with respect to the turbulence alone. For either interpretation, we arrive at the same results.

Another common metric for system performance is capacity. Ergodic capacity is the maximum rate that reliable communication can be achieved, assuming the communication duration is long enough to experience all channel states. Intuitively, this means channel coding can eventually average over the channel states, hence the average capacity is of value. An atmospheric coherence time can be up to 100 ms, implying a system needs to code over about 10 seconds to achieve ergodic channel capacity. If a system's delay requirements preclude coding over many atmospheric states, outage capacity is an alternative notion that better describes achievable performance:

$$\begin{aligned} P_{outage}(R) &= \Pr(C_i < R) \\ &= \Pr(\log(1 + \mathrm{SNR}\phi) < R) \end{aligned} \tag{2.84}$$

where R is some desired rate, C_i is the instantaneous channel capacity for a particular atmospheric realization, and ϕ is a sufficient statistic for detection. The notion of instantaneous channel capacity is justified for systems where the rate is much higher than the atmospheric coherence time, so that long code words may be transmitted over a particular atmospheric realization. If we wish to guarantee the outage probability $P_{outage}(R)$ is less than some ϵ, the largest attainable rate of transmission is called the ϵ-capacity:

$$C_\epsilon = \log\left(1 + F^{-1}(1-\epsilon)\ \mathrm{SNR}\right) \tag{2.85}$$

where F is the complementary cumulative distribution function of the sufficient statistic ϕ.

2.5.4 Singular Value Distribution

We decouple the input-output relationship of $\mathbf{H}$ with a singular value decomposition (SVD):

$$\frac{1}{\sqrt{n_{rx}}}\mathbf{H} = \mathbf{U}\mathbf{\Gamma}\mathbf{V}^\dagger \tag{2.86}$$

where the i^{th} column of $\mathbf{U}$ is an output eigenmode, the i^{th} row of $\mathbf{V}$ is an input eigenmode, and the $\mathsf{i},\mathsf{i}^{th}$ entry of the diagonal matrix Γ is γ_i, whose square is the fractional power transfer for the i^{th} input/output eigenmode. We define $\vec{v}_\mathsf{i}$ to be column i of matrix $\mathbf{V}$ and $\vec{u}_\mathsf{i}$ to be column i of matrix $\mathbf{U}$. For the context of this thesis, an *eigenmode* is a particular spatial field distribution, or spatial mode. Using the SVD to transform $\vec{y} = \sqrt{\frac{\mathrm{SNR}}{n_{rx}}}\mathbf{H}\vec{x} + \vec{w}$ into parallel Gaussian channels, we arrive at:

$$\begin{aligned}
\tilde{y}_1 &= \sqrt{\mathrm{SNR}}\gamma_1\tilde{x}_1 + \tilde{w}_1 \\
\tilde{y}_2 &= \sqrt{\mathrm{SNR}}\gamma_2\tilde{x}_2 + \tilde{w}_2 \\
\vdots \quad &\quad \vdots \quad\quad \vdots \\
\tilde{y}_{n_{\min}} &= \sqrt{\mathrm{SNR}}\gamma_{n_{\min}}\tilde{x}_{n_{\min}} + \tilde{w}_{n_{\min}}
\end{aligned} \tag{2.87}$$

where $n_{\min} = \min(n_{tx}, n_{rx})$. The vectors $\tilde{\vec{x}}$, $\tilde{\vec{y}}$, and $\tilde{\vec{w}}$ are related to the vectors $\vec{x}$, $\vec{y}$, and $\vec{w}$ through the usual SVD, such as in [48]. Note $\tilde{w}_{\text{i}}$ retains its circularly symmetric complex Gaussian distribution. We denote the variance of $\tilde{w}_{\text{i}}$ as $\sigma^2 = 1$.

Chapter 3

Perfect Channel State Information

This chapter focuses on the performance of sparse aperture communication systems when the channel information is *perfectly* known by the transmitter. As stated in the previous chapter, minimizing bit error rate (BER) provides the maximum protection against fading. Because turbulence induced fading, not link capacity, is the primary limitation of atmospheric free space optical communication systems, the first section provides closed-form expressions for average and outage BER in homogeneous turbulence. The next section generalizes these results for inhomogeneous turbulence. Despite capacity being an incorrect performance metric for free space optical communication systems, some may wish to have knowledge of the capacity. As such, we include closed-form expressions for capacity in the last section of the chapter.

3.1 Optimal Solution for Homogeneous Isotropic Known Turbulence

In this section, we find the performance of sparse aperture systems under simplified conditions: we assume perfect knowledge of the instantaneous Green's function at the receiver, homogeneous isotropic turbulence, and aperture spacing sufficient to ensure independent link statistics. On the basis of these simplifying assumptions, we find closed-form performance expressions for various spatial diversity communica-

tion schemes, which we group based on the amount and quality of turbulence state information at the transmitter:

- Perfect knowledge of the channel transfer matrix: because this system will predistort the wavefront for optimal propagation, we call it the *optimal wavefront predistortion* scheme.
- Knowledge of the transmitter with the best performance: because this system selects the transmitter with the best performance, we will call it the *selection diversity* scheme.
- No knowledge of channel: because this system does not require feedback, we will call this the *open loop diversity* scheme.

While there are many schemes that operate with different transmitter turbulence state information, we only describe and analyze a subset with engineering significance. For example, we will study the case with perfect knowledge of the input mode with the best performance along with an optimal modulation and demodulation because this scheme provides a lower-limit on the achievable bit error rate. Further, this lower limit provides us with a way to calculate the inefficiency introduced by limited or imperfect information at the transmitter and/or suboptimal modulation and demodulation schemes. On the other end, we will study the case where the transmitter has no information about the channel because it provides performance where the feedback link has been completely severed. We start by analyzing the performance of optimal wavefront predistortion systems.

3.1.1 Optimal Wavefront Predistortion

For this section, we assume instantaneous *channel state information* (CSI) measured by the receiver is perfectly fed back to the transmitter. Early work on this topic was conducted by Poon et al. [42]. Implied in the assumption of perfect transmitter CSI is a feedback path from the receiver to the transmitter of sufficiently high rate and low delay to allow for some minimum amount of channel information to be received

at the transmitter before the atmospheric state has changed. The delay is required to be much less than an atmospheric correlation time, on the order of 1 to 100 ms, which is reasonable for communication systems with link distances on the order of tens of kilometers.

Asymptotic Analysis: Squared Singular Value Distribution

The ultimate goal of this chapter is to find the performance of the sparse aperture system. The performance is entirely determined by the distribution of squared singular values of the channel transfer matrix:

$$\frac{1}{\sqrt{n_{rx}}}\mathbf{H} = \mathbf{U}\mathbf{\Gamma}\mathbf{V}^{\dagger} \tag{3.1}$$

where the i^{th} column of $\mathbf{U}$ is an output eigenmode, the i^{th} column of $\mathbf{V}$ is an input eigenmode, and the $\mathsf{i},\mathsf{i}^{th}$ entry of the diagonal matrix $\mathbf{\Gamma}$ is the singular value, or diffraction gain, associated with the i^{th} input/output eigenmode. Consequently, we calculate the distribution of singular values (specifically, we calculate the distribution of squared singular values) in this section, then use the result to calculate average BER and capacity in following sections. For finite n_{rx} and n_{tx}, there are limited squared singular value distribution results. However, more insightful results come from considering the asymptotic spectrum of $\frac{1}{\sqrt{n_{rx}}}\mathbf{H}$. Asymptotic spectrum refers to the distribution of squared singular values for a particular matrix as the number of receive and transmit apertures go to infinity, $n_{tx}, n_{rx} \to \infty$, while the ratio of the number of transmit apertures to the number of receive apertures is fixed, $\beta = n_{tx}/n_{rx}$.

Theorem 1 *For a sparse aperture communication system with uniform average illumination of the receive apertures (i.e., all receive apertures fall within the main lobe of the propagating beam) and well-developed turbulence (i.e., $\sigma_{\phi}^2 \gg 2\pi$) for a single atmospheric state, as the number of transmit apertures and receive apertures asymptotically approaches infinity, the empirical eigenvalue distribution of $\mathbf{H}\mathbf{H}^{\dagger}/n_{rx}$*

converges almost surely to the Marcenko-Pastur density:

$$f_{\gamma^2}(x;\beta) = (1-\beta)^+\delta(x) + \frac{\sqrt{\left(x-\left(1-\sqrt{\beta}\right)^2\right)^+\left(\left(1+\sqrt{\beta}\right)^2-x\right)^+}}{2\pi x} \tag{3.2}$$

where $\beta = \dfrac{n_{tx}}{n_{rx}}$ *and* $(x)^+ = \max(x,0)$. *Because the nonzero squared singular values of* $\mathbf{H}/\sqrt{n_{rx}}$ *are the nonzero eigenvalues of* $\mathbf{H}\mathbf{H}^\dagger/n_{rx}$, *the Marcenko-Pastur density provides the empirical squared singular value distribution of* $\mathbf{H}/\sqrt{n_{rx}}$.

Proof. For some matrix $\mathbf{A}$, Bai [3] showed that the empirical eigenvalue distribution of $\mathbf{A}\mathbf{A}^\dagger$ asymptotically converges with probability one to the Marcenko-Pastur density if the entries of $\mathbf{A}$ are complex random variables with the following properties:

- zero mean,
- variance of $1/n_{rx}$,
- fourth moment decreases at least as fast as $1/n_{rx}^2$,
- independent,
- and identically distributed.

Because the nonzero squared singular values of $\mathbf{A}$ are the nonzero eigenvalues of $\mathbf{A}\mathbf{A}^\dagger$, the empirical eigenvalue distribution of $\mathbf{A}\mathbf{A}^\dagger$ provides the empirical squared singular value distribution of $\mathbf{A}$. Thus, we must show that the normalized channel transfer matrix $\frac{1}{\sqrt{n_{rx}}}\mathbf{H}$ satisfies these conditions. As we showed in Section 2.3.2, well-developed turbulence implies that the elements of $\mathbf{H}$ are zero mean, $\mathbb{E}[h_{\mathsf{kj}}/\sqrt{n_{rx}}] = 0$. By conservation of energy, the variance condition is satisfied:

$$\mathrm{var}\left(\frac{1}{\sqrt{n_{rx}}}h_{\mathsf{kj}}\right) = \frac{1}{n_{rx}}\mathbb{E}\left[e^{2\chi(\vec{\rho}_{\mathsf{k}},\vec{\rho}_{\mathsf{j}}')}\right] = \frac{1}{n_{rx}} \tag{3.3}$$

Again by conservation of energy, the fourth moment condition is satisfied:

$$\mathbb{E}\left[\left|\frac{1}{\sqrt{n_{rx}}}h_{\mathsf{kj}}\right|^4\right] = \frac{1}{n_{rx}^2}\mathbb{E}\left[e^{4\chi(\vec{\rho}_{\mathsf{k}},\vec{\rho}_{\mathsf{j}}')}\right] = \frac{1}{n_{rx}^2}e^{4\sigma_\chi^2} \tag{3.4}$$

Because each ray traverses a different path from transmitter k to receiver j, the entries of $\mathbf{H}$ will be uncorrelated, and thus approximately independent for our purposes, provided transmit apertures are separated by at least a transmit plane correlation length and the receive apertures are separated by at least a receive plane correlation length. If we assume that all receive apertures fall within the main lobe of the propagating beam and that the area of the transmit and receive apertures are all equal (note that the area of a transmit aperture does not have to equal the area of a receive aperture), the amplitude statistics are approximately identically distributed for all h_{kj}. Thus, we have shown that the Marcenko-Pastur density is, with probability one, the empirical squared singular value distribution (up to a normalization factor) of the channel transfer matrix $\frac{1}{\sqrt{n_{rx}}}\mathbf{H}$ for the sparse aperture communication systems. $\square$

As a corollary to Theorem 1, the number of eigenmodes corresponding to nonzero squared singular values converges, almost surely, to $\min(n_{tx}, n_{rx})$. Additionally, the maximum squared singular value converges, almost surely, to $\gamma_{\max}^2 = (1+\sqrt{\beta})^2$ while the minimum nonzero squared singular value converges, almost surely, to $\gamma_{\min}^2 = (1-\sqrt{\beta})^2$. The squared singular value distribution has an interesting structure; $\beta > 1$ gives larger squared singular than the case where $\beta < 1$: this implies that the feedback link is more important for systems with more transmit apertures than receive apertures. Figure 3-1 shows the Marcenko-Pastur density for various system geometries.

The uniform illumination of all receive apertures does not restrict the applicability of Theorem 1: no practical system would be designed such that there are receive apertures that are not illuminated by the main lobe. For all receive apertures to be illuminated by the main lobe of the beam, the maximum extent of the convex hull of

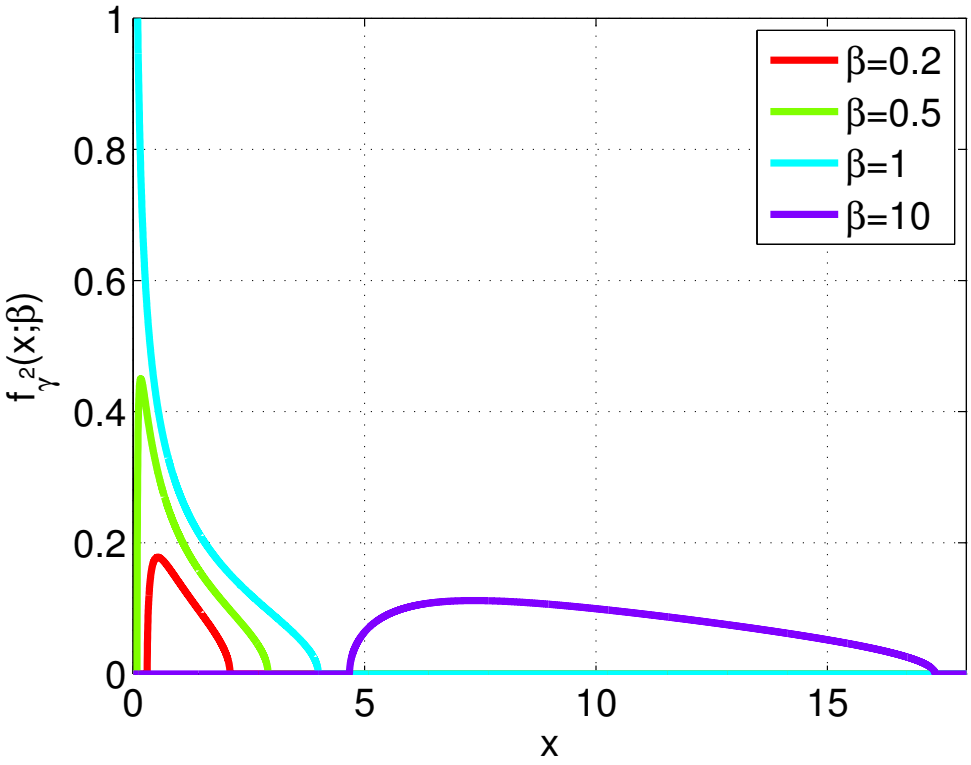

Figure 3-1: Marcenko-Pastur density: Probability density function of diffraction gain γ^2 under different transmitter/receiver aperture configurations where $\beta = n_{tx}/n_{rx}$. Note the impulse function at the origin, if present, is not shown.

the receive apertures d_{rx} must satisfy:

$$d_{rx} < \frac{2\lambda L}{\mathsf{w}} - d_{tx} \tag{3.5}$$

where d_{tx} is the maximum extent of the convex hull of the transmit apertures and w is the radius of a single transmit aperture. Thus, there is a constraint on the extent of the convex hull of both the transmit apertures and the receive apertures. We can increase the extent of the convex hull of the transmit apertures by adding a linear phase to the transmit apertures so that they 'point' toward the receiver.

Theorem 1 assumes a large number of apertures. The theorem's usefulness depends on the rate of convergence of the empirical distribution to the asymptotic result: if 10 transmit apertures and 10 receive apertures are required for approximate convergence to the Marcenko-Pastur distribution, then the theory is very useful. On

the other hand, if 1000 transmit apertures and 1000 receive apertures are required for approximate convergence to the Marcenko-Pastur distribution, then the theory becomes much more limited in usefulness. For example, let us consider a system with a link range of 10 km and 100 transmit apertures and 100 receive apertures (each in a 10-by-10 grid). For mild to moderate turbulence, the transmit apertures and receive apertures must be placed about a centimeter apart to ensure independent statistics. Thus, all the transmit (receive) apertures will fit into a 10 cm by 10 cm patch, which is a very reasonable form factor for today's communication systems. For this example system, does the Marcenko-Pastur distribution approximate the empirical squared singular value distribution? Figure 3-2 presents a comparison of the squared singular value distribution of simulation versus theory for various cases where the number of transmit apertures is 100. To create the histogram, we simulated many atmospheric states and calculated the empirical distribution of the squared singular values of these states. We see, even for the case with 100 transmit apertures and 100 receive apertures, that the simulated distribution has very nearly converged to the Marcenko-Pastur density. Therefore, the theory is applicable for practical systems. As a note, we present non-asymptotic results for one, two, and three transmit apertures later in Section 3.1.1.

The empirical squared singular value distribution in Theorem 1 does not depend on turbulence strength or transmitter/receiver geometry as long as the transmit and receive apertures are separated by at least a coherence length and the receive apertures are uniformly illuminated on average. In fact, the turbulence could be distributed in some way other than log-normal, as Rytov's method predicts. This is surprising to some. In some sense, the fact that the spectral distribution of squared singular values of a wide class of independent identically distributed random matrices converge to the Marcenko-Pastur distribution is analogous to the central limit theorem: under the central limit theorem, the sum of a wide class of independent identically distributed random variables converges to the Gaussian distribution. The underlying distribution of the entries of the channel transfer matrix does impact the convergence rate, however. The empirical squared singular value distribution converges to

the Marcenko-Pastur density for a much smaller number of transmit/receive apertures when the log-amplitude variance σ_χ^2 is small. Fortunately, for strong turbulence where convergence is slower we can expect many more transmit apertures in a given area (because the coherence length is small in strong turbulence).

Two power methods to measure the distance between two distributions, and thus the convergence rate, are the Kolmogorov distance and Cramér-von-Mises distance. The Kolmogorov distance is defined to be:

$$D_{n_{tx}} = \sup_x |F_{\gamma^2}(x; n_{tx}) - F_{\gamma^2}(x; \beta)| \tag{3.6}$$

where sup is the supremum, $F_{\gamma^2}(x;\beta)$ is the cumulative distribution function (cdf) of $f_\gamma^2(x;\beta)$ and $F_{\gamma^2}^*(x; n_{tx})$ is the empirical cdf created by averaging many realizations of the channel state with n_{tx} transmit apertures:

$$F_{\gamma^2}^*(x; n_{tx}) = \frac{1}{n_{tx}} \sum_{i=1}^{n_{tx}} I\left(\gamma_i^2 \leq x\right) \tag{3.7}$$

where γ_i^2 is an observation and $I(A)$ is the indicator of event A. Gotze et al. [18] showed that the Kolmogorov distance between the spectral distribution function and the distribution function of the Marcenko-Pastur law is of order $O(n_{tx}^{-1/2})$, under the condition that β is bounded away from one.

With regard to the Cramér-von-Mises distance, simulation shows that the empirical distribution converges at a polynomial rate. The Cramér-von-Mises criterion is defined as:

$$\omega^2 = \int_{-\infty}^{\infty} \left[F_{\gamma^2}^*(x; n_{tx}) - F_{\gamma^2}(x; \beta)\right]^2 dF_{\gamma^2}(x) \tag{3.8}$$

Figure 3-3 shows ω^2 for a Monte Carlo simulation versus number of receive apertures for various β and σ_χ^2.

Based on simulation, the convergence of ω^2 with n_{rx} is approximately a power law. We define the convergence exponent at α:

$$\omega^2 \propto n_{tx}^{-\alpha} \tag{3.9}$$

Simulation shows that α is about 2, invariant of β or σ_χ^2. We conclude that the Marcenko-Pastur density is practically very useful, even for systems with moderate diversity. For a 3×3 grid of receive apertures and a 3×3 grid of transmit apertures, we expect the empirical distribution to be within a Cramér-von-Mises distance of 10^{-4} from the asymptotic distribution. For transmission through thin clouds, where there may be millions of independent channels, convergence is very good.

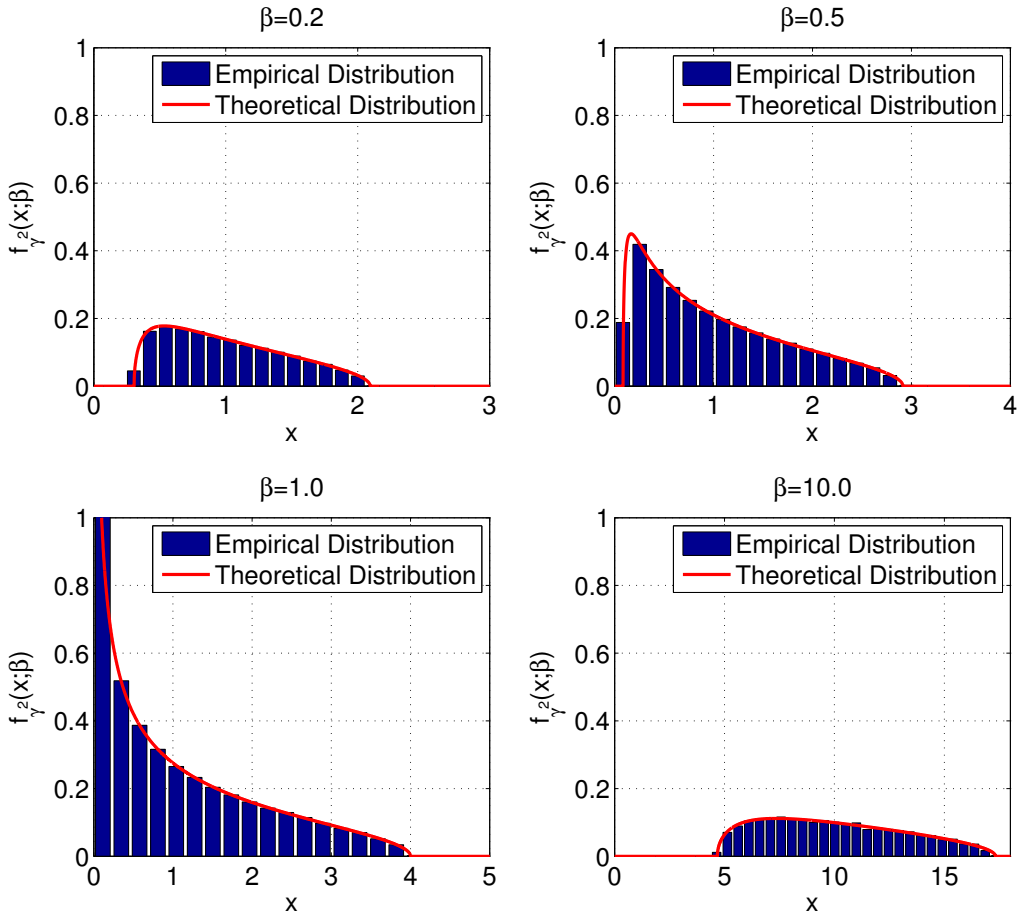

Figure 3-2: Comparison of Marcenko-Pastur density with simulation: Probability density function of diffraction gain γ^2 under different transmitter/receiver aperture configurations along with simulated squared singular value distribution. For $\beta = 0.2$, $n_{tx} = 100$ and $n_{rx} = 500$. For $\beta = 0.5$, $n_{tx} = 100$ and $n_{rx} = 100$. For $\beta = 1$, $n_{tx} = 100$ and $n_{rx} = 100$. For $\beta = 10$, $n_{tx} = 100$ and $n_{rx} = 10$.

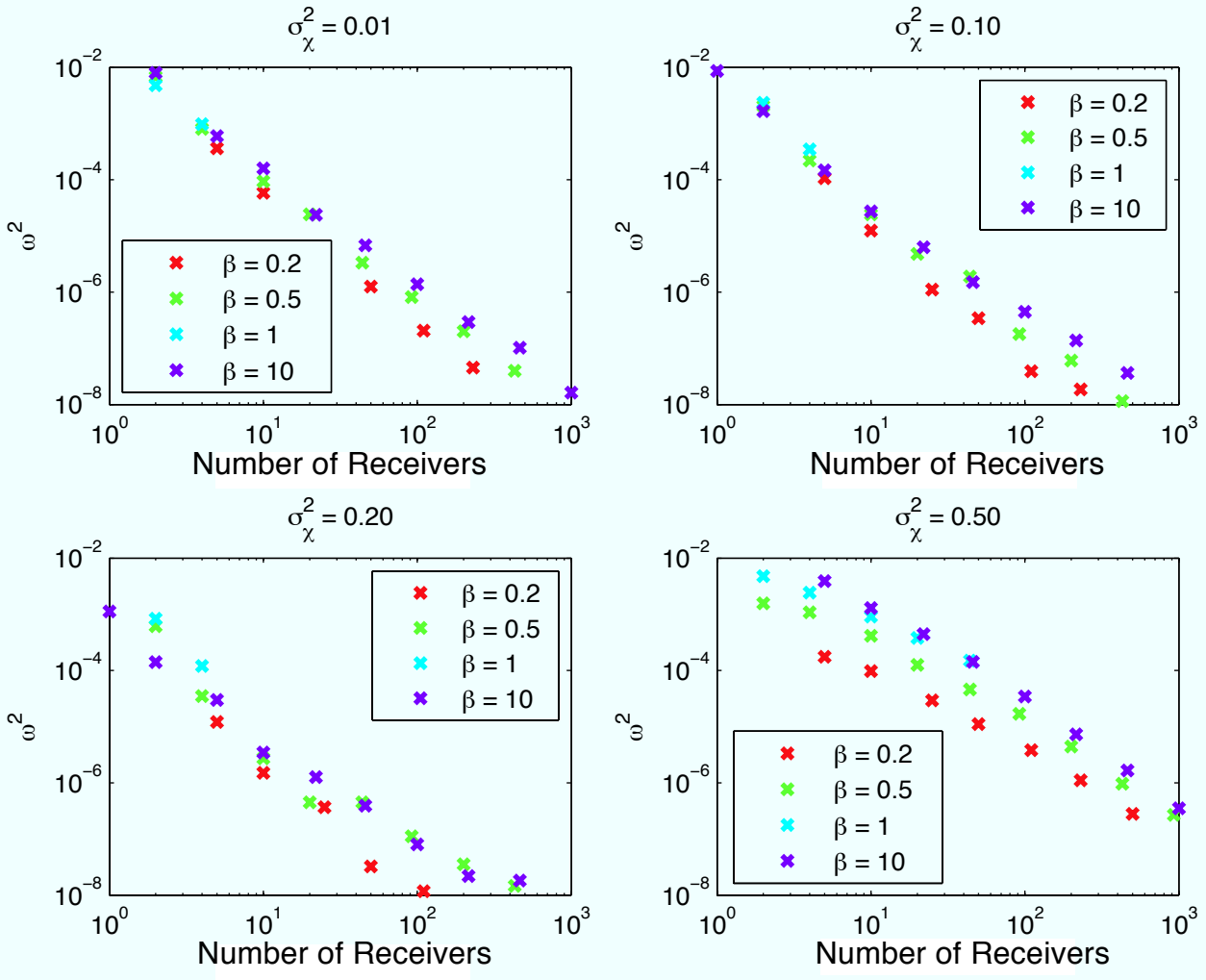

Figure 3-3: Cramér-von-Mises criterion for a Monte Carlo simulation versus number of receive apertures (n_{rx}) for various β and σ_χ^2.

Asymptotic Analysis: Average Bit Error Rate

In this section, we present the performance of sparse aperture systems with wavefront control and coherent detection. As we have argued, the bit error rate is the appropriate metric. Our goal is to now find the spatial field distribution for a known atmospheric state that will minimize the BER. Assuming binary phase shift keying (BPSK), the problem can be formulated as:

$$\vec{x}^* = \arg \min_{\vec{x}:\|\vec{x}\|^2=1} Q\left(\sqrt{2\mathrm{SNR}|\phi_s|^2}\right) \tag{3.10}$$

where $\|\cdot\|$ is the vector norm, SNR is the signal to noise ratio as defined in Chapter 2, $Q(\cdot)$ is the q-function, and ϕ_s is the recombination of the *signal* portion of the received field. Other modulation types such as quadrature phase shift keying are certainly possible. We focus on BPSK because it provides the best protection against fading. The optimization in (3.10) finds the spatial field distribution, $\vec{x}^*$, that propagates most efficiently through the turbulent atmosphere. Theorem 2 gives the solution to equation (3.10).

Theorem 2 *The spatial field distribution that minimizes instantaneous BER, as formulated in (3.10), is given by:*

$$\vec{x}^* = a\vec{v}_{\max}(\mathbf{H}) \tag{3.11}$$

where we have used that $\vec{v}_{\max}(\mathbf{H})$ *is the input eigenvector of* $\mathbf{H}$ *associated with the maximum squared singular value* $\gamma^2_{\max}$ *of* $\mathbf{H}$*. We will simply use* $\vec{v}_{\max}$ *instead of* $\vec{v}_{\max}(\mathbf{H})$ *when the context is clear. Data is encoded by variation of* $a \in \mathbb{C}$*, which is spatially constant at a particular time. For example, to transmit a bit* $C[n] \in \{0, 1\}$ *using binary phase shift keying (BPSK):* $a[n] = e^{i\pi C[n]}$*. A sufficient statistic for optimum detection is:*

$$\phi = Re\{\vec{u}^{\dagger}_{\max}\vec{y}\} \tag{3.12}$$

where ϕ *is the sufficient statistic and* $\vec{u}_{\max}$ *is the output eigenvector of* $\mathbf{H}$ *associated with the maximum squared singular value. The associated optimal instantaneous probability of error for channel state* $\mathbf{H}$ *is:*

$$\Pr(\text{error}|\mathbf{H}) = Q\left(\sqrt{2\text{SNR}\gamma^2_{\max}}\right) \tag{3.13}$$

Proof. For binary transmission of data through a fixed atmosphere, the transmit vector can take on one of two vectors: $\vec{x} \in \{\vec{x}_A, \vec{x}_B\}$. We assume, without loss of generality, that $\vec{x}$ takes on $\vec{x}_A$ and $\vec{x}_B$ with equal probability. Consequently, we can

write the transmit vector as:

$$\vec{x} = x\left(\frac{\vec{x}_A - \vec{x}_B}{2}\right) + \left(\frac{\vec{x}_A + \vec{x}_B}{2}\right) \tag{3.14}$$

where the information is in the scalar $x \in \{-1, 1\}$. Because $\vec{x}$ takes on $\vec{x}_A$ and $\vec{x}_B$ with equal probability, the scalar x takes on values of 1 and -1 with equal probability. Additionally, the unit energy constraint on $\vec{x}$ implies that both transmit vectors $\vec{x}_A$ and $\vec{x}_B$ must also have unit energy. We write the received vector $\vec{y}$ as:

$$\vec{y} - \mathbf{H}\left(\frac{\vec{x}_A + \vec{x}_B}{2}\right) = \sqrt{\text{SNR}}\mathbf{H}\left(\frac{\vec{x}_A - \vec{x}_B}{2}\right)x + \vec{w} \tag{3.15}$$

We see the information is contained in a one-dimensional subspace of the n_{rx}-dimensional receive space. The subspace is:

$$\vec{p} = \frac{\mathbf{H}\vec{x}_A - \mathbf{H}\vec{x}_B}{\|\mathbf{H}\vec{x}_A - \mathbf{H}\vec{x}_B\|} \tag{3.16}$$

The power received in $\vec{y}$ that is orthogonal to $\vec{p}$ is exclusively noise. Further, because the entries of $\vec{w}$ are circularly symmetric and independent, the noise components in directions orthogonal to $\vec{p}$ are independent of the noise in the direction of $\vec{p}$. This means that the components of the received vector $\vec{y}$ that are orthogonal to $\vec{p}$ are *irrelevant* for detection and can be ignored. We ignore the component of the noise orthogonal to the signal by projecting the received vector down onto the signal space defined by $\vec{p}$:

$$\begin{aligned}\phi &= Re\left\{\vec{p}^{\,\dagger}\left(\vec{y} - \sqrt{\text{SNR}}\mathbf{H}\left(\frac{\vec{x}_A + \vec{x}_B}{2}\right)\right)\right\} \\ &= Re\left\{\vec{p}^{\,\dagger}\vec{y}\right\}\end{aligned} \tag{3.17}$$

where we have ignored $\mathbf{H}\left(\frac{\vec{x}_A+\vec{x}_B}{2}\right)$ because it does not contain any information. Consequently, we arrive at the following *scalar* detection problem:

$$\begin{aligned}\phi &= Re\left\{\vec{p}^{\,\dagger}\vec{y}\right\} \\ &= Re\left\{\left(\frac{\mathbf{H}\vec{x}_A-\mathbf{H}\vec{x}_B}{\|\mathbf{H}\vec{x}_A-\mathbf{H}\vec{x}_B\|}\right)^{\dagger}\left(\sqrt{\mathrm{SNR}}\mathbf{H}\left(\frac{\vec{x}_A-\vec{x}_B}{2}\right)x+\vec{w}\right)\right\} \\ &= \frac{\sqrt{\mathrm{SNR}}}{2}\|\mathbf{H}(\vec{x}_A-\vec{x}_B)\|x+Re\{\tilde{w}\}\end{aligned} \tag{3.18}$$

where $\tilde{w}$ has the same distribution as each element of $\vec{w}$. As a result, ϕ conditioned on x is normally distributed:

$$\phi|x \sim \mathcal{N}\left(\frac{\sqrt{\mathrm{SNR}}}{2}\|\mathbf{H}(\vec{x}_A-\vec{x}_B)\|x, 1\right) \tag{3.19}$$

The optimal detector, with the smallest probability of error, chooses the symbol that is most likely to have been transmitted given the received signal.

$$Pr(x=1|\phi) \underset{x=1}{\overset{x=-1}{\lessgtr}} Pr(x=-1|\phi) \tag{3.20}$$

Because both symbols are equally likely, we can use Bayes' rule to simplify.

$$\begin{aligned}\frac{1}{\sqrt{\pi}}\exp\left(-\frac{1}{2}\left(\phi-\frac{\sqrt{\mathrm{SNR}}}{2}\|\mathbf{H}(\vec{x}_A-\vec{x}_B)\|\right)^2\right) &\underset{x=1}{\overset{x=-1}{\lessgtr}} \\ \frac{1}{\sqrt{\pi}}\exp\left(-\frac{1}{2}\left(\phi+\frac{\sqrt{\mathrm{SNR}}}{2}\|\mathbf{H}(\vec{x}_A-\vec{x}_B)\|\right)^2\right)&\end{aligned} \tag{3.21}$$

Simplifying further gives the nearest neighbor detection rule:

$$\begin{aligned}&\left|\phi-\frac{\sqrt{\mathrm{SNR}}}{2}\|\mathbf{H}(\vec{x}_A-\vec{x}_B)\|\right| \underset{x=-1}{\overset{x=1}{\lessgtr}} \left|\phi+\frac{\sqrt{\mathrm{SNR}}}{2}\|\mathbf{H}(\vec{x}_A-\vec{x}_B)\|\right| \\ &\rightarrow \phi \underset{x=1}{\overset{x=-1}{\lessgtr}} 0\end{aligned} \tag{3.22}$$

The probability of error for this detection is then:

$$\begin{aligned}
\Pr(\text{error}|\mathbf{H}) &= \frac{1}{2}\Pr(\text{error}|\mathbf{H}, x=1) + \frac{1}{2}\Pr(\text{error}|\mathbf{H}, x=-1) \\
&= \Pr(\text{error}|\mathbf{H}, x=1) \\
&= \frac{1}{\sqrt{2\pi}}\int_0^\infty \exp\left(-\left(z - \frac{\sqrt{\text{SNR}}}{2}\|\mathbf{H}(\vec{x}_A - \vec{x}_B)\|\right)^2\right) dz \\
&= Q\left(\sqrt{\text{SNR}\frac{\|\mathbf{H}(\vec{x}_A - \vec{x}_B)\|^2}{2}}\right)
\end{aligned} \tag{3.23}$$

Consequently, we have an expression showing the dependence of BER with SNR and the choice of transmit signals. We minimize BER by simply selecting the transmit signals $\vec{x}_A$ and $\vec{x}_B$ that maximize $\|\mathbf{H}(\vec{x}_A - \vec{x}_B)\|^2$.

$$\begin{aligned}
\{x_A, x_B\} &= \underset{x_A, x_B : \|x_A\|^2 = \|x_B\|^2 = 1}{\text{argmin}} Q\left(\sqrt{\text{SNR}\frac{\|\mathbf{H}(\vec{x}_A - \vec{x}_B)\|^2}{2}}\right) \\
&= \underset{x_A, x_B : \|x_A\|^2 = \|x_B\|^2 = 1}{\text{argmax}} \|\mathbf{H}(\vec{x}_A - \vec{x}_B)\|^2
\end{aligned} \tag{3.24}$$

Because each transmit vector $\vec{x}_A$ and $\vec{x}_B$ is unit energy, and by the triangle inequality ($\|\vec{x}_A + \vec{x}_B\|^2 \leq \|\vec{x}_A\|^2 + \|\vec{x}_B\|^2$), the BER minimizing transmit vectors must be antipodal: $\vec{x}_A = -\vec{x}_B$. This simplifies the minimization problem:

$$\begin{aligned}
\vec{x}_A &= \underset{x_A : \|x_A\|^2 = 1}{\text{argmin}} Q\left(\sqrt{2\text{SNR}\|\mathbf{H}\vec{x}_A\|^2}\right) \\
&= \underset{x_A : \|x_A\|^2 = 1}{\text{argmax}} \|\mathbf{H}\vec{x}_A\|^2 \\
&= \underset{x_A : \|x_A\|^2 = 1}{\text{argmax}} \vec{x}_A{}^\dagger \mathbf{H}^\dagger \mathbf{H} \vec{x}_A \\
&= \underset{x_A : \sum_{\mathsf{i}}^{n_{tx}} |\alpha_{\mathsf{i}}|^2 = 1}{\text{argmax}} \left(\sum_{\mathsf{j}=1}^{n_{tx}} \alpha_{\mathsf{j}}{}^\dagger \vec{v}_{\mathsf{i}=1}^\dagger\right) \mathbf{H}^\dagger \mathbf{H} \left(\sum_{\mathsf{i}=1}^{n_{tx}} \alpha_{\mathsf{i}} \vec{v}_{\mathsf{i}}\right) \\
&= \underset{x_A : \sum_{\mathsf{i}}^{n_{tx}} |\alpha_{\mathsf{i}}|^2 = 1}{\text{argmax}} \sum_{\mathsf{i}=1}^{n_{tx}} |\alpha_{\mathsf{i}}|^2 \gamma_{\mathsf{i}}(\mathbf{H}) \\
&= \vec{v}_{\max}
\end{aligned} \tag{3.25}$$

where we have written $\vec{x}_A$ as a linear combination of the orthonormal basis formed by the input eigenmodes of the matrix $\mathbf{H}$: $\vec{x}_A = \sum_{\mathsf{i}}^{n_{tx}} \alpha_{\mathsf{i}} \vec{v}_{\mathsf{i}}$ where $\alpha_{\mathsf{i}} = \vec{v}_{\mathsf{i}}^{\,\dagger} \vec{x}_A$. By the non-negativity of the squared singular values of $\mathbf{H}$, the last expression is solved by selecting $\alpha_1 = 1$, $\alpha_{\mathsf{i}} = 0, \mathsf{i} = 2 \ldots n_{tx}$. We have used the convention that $\gamma_1 \geq \gamma_2 \geq \cdots \geq \gamma_{n_{tx}}$. As a result, the optimal transmit vectors for a given atmospheric state are $\vec{x}_A = -\vec{x}_B = \vec{v}_{\max}$. The associated probability of error is:

$$\Pr(\text{error}|\mathbf{H}) = Q(\sqrt{2\text{SNR}\gamma_{\max}^2}) \tag{3.26}$$

And the optimal detector is:

$$\phi = Re\{\vec{v}_{\max}^{\,\dagger} \vec{y}\} \tag{3.27}$$

□

We showed that the predistortion and recombination scheme given in Theorem 2 is optimal, in the sense that it minimizes BER, for the sparse aperture system. The scheme presented in the theorem is, in fact, optimal for a much broader class of systems: the condition that each transmit receive aperture pair experience independent fading is *not* required for the scheme to be optimal. Thus, Theorem 2 provides the optimal predistortion and recombination scheme for systems with transmit (or receive) apertures spaced more closely to one another than a coherence length.

Additionally, Theorem 2 can be applied to large, with respect to the atmospheric coherence length, aperture systems that have the ability to predistort the transmitted wave. To apply the theorem, divide up the large transmit aperture into small elements. The elements should be much smaller than the atmospheric coherence length at the transmitter. Each element then represents a transmit aperture in the context of Theorem 2. The receive aperture should similarly be divided up into elements that are much smaller than the atmospheric coherence length at the receiver. Each element then represents a receive aperture in the context of Theorem 2.

While an equation for instantaneous probability of error is provided, we have not presented a closed-form solution for the maximum squared singular value $\gamma_{\max}^2$ and, therefore, have not yet presented a closed-form expression for probability of error.

We now calculate the maximum squared singular value and provide a closed-form expression for turbulence average bit error rate.

For BPSK modulation, the turbulence average BER is:

$$\begin{aligned}\mathbb{E}[\Pr(\text{error})] &= \int_0^\infty \Pr(\text{error}|x) f_{\gamma^2_{\max}}(x) dx \\ &= \int_0^\infty Q\left(\sqrt{2\text{SNR}x}\right) f_{\gamma^2_{\max}}(x) dx\end{aligned} \tag{3.28}$$

where $f_{\gamma^2_{\max}}(x)$ is the pdf of the largest squared singular value. This result is general for any BPSK sparse aperture optical communication system, but depends on an unknown pdf, $f_{\gamma^2_{\max}}(x)$. The pdf for the largest squared singular value is only known in the asymptotic case. From Theorem 1 we know that, as the number of apertures grows large, the pdf of the largest squared singular value converges almost surely to:

$$\lim_{n_{tx}\to\infty} f_{\gamma^2_{\max}}(x) = \delta\left(x - \left(1+\sqrt{\beta}\right)^2\right) \tag{3.29}$$

where $\delta(\cdot)$ is the Dirac delta. Using (3.29) to evaluate (3.28) provides a closed-form expression for the probability of error:

$$\begin{aligned}\lim_{n_{tx}\to\infty} \mathbb{E}[\Pr(\text{error})] &= \int_0^\infty Q\left(\sqrt{2\text{SNR}x}\right) \delta\left(x - \left(1+\sqrt{\beta}\right)^2\right) dx \\ &= Q\left(\sqrt{2\text{SNR}\left(1+\sqrt{\beta}\right)^2}\right)\end{aligned} \tag{3.30}$$

While this result is only exact in the asymptotic case, it provides a very good approximation for a finite but large number of apertures. The $\left(1+\sqrt{\beta}\right)^2$ term is the power gain over a system the same system without wavefront predistortion. Specifically, it is the gain over a system with the same geometry, no turbulence state information at the transmitter, coherent detection, and optimal recombination. This power gain term results from the ability to allocate all the system transmit power into the spatial mode with the best propagation performance. Essentially, we select the mode with the best constructive interference for the particular receiver aperture geometry and atmospheric state. As the number of receive apertures becomes much larger than

the number of transmit apertures, $\beta \to 0$, the system performance approaches that of the system without wavefront predistortion. This is an expected result. As the system becomes very asymmetric, the ability to predistort the wavefront is lost.

Many would expect a balanced system, with an equal number of transmit and receive apertures, to provide the best performance. Indeed, additional diversity at the transmitter or receiver always increases performance (provided that power collected at the receiver is not reduced by adding additional transmit or receive apertures). The $\left(1+\sqrt{\beta}\right)^2$ term does not imply that more transmitters relative to the number or receivers is beneficial.

The gain, in terms of probability of error, of moving to a diversity system with wavefront predistortion is:

$$\frac{\mathbb{E}[\Pr(\text{error}|\text{sparseaperture})]}{\mathbb{E}[\Pr(\text{error}|\text{nodiversity})]} = e^{-\left((1+\sqrt{\beta})^2-1\right)\text{SNR}} \tag{3.31}$$

where we have bounded the probability of error with the Chernoff bound of the q-function to derive the expression. At high-SNR, using the sparse aperture system provides a large gain in BER compared to the no diversity system. At low-SNR, the advantage of the more sophisticated system is less pronounced.

It is clear, in the asymptotic case, that the average BER does not depend on turbulence strength. Effectively, the many apertures act to average out the spatial variation induced by the atmospheric turbulence. Turbulence strength does factor into the system design; in stronger turbulence, apertures may be placed more closely together while in weaker turbulence, they must be placed farther apart. Further, stronger turbulence causes slower convergence to the Marcenko-Pastur density; which means more apertures are required for (3.30) to be valid.

Lastly, as the total aperture size increases for a single aperture system, the power gain saturates as the aperture size approaches the correlation length. We have shown that the sparse aperture system, however, does not saturate with total aperture size. Indeed, the number of apertures used is only limited by form factor constraints and the requirement for uniform illumination.

A Monte-Carlo simulation was performed to validate the theory presented in (3.30). In the simulation, we assumed that the instantaneous atmospheric state was available at the transmitter. For a single atmospheric state, an equiprobable binary source was encoded according to (3.11), transmitted through the simulated atmosphere, detected coherently, and the number of raw bit errors recorded. This process was repeated many times with independent realizations of the atmosphere to arrive at the average BER presented in Figure 3-4. In the figure, we show theory and simulation versus SNR. The number of transmit apertures was 100, 100, 200 and the number of receive apertures was 100, 50, 20 giving $\beta = 1$, $\beta = 0.5$, and $\beta = 0.1$.

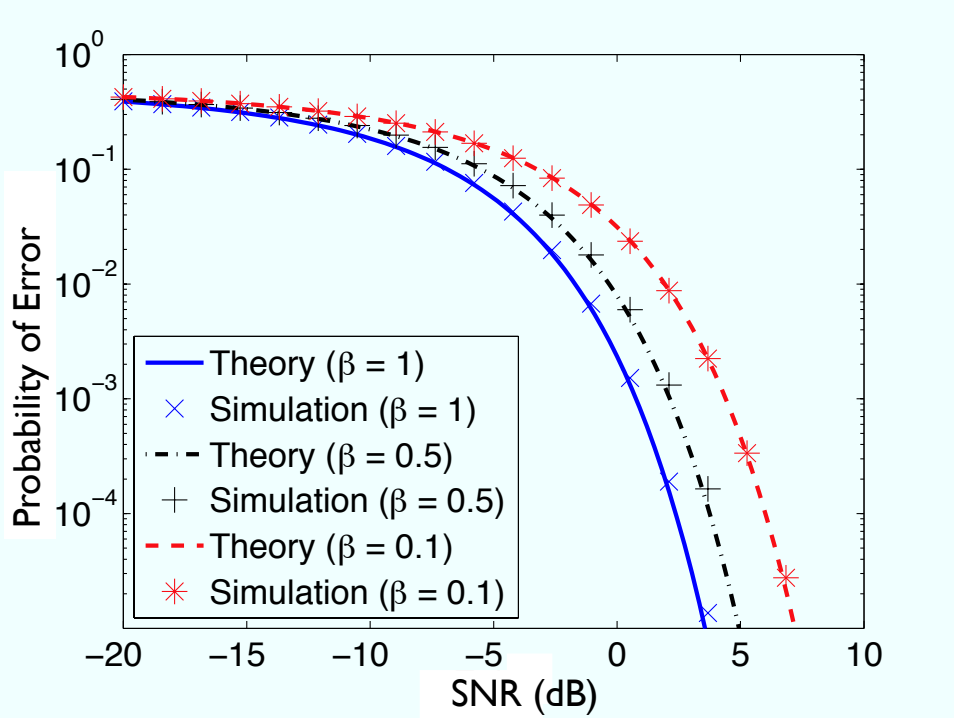

Figure 3-4: BER versus SNR: A comparison of Monte-Carlo simulation and theory for binary phase shift keying with $\sigma_\chi^2 = 0.1$. The number of transmit apertures was 100, 100, 200 and the number of receive apertures was 100, 50, 20 giving $\beta = 1$, $\beta = 0.5$, and $\beta = 0.1$.

From the figure, we see very good agreement between theory and simulation. As we stated earlier, the theory provides an approximate solution to any system with a large but finite number of apertures. Here, we see the approximation is very close to the theory.

Asymptotic Analysis: Outage Probability

There are many ways to measure the variability in system performance due to fading. Outage probability defined in terms of BER is particularly useful because it guarantees at least some minimum performance some fraction of the time. Formally, the outage probability associated with some BER, P^*, is the probability that any given atmospheric state will yield an instantaneous BER more than P^*:

$$\begin{aligned} P_{\text{out}}(P^*) &= \Pr\left(P_i \geq P^*\right) \\ &= 1 - F_{BER}(P^*) \end{aligned} \tag{3.32}$$

where P_{out} is the outage probability, P_i is the instantaneous probability of bit-error, P^* is the minimum performance we wish to guarantee in terms of BER, and $F_{BER}(\cdot)$ is the BER cumulative distribution function (cdf). The following theorem provides an asymptotic expression for the outage probability:

Theorem 3 *The probability of outage, P_{out}, associated with a desired probability of error, P^* is asymptotically given by:*

$$\begin{aligned} \lim_{n_{tx},n_{rx}\to\infty} P_{\text{out}}(s) &= \exp\left(-\int_s^\infty (x-s)\, q^2(x)dx\right), \\ s &= \frac{(Q^{-1}\left(P^*\right))^2/(2\text{SNR}) - \left(1+\sqrt{\frac{n_{tx}}{n_{rx}}}\right)^2}{\left(1+\sqrt{\frac{n_{tx}}{n_{rx}}}\right)\left(\frac{1}{\sqrt{n_{tx}}}+\frac{1}{\sqrt{n_{rx}}}\right)^{1/3}} \end{aligned} \tag{3.33}$$

where $Q^{-1}(\cdot)$ is the inverse Q-function and $q(x)$ is the function that solves the nonlinear Painlevé II differential equation:

$$q''(x) = xq(x) + 2q^3(x) \tag{3.34}$$

with the associated boundary condition:

$$q(x) \sim Ai(x), x \to \infty \tag{3.35}$$

where $Ai(x)$ is the Airy function, given by:

$$Ai(x) = \frac{1}{\pi}\int_0^\infty \cos\left(\frac{1}{3}t^3 + xt\right) dt \tag{3.36}$$

Proof. Starting from the definition of probability of outage:

$$\begin{aligned} P_{\text{out}}(P^*) &= Pr(P_i > P^*) \\ &= Pr\left(Q\left(\sqrt{2\text{SNR}\gamma_{\max}^2}\right) > P^*\right) \\ &= Pr\left(\gamma_{\max}^2 < \frac{\left(Q^{-1}(P^*)\right)^2}{2\text{SNR}}\right) \\ &= F_{\gamma_{\max}^2}\left(\frac{\left(Q^{-1}(P^*)\right)^2}{2\text{SNR}}\right) \end{aligned} \tag{3.37}$$

where $F_{\gamma_{\max}^2}$ is the cdf of the largest eigenvalue of $\mathbf{H}^\dagger\mathbf{H}$. To find $F_{\gamma_{\max}^2}$, we first note that a complex matrix $\mathbf{Q}$ with independent circularly symmetric Gaussian entries such that $Re\{q_{\mathsf{kj}}\}, Im\{q_{\mathsf{kj}}\} \sim \mathcal{N}(0, 1/2)$, the largest eigenvalue of $\mathbf{Q}^\dagger\mathbf{Q}$, with the proper normalization, converges almost surely to the Tracy-Widom distribution [23]:

$$\frac{\gamma_{\max}^2 - \left(1 + \sqrt{\frac{n_{tx}}{n_{rx}}}\right)^2}{\left(1 + \sqrt{\frac{n_{tx}}{n_{rx}}}\right)\left(\frac{1}{\sqrt{n_{tx}}} + \frac{1}{\sqrt{n_{rx}}}\right)^{1/3}} \sim W_2 \tag{3.38}$$

where $\gamma_{\max}^2$ is the largest eigenvalue of $\mathbf{Q}^\dagger\mathbf{Q}$ and W_2 is the Tracy-Widom distribution. First we will show that the real and imaginary parts of the h_{kj} are zero mean random variables with variance equal to one half. Next we will show that the entries of $\mathbf{H}^\dagger\mathbf{H}$ are asymptotically Gaussian, and thus the largest squared singular value of $\mathbf{H}$ is governed by the Tracy-Widom distribution. The mean of the real part of $\mathbf{H}$ is:

$$\begin{aligned} \mathbb{E}[Re\{h_{ij}\}] &= \mathbb{E}[Re\{e^{\chi + j\phi}\}] \\ &= \mathbb{E}[e^{\chi}\cos\phi] \\ &= \mathbb{E}[e^{\chi}]\mathbb{E}[\cos\phi] \\ &= 0 \end{aligned} \tag{3.39}$$

where we have used that the atmosphere is log-normally distributed with e^{χ} and $\cos\phi$ uncorrelated with each other. Note that in Chapter 2 we stated that χ and ϕ are *not* independent random variables. Because the phase variation is much larger than 2π e^{χ} and $\cos\phi$ are indeed approximately uncorrelated. Similarly, the imaginary part of $\mathbf{H}$ is zero mean:

$$\begin{aligned}\mathbb{E}[Im\{h_{ij}\}] &= \mathbb{E}[Im\{e^{\chi+j\phi}\}] \\ &= \mathbb{E}[e^{\chi}\sin\phi] \\ &= \mathbb{E}[e^{\chi}]\mathbb{E}[\sin\phi] \\ &= 0\end{aligned} \tag{3.40}$$

The variance of the real part of $\mathbf{H}$ is:

$$\begin{aligned}Var[Re\{h_{ij}\}] &= \mathbb{E}[(Re\{h_{ij}\})^2] \\ &= \mathbb{E}[e^{2\chi}\cos^2\phi] \\ &= \mathbb{E}[e^{2\chi}]\mathbb{E}[\cos^2\phi] \\ &= 1/2\end{aligned} \tag{3.41}$$

where we used that $\mathbb{E}[e^{2\chi}] = 1$ by conservation of energy. Similarly, the variance of the imaginary part of $\mathbf{H}$ is:

$$\begin{aligned}Var[Im\{h_{ij}\}] &= \mathbb{E}[(Im\{h_{ij}\})^2] \\ &= \mathbb{E}[e^{2\chi}\sin^2\phi] \\ &= \mathbb{E}[e^{2\chi}]\mathbb{E}[\sin^2\phi] \\ &= 1/2\end{aligned} \tag{3.42}$$

Thus, the mean and variance of $\mathbf{H}$ are the same as the mean and variance of $\mathbf{Q}$. While the entries of $\mathbf{H}$ are not circularly symmetric Gaussian, by central limit theorem the entries of $\mathbf{H}^{\dagger}\mathbf{H}$ are asymptotically Gaussian. Thus, the entries of $\mathbf{H}^{\dagger}\mathbf{H}$ are distributed the same as the entries of $\mathbf{Q}^{\dagger}\mathbf{Q}$ when there are many transmit and receive apertures.

Therefore, the theorem is proved for the asymptotic case.

□

The outage probability 3 dB point is about $\left(1+\sqrt{\beta}\right)^2$, which agrees with the empirical cdf described by the Marcenko-Pastur distribution. Figure 3-5 shows the probability of outage versus desired BER for various numbers of apertures. From the figure, we see that increasing the number of apertures causes the outage probability curve to decrease much faster. Calculating the integral and associated nonlinear differential equation in Theorem 3 is computationally intensive. Corollary 1 provides a high-SNR bound, in terms of elementary functions, that is much easier to compute.

Corollary 1 *The high-SNR probability of outage, P_{out}, associated with a desired probability of error, P^* is asymptotically:*

$$\lim_{n_{tx},n_{rx}\to\infty} P_{\text{out}}(s) = e^{\frac{-|s|^3}{12}}, s \ll 0$$

$$s = \frac{\left(Q^{-1}\left(P^*\right)\right)^2/(2\text{SNR}) - \left(1+\sqrt{\frac{n_{tx}}{n_{rx}}}\right)^2}{\left(1+\sqrt{\frac{n_{tx}}{n_{rx}}}\right)\left(\frac{1}{\sqrt{n_{tx}}}+\frac{1}{\sqrt{n_{rx}}}\right)^{1/3}} \tag{3.43}$$

Proof. The Tracy-Widom distribution has the following tail [10]:

$$\lim_{s\to-\infty} W_2(s) = exp\left(-|s|^3/12\right) \tag{3.44}$$

Substituting this expression into the proof of Theorem 3 proves the corollary. □

From Corollary 1, it is easy to prove the outage probability approaches a step function as the number of apertures goes to infinity. This corollary shows that a system designer can achieve any desired nonzero outage probability by adding apertures, limited only by the ability to satisfy the assumption of uniform illumination. The expression in Corollary 1 is still difficult to interpret. As such, we now specialize the corollary for the case where $n_{tx} = n_{rx} = n$:

Corollary 2 *For the special case where $n_{tx} = n_{rx} = n$, probability of outage, P_{out}, associated with a desired probability of error, P^* is asymptotically:*

$$\lim_{n_{tx},n_{rx}\to\infty} P_{\text{out}}(P^*) = \exp\left(\frac{-\sqrt{n}}{192}\left(4 - \frac{(Q^{-1}(P^*))^2}{2\text{SNR}}\right)^3\right),\ P_{\text{out}} \ll 1 \tag{3.45}$$

Proof. Substituting $n_{tx} = n_{rx} = n$ into Corollary 1 and simplifying proves the theorem. □

So, we see that for a given SNR and desired BER, the outage probability decreases as $\exp(-\sqrt{n})$.

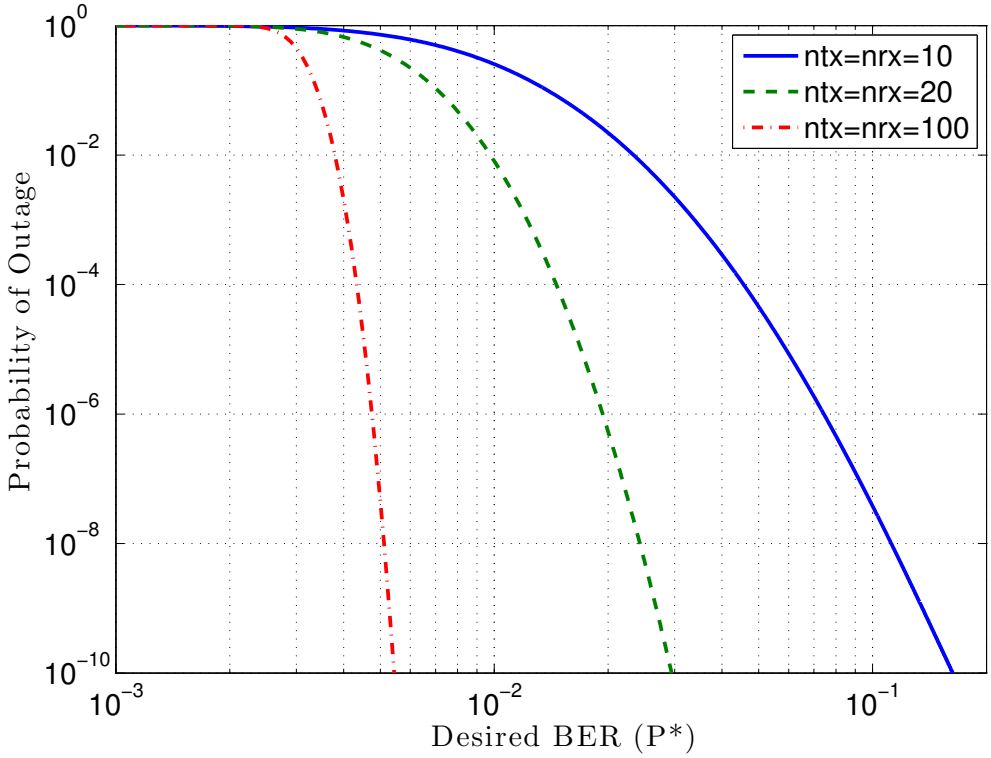

Figure 3-5: Wavefront predistortion probability of outage versus BER: Probability of outage versus desired BER for various numbers of apertures and SNR=1.

Asymptotic Analysis: Finite Aperture Power Margin

Here we define finite aperture power margin in two equivalent ways. The first way defines power margin as a comparison between the finite aperture system and the

asymptotic system: *finite aperture power margin* is the multiplicative power increase required for the finite sparse aperture system to perform at least as well as the infinite sparse aperture system, at least P_{out} fraction of the time. The second, equivalent way, defines finite aperture power margin as a comparison between the sparse aperture system in and out of a fading environment: *finite aperture power margin* is the power increase required to overcome fading, at least P_{out} fraction of the time. Mathematically, finite aperture power margin is:

$$m = \arg_m \left\{ \Pr \left[Q\left(\sqrt{(2\gamma_{\max}^2 \text{SNR})\, m} \right) \geq Q\left(\sqrt{2\left(1+\sqrt{\beta}\right)^2 \text{SNR}} \right) \right] = P_{\text{out}} \right\} \tag{3.46}$$

where P_{out} is the desired outage probability and $\gamma_{\max}^2$ is a random variable. In general, the finite aperture margin will be a function of outage probability; requiring a smaller outage probability will increase the required finite aperture power margin.

Corollary 3 *The finite aperture power margin at a specific outage probability P_{out} for wavefront predistortion is:*

$$\begin{aligned} m &= \frac{1}{1 - \frac{\left(\frac{1}{\sqrt{n_{tx}}}+\frac{1}{\sqrt{n_{rx}}}\right)^{1/3}}{1+\sqrt{\frac{n_{tx}}{n_{rx}}}} \left(12 \log\left(\frac{1}{P_{\text{out}}}\right)\right)^{1/3}} \\ &\approx 1 + \frac{\left(\frac{1}{\sqrt{n_{tx}}}+\frac{1}{\sqrt{n_{rx}}}\right)^{1/3}}{1+\sqrt{\frac{n_{tx}}{n_{rx}}}} \left(12 \log\left(\frac{1}{P_{\text{out}}}\right)\right)^{1/3}, n_{tx}, n_{rx} \gg 1 \end{aligned} \tag{3.47}$$

To gain additional insight, we look at the specific case where $n = n_{tx} = n_{rx}$, a balanced system:

$$\begin{aligned} m &= \frac{1}{1 - \left(\frac{3}{\sqrt{n}} \log\left(\frac{1}{P_{\text{out}}}\right)\right)^{1/3}} \\ &\approx 1 + \left(\frac{3}{\sqrt{n}} \log\left(\frac{1}{P_{\text{out}}}\right)\right)^{1/3}, n_{tx}, n_{rx} \gg 1 \end{aligned} \tag{3.48}$$

Proof. Starting from the definition of finite aperture power margin,

$$m = \arg_m \left\{ \Pr \left[Q\left(\sqrt{(2\gamma_{\max}^2 \mathrm{SNR})\, m} \right) \geq Q\left(\sqrt{2\left(1+\sqrt{\beta}\right)^2 \mathrm{SNR}} \right) \right] = P_{\text{out}} \right\} \tag{3.49}$$

Simplifying we get:

$$F_{\gamma_{\max}^2}\left(\frac{\mu_{n_{tx}n_{rx}}}{m} \right) = P_{\text{out}} \tag{3.50}$$

where $F_{\gamma_{\max}^2}$ is the cdf of the maximum squared singular value and $\mu_{n_{tx}n_{rx}} = \left(1+\sqrt{\beta}\right)^2$. While we know $F_{\gamma_{\max}^2}$ from Theorem 3, we will instead use the approximation for $F_{\gamma_{\max}^2}$ in Corollary 1:

$$P_{\text{out}} = exp\left(-\frac{1}{12} \left| \frac{\mu_{n_{tx}n_{rx}}}{\sigma_{n_{tx}n_{rx}}} \left(\frac{1}{m} - 1 \right) \right|^3 \right) \tag{3.51}$$

where $\sigma_{n_{tx}n_{rx}} = \frac{\left(\frac{1}{\sqrt{n_{tx}}}+\frac{1}{\sqrt{n_{rx}}}\right)^{1/3}}{1+\sqrt{\frac{n_{tx}}{n_{rx}}}}$. Solving for m proves the corollary. Equation (3.48) is then found by using $n = n_{tx} = n_{rx}$. $\square$

As we would expect, finite aperture power margin is not a function of SNR. This implies that the amount of power margin required to achieve turbulence-free equivalent performance does not depend on the SNR, only the number of apertures and the desired outage probability. An interesting interpretation of the finite aperture power margin is this: it is the *value*, in terms of transmit power, of adding additional apertures.

Figure 3-6 shows Corollary 3 for a balanced system as a function of the number of receive apertures for various outage probabilities. In the figure, we show only the finite aperture power margin in the regime where the corollary is applicable. When operating around $n \approx \log_e(1/P_{\text{out}})$ adding additional apertures greatly reduces required transmit power: each additional transmit has a high power value. However, as the number of apertures becomes large $n \gg \log_e(1/P_{\text{out}})$, adding additional apertures reduces the required transmit power quite slowly, as $1/n^{1/6}$: each additional transmitter has a low power value.

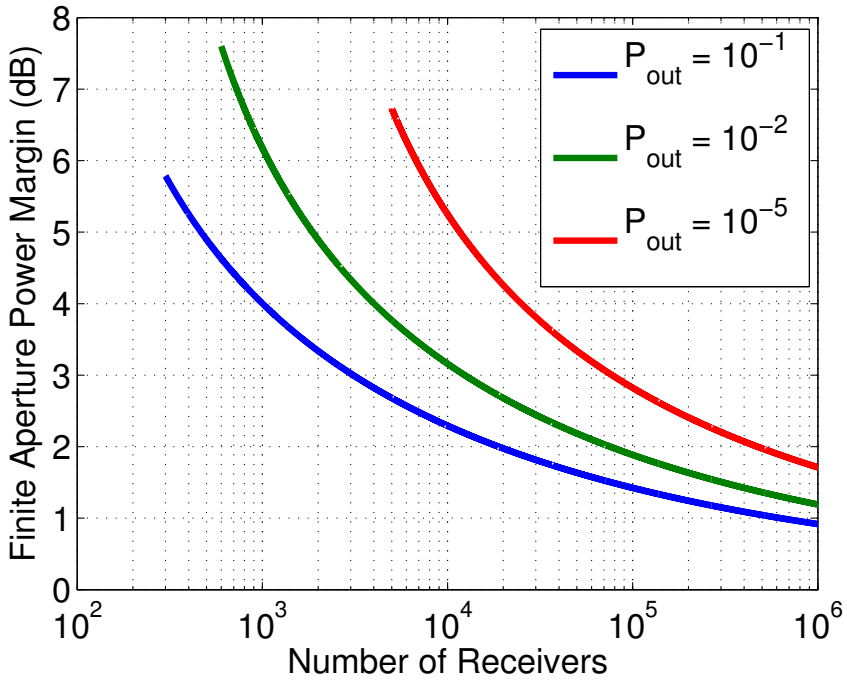

Figure 3-6: Finite aperture power margin: Finite aperture power margin for balanced wavefront predistortion system versus number of receive apertures for various outage probabilities.

Finite Analysis: Average BER, Outage BER, and Finite Aperture Power Margin

Thus far, we have presented results for systems with a large number of transmit and receive apertures. While the large number of apertures results provide important insights and design intuition, we also wish to calculate the performance of systems with $n_{tx} = n_{rx} = 1$ and $n_{tx} = n_{rx} = 2$. While these results are not as clean, and are much more difficult to interpret, they provide an end point for the asymptotic results. In this subsection, we calculate average BER, outage probability, and finite aperture power margin for systems with a small number of apertures ($n_{tx} = n_{rx} < 3$).

Single Aperture System For the single aperture system, $n_{tx} = n_{rx} = 1$, the exact average BER is given by:

$$\begin{aligned}\mathbb{E}_h[\Pr(\text{error})] &= \int_0^\infty \Pr(\text{error}|s) f_{|h|^2}(s) ds \\ &= \int_0^\infty Q(\sqrt{2\text{SNR}s}) \frac{1}{s\sqrt{8\pi\sigma_\chi^2}} \exp\left(\frac{-\left(\log s + 2\sigma_\chi^2\right)^2}{8\sigma_\chi^2}\right) ds\end{aligned} \tag{3.52}$$

where h is the turbulence state matrix $\mathbf{H}$ when there is only a single element. This expression must be calculated via numeric integration, which fails to provide any insights about the dependencies. Here we provide the following closed-form approximation:

Theorem 4 *The average bit error rate for a single aperture system is:*

$$\mathbb{E}_h[\Pr(\text{error})] \approx Q\left(\frac{1}{2\sigma_\chi} \log \text{SNR} - \sigma_\chi\right) \tag{3.53}$$

Proof. From the definition of average BER, we have:

$$\begin{aligned}\mathbb{E}_h[\Pr(\text{error})] &= \int_0^\infty \Pr(\text{error}|s) f_{|h|^2}(s) ds \\ &= \int_0^{s^*} \Pr(\text{error}|s) f_{|h|^2}(s) ds + \int_{s^*}^\infty P(\text{error}|s) f_{|h|^2}(s) ds\end{aligned} \tag{3.54}$$

If a system is in a deep fade, say $|h|^2\text{SNR} < 1$, we would expect a very high BER. Conversely, if a system is not experiencing a deep fade, $|h|^2\text{SNR} > 1$, we would expect a very low BER. Following that intuition, we now make the approximation that there will always be an error in a deep fade, $\Pr(\text{error}|s) = 1/2, \forall s < s*$, and it never makes an error when not in a deep fade, $\Pr(\text{error}|s) = 0, \forall s > s*$. Setting $s^* = 1/\text{SNR}$, we find:

$$\begin{aligned}\mathbb{E}_h[\Pr(\text{error})] &\approx \int_0^{1/\text{SNR}} (1/2) f_{|h|^2}(s) ds \\ &= (1/2) F_{|h|^2}(1/\text{SNR})\end{aligned} \tag{3.55}$$

Using the lognormal model of atmospheric turbulence, we prove the theorem. □

Because the approximation is so coarse, this theorem is not useful for calculating exact BER. It does capture the interplay between the turbulence strength σ_χ and SNR. Next we present a closed-form expression for the outage probability of the single aperture system.

Theorem 5 *The probability of outage for a single aperture system is [29]:*

$$P_{\text{out}} = Q\left(\frac{1}{2\sigma_\chi}\log\left(\frac{2\text{SNR}}{\left(Q^{-1}(P^*)\right)^2}\right) - \sigma_\chi\right) \tag{3.56}$$

Proof. From the definition of outage probability, we write:

$$\begin{aligned} P_{\text{out}} &= \Pr\left(Q\left(\sqrt{2\text{SNR}|h|^2}\right) \geq P^*\right) \\ &= \Pr\left(|h|^2 \leq \frac{\left(Q^{-1}(P^*)\right)^2}{2\text{SNR}}\right) \\ &= F_{|h|^2}\left(\frac{\left(Q^{-1}(P^*)\right)^2}{2\text{SNR}}\right) \end{aligned} \tag{3.57}$$

where P^* is the desired BER and $F_{|h|^2}(\cdot)$ is the cdf of $|h|^2$. Noting that $|h|^2$ is log-normally distributed, $|h|^2 = e^\chi$ where $\chi \sim \mathcal{N}\left(-2\sigma_\chi^2, 4\sigma_\chi^2\right)$, we prove the theorem. □

Finally, we calculate the finite aperture power margin for the single aperture system. The finite aperture power margin, in this case, is the multiplicative power increase required for the single sparse aperture system to perform at least as well as the infinite sparse aperture system, at least P_{out} fraction of the time.

Corollary 4 *The finite aperture power margin m for the single aperture system is given by:*

$$m = \left(1 + \sqrt{\beta}\right)^2 e^{2\sigma_\chi^2 + 2\sigma_\chi Q^{-1}(P_{\text{out}})} \tag{3.58}$$

where β is the ratio of the number of transmit apertures to receive apertures for the comparison infinite sparse aperture system.

Proof. We begin with the definition of the finite aperture power margin:

$$m = \arg_m \left\{ \Pr \left[Q\left(\sqrt{(2|h|^2 \mathrm{SNR})\, m} \right) \geq Q\left(\sqrt{2\left(1+\sqrt{\beta}\right)^2 \mathrm{SNR}} \right) \right] = P_{\text{out}} \right\} \tag{3.59}$$

Simplifying gives:

$$m = \arg_m \left\{ \Pr \left[|h|^2 \leq \frac{\left(1+\sqrt{\beta}\right)^2}{m} \right] = P_{\text{out}} \right\} \tag{3.60}$$

Using the cdf for $|h|^2$ from Theorem 5 gives:

$$P_{\text{out}} = Q\left(\frac{1}{2\sigma_\chi} \log\left(\frac{m}{\left(1+\sqrt{\beta}\right)^2} \right) - \sigma_\chi \right) \tag{3.61}$$

Solving for m proves the corollary. □

Figure 3-7 shows the finite aperture power margin for a single aperture transmit and receive system versus desired BER for various values of turbulence strength. As expected, the margin increases as the desired BER becomes smaller. In stronger turbulence, the margin increases faster as the desired BER becomes smaller. This is intuitively satisfying, diversity has a larger impact in strong turbulence and a smaller impact in weak turbulence.

Multiple Transmit, Multiple Receive Aperture System The analysis of the multiple transmit aperture, multiple receive aperture system is considerably more challenging than the analysis of the one transmit aperture, one receive aperture system. Accordingly, we will focus on the most important and relevant of the metrics: outage probability. The following outage probability upper and lower bound are valid for any number of transmit and receive apertures.

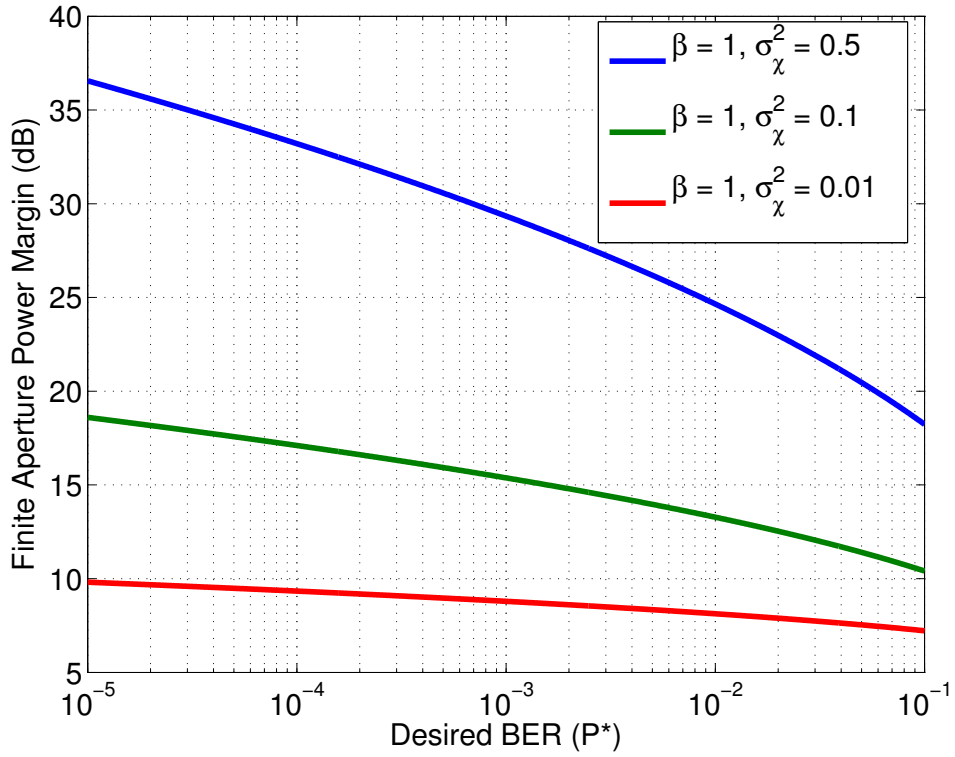

Figure 3-7: Finite aperture power margin: Finite aperture power margin for single aperture transmit and receive system versus desired BER for various values of σ_χ^2.

Theorem 6 *The probability of outage for a multiple transmit aperture, multiple receive aperture system with wavefront predistortion is lower and upper bounded by:*

$$Q\left(\frac{\log\left(\frac{n_{tx}^2 n_{rx}^2}{e^{4\sigma_\chi^2}-1+n_{tx}n_{rx}}\right)-\log\left(\frac{\mathrm{SNR}}{n_{\min}n_{rx}(Q^{-1}(P^*))^2}\right)}{\sqrt{\log\left(\frac{e^{4\sigma_\chi^2}-1}{n_{rx}n_{tx}}+1\right)}}\right)\leq P_{\mathrm{out}}(P^*)$$
$$P_{\mathrm{out}}(P^*)\leq Q\left(\frac{\log\left(\frac{n_{tx}^2 n_{rx}^2}{e^{4\sigma_\chi^2}-1+n_{tx}n_{rx}}\right)-\log\left(\frac{\mathrm{SNR}}{n_{rx}(Q^{-1}(P^*))^2}\right)}{\sqrt{\log\left(\frac{e^{4\sigma_\chi^2}-1}{n_{rx}n_{tx}}+1\right)}}\right) \tag{3.62}$$

Proof. We wish to find the squared singular values of $\frac{1}{\sqrt{n_{rx}}}\mathbf{H}$ or, equivalently, the eigenvalues of $\frac{1}{n_{rx}}\mathbf{H}^\dagger\mathbf{H}$. We begin by upper and lower bounding the maximum eigenvalue of $\mathbf{H}^\dagger\mathbf{H}$:

$$\frac{1}{n_{\min}}\mathrm{Tr}\left(\mathbf{H}^\dagger\mathbf{H}\right)\leq\gamma_{\max}^2\left(\mathbf{H}^\dagger\mathbf{H}\right)\leq\mathrm{Tr}\left(\mathbf{H}^\dagger\mathbf{H}\right) \tag{3.63}$$

where $n_{\min} = \min(n_{tx}, n_{rx})$ and $\gamma^2_{\max}\left(\mathbf{H}^\dagger\mathbf{H}\right)$is the maximum eigenvalue of $\mathbf{H}^\dagger\mathbf{H}$. We have used that, for a symmetric matrix, the maximum eigenvalue must be less than the sum of the eigenvalues and that the maximum eigenvalue must be more than the average non-zero eigenvalue. Relating the maximum eigenvalue of $\gamma^2_{\max}\left(\mathbf{H}^\dagger\mathbf{H}\right)$ to the maximum eigenvalue of $\gamma^2_{\max}\left(\frac{1}{n_{rx}}\mathbf{H}^\dagger\mathbf{H}\right)$, $\gamma^2_{\max}\left(\mathbf{H}^\dagger\mathbf{H}\right) = n_{rx}\gamma^2_{\max}\left(\frac{1}{n_{rx}}\mathbf{H}^\dagger\mathbf{H}\right)$, we arrive at:

$$\frac{1}{n_{\min}}\mathrm{Tr}\left(\mathbf{H}^\dagger\mathbf{H}\right) \leq n_{rx}\gamma^2_{\max} \leq \mathrm{Tr}\left(\mathbf{H}^\dagger\mathbf{H}\right) \tag{3.64}$$

Using the definition of the trace operation we arrive at the following bound:

$$\frac{1}{n_{\min}}\sum_{\mathsf{k}=1}^{n_{tx}}\sum_{\mathsf{j}=1}^{n_{rx}}|h_{\mathsf{kj}}|^2 \leq n_{rx}\gamma^2_{\max} \leq \sum_{\mathsf{k}=1}^{n_{tx}}\sum_{\mathsf{j}=1}^{n_{rx}}|h_{\mathsf{kj}}|^2 \tag{3.65}$$

Since the log amplitude of the channel state is normally distributed, we approximate the summation as also being log normal:

$$\left(\sum_{\mathsf{k}=1}^{n_{tx}}\sum_{\mathsf{j}=1}^{n_{rx}}|h_{\mathsf{kj}}|^2\right) \sim \mathrm{Log}{-}\mathcal{N}\left(\log\left(\frac{8}{\sqrt{e^{4\sigma_\chi^2}+3}}\right), \log\left[\frac{e^{4\sigma_\chi^2}+3}{4}\right]\right) \tag{3.66}$$

where we have used that $|h_{\mathsf{kj}}|^2 \sim \mathrm{Log}{-}\mathcal{N}\left(-2\sigma_\chi^2, 4\sigma_\chi^2\right)$ and that z, the sum of n independent identically distributed log normal random variables with mean μ and variance σ^2, is distributed as [41]:

$$z \sim \mathrm{Log}{-}\mathcal{N}\left(\log n + \mu + \frac{\sigma^2}{2} - \frac{1}{2}\log\left[\frac{e^{\sigma^2}-1}{n}+1\right], \log\left[\frac{e^{\sigma^2}-1}{n}+1\right]\right) \tag{3.67}$$

Finally, the bound on the outage probability is established by the definition of outage probability:

$$\Pr\left(\gamma^2_{\max} \leq \frac{n_{\min}n_{rx}(Q^{-1}(P^*))^2}{\mathrm{SNR}}\right) \leq P_{\mathrm{out}}(P^*) \leq \Pr\left(\gamma^2_{\max} \leq \frac{n_{rx}(Q^{-1}(P^*))^2}{\mathrm{SNR}}\right) \tag{3.68}$$

□

To validate the upper and lower bound on outage probability for a multiple transmit aperture, multiple receive aperture sparse aperture system, we calculated the

outage probability using a Monte Carlo simulation of a two transmit aperture, two receive aperture system. For the simulation, we randomly generated many atmospheric states, calculated the largest squared singular value for each state, and used the results to calculate the outage probability. Figure 3-8 shows the results of the simulation along with the upper and lower bound on outage probability presented in Theorem 6. For the figure, $\sigma_\chi^2 = 0.2$ and SNR $= 1$.

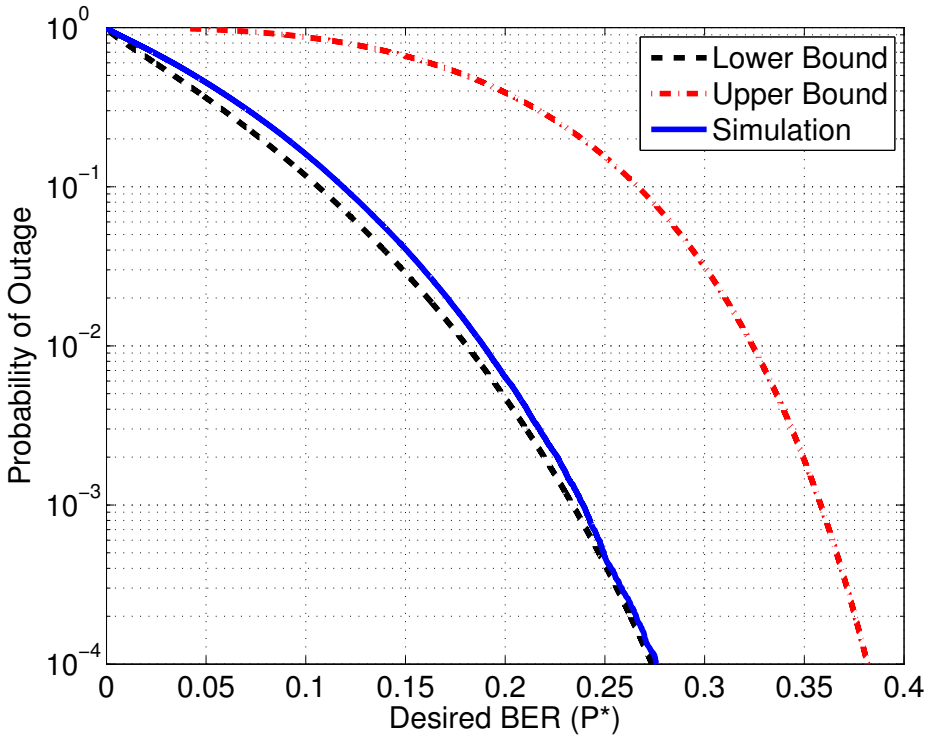

Figure 3-8: Probability of outage versus desired BER, P^*, for a two transmit aperture two receive aperture system: This figure shows the outage probability for a simulated two transmit aperture by two receive aperture system along with the upper and lower bound on outage probability presented in Theorem 6. For the figure, $\sigma_\chi^2 = 0.2$ and SNR $= 1$.

From the simulation, it is clear that the lower bound on outage probability is much tighter than the upper bound. Generally, for system geometries with $n_{tx} < 5$ and $n_{rx} < 5$, the lower bound will be tight. As a result, we use the lower bound to calculate the finite aperture power margin. The finite aperture power margin, in this case, is the multiplicative power increase required for the multiple transmit aperture,

multiple receive aperture sparse aperture system to perform at least as well as the infinite sparse aperture system, at least P_{out} fraction of the time.

Corollary 5 *The finite aperture power margin m for sparse aperture systems with fewer than five transmit apertures and fewer than five receive apertures is given by:*

$$m = n_{rx}\left(1+\sqrt{\beta}\right)^2 \exp\left(\log\left(\frac{e^{4\sigma_\chi^2}-1+n_{tx}n_{rx}}{n_{tx}^2 n_{rx}^2}\right) + Q^{-1}(P_{\text{out}})\sqrt{\log\left(\frac{e^{4\sigma_\chi^2}-1}{n_{tx}n_{rx}}+1\right)}\right) \tag{3.69}$$

where β is the ratio of the number of transmit apertures to receive apertures for the comparison infinite sparse aperture system.

Proof. We begin with the definition of the finite aperture power margin:

$$m = \arg_m\left\{\Pr\left[Q\left(\sqrt{(2\gamma_{\max}^2\text{SNR})\,m}\right) \geq Q\left(\sqrt{2\left(1+\sqrt{\beta}\right)^2\text{SNR}}\right)\right] = P_{\text{out}}\right\} \tag{3.70}$$

Simplifying gives:

$$m = \arg_m\left\{\Pr\left[\gamma_{\max}^2 \leq \frac{\left(1+\sqrt{\beta}\right)^2}{m}\right] = P_{\text{out}}\right\} \tag{3.71}$$

Using the cdf for $\gamma_{\max}^2$ from Theorem 6 gives:

$$P_{\text{out}} = Q\left(\frac{\log\left(\frac{n_{tx}^2 n_{rx}^2}{e^{4\sigma_\chi^2}-1+n_{tx}n_{rx}}\right) + \log\left(\frac{m}{n_{rx}\left(1+\sqrt{\beta}\right)^2}\right)}{\sqrt{\log\left(\frac{e^{4\sigma_\chi^2}-1}{n_{rx}n_{tx}}+1\right)}}\right) \tag{3.72}$$

Solving for m proves the corollary. □

Figure 3-9 shows the finite aperture power margin for a two aperture transmit and two receive system versus desired BER for various values of turbulence strength. As expected, the margin increases as the desired BER becomes smaller. In stronger turbulence, the margin increases faster as the desired BER becomes smaller. This is intuitively satisfying, diversity has a larger impact in strong turbulence and a smaller impact in weak turbulence.

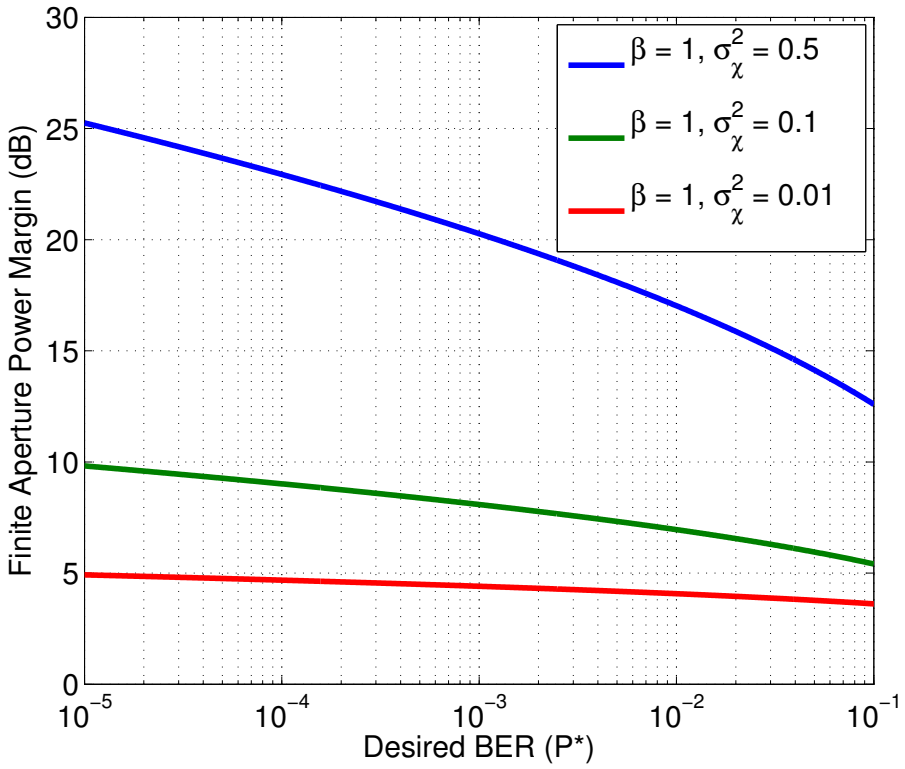

Figure 3-9: Finite aperture power margin: Finite aperture power margin for two aperture transmit and two receive system versus desired BER for various values of σ_χ^2.

Finite Aperture Power Margin

We conclude this subsection on the performance of the sparse aperture system with wavefront predistortion by comparing the margin results for both the finite and asymptotic analysis. Figure 3-10 shows the finite aperture power margin for balanced wavefront predistortion system versus number of receive apertures for various outage probabilities. This figure shows results for:

- a one transmit aperture and one receive aperture system
- a two transmit aperture and two receive aperture system
- a three transmit aperture and three receive aperture system
- an asymptotically many transmit and receive apertures system

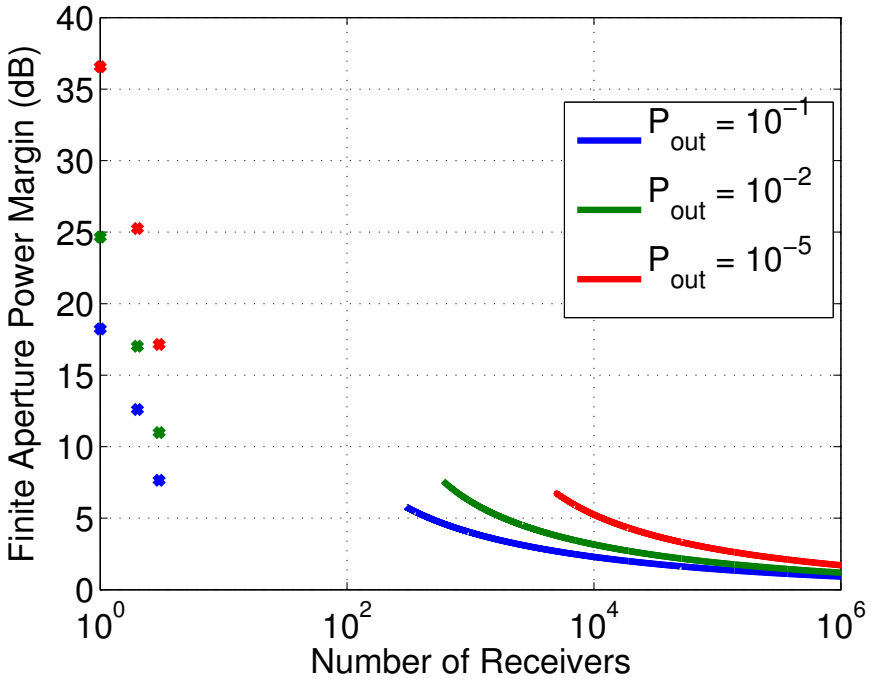

Figure 3-10: Finite aperture power margin: Finite aperture power margin for balanced wavefront predistortion system versus number of receive apertures for various outage probabilities. This figure shows the finite results with $\sigma_\chi^2 = 0.5$ along with the asymptotic results.

From the figure, we see that diversity can decrease the necessary power required to achieve 10^{-5} outage performance by more than 35 dB compared to a single transmit/receive aperture system. Relative to a single transmit/receive aperture system, a two transmit/two receive aperture system requires 10 dB less power to achieve the same 10^{-5} outage performance. Relative to a single transmit/receive aperture system, a three transmit/three receive aperture system requires 20 dB less power to achieve the same 10^{-5} outage performance.

3.1.2 Selection Transmit Diversity

Another scheme, termed selection transmit diversity, is to allocate all transmit power to the transmit aperture that will minimize the instantaneous bit error rate. This scheme is attractive because no phase control is necessary and the power only needs to be switched. The wavefront predistortion scheme required both phase control

and power splitting between all transmit apertures. Additionally, only an integer from $1 \ldots n_{tx}$ needs to be relayed to the transmitter; the feedback link can be very low rate. The following provides the transmission and demodulation scheme that minimizes BER for selection transmit diversity:

Definition 1 *The BER minimizing power allocation for the selection transmit diversity is:*

$$\vec{x}_s = \begin{cases} 1 & \mathsf{k} = \mathsf{k}^* \\ 0 & \mathsf{k} \neq \mathsf{k}^* \end{cases} \quad \forall \mathsf{k} \in 1..n_{tx} \tag{3.73}$$

Where k^* *is the transmitter associated with the maximum received power:*

$$\mathsf{k}^* = \arg\max_{\mathsf{k}} \|\vec{h}_{\mathsf{k}}\|^2 \tag{3.74}$$

where $\|\vec{h}_{\mathsf{k}}\|^2$ *is the norm squared of the* k^{th} *column of the channel transfer matrix* $\mathbf{H}$*. We define* $\vec{h}_{\max}$ *to be the channel transfer matrix column associated with* k^**:*

$$\vec{h}_{\max} = \vec{h}_{\mathsf{k}^*} = \max_{\mathsf{k}} \|\vec{h}_{\mathsf{k}}\|^2 \tag{3.75}$$

A spatially matched filter is the optimal receiver. Thus we can form a sufficient statistic ϕ*:*

$$\phi = \frac{1}{\|\vec{h}_{\max}\|} Re\left\{\vec{h}_{\max}^{\dagger}\vec{y}\right\} \tag{3.76}$$

where the normalization is selected such that:

$$\left\| \frac{\vec{h}_{\max}}{\|\vec{h}_{\max}\|} \right\|^2 = 1 \tag{3.77}$$

Proof. Here we show that this transmit scheme minimizes the BER among possible selection diversity techniques.

$$\begin{aligned}\mathsf{k}^* &= \arg\min_{|\phi_s|^2} Q\left(\sqrt{\frac{2\mathrm{SNR}}{n_{rx}}|\phi_s|^2}\right) \\ &= \arg\min_{\mathsf{k}=1\ldots n_{tx}} Q\left(\sqrt{\frac{2\mathrm{SNR}}{n_{rx}}\|h_{\mathsf{k}}\|^2}\right) \\ &= \arg\max_{\mathsf{k}=1\ldots n_{tx}} \|h_{\mathsf{k}}\|^2\end{aligned} \tag{3.78}$$

where ϕ_s is the signal portion of the sufficient statistic. Thus we have proved that, among selection diversity techniques, allocating power to the transmitter associated with the maximum received power minimizes BER. □

While the selection transmitter is less complex and the feedback rate is smaller for selection transmit diversity compared to wavefront predistortion diversity, its performance in terms of average BER and outage probability is significantly reduced. Theorem 7 and 8 quantify the performance of this suboptimal scheme.

Theorem 7 *For uncoded binary phase shift keying with selection transmit diversity, the probability of error averaged over all atmospheric states, converges almost surely as the number of transmit and receive apertures gets very large to:*

$$\lim_{n_{tx},n_{rx}\to\infty} \mathbb{E}_{\mathbf{H}}\left[P_e\right] = Q\left(\sqrt{2\mathrm{SNR}\left(1+\sqrt{\frac{\alpha\log\left(n_{tx}\right)}{n_{rx}}}\right)}\right) \tag{3.79}$$

where $\alpha = 2\left(e^{4\sigma_\chi^2}-1\right)$.

Proof. The average error probability is given by the following expression:

$$\mathbb{E}_{\mathbf{H}}\left[P_e\right] = \int_{-\infty}^{\infty} f_{|\phi_s|^2}(s) Q\left(\sqrt{2\mathrm{SNR}s}\right) ds \tag{3.80}$$

where $f_{|\phi_s|^2}(s)$ is the probability density function of the signal part of the sufficient statistic, $|\phi_s|^2 = \frac{1}{n_{rx}}\|\vec{h}_{\max}\|^2$. Therefore, we must find the distribution of $\frac{1}{n_{rx}}\|\vec{h}_{\max}\|^2$.

First we note that, by central limit theorem, $|\phi_s|^2$ is approximately Gaussian:

$$|\phi_s|^2 = \frac{1}{n_{rx}}\|\vec{h}_{\mathsf{k}}\|^2 \sim \mathcal{N}\left(1, \sqrt{\frac{\left(e^{4\sigma_\chi^2}-1\right)}{n_{rx}}}\right) \tag{3.81}$$

We define ξ_{k} as:

$$\xi_{\mathsf{k}} = \frac{\frac{1}{n_{rx}}\|h_{\mathsf{k}}\|^2 - 1}{\sqrt{\frac{1}{n_{rx}}\left(e^{4\sigma_\chi^2}-1\right)}} \tag{3.82}$$

where we have chosen the particular normalization such that $\xi_{\mathsf{k}} \sim \mathcal{N}(0,1)$. With probability one, the maximum of $(\xi_1, \ldots, \xi_{n_{tx}})$, is $\sqrt{2\log n_{tx}}$ [13]:

$$\begin{aligned} &\Pr\left(\lim_{n_{tx}\to\infty}(2\log(n_{tx}))^{-1/2}\max_{1<\mathsf{k}\leq n_{tx}}\xi_{\mathsf{k}} = 1\right) = 1 \\ &\to \Pr\left(\lim_{n_{tx}\to\infty}(2\log(n_{tx}))^{-1/2}\max_{1<\mathsf{k}\leq n_{tx}}\frac{\frac{1}{n_{rx}}\|\vec{h}_{\mathsf{k}}\|^2 - 1}{\sqrt{\frac{1}{n_{rx}}\left(e^{4\sigma_\chi^2}-1\right)}} = 1\right) = 1 \end{aligned} \tag{3.83}$$

Solving for $\frac{1}{n_{rx}}\|h_{\mathsf{k}}\|^2$ indicates that the pdf of $f_{|\phi_s|^2}(s)$ converges almost surely to:

$$f_{|\phi_s|^2}(s) = \delta\left(s - \left(1 + \sqrt{2\left(e^{4\sigma_\chi^2}-1\right)\frac{\log n_{tx}}{n_{rx}}}\right)\right) \tag{3.84}$$

Because of the sifting property of the Dirac delta, we arrive at the following expression for average error probability:

$$\begin{aligned} \lim_{n_{tx}\to\infty}\mathbb{E}_{\mathbf{H}}\left[P_e\right] &= \lim_{n_{tx}\to\infty}\int_{-\infty}^{\infty} f_{|\phi_s|^2}(s)Q\left(\sqrt{2\mathrm{SNR}s}\right)ds \\ &= \int_{-\infty}^{\infty}\delta\left(s - \left(1 + \sqrt{2\left(e^{4\sigma_\chi^2}-1\right)\frac{\log n_{tx}}{n_{rx}}}\right)\right)Q\left(\sqrt{2\mathrm{SNR}s}\right)ds \\ &= Q\left(\sqrt{2\mathrm{SNR}\left(1 + \sqrt{2\left(e^{4\sigma_\chi^2}-1\right)\frac{\log\left(n_{tx}\right)}{n_{rx}}}\right)}\right) \end{aligned} \tag{3.85}$$

□

We note that the average power gain due the feedback link is much lower for selection transmit diversity than for wavefront predistortion diversity. Specifically,

the average power gain due to feedback for selection transmit diversity increases proportional to $\sqrt{\log(n_{rx})}$ while the average power gain due to feedback for wavefront predistortion increases proportional to n_{tx}. As such, the wavefront predistortion system performs much better than the selection transmit diversity scheme. Next we find the outage probability for selection transmit diversity.

Theorem 8 *For uncoded binary phase shift keying with optimal selection transmit diversity, the probability of outage converges almost surely as the number of transmit and receive apertures gets very large to:*

$$\begin{aligned} P_{\text{out}}(s) &= \left(Q\left(-\sqrt{\frac{n_{rx}}{(e^{4\sigma_\chi^2}-1)}}\,(s-1) \right) \right)^{n_{tx}} \\ &\leq \frac{1}{2^{n_{tx}}} exp\left(\frac{-n_{tx}n_{rx}(s-1)^2}{2\left(e^{4\sigma_\chi^2}-1\right)} \right), \forall s \ll 1 \end{aligned} \tag{3.86}$$

where $s = (Q^{-1}(P^*))^2/2\text{SNR}$ *for a desired outage threshold* P^*.

Proof. With the spatial matched filter, the outage probability is:

$$\begin{aligned} P_{\text{out}}(P^*) &= Pr\left(Q\left(\sqrt{\frac{2\text{SNR}}{n_{rx}}\|\vec{h}_{\max}\|^2} \right) \geq P^* \right) \\ &= Pr\left(\frac{1}{n_{rx}}\|\vec{h}_{\max}\|^2 \leq \frac{Q^{-1}(P^*)}{2\text{SNR}} \right) \end{aligned} \tag{3.87}$$

Using the change of variables $s = (Q^{-1}(P^*))^2/2\text{SNR}$ gives:

$$\begin{aligned} P_{\text{out}}(s) &= Pr\left(\|\vec{h}_{\max}\|^2 \leq s \right) \\ &= Pr\left(\|\vec{h}_1\|^2 \leq s, \|\vec{h}_2\|^2 \leq s, ..., \|\vec{h}_{n_{tx}}\|^2 \leq s \right) \\ &= \left[Pr\left(\|\vec{h}_1\|^2 \leq s \right) \right]^{n_{tx}} \end{aligned} \tag{3.88}$$

where we have used the fact that the random variable $\|\vec{h}_{\mathsf{k}}\|^2$ is iid for all k. Substituting in the definition of $\|\vec{h}_1\|^2$, we get:

$$P_{\text{out}}(s) = \left[\Pr\left(\frac{1}{n_{rx}}\sum_{\mathsf{j}=1}^{n_{rx}}|h_{1\mathsf{j}}|^2 \leq s\right)\right]^{n_{tx}} \tag{3.89}$$

While there is no closed-form expression for the distribution of $\sum_{\mathsf{j}=1}^{n_{rx}}|h_{1\mathsf{j}}|^2$, we can apply the central limit theorem as the number of receive apertures becomes large:

$$\frac{1}{n_{rx}}\sum_{\mathsf{j}=1}^{n_{rx}}|h_{1\mathsf{j}}|^2 \sim \mathcal{N}\left(1, \sqrt{\frac{e^{4\sigma_\chi^2}-1}{n_{rx}}}\right) \tag{3.90}$$

The resulting outage probability is then:

$$P_{\text{out}}(s) = \left(\frac{1}{2}\text{erfc}\left(-\sqrt{\frac{n_{rx}}{2(e^{4\sigma_\chi^2}-1)}}\,(s-1)\right)\right)^{n_{tx}} \tag{3.91}$$

where erfc is the complementary error function. Finally, using the Chernoff bound of the Q-function, $Q(x) \leq \frac{1}{2}\exp(-x^2/2)$ we arrive at the bound on outage performance. □

The bound presented in Theorem 8 is only good for $s \ll 1$, which corresponds to a low outage probability region. This bound shows that the product $n_{tx} \times n_{rx}$ is what governs how fast the outage probability falls off. From the exact expression, we see that the number of receive apertures only interacts through the error function, thus increasing the number of receive apertures does not change the average probability of error. Increasing the number of receive apertures does, however, exponentially decrease the outage probability for any $P^* > \mathbb{E}[P]$. Physically, we see that increasing the number of receive apertures tends to average out the turbulence thus reducing the probability of outage while not increasing the average power received. As a result, average probability of error is not a function of the number of receive apertures.

The number of transmit apertures interacts by exponentiating the entire expression. Therefore, we see that increasing the number of transmit apertures both de-

creases the average probability of error and decreases the average probability of outage. Physically this decrease in both average and outage probability is reasonable:

- *decrease outage probability:* increasing the number of transmit apertures, each seeing independent channel states, decreases the likelihood the system will experience a deep fade.

- *decrease average probability of error:* because the system allocates all of its power to the transmitter with the best performance, increasing the number of transmit apertures increases the likelihood that the system will have a transmitter with exceptional performance. Because the performance gain depends on transmit apertures with performance in the tails of the distribution, the decrease in average BER resulting from increasing the number of transmit apertures is generally very slow.

Finally, we define *selection transmit diversity power margin* as the multiplicative power increase required for the finite sparse aperture system with the use of section transmit diversity to perform at least as well as the infinite sparse aperture system with the use of wavefront predistortion, at least P_{out} fraction of the time. Thus, selection transmit diversity power margin is a comparison between a finite aperture selection diversity system and an infinite aperture wavefront predistortion system.

Corollary 6 *The selection transmit diversity power margin at a specific outage probability* P_{out} *is:*

$$m = \frac{\left(1 + \sqrt{\frac{n_{tx}}{n_{rx}}}\right)^2}{1 + Q^{-1}\left(P_{\text{out}}^{1/n_{tx}}\right)\sqrt{\frac{e^{4\sigma_\chi^2}-1}{n_{rx}}}} \tag{3.92}$$

Proof. Starting from the definition of diversity power margin,

$$m = \arg_m \left\{ \Pr\left[Q\left(\sqrt{\left(\frac{2\|\vec{h}_{\max}\|^2}{n_{rx}} \text{SNR} \right) m} \right) \geq Q\left(\sqrt{2\left(1+\sqrt{\beta}\right)^2 \text{SNR}} \right) \right] = P_{\text{out}} \right\} \tag{3.93}$$

Simplifying we get:

$$F_{\|\vec{h}_{\max}\|^2}\left(\frac{(1+\sqrt{\frac{n_{rx}}{n_{tx}}})^2}{m}\right) = P_{\text{out}} \tag{3.94}$$

where $F_{\|\vec{h}_{\max}\|^2}$ is the cdf of $\frac{\|\vec{h}_{\max}\|^2}{n_{rx}}$. Using the cdf for $\|\vec{h}_{\max}\|^2$ from Theorem 8 and solving for m proves the corollary. $\square$

We defer the comparison of the wavefront predistortion margin and selection transmit margin to Subsection 3.1.4 and now continue to analyze the sparse aperture system without feedback.

3.1.3 Open Loop Transmitter Diversity

If the feedback link is broken, not set up yet, or has a delay that exceeds the atmospheric coherence time, the transmitter will have no channel state information. This situation represents a lower limit on diversity system performance. In this subsection, we define the optimal communication scheme with no transmitter channel state information and give average and outage performance. First, we describe the communication scheme.

Definition 2 *Because the transmitter has no channel state information, an optimal transmission scheme is simply equal power on each transmitter:*

$$x_{\mathsf{k}} = \frac{1}{\sqrt{n_{tx}}} \forall \mathsf{k} \in \{1...n_{tx}\} \tag{3.95}$$

The optimal recombination scheme is a spatial matched filter:

$$\phi = \frac{1}{\|\vec{h}_{\text{sum}}\|} Re\left\{\vec{h}_{\text{sum}}^{\dagger}\vec{y}\right\} \tag{3.96}$$

where we define $\vec{h}_{\text{sum}}$ *as:*

$$\vec{h}_{\text{sum}} = \sum_{\mathsf{j}=1}^{n_{tx}} \vec{h}_{\mathsf{j}} \tag{3.97}$$

where the normalization was chosen such that:

$$\left\| \frac{\vec{h}_{\text{sum}}}{\|\vec{h}_{\text{sum}}\|} \right\|^2 = 1 \tag{3.98}$$

Theorem 9 *For uncoded binary phase shift keying with no channel state information (CSI) at the transmitter, as the number of transmit apertures becomes large the outage probability is:*

$$\lim_{n_{tx}\to\infty} P_{\text{out}}(P^*) = \frac{\gamma\left(n_{rx}, \frac{n_{rx}\left(Q^{-1}(P^*)\right)^2}{2\text{SNR}}\right)}{(n_{rx}-1)!} \tag{3.99}$$

where $\gamma(\cdot,\cdot)$ is the lower incomplete Gamma function given by:

$$\gamma(s,x) = \int_0^x t^{s-1}e^{-t}dt \tag{3.100}$$

We have placed no assumption on the number of receive apertures.

Proof. By definition, the probability of outage for some desired BER P^* is:

$$P_{\text{out}}(P^*) = \Pr\left(Q\left(\sqrt{\frac{2\text{SNR}\|\vec{h}_{\text{sum}}\|^2}{n_{rx}n_{tx}}}\right) > P^*\right) \tag{3.101}$$

Rearranging the terms gives:

$$P_{\text{out}}(P^*) = \Pr\left(\frac{2}{n_{tx}}\|\vec{h}_{\text{sum}}\|^2 < \frac{n_{rx}(Q^{-1}(P^*))^2}{\text{SNR}}\right) \tag{3.102}$$

Thus we must find the cdf of $\frac{2}{n_{tx}}\|\vec{h}_{\text{sum}}\|^2$. Using the definition of $\|\vec{h}_{\text{sum}}\|^2$ we arrive at the following expression:

$$\frac{2}{n_{tx}}\|\vec{h}_{\text{sum}}\|^2 = \sum_{\mathsf{j}=1}^{n_{rx}} \left| \sqrt{\frac{2}{n_{tx}}} \sum_{\mathsf{k}=1}^{n_{tx}} h_{\mathsf{kj}} \right|^2 \tag{3.103}$$

By central limit theorem, as the number of transmit apertures becomes large, the term inside the absolute value squared a circularly symmetric Gaussian random variable:

$$\sqrt{\frac{2}{n_{tx}}}\sum_{\mathsf{k}=1}^{n_{tx}} h_{\mathsf{kj}} \sim \mathcal{CN}\left(0, \frac{1}{2}\right) \tag{3.104}$$

where we have used that the atmosphere does not absorb energy, that the apertures experience independent fades, and that the amplitude fluctuations are approximately uncorrelated from the exponentiated phase fluctuations. We should note that, so long as the number of transmit apertures is large, increasing the number of transmit apertures does not change the distribution of the summation. Thus, the final outage calculations will not depend on the number of transmit apertures. The cdf of $\frac{2}{n_{tx}}\|\vec{h}_{\text{sum}}\|^2$ is distributed as a chi-square distribution with $2n_{rx}$ degrees of freedom.

$$\left|\sqrt{\frac{2}{n_{tx}}}\sum_{\mathsf{k}=1}^{n_{tx}} h_{\mathsf{kj}}\right|^2 \sim \chi^2_2 \tag{3.105}$$

The sum of n independent chi-square random variables with two degrees of freedom is a chi-square distribution with $2n$ degrees of freedom. Consequently, we arrive at the distribution of $\frac{2}{n_{tx}}\|\vec{h}_{\text{sum}}\|^2$:

$$\frac{2}{n_{tx}}\|\vec{h}_{\text{sum}}\|^2 = \sum_{\mathsf{j}=1}^{n_{rx}}\left|\sqrt{\frac{2}{n_{tx}}}\sum_{\mathsf{k}=1}^{n_{tx}} h_{\mathsf{kj}}\right|^2 \sim \chi^2_{2n_{rx}} \tag{3.106}$$

Finally, using the cdf of the chi-square distribution we find the probability of outage:

$$P_{\text{out}}(s) = \frac{\gamma\left(n_{rx}, \frac{n_{rx}(Q^{-1}(P^*))^2}{\text{SNR}}\right)}{\Gamma(n_{rx})} = \frac{\gamma\left(n_{rx}, \frac{n_{rx}(Q^{-1}(P^*))^2}{\text{SNR}}\right)}{(n_{rx}-1)!} \tag{3.107}$$

□

Analysis using the lower incomplete gamma function used to calculate the outage probability of the open loop sparse aperture system is difficult. As a result, in Corollary 7 we present a simplified expression for outage probability that is valid when the number of receive apertures and transmit apertures is very large.

Corollary 7 *For uncoded binary phase shift keying with no CSI at the transmitter, as the number of transmit and receive apertures becomes large, the outage probability is:*

$$\lim_{n_{tx},n_{rx}\to\infty} P_{\text{out}}(P^*) = Q\left(\left(1 - \frac{\left(Q^{-1}\left(P^*\right)\right)^2}{2\text{SNR}}\right)\sqrt{n_{rx}}\right) \tag{3.108}$$

Proof. We prove this corollary in two ways: we can invoke the central limit theorem on the sum of the squared terms in equation (3.103) or we can look at the limiting exact distribution in equation (3.107). Using the second method, we find:

$$\lim_{n_{rx}\to\infty} \frac{\gamma(n_{rx}, sn_{rx})}{(n_{rx}-1)!} = \mathcal{N}^{(cdf)}\left(s; 1, \frac{1}{\sqrt{n_{rx}}}\right) \tag{3.109}$$

where $s = (Q^{-1}(P^*))^2/(2\text{SNR})$. $\square$

We define *open loop diversity power margin* as the multiplicative power increase required for the finite sparse aperture system with transmit and receive diversity with no CSI at the transmitter to perform at least as well as the infinite sparse aperture system using wavefront predistortion, at least P_{out} fraction of the time. Thus, open loop diversity power margin is a comparison between a finite aperture open loop diversity system and an infinite aperture wavefront predistortion system.

Corollary 8 *As the number of transmit apertures becomes large, the open loop diversity power margin at a specific outage probability P_{out} is:*

$$\begin{aligned} m &= \frac{2n_{rx}(1+\sqrt{\frac{n_{tx}}{n_{rx}}})^2}{F^{-1}_{\chi^2}(P_{\text{out}}; 2n_{rx})} \\ &\approx \frac{\left(1+\sqrt{\frac{n_{tx}}{n_{rx}}}\right)^2}{1-\left(\sqrt{1/n_{rx}}\right)Q^{-1}(P_{\text{out}})}, n_{rx} > 20\left(Q^{-1}(P_{\text{out}})\right)^2 \\ &\approx \left(1+\sqrt{\frac{n_{tx}}{n_{rx}}}\right)^2\left(1+\sqrt{\frac{1}{n_{rx}}}Q^{-1}(P_{\text{out}})\right), n_{rx} \gg 20\left(Q^{-1}(P_{\text{out}})\right)^2 \end{aligned} \tag{3.110}$$

where $F^{-1}_{\chi^2}(\,\cdot\,; n)$ is the inverse chi-square distribution with n degrees of freedom.

Proof. Starting from the definition of diversity power margin,

$$\begin{aligned} P_{\text{out}} &= \Pr\left[Q\left(\sqrt{(2\text{SNR}|\phi_s|^2)\,m}\right) \geq Q\left(\sqrt{2\left(1+\sqrt{\beta}\right)^2 \text{SNR}}\right)\right] \\ &= \Pr\left[|\phi_s|^2 \leq \frac{\left(1+\sqrt{\frac{n_{tx}}{n_{rx}}}\right)^2}{m}\right] \\ &= \Pr\left[\frac{2\|\vec{h}_{\text{sum}}\|^2}{n_{rx}} \leq \frac{2n_{rx}\left(1+\sqrt{\frac{n_{tx}}{n_{rx}}}\right)^2}{m}\right] \end{aligned} \tag{3.111}$$

Noting that $\frac{2\|\vec{h}_{\text{sum}}\|^2}{n_{rx}}$ is random variable with a chi-square with $2n_{rx}$ degrees of freedom distribution, we arrive at the following expression:

$$P_{\text{out}} = F_{\chi^2}\left(\frac{2n_{rx}(1+\sqrt{\frac{n_{rx}}{n_{tx}}})^2}{m}\right) \tag{3.112}$$

where $F_{\chi^2}(\,\cdot\,;n)$ is the chi-square distribution with n degrees of freedom. Solving for m proves the equality in equation (3.110). Using the normal approximation for large n_{rx} (specifically, $n_{rx} > 20(Q^{-1}(P_{\text{out}}))^2$) gives the following expression for outage probability in terms of open loop diversity power margin:

$$P_{\text{out}} = Q\left(\sqrt{n_{rx}}\left(1-\frac{\left(1+\sqrt{\frac{n_{tx}}{n_{rx}}}\right)^2}{m}\right)\right) \tag{3.113}$$

Solving for m proves the first approximation in equation (3.110). Finally, a Taylor series expansion gives the last approximation in equation (3.110). □

Figure 3-11 shows applicability of the margin bounds for $P_{\text{out}} = 10^{-5}$ and $P_{\text{out}} = 10^{-10}$. The solid line denotes the exact expression, with the linear and normal approximations shown as dashed lines. The 'approximation valid' line, placed at $n = 20\left(Q^{-1}(P_{\text{out}})\right)^2$ shows where we expect the bounds to begin to be tight. For $n < 20\left(\text{erfc}^{-1}(2P_{\text{out}})\right)^2$, the bounds are very loose with the normal bound approaching infinity as $n \approx 2\left(Q^{-1}(P_{\text{out}})\right)^2$.

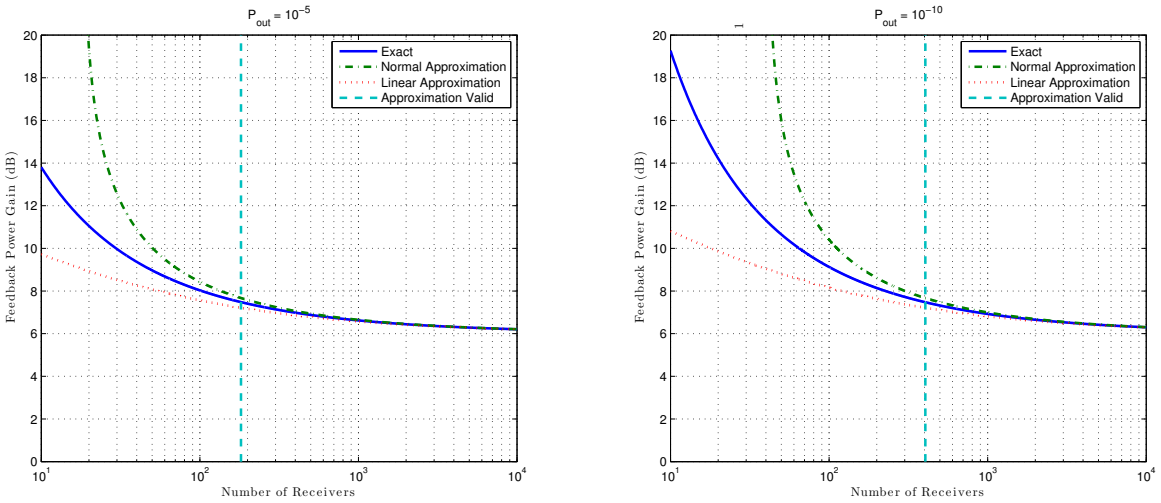

Figure 3-11: Open loop diversity power margin bounds for balanced sparse aperture system: The applicability of the margin bounds is shown for $P_{\text{out}} = 10^{-5}$ and $P_{\text{out}} = 10^{-10}$. The solid line denotes the exact expression, with the linear and normal approximations shown as dashed lines.

This corollary has an interesting alternative interpretation: it provides a value, in terms of power gain, of channel state information at the transmitter. The open loop diversity power margin is the additional power that a system with no channel state information needs to perform as well as a system with perfect CSI at least P_{out} fraction of the time. An alternative name *feedback power gain* could be used because it represents the equivalent power gain enabled by feedback.

Figure 3-12 shows the open loop diversity power margin (or, alternatively, the feedback power gain). As the outage probability is reduced, the feedback power gain is greatly increased: if a system is required to operate at a low outage probability, the value of the feedback information is very high. As the number of apertures increases, the value of feedback is diminished. Asymptotically, as the number of apertures gets very large the feedback power gain approaches the average gain value of $(1 + \sqrt{n_{tx}/n_{rx}})^2$.

Finally, we present the asymptotic average BER for the sparse aperture system with no channel state information.

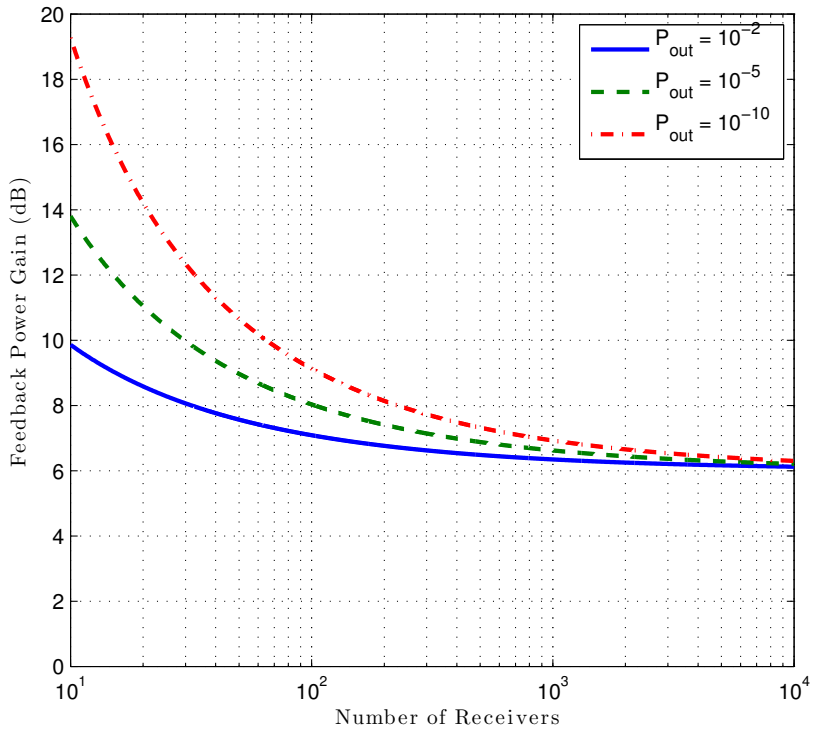

Figure 3-12: Feedback power gain: The additional power that an open loop system needs to perform as well as the wavefront predistortion system versus number of receivers for a balanced sparse aperture system.

Theorem 10 *For uncoded binary phase shift keying with no CSI at the transmitter, the turbulence average BER is:*

$$\lim_{n_{rx},n_{rx}\to\infty} \mathbb{E}_{\mathbf{H}}[P_e] = Q\left(\sqrt{2\text{SNR}}\right) \tag{3.114}$$

Proof. By definition, the turbulence average BER is:

$$\mathbb{E}_{\mathbf{H}}[P_e] = \int_{-\infty}^{\infty} f_{|\phi_s|^2}(s) Q\left(\sqrt{2\text{SNR}s}\right) ds \tag{3.115}$$

where $f_{|\phi_s|^2}(s)$ is the pdf of the sufficient statistic. From Corollary 7, we know the asymptotic probability distribution of $f_{|\phi_s|^2}(s)$:

$$\mathbb{E}_{\mathbf{H}}[P_e] = \int_{-\infty}^{\infty} \mathcal{N}\left(s; 1, \frac{1}{\sqrt{n_{rx}}}\right) Q\left(\sqrt{2\text{SNR}s}\right) ds \tag{3.116}$$

Noting that as the number of receive apertures increases, the normal distribution approaches an impulse and the average BER:

$$\begin{aligned}\lim_{n_{rx}\to\infty}\int_{-\infty}^{\infty}\mathcal{N}\left(s;1,\frac{1}{\sqrt{n_{rx}}}\right)Q\left(\sqrt{2\mathrm{SNR}s}\right)ds \\ =\int_{-\infty}^{\infty}\delta(s-1)Q\left(\sqrt{2\mathrm{SNR}s}\right)ds=Q\left(\sqrt{2\mathrm{SNR}}\right)\end{aligned} \tag{3.117}$$

□

3.1.4 Comparison of Schemes

In this section, we will give a system designer some guidance when deciding which diversity system to use: wavefront predistortion, selection, or open loop. While the wavefront predistortion scheme has additional costs because it requires feedback and hardware to predistort the transmitted wave, open loop has additional cost because it must send significantly more power to achieve the same performance.

To compare systems, we define *spatial modulation gain* to be the average power gain due to spatial modulation relative to the average power with no spatial modulation. The metric provides a rough value in terms of SNR of a particular modulation scheme. By definition, the open loop system attains 0 dB of spatial modulation gain. For a balanced system, comparing the asymptotic BER given for wavefront predistortion in (3.30) with the asymptotic BER for open loop given in (3.114), we see that an open loop system, on average, performs as well as a wavefront predistortion system with 6 dB less transmit power. The spatial modulation gain for the different systems we have discussed is:

- Open loop, spatial modulation gain: 1
- Selection, spatial modulation gain: $1+\sqrt{2(\exp(4\sigma_\chi^2)-1)\log(n_{tx})/n_{rx}}$
- Wavefront predistortion, spatial modulation gain: $\left(1+\sqrt{n_{tx}/n_{rx}}\right)^2$

Figure 3-13 shows the spatial modulation gain for all three systems versus number of receive apertures for a fixed 100 transmit apertures. We see that, as the number of

receive apertures becomes large compared to the number of transmit apertures, the modulation gain converges to 0 dB for all three systems. Intuitively, this is because the large number of receive apertures tends to average out any modulation from the transmitter.

Similarly, Figure 3-14 shows the spatial modulation gain for all three systems versus number of transmit apertures for a fixed 100 receive apertures. As the number of transmit apertures becomes large compared to the number of receive apertures, the modulation gain grows unbounded. Intuitively, the more transmit apertures the higher the probability the system will be able to exploit a favorable turbulence state.

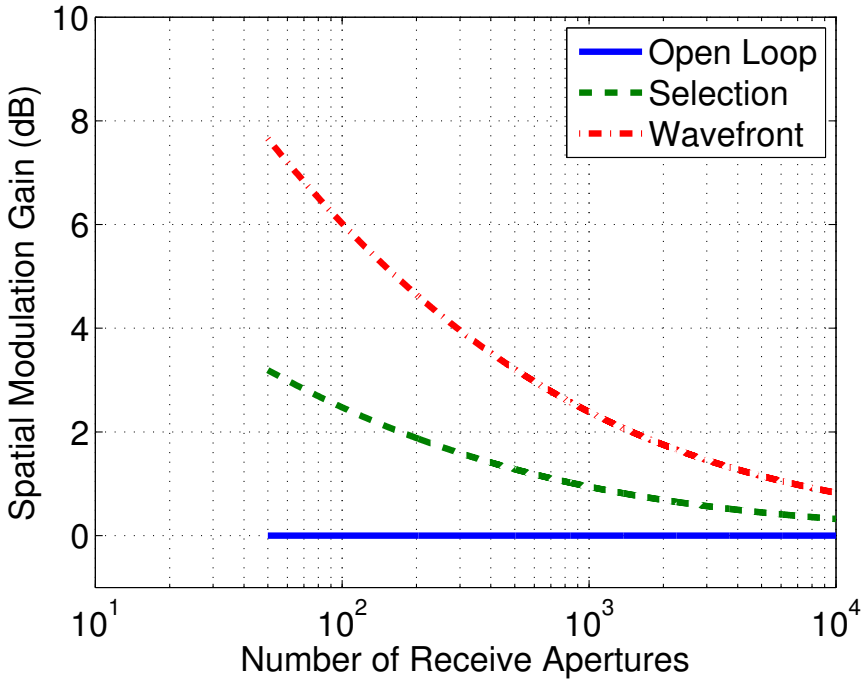

Figure 3-13: Spatial modulation gain: Spatial modulation gain of open loop, selection, and wavefront predistortion schemes versus number of receive apertures for a 100 transmit apertures and $\sigma_\chi^2 = 0.5$.

This average result, however, can be misleading for any real world system because instantaneous BER fluctuation around the mean can cause catastrophic outages. Figure 3-15 shows a comparison of outage probability for open loop, selection, and wavefront predistortion systems with $n_{tx} = n_{rx} = 100$. Because the outage probability for the open loop system falls off relatively slowly, it requires more than the

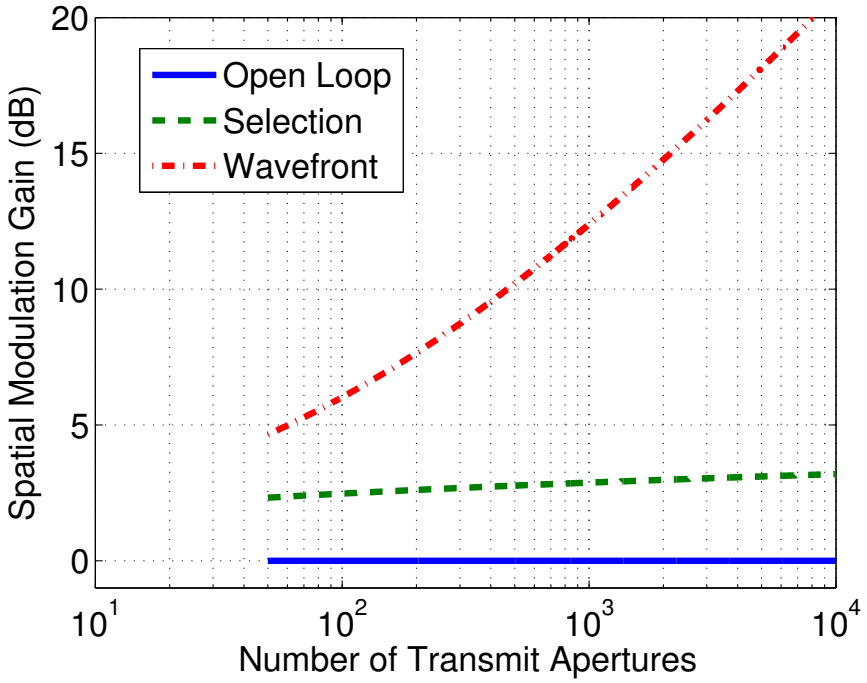

Figure 3-14: Spatial modulation gain: Spatial modulation gain of open loop, selection, and wavefront predistortion schemes versus number of transmit apertures for a 100 receive apertures and $\sigma_\chi^2 = 0.5$.

average power gain, the spatial diversity gain, to perform as well as the wavefront predistortion system with a reasonable outage probability.

We conclude this section with a comparison of margin for each diversity scheme (wavefront predistortion, selection, and open loop). Figure 3-16 shows finite aperture power margin for balanced systems versus number of receive apertures. In the figure, finite aperture power margin for wavefront predistortion diversity is shown in blue, diversity power margin for selection diversity is shown in red, and diversity power margin for open loop is shown in green. The finite aperture power margin for wavefront predistortion begins at 17 dB for a one transmit aperture/one receive aperture system (a one-by-one system) and decreases rapidly to 9 dB for a two-by-two system and 5 dB for a three-by-three system. As the number of transmit and receive apertures gets to be large, the finite aperture power margin for wavefront predistortion approaches 0 dB. Open loop diversity power margin begins at 14 dB at $n_{tx} = n_{rx} = 20$ then decreases rapidly to its 6 dB asymptote. Thus wavefront

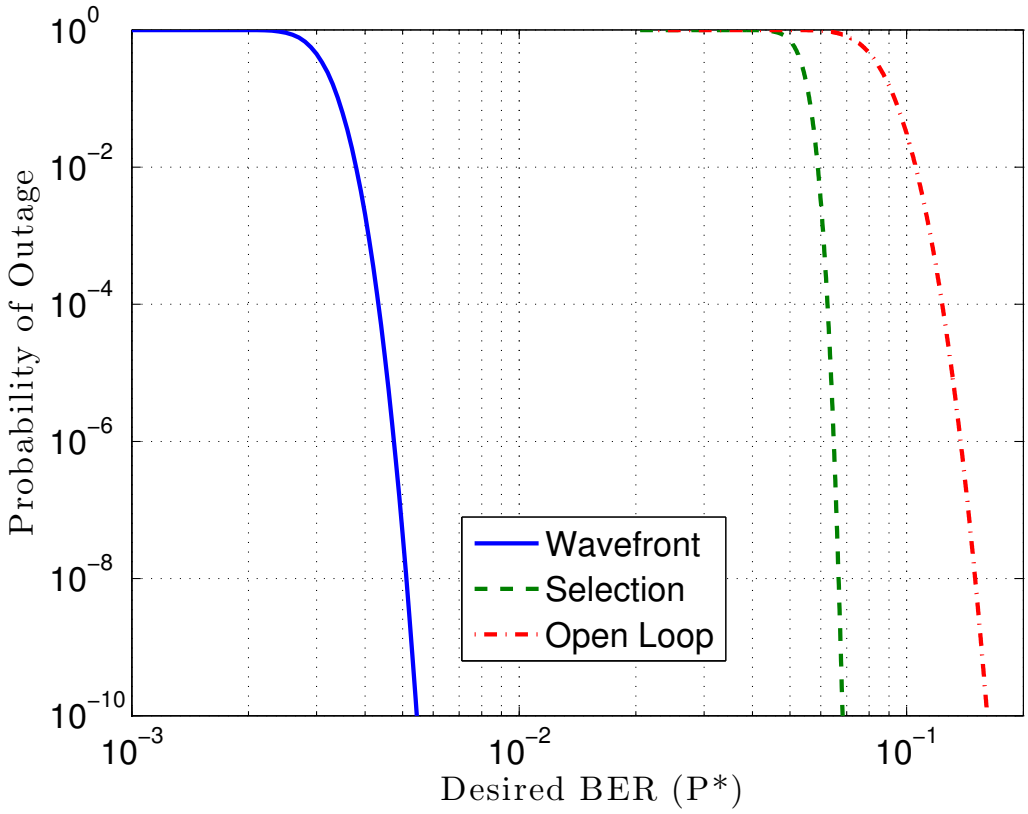

Figure 3-15: Comparison of outage probability: Outage probability for open loop, selection, and wavefront predistortion schemes versus desired BER for $n_{tx} = n_{rx} = 100$, SNR $= 1$, and $\sigma_\chi^2 = 0.5$.

predistortion provides a *large* gain over open loop in the 2 to 100 aperture region. For a large number of transmit and receive apertures wavefront predistortion provides 6 dB gain over open loop. Selection diversity power margin has approximately the same asymptote (as the number of apertures becomes large) as open loop diversity power margin, but does not increase nearly as quickly as the open loop system as the number of apertures becomes small. Thus selection diversity does not provide significant gain compared to the simpler open loop system when the number of transmit and receive apertures are large. Selection diversity does provide significant gain compared to open loop when the number of transmit and receive apertures are small. As a result, selection diversity should never be used for systems with a large number of transmitters. When the number of transmit and receive apertures is small, transmit diversity should be used if wavefront predistortion is unavailable. In summary, for

balanced systems wavefront predistortion requires the least margin and thus should be used when a sufficient feedback link is available. If a sufficient feedback link is unavailable, selection diversity should be used in the small number of aperture regime ($n_{tx} = n_{rx} < 500$) and open loop should be used in the large number of aperture regime ($n_{tx} = n_{rx} > 500$).

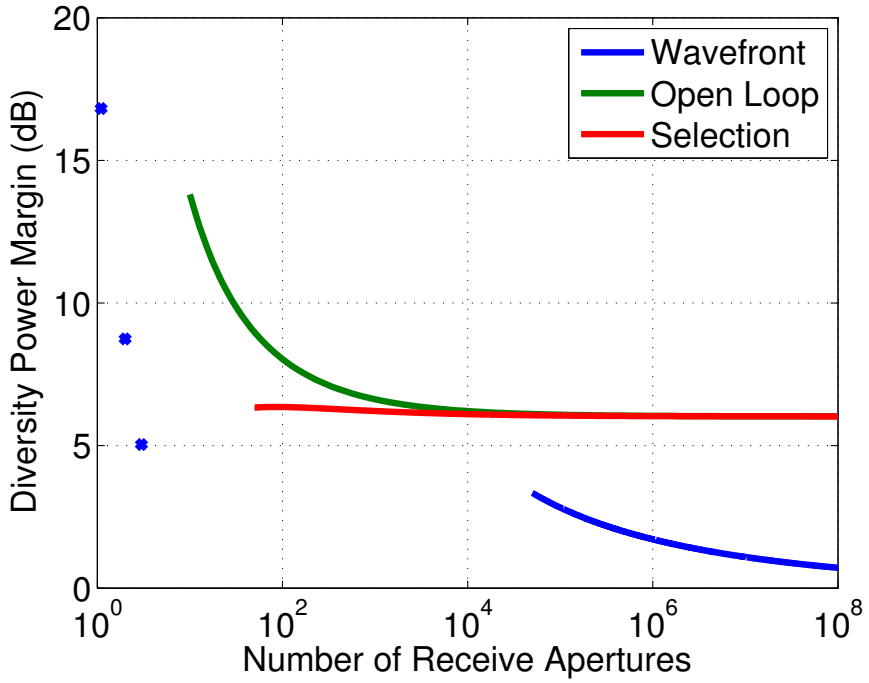

Figure 3-16: Diversity power margin: Diversity power margin for balanced systems versus number of receive apertures for wavefront predistortion diversity, selection diversity, and open loop diversity. In this figure, $\sigma_\chi^2 = 0.1$ and $P_{\text{out}} = 10^{-5}$.

Figure 3-17 shows the diversity power margin versus number of transmit apertures with a fixed number of receive apertures, $n_{rx} = 100$. As the number of transmit apertures increases, the wavefront predistortion becomes a better approximation for an infinite aperture system and, as such, the finite aperture power margin approaches 0 dB. As the number of transmit apertures increases, both selection and open loop diversity power margin increase rapidly. This is because, as the number of transmit apertures becomes large relative to the number of receive apertures, the wavefront predistortion system is able to exploit advantageous turbulence states while open loop and selection are not. Thus, for systems with many more transmit apertures

than receive apertures, wavefront predistortion should be used. For systems with many more receive apertures than transmit apertures, wavefront predistortion and selection diversity do not provide significant performance gains and, as a result, open loop diversity should be used.

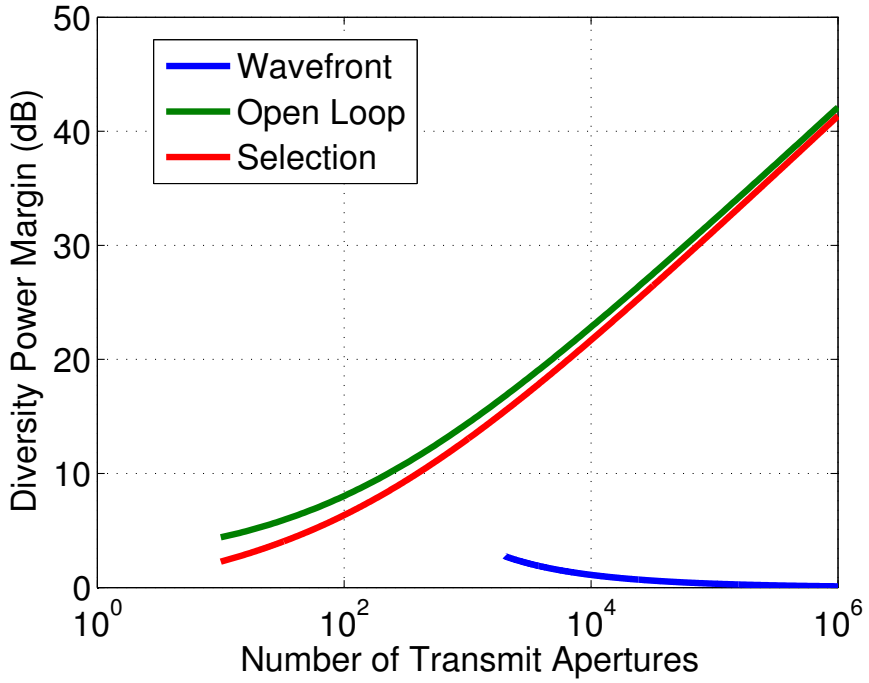

Figure 3-17: Diversity power margin: Diversity power margin for wavefront predistortion system versus β for wavefront predistortion diversity, selection diversity, and open loop diversity. In this figure, $\sigma_\chi^2 = 0.1$, $P_{\text{out}} = 10^{-5}$ and $n_{rx} = 100$.

3.2 System Performance in Inhomogeneous Turbulence

Thus far, we have been concerned with system performance in homogeneous turbulence. This implies a horizontal link or a limited vertical link. For the case of a vertical link over kilometers, such as an aircraft or satellite terminal to a ground terminal, turbulence will be inhomogeneous. The limiting Marcenko-Pastur distribution is still valid provided the conditions in Theorem 1 are satisfied.

To quantify the effects of the inhomogeneous turbulence, we define the average wavefront predistortion gain:

$$P_{\text{gain}} = \left(1 + \sqrt{\beta}\right)^2 \tag{3.118}$$

which represents the average power gain of a diversity system *with* wavefront predistortion compared with a diversity system *without* wavefront predistortion. For scenarios with small wavefront predistortion gain, there is negligible benefit to implementing wavefront predistortion. On the other hand, for scenarios with a large wavefront predistortion gain, there is significant benefit to implementing wavefront predistortion. If we wish to maximize the protection against fading (e.g., we use as many transmit and receive apertures as possible given a form factor constraint), for a transmitter and receiver of linear extent L, the average wavefront predistortion gain is:

$$\begin{aligned} P_{\text{gain}}^{\text{g-ac}} &= \left(1 + \frac{\text{floor}\left(\frac{L}{\rho_g}\right) + 1}{\text{floor}\left(\frac{L}{\rho_s}\right) + 1}\right)^2 \\ P_{\text{gain}}^{\text{ac-g}} &= \left(1 + \frac{\text{floor}\left(\frac{L}{\rho_s}\right) + 1}{\text{floor}\left(\frac{L}{\rho_g}\right) + 1}\right)^2 \end{aligned} \tag{3.119}$$

where $P_{\text{gain}}^{\text{g-ac}}$ is the average wavefront predistortion gain for a system with transmit apertures on the ground and receive apertures on an aircraft or spacecraft and $P_{\text{gain}}^{\text{ac-g}}$ is the average wavefront predistortion gain for a system with transmit apertures on an aircraft or spacecraft and receive apertures on the ground. The variable ρ_g is the correlation length measured on the ground and ρ_s is the correlation length measured at some altitude L above the surface:

$$\begin{aligned} \rho_g &= \left[2.91k^2 \int_0^L C_n^2(z)(z/L)^{5/3} dz\right]^{-3/5} \\ \rho_s &= \left[2.91k^2 \int_0^L C_n^2(z)(1 - z/L)^{5/3} dz\right]^{-3/5} \end{aligned} \tag{3.120}$$

where $C_n^2(z)$ is the atmospheric structure constant. As the extent L grows very large, the function approaches:

$$\lim_{L\to\infty} P_{gain} = \left(1 + \frac{\rho_s}{\rho_g}\right)^2 \tag{3.121}$$

This approximate equation is only valid when there are many coherence lengths within the transmit and receive form factor. In its region of validity, it is apparent that the average wavefront predistortion gain given in (3.119) is a discretized version of the limiting average wavefront predistortion gain given in (3.121). Equation (3.121) is therefore a useful metric for inhomogeneous turbulence average wavefront predistortion gain. Figure 3-18 shows the average wavefront predistortion gain for a ground to aircraft/spacecraft platform and an aircraft/spacecraft to ground platform. We assumed a vertical clear air path with the structure constant variation shown in Figure 3-19 [35]. The structure constant data shown in the figure is the average of data from three consecutive days, each day's data consisting of one profile taken during daylight hours [35]. For the power gain calculation, we assumed that the structure constant was zero where data were not present. As a result, the wavefront predistortion power gain curves represent a lower bound on the actual wavefront predistortion power gain achievable under similar conditions. For the figure, the red line denotes the altitude of an operational predator drone, the cyan line denotes the altitude of a commercial aircraft, the purple line denotes a low earth satellite altitude and the yellow line denotes the altitude of a geosynchronous satellite. For the ground to aircraft/spacecraft link, the wavefront predistortion power gain starts at 0 dB because the turbulence path between transmitter and receiver is too short for the transmitter and receiver to experience many independent sublinks (we use the term *sublink* to indicate a single transmit aperture to receiver aperture connection within a diversity system with many such sublinks). At a vertical path length of approximately 40 m the ground to aircraft/spacecraft wavefront predistortion gain begins to rapidly increase as turbulence allows the transmitter and receiver to experience many independent sublinks. At approximately 100 km vertical link distance, the wavefront predistortion gain levels off because Earth's atmosphere approaches vacuum. Similarly for the

aircraft/spacecraft to ground link, the wavefront predistortion power gain starts at 0 dB because the turbulence path between transmitter and receiver is too short for the transmitter and receiver to experience many independent sublinks. At a vertical path length of approximately 40 m the aircraft/spacecraft to ground wavefront predistortion gain begins to rapidly increase as turbulence allows the transmitter and receiver to experience many independent sublinks. The aircraft/spacecraft to ground wavefront predistortion gain reaches a maximum of 6 dB for a vertical path length of approximately 100 m, then begins to decrease rapidly as fewer and fewer independent sublinks are experienced by the transmitter.

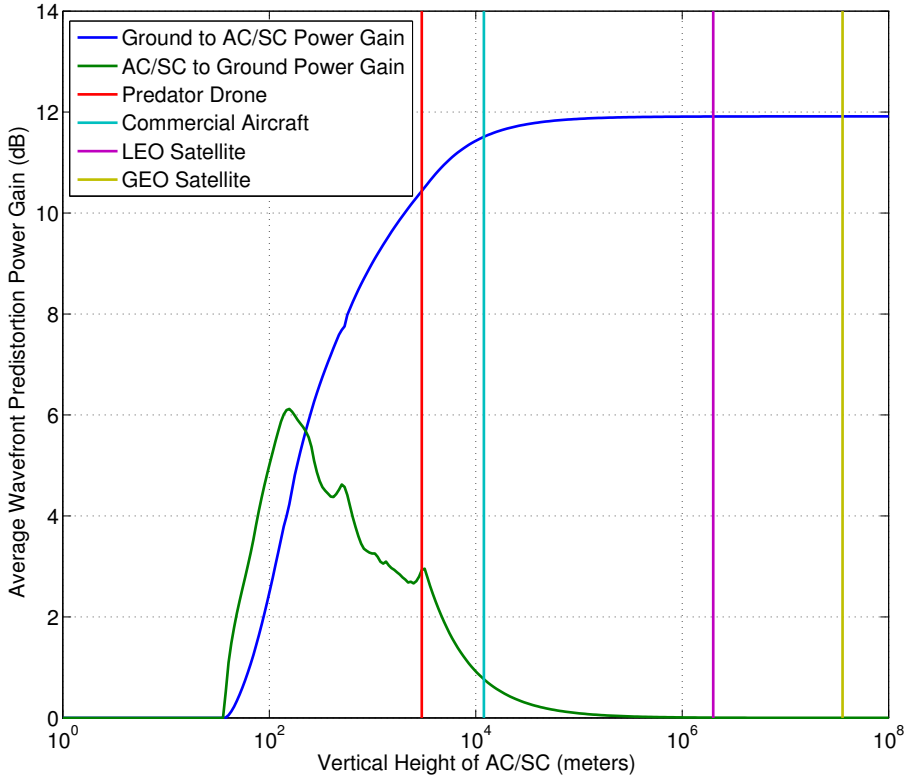

Figure 3-18: Average wavefront predistortion power gain in inhomogeneous turbulence: Ground to aircraft and aircraft to ground average wavefront predistortion power gain for clear air vertical turbulence as a function of altitude above sea level. For this figure, the total area of the transmitter and receiver is 0.09 m^2.

From figure 3-18 we see that wavefront predistortion is much more useful for the ground to aircraft/spacecraft link than the aircraft/spacecraft to ground link. For the

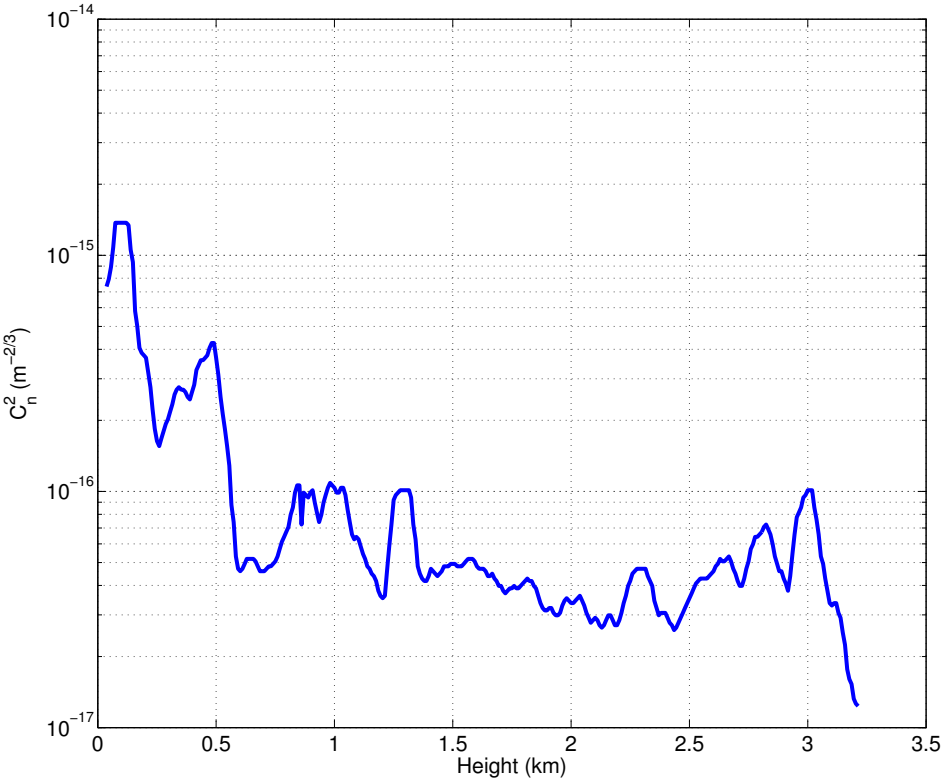

Figure 3-19: Airplane-borne temperature sensor determination of C_n^2 versus height.

ground to aircraft/spacecraft link, the average wavefront distortion gain exceeds 10 dB for all example platforms shown in the figure. In contrast, for the aircraft/spacecraft to ground link the average wavefront predistortion gain is approximately 3 dB for the predator drone altitude and is less than 1 dB for all other platforms shown in the figure. Physically this is because the turbulence is near the transmitter for the ground to aircraft/spacecraft link while the turbulence is very far from the transmitter for the aircraft/spacecraft to ground link. With the transmitter far from the turbulence, it is unable to predistort the wave to undo the turbulence.

Alternatively, if we wish to minimize average BER, for a transmitter and receiver of linear extent L the wavefront predistortion power gain is:

$$\begin{aligned} P_{\text{gain}}^{\text{g}-\text{ac}} &= \left(1+\frac{L}{\rho_g}\right)^2 \\ P_{\text{gain}}^{\text{ac}-\text{g}} &= \left(1+\frac{L}{\rho_s}\right)^2 \end{aligned} \tag{3.122}$$

which is valid when the transmitter experiences many independent sublinks. Figure 3-20 shows the average wavefront predistortion power gain for clear air vertical turbulence as a function of altitude above sea level for the case where we have maximized the wavefront predistortion gain. For the figure, the red line denotes the altitude of an operational predator drone, the cyan line denotes the altitude of a commercial aircraft, the purple line denotes a low earth satellite altitude and the yellow line denotes the altitude of a geosynchronous satellite.

Comparing figure 3-20 and figure 3-18, it is clear that maximizing the outage protection or minimizing average BER has little effect on the wavefront predistortion gain of the ground to aircraft/spacecraft link. The comparison shows, however, that maximizing the outage protection or minimizing average BER gives different results for the wavefront predistortion gain of the aircraft/spacecraft to ground link. This is because, for the aircraft/spacecraft to ground link, we sacrifice receive apertures, and thus independent sublinks between transmit and receive apertures. This decreases average BER at the expense of outage protection.

Table 3.1 provides a summary of the applicability of diversity and wavefront predistortion for the vertical clear air link. The particular vertical link numbers given in the table are specific to the structure constant profile used. Despite this, the table should give a good general idea regarding the regions of applicability.

3.3 Expected Channel Capacity

We now calculate the capacity of the sparse aperture system with wavefront predistortion and coherent detection. Generally, the noisy-channel coding theorem states that

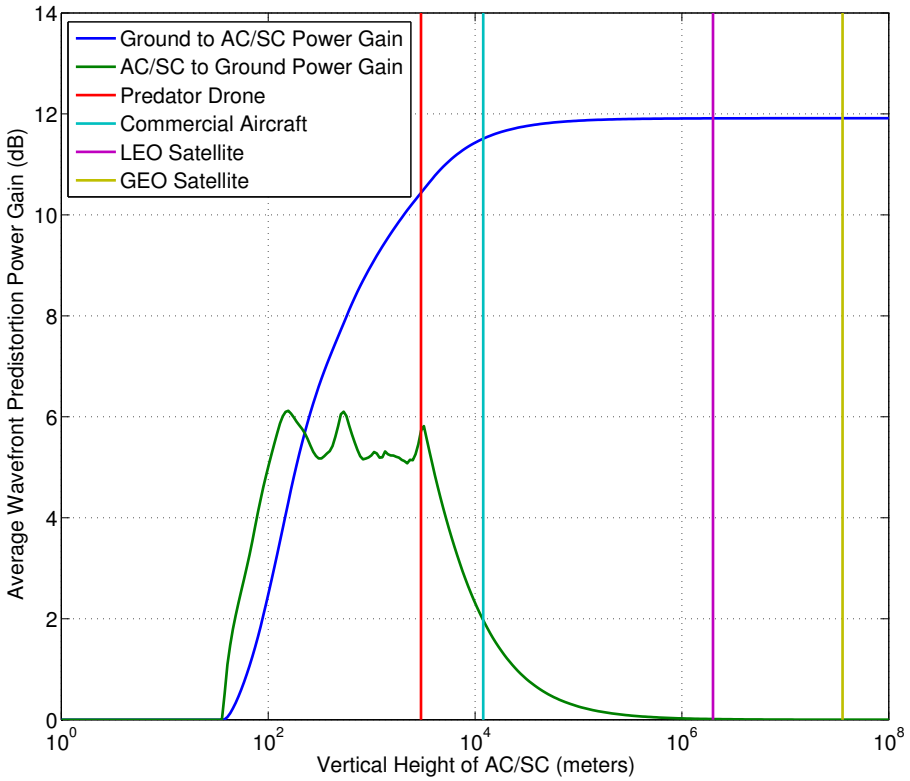

Figure 3-20: Average wavefront predistortion power gain in inhomogeneous turbulence: Ground to aircraft and aircraft to ground average wavefront predistortion power gain for clear air vertical turbulence as a function of altitude above sea level. For this figure, the total area of the transmitter and receiver is 0.09 m^2.

capacity is the highest rate that can be achieved with an arbitrarily low probability of error. More formally, capacity is the highest rate for which there exists a code of length N that can be decoded with arbitrarily small probability of error. The notion of capacity is not always applicable; for example, the noisy-channel coding theorem is not applicable if the atmospheric state changes before a code word of length N can be sent. Practically, if the time to transmit a single code word exceeds the overall system delay requirements (for example, for voice over internet protocol the delay, from mouth to ear, must be less than 150 ms) then the noisy-channel theorem cannot be applied. For the time being, we will assume the atmospheric state is constant over the time required to send a code word and that the system delay requirements do not limit the use of the theorem.

Table 3.1: Applicability of wavefront predistortion in inhomogeneous turbulence. *No Diversity* means that neither diversity nor wavefront predistortion is possible. *Wavefront Predistortion* means that either diversity or wavefront predistortion is possible, but wavefront predistortion provides significant gain over diversity. *Diversity* means diversity is possible, but wavefront predistortion is not possible.

Vertical Link Distance	Ground to AC/SC Link	AC/SC to Ground Link
0 km to 0.04 km	No Diversity	No Diversity
0.04 km to 100 km	Wavefront Predistortion	Wavefront Predistortion
100 km and up	Wavefront Predistortion	Diversity

We showed in the introduction that the system can be decomposed into parallel Gaussian channels. From Chapter 2 the parallel channel is:

$$\begin{aligned} \tilde{y}_1 &= \sqrt{\mathrm{SNR}}\gamma_1\tilde{x}_1 + \tilde{w}_1 \\ \tilde{y}_2 &= \sqrt{\mathrm{SNR}}\gamma_2\tilde{x}_2 + \tilde{w}_2 \\ \vdots \quad & \quad \vdots \quad \quad \vdots \\ \tilde{y}_{n_{\min}} &= \sqrt{\mathrm{SNR}}\gamma_{n_{\min}}\tilde{x}_{n_{\min}} + \tilde{w}_{n_{\min}} \end{aligned} \tag{3.123}$$

where $n_{\min} = \min(n_{tx}, n_{rx})$. The constraint that $\mathbb{E}[\|\vec{x}\|^2] = 1$ implies a constraint on the energy allocated to $\tilde{x}_{\mathsf{i}}$ (assuming no energy is allocated to eigenmodes associated with squared singular values with a value of zero):

$$\sum_{\mathsf{i}=1}^{n_{\min}} E_{\mathsf{i}} = 1 \tag{3.124}$$

where E_{i} is the energy in $\tilde{x}_{\mathsf{i}}$, $|\tilde{x}_{\mathsf{i}}|^2 = E_{\mathsf{i}}$. For a channel that can be decomposed into parallel Gaussian channels, the expected channel capacity is well known to be [14]:

$$\mathbb{E}[\mathrm{C}] = \mathbb{E}\left[\sum_{\mathsf{i}=1}^{\infty} \log\left(1 + \gamma_{\mathsf{i}}^2 E_{\mathsf{i}}^* \mathrm{SNR}\right)\right] \tag{3.125}$$

where E_{i}^* is the power allocation that maximizes the expression. The optimal power allocation (OPA) is the so-called water filling technique:

$$E_{\mathsf{i}}^* = \left(\mu + \frac{1}{\mathrm{SNR}\gamma_{\mathsf{i}}^2}\right)^+ \tag{3.126}$$

where $(x)^+ = \max(x, 0)$ and μ is selected to satisfy the energy constraint $\sum_{\mathsf{i}=1}^{n_{\min}} E_{\mathsf{i}} = 1$.

Thus, capacity is attained by measuring the channel state, adjusting the codebook, and adjusting the power allocated to each eigenmode accordingly. By varying the phase and power of each transmitter, we can adjust the power allocated to each eigenmode independently. For the optimal power allocation, E_{i}^*, the associated transmit vector is:

$$\vec{x} = \sum_{\mathsf{i}=1}^{n_{\min}} \vec{v}_{\mathsf{i}} \sqrt{E_{\mathsf{i}}^*} \tag{3.127}$$

Various modulation schemes can be used in conjunction with the optimal power allocation. For example, if we wish to transmit a $n_{\min}$-length code word across the $n_{\min}$-independent channels during bit period n with binary phase shift keying (BPSK), the phase of each transmit vector should be set to:

$$\vec{x}[n] = \sum_{\mathsf{i}=1}^{n_{\min}} \vec{v}_{\mathsf{i}} \sqrt{E_{\mathsf{i}}^*} e^{j\pi C_{\mathsf{i}}[n]} \tag{3.128}$$

where $C_{\mathsf{i}}[n] \in \{0, 1\}$ is the i^{th} bit of the word transmitted during bit period n.

While we can implement a system with the optimal power allocation scheme, no analytic solution exits for the expected capacity in equation (3.125). Instead, we present the solution to a suboptimal power allocation scheme that allocates power equally to all nonzero eigenmodes. We show this suboptimal power allocation scheme provides a tight bound to the capacity-maximizing performance, especially at high received SNR levels.

Theorem 11 *As the number of transmit and receive apertures grow, the expected capacity for the sparse aperture system with wavefront predistortion asymptotically*

converges and is lower bounded by:

$$\mathbb{E}[\mathrm{C}] \geq n_{tx} \log\left(1 + \frac{\mathrm{SNR}}{n_{\min}} - \frac{1}{4}\mathcal{F}\left(\frac{\mathrm{SNR}}{n_{\min}}, \beta\right)\right) + n_{rx} \log\left(1 + \frac{\mathrm{SNR}\beta}{k} - \frac{1}{4}\mathcal{F}\left(\frac{SNR}{n_{\min}}, \beta\right)\right)$$
$$\cdots - \frac{n_{rx} n_{\min}}{4\mathrm{SNR}}\mathcal{F}\left(\frac{\mathrm{SNR}}{n_{\min}}, \beta\right)$$
$$\mathcal{F}\left(\frac{\mathrm{SNR}}{n_{\min}}, \beta\right) = \left(\sqrt{\frac{\mathrm{SNR}}{n_{\min}}(1+\sqrt{\beta})^2 + 1} - \sqrt{\frac{\mathrm{SNR}}{n_{\min}}(1-\sqrt{\beta})^2 + 1}\right)^2 \tag{3.129}$$

Where the bound is tight when the SNR is sufficient to ensure that power is allocated to every eigenmode associated with a nonzero squared singular value:

$$\mathrm{SNR} \geq \frac{2\min(1, \beta^{3/2})}{|1-\sqrt{\beta}||1-\beta|} \tag{3.130}$$

Proof. Starting with the definition of capacity for equal power allocation to eigenmodes associated with nonzero squared singular values:

$$\mathbb{E}[\mathrm{C}] = \mathbb{E}\left[\sum_{\mathsf{i}=1}^{n_{\min}} \log\left(1 + \frac{\gamma_{\mathsf{i}}^2}{n_{\min}}\mathrm{SNR}\right)\right] \tag{3.131}$$

where we have used that there will be $n_{\min}$ spatial degrees of freedom implying $n_{\min}$ nonzero squared singular values. As the number of transmit and receive apertures grows, the width between squared singular values goes to zero and they represent a finer and finer sampling of the continuous squared singular value distribution. So, a good approximation to the capacity is:

$$\lim_{n_{tx}, n_{rx} \to \infty} \mathbb{E}[\mathrm{C}] = n_{\min} \int_0^\infty \log\left(1 + \frac{x}{n_{\min}}\mathrm{SNR}\right) f_{\gamma^2}(x) dx \tag{3.132}$$

Applying the general capacity expression to the specific case of the sparse aperture system with high-SNR in turbulence, we arrive at:

$$\lim_{n_{tx},n_{rx}\to\infty} \frac{1}{n_{\min}}\mathbb{E}[\mathrm{C}] = \ldots$$
$$\int_{(1-\sqrt{\beta})^2}^{(1+\sqrt{\beta})^2} \log\left(1+\frac{x}{n_{\min}}\mathrm{SNR}\right)\frac{\sqrt{\left(x-(1-\sqrt{\beta})^2\right)\left((1+\sqrt{\beta})^2-x\right)}}{2\pi x}dx \tag{3.133}$$

Where we have used Theorem 1 which states that, for a sparse aperture communication system with uniform average illumination of the receive apertures and well-developed turbulence (i.e., $\sigma_\phi^2 \gg 2\pi$) for a single atmospheric state, as the number of transmit apertures and receive apertures asymptotically approaches infinity, the empirical squared singular value distribution converges almost surely to the Marcenko-Pastur density. With a change of variables, this expression has been evaluated in [50]. Thus the theorem is proven. $\square$

It is common to describe optimal power allocation as water filling: consider the thought experiment where we plot the values of $1/(\mathrm{SNR}\gamma_{\mathsf{i}})$ versus the squared singular value index, i, and imagine the line traced out as a vat which may hold water. Power is allocated to eigenmodes such that the water level is constant $1/\mu$. Power is first allocated to the eigenmodes with the largest squared singular value, the lowest point in the vat. As power is increased, it is allocated to weaker and weaker eigenmodes. Thus power is allocated to the various eigenmodes in the same way water would be allocated if it were poured into the vat.

When the water level is deep, the difference between equal power allocation capacity and optimal power allocation capacity is small. The water level is deep when the SNR is large compared with the reciprocal of the nonzero eigenvalues, which is true when β is bounded from one (e.g., a small vat) or the SNR is large (e.g., a lot of water). Consequently, the difference between equal power allocation capacity and optimal power allocation capacity is asymptotically zero as SNR gets very large or

β is very far from one. Finally we note that over a wide range of SNR, the gain of optimal power allocation versus equal power allocation is small.

The bound on average capacity is a complicated function and, as a result, it is difficult to gain intuition from Theorem 11. Accordingly, we present an asymptotic expression for the expected capacity to better elucidate the dependencies. In the limit as SNR grows, the average capacity lower bound approaches the following limit:

$$\lim_{n_{tx},n_{rx}\to\infty} \mathbb{E}[\mathrm{C}] \geq \begin{cases} n_{tx} \log\left(\frac{\mathrm{SNR}}{n_{tx}}\left(1-\frac{n_{tx}}{n_{rx}}\right)\right) & n_{tx} < n_{rx} \\ n_{tx} \log\left(\frac{\mathrm{SNR}}{3n_{tx}}\right) & n_{tx} = n_{rx} \\ n_{rx} \log\left(\frac{\mathrm{SNR}}{n_{rx}}\left(\frac{n_{tx}}{n_{rx}}-1\right)\right) & n_{tx} > n_{rx} \end{cases} \tag{3.134}$$

For a fixed number of receive apertures, capacity scales very differently for the cases where $n_{tx} > n_{rx}$ and $n_{tx} < n_{rx}$:

- $n_{tx} < n_{rx}$: capacity scales *linearly* with the number of transmit apertures
- $n_{tx} > n_{rx}$: capacity scales *logarithmically* with the number of transmit apertures

In both cases, the capacity scales logarithmically with SNR. Consequently, in the $n_{tx} < n_{rx}$ regime it is more efficient to increase capacity by adding additional transmit apertures than by increasing SNR. In the $n_{rx} < n_{tx}$ regime, capacity can be increased by either adding additional transmit apertures or increasing SNR.

For a fixed number of transmit apertures, capacity *increases* as the number of receive apertures *decrease*. The power increase (per receive aperture) more than compensates for the decrease in the number of parallel channels ($n_{\min}$). This intuition is only valid in the regime where there are many transmit and receive apertures.

Figure 3-21 shows the SNR threshold for Theorem 11 to be valid as a function of β. Near $\beta = 1$ a very large SNR is required for the theorem to be valid. For values of $\beta > 3$ and $\beta < 1/3$, an SNR of one is sufficient for the theorem to be valid. Note that an analytic solution for the expected capacity of a balanced system ($\beta = 1$) is known only for asymptotically large SNR. The fact that no solution exists for the low-SNR and β near one motivates us to find another bound that is useful in this region. As

a result, we present a bound based on allocating all power to the highest eigenvalue that is valid for any SNR, but is tight for low-SNR.

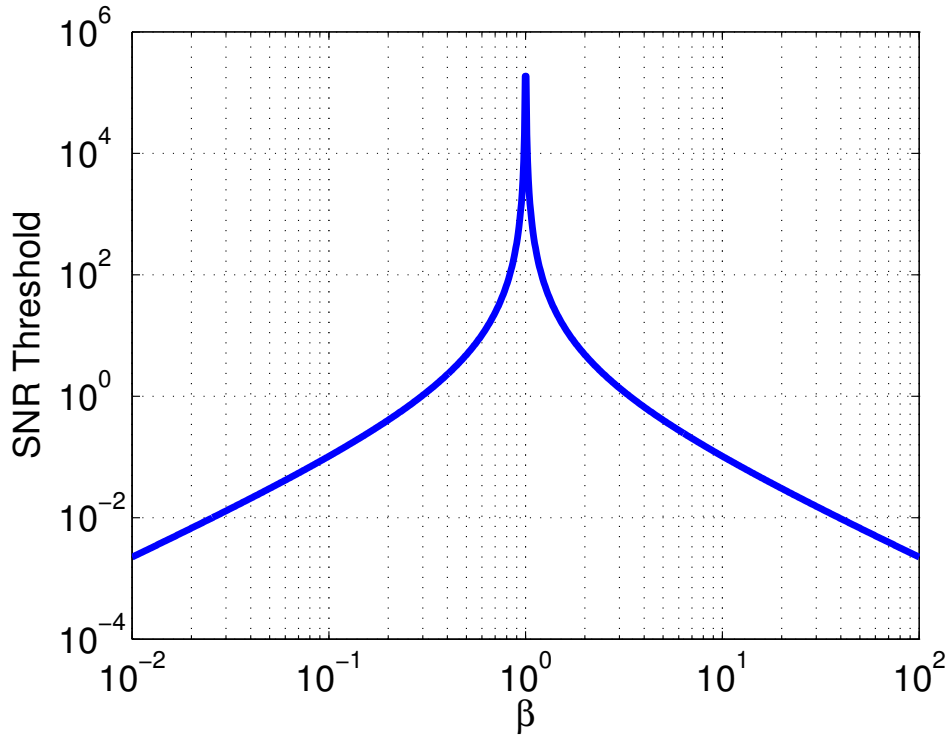

Figure 3-21: SNR threshold for Theorem 11 to be valid as a function of β.

Figure 3-22 shows the expected asymptotic capacity lower bound (solid black line) given in equation (3.129) as a function of SNR. In each panel in the figure, the ratio of number of transmit apertures to receive apertures is the same while the total number of apertures is varied: the upper-left panel shows $n_{tx} = 4, n_{rx} = 1$, the upper-right panel shows $n_{tx} = 8, n_{rx} = 2$, the lower panel plot shows $n_{tx} = 20, n_{rx} = 5$ and the lower right plot shows $n_{tx} = 40, n_{rx} = 10$. In all panels, the high-SNR equation for expected capacity, equation (3.134), is shown as a blue line. A Monte-Carlo simulation of capacity with optimal power allocation is shown as red '+' symbols. For this simulation, many independent turbulence states were generated. The optimal power allocation and the associated capacity for each state were calculated and displayed as a red '+'. Finally the capacity for equal power allocation (EPA) of a single simulated atmospheric state is shown as magenta 'x' symbols. For this simulation, many inde-

pendent turbulence states were generated. Each eigenmode associated with a nonzero squared singular value was allocated equal power and the associated capacity for each state was calculated and displayed as magenta 'x' symbols. All simulations were performed with an atmospheric $\sigma_\chi^2 = 0.1$. The EPA simulation is in excellent agreement with the asymptotic theory. Note that the asymptotic theory provided under EPA is a very good bound for the expected capacity under optimal. Because the optimal scheme—water-filling—approaches equal power allocation at high-SNR, we expect a very good bound at high-SNR. Because the eigenvalue density for small β is bounded away from zero, we expect the EPA scheme to provide closer bounds for small values of β (i.e., EPA must provide less power to small eigenvalues when β is small). Finally, the variation around the average capacity decreases rapidly. By $n_{tx} = 20$ and $n_{rx} = 5$, the average capacity bound is a good approximation for the capacity of a *single* turbulence state. For $n_{tx} = 4$ and $n_{rx} = 1$, the average capacity bound can be very different from the capacity of any particular turbulence realization.

We have given a closed-form expression for the equal power allocation capacity, which is a bound for the optimal power allocation capacity. While this bound is tight when β is far from one or when the SNR is high, we now proceed to develop another useful bound to the optimal power allocation capacity. This second bound, which is tight for asymptotically low-SNR, is based on the intuition that at low received power, the optimal scheme is to allocate all the transmit power to the eigenmode associated with the largest squared singular value. For low-SNR, the optimal water filling scheme allocates all the power to the strongest eigenmode. So, the expected capacity is:

$$\begin{aligned} \lim_{\mathrm{SNR}\to\mathrm{small}} \mathbb{E}[\mathrm{C}] &= \log\left(1 + \mathrm{SNR}\left(\max_{\mathsf{i}} \gamma_{\mathsf{i}}\right)\right) \\ &= \log\left(1 + \mathrm{SNR}\left(1 + \sqrt{\beta}\right)^2\right) \\ &\approx \mathrm{SNR}\left(1 + \sqrt{\beta}\right)^2 \end{aligned} \tag{3.135}$$

where we arrived at the last inequality with a Taylor series expansion $\log(1 + |x|) \approx |x|, |x| \ll 1$. We see that capacity varies linearly with SNR. Additionally when

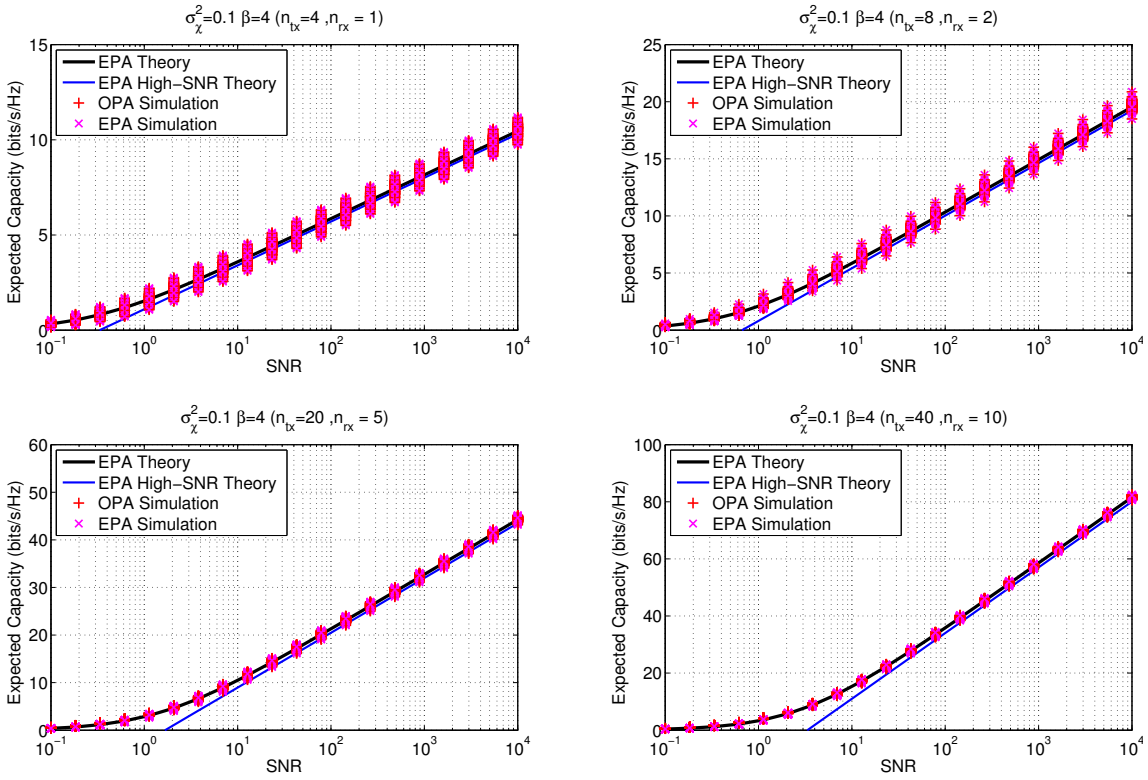

Figure 3-22: Expected channel capacity versus SNR, theory and simulation: The solid black line is the expected asymptotic capacity lower bound given in equation (3.129). The blue line is the high-SNR capacity approximation. The red '+' symbols are the results of simulation with optimal power allocation and the magenta 'x' symbols are the results of simulation with equal power allocation. All simulations were performed with an atmospheric $\sigma_\chi^2 = 0.1$.

$n_{tx} > n_{rx}$, capacity varies approximately linearly with the number of transmit apertures. Therefore it is equally efficient, in the low-SNR region, to increase capacity by increasing SNR or by increasing the number of transmit apertures.

Figure 3-23 shows the expected capacity in the low-SNR region as a function of SNR. The solid black line is the asymptotic capacity lower bound given in equation (3.129). The high-SNR and low-SNR bounds on capacity are shown as blue and red lines, respectively. The cyan '+' symbols are the results of a simulation with optimal power allocation and the magenta 'x' symbols are the results of simulation with equal power allocation. For SNR < 1 the low-SNR bound is in excellent agreement with the optimal power allocation simulation.

We conclude this section by noting that the optimal power allocation scheme maximizing capacity in the small SNR regime is the same as the optimal scheme for minimizing BER: allocate all transmit power to the eigenmode associated with largest squared singular value. Thus, a system designed to maximize capacity with optimal power allocation will automatically 'switch' to outage protection mode when a fade occurs. When not in a fade, the system will opportunistically maximize the data transfer through the advantageous channel. Because the bandwidth of the free space optical channel is very large compared to typical system bit-rate requirements, the complexity associated with transmitting information on multiple modes typically not justified. If situation arise where multiple mode data transmission is necessary, future research could focus on the performance of such a system. We have provided the asymptotic average performance, but have not provided finite or ϵ-capacity analysis necessary for a full exploration of such a system. Finite analysis will require an analytic expression for the squared singular value distribution for finite matrices. ϵ-capacity analysis will require an understanding of the way the squared singular value distribution typically deviates from the Marcenko-Pastur distribution.

3.4 Alternative Normalization

We conclude by restating key results from this chapter with an alternative normalization:

$$\vec{y} = \sqrt{\frac{\mathrm{SNR}}{N}}\mathbf{H}\vec{x} + \vec{w} \tag{3.136}$$

where N can be any function of the number of transmit apertures and receive apertures. Under this normalization, the empirical eigenvalue distribution of $\mathbf{H}\mathbf{H}^{\dagger}/N$ is:

$$f_{\gamma^2}(x;\beta) = (1-\beta)^{+}\delta(x) + \frac{\sqrt{\left(x - \left(\sqrt{\frac{n_{rx}}{N}} - \sqrt{\frac{n_{tx}}{N}}\right)^2\right)^{+}\left(\left(\sqrt{\frac{n_{rx}}{N}} + \sqrt{\frac{n_{tx}}{N}}\right)^2 - x\right)^{+}}}{2\pi x n_{rx}/N} \tag{3.137}$$

Similarly the empirical eigenvalue distribution of $\mathbf{H}^\dagger\mathbf{H}/N$ is:

$$f_{\gamma^2}(x;\beta) = \left(1-\frac{1}{\beta}\right)^+ \delta(x) + \frac{\sqrt{\left(x-\left(\sqrt{\frac{n_{rx}}{N}}-\sqrt{\frac{n_{tx}}{N}}\right)^2\right)^+\left(\left(\sqrt{\frac{n_{rx}}{N}}+\sqrt{\frac{n_{tx}}{N}}\right)^2-x\right)^+}}{2\pi x n_{tx}/N} \tag{3.138}$$

For both $\mathbf{H}^\dagger\mathbf{H}/N$ and $\mathbf{H}\mathbf{H}^\dagger/N$, the maximum nonzero eigenvalue value is:

$$\gamma^2_{\max} = \left(\sqrt{\frac{n_{rx}}{N}}+\sqrt{\frac{n_{tx}}{N}}\right)^2 \tag{3.139}$$

while the minimum nonzero eigenvalue is:

$$\gamma^2_{\min} = \left(\sqrt{\frac{n_{rx}}{N}}-\sqrt{\frac{n_{tx}}{N}}\right)^2 \tag{3.140}$$

Thus it is clear that for any symmetric normalization (where transmit and receive apertures are treated the same) the nonzero eigenvalue distribution is the same for both $\mathbf{H}^\dagger\mathbf{H}/N$ and $\mathbf{H}\mathbf{H}^\dagger/N$. The average BER as the number of apertures grows, using optimal wavefront predistortion, and with the generalized normalization is:

$$\lim_{n_{tx},n_{rx}\to\infty} \mathbb{E}[\Pr(\text{error})] = Q\left(\sqrt{2\text{SNR}\left(\sqrt{\frac{n_{rx}}{N}}+\sqrt{\frac{n_{tx}}{N}}\right)^2}\right) \tag{3.141}$$

The average BER as the number of apertures grows, using selection transmission, and with the generalized normalization is:

$$\lim_{n_{tx},n_{rx}\to\infty} \mathbb{E}[\Pr(\text{error})] = Q\left(\sqrt{\frac{2\text{SNR}}{N}\left(n_{rx}+\sqrt{2\left(e^{4\sigma^2}-1\right)\log(n_{tx})n_{rx}}\right)}\right) \tag{3.142}$$

Finally, the average BER as the number of apertures grows, using open loop transmission, and with the generalized normalization is:

$$\lim_{n_{tx},n_{rx}\to\infty} \mathbb{E}[\Pr(\text{error})] = Q\left(\sqrt{\frac{2\text{SNR}n_{rx}}{N}}\right) \tag{3.143}$$

It is now clear why $N = n_{rx}$ is the preferred normalization: it is the only normalization that gives sparse aperture without wavefront predistortion performance that does not depend on the number of apertures. As a result, we are able to easily study the improvement of spatial modulation over open loop systems.

For clarity, we now present three concrete examples. In all three examples we assume perfect knowledge of the channel state at the receiver, and optimal recombination. First we calculate the performance of a fixed system (e.g., there is no control over the number and size of all the apertures) both with and without feedback. Because the system is fixed, no normalization is necessary. In this case, the asymptotic average performance without feedback is:

$$\lim_{n_{tx},n_{rx}\to\infty} \mathbb{E}[\Pr(\text{error})] = Q\left(\sqrt{2\text{SNR}n_{rx}}\right) \tag{3.144}$$

And the asymptotic average performance with feedback is:

$$\lim_{n_{tx},n_{rx}\to\infty} \mathbb{E}[\Pr(\text{error})] = Q\left(\sqrt{2\text{SNR}\left(\sqrt{n_{rx}}+\sqrt{n_{tx}}\right)^2}\right) \tag{3.145}$$

We see that without feedback, only the number of receive apertures contributes to increasing performance. With the feedback link and wavefront predistortion, the number of receiver apertures *or* the number of transmit apertures contributes to increasing performance. In this case, the value of the feedback is the ratio of $\left(\sqrt{n_{rx}}+\sqrt{n_{tx}}\right)^2$ and n_{rx}. Simplifying, we see that the value of the feedback is $P_{\text{gain}} = \left(1+\sqrt{\beta}\right)^2$. For the second example, we modify the fixed system so that we can choose which side is the transmitter and which side is the receiver and calculate the performance both with and without feedback. Because we can choose which is the transmitter and receiver, we will always choose the arrangement where the transmitter has fewer apertures. This arrangement is preferable because it performs better when there is no feedback and because it requires a lower rate feedback link. In this case, the asymptotic average performance without feedback is:

$$\lim_{n_{tx},n_{rx}\to\infty} \mathbb{E}[\Pr(\text{error})] = Q\left(\sqrt{2\text{SNR}\max(n_{tx},n_{rx})}\right) \tag{3.146}$$

And the asymptotic average performance with feedback is:

$$\lim_{n_{tx},n_{rx}\to\infty} \mathbb{E}[\Pr(\text{error})] = Q\left(\sqrt{2\text{SNR}\left(\sqrt{n_{rx}}+\sqrt{n_{tx}}\right)^2}\right) \tag{3.147}$$

With the feedback link and wavefront predistortion, the number of receiver apertures *or* the number of transmit apertures contributes to increasing performance. In this case, the value of the feedback is the ratio of $\left(\sqrt{n_{rx}}+\sqrt{n_{tx}}\right)^2$ and $\max(n_{tx}, n_{rx})$. Simplifying, we see that the value of the feedback is:

$$P_{\text{gain}} = \left(1+\sqrt{\frac{\min(n_{tx}, n_{rx})}{\max(n_{tx}, n_{rx})}}\right)^2 \tag{3.148}$$

For the third case, we consider the bidirectional communication system with a fixed number and size of apertures. For this case, we calculate the performance of the worst case (without feedback) link and then calculate the performance of the same link with feedback. The open loop system with the worst case performance is the one with the fewest receive apertures. Thus the asymptotic average performance without feedback is:

$$\lim_{n_{tx},n_{rx}\to\infty} \mathbb{E}[\Pr(\text{error})] = Q\left(\sqrt{2\text{SNR}\min(n_{tx}, n_{rx})}\right) \tag{3.149}$$

And the asymptotic average performance with feedback is:

$$\lim_{n_{tx},n_{rx}\to\infty} \mathbb{E}[\Pr(\text{error})] = Q\left(\sqrt{2\text{SNR}\left(\sqrt{n_{rx}}+\sqrt{n_{tx}}\right)^2}\right) \tag{3.150}$$

With the feedback link and wavefront predistortion, the number of receiver apertures *or* the number of transmit apertures contributes to increasing performance. In this case, the value of the feedback is the ratio of $\left(\sqrt{n_{rx}}+\sqrt{n_{tx}}\right)^2$ and $\min(n_{tx}, n_{rx})$. Simplifying, we see that the value of the feedback is:

$$P_{\text{gain}} = \left(1+\sqrt{\frac{\max(n_{tx}, n_{rx})}{\min(n_{tx}, n_{rx})}}\right)^2 \tag{3.151}$$

Thus we see that, depending on the specific design constraints, the feedback power gain can be very different.

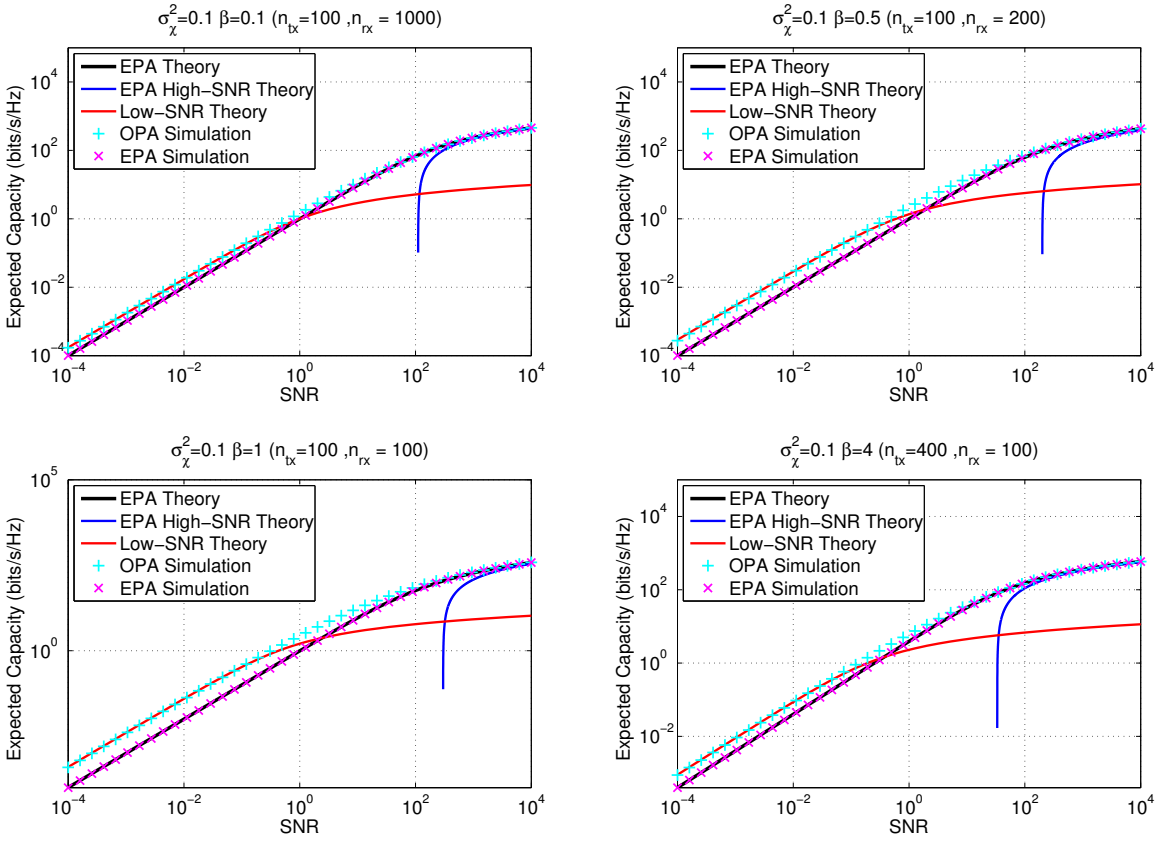

Figure 3-23: Expected channel capacity showing low-SNR region: The solid black line is the expected asymptotic capacity lower bound given in equation (3.129). The blue line is the high-SNR capacity approximation. The red line is the expected asymptotic capacity lower bound for lower SNR given in equation (3.135). The cyan '+' symbols are the results of simulation with optimal power allocation and the magenta 'x' symbols are the results of simulation with equal power allocation. All simulations were performed with an atmospheric $\sigma_\chi^2 = 0.1$.

Chapter 4

On the Time Dynamics of Optical Communication through Atmospheric Turbulence with Feedback

In this chapter, we develop closed-form analytic expressions for the effects of the dynamic atmosphere on system performance. The major consequence of the dynamic channel state is that the system's estimate of the channel may grow stale, causing the transmitter to couple into spatial modes that propagate suboptimally and the receiver to tune away from the information bearing spatial mode. Specifically, we show how system performance degrades as the transmitter's channel state estimate becomes stale or both the receiver's and transmitter's estimate becomes stale. This will allow us to address the impact of a lag in receiver channel state tracking.

We generalize our analysis to allow dynamically changing turbulence with finite rate latent feedback in an attempt to answer design questions important to system implementation and deployment. How much do feedback delay and computational time impact performance? Given a system geometry, what feedback rate is needed to take full advantage of the diversity? If the feedback link has a rate of r, what is

the best performance possible? How often does the transmitter need channel state updates? At each update, what information does the transmitter need? In terms of feedback information, we have two degrees of freedom: how often to feed back an update, and what information is fed back at each update. If we feed back very infrequently with respect to the channel coherence time, we would need to send back a full set of channel state information. If we update the state information more frequently, we may not have to transmit the full set of channel state information. For example, if we update the state information at a tenth of the channel coherence time, we could possibly feed back a state update, or perturbation, instead of the full set of channel state information (CSI). Finally, given a system geometry and performance requirements, what is the trade between increasing transmit power and increasing feedback rate?

Communication systems are designed with the worst-case performance as the primary driver of scale and expense. As a result, we wish to utilize the feedback link in a way that achieves the *best* worst-case performance, the so called maximin problem:

$$\mathrm{BER}^* = \min_{\text{feedback schemes}} \left(\max_t \mathrm{BER} \right) \tag{4.1}$$

where BER (bit error rate) is the probability of error averaged over all atmospheric states, the maximization is over time, and the minimization is over all possible feedback schemes. We find a scheme that achieves the best worst-case performance by breaking the problem into coupled subproblems: the channel time dynamics and the description of the channel state.

First, using results from rate distortion theory we find the best possible performance given some number of bits to describe the channel state. We also show exactly what information to feed back to achieve the best performance. Next, we derive the effects of atmospheric time dynamics and channel state estimate latencies, both at the transmitter and receiver. Finally, we combine the reduction in performance because of the limited number of bits to describe each channel state with the reduction in performance due to channel time dynamics and latencies to quantify the effect of the

dynamic atmosphere channel on the performance of systems that use feedback with wavefront predistortion. We will provide the optimal performance of a system given the fundamental design parameters: wind direction, atmospheric structure constant, number of transmit and receive apertures, and feedback bit rate and latency.

4.1 Feedback Link Description

We assume a fixed atmosphere, with a limited amount of feedback information, R_u bits, to describe the atmospheric state to the transmitter. We would like to find a scheme that efficiently uses those bits to minimize the bit error rate resulting from wavefront predistortion based on the feedback information. Notionally, we can express the problem as:

$$\min_{R \leq R_u} \text{BER} \tag{4.2}$$

where R is the number of bits fed back and R_u is the maximum number of bits that can be fed back. We have not yet specified if we want to minimize average BER or the BER for a given outage probability. Because the feedback information is used to tune the amplitude and phase of each transmit aperture, the minimization translates to selecting a spatial field distribution for a given channel realization that can be fed back in less than R_u bits and achieves the minimum BER. We can reformulate the problem as finding a mapping $g(\cdot) : \mathbb{C}^{n_{tx} \times n_{rx}} \rightarrow \mathbb{C}^{n_{tx}}$ from the channel transfer matrix to a set of amplitude and phase tuning coefficients:

$$g^*(\cdot) = \arg \min_{g(\mathbf{H}_c): H(g(\mathbf{H}_c)) \leq R_u} \text{BER} \tag{4.3}$$

where $H(\vec{x})$ is a function whose output is the average number of bits that it takes to describe $\vec{x}$ and $\mathbf{H}_c$ is the current atmospheric state. If we view the transmit field distribution as a vector in a metric space (the *transmit vector*), then the power constraint implies that set of all possible transmit vectors must, on average, lie on a $2n_{tx}$ dimensional unit sphere. Figure 4-1 shows a notional view of this metric space when the number of transmit apertures is equal to two. The vectors $\vec{v}_{max}$ and $\vec{v}_{min}$

are input eigenvectors of a sample atmospheric state. As the field propagates through the channel, the unit sphere is stretched and rotated, as shown in the figure. The vectors $\vec{u}_{max}$ and $\vec{u}_{min}$ are output eigenvectors of a sample atmospheric state.

The limit on the amount of feedback information implies that the function $g(\cdot)$ will necessarily produce a distorted representation of the information so that it can be fed back with less than R_u bits. The function $g(\cdot)$ that produces the distorted representation is generally referred to as *quantization*. We refer to the vector that we calculate to be the optimal transmit vector as the *ideal transmit vector* and the distorted transmit vector as the *quantized transmit vector*. There are many functions $g(\cdot)$ to quantize the ideal transmit vector; a candidate function is to uniformly quantize the real and imaginary part of each element of the ideal transmit vector. Figure 4-1 shows an example of a uniform quantizer: for a particular atmospheric realization the uniform quantizer would select the grid point (shown as gray squares in the figure) closest to the ideal transmit vector and feed back the index associated with grid point. The grid point associated with the index is then the quantized transmit vector. Uniform quantization is simple but inherently inefficient as it makes no use of a priori information about the structure of the ideal transmit vector. For example, the uniform quantizer does not use the a priori information that the ideal transmit vector must have unit length on average. If we have a very large amount of feedback information, the grid points can be placed very close to one another, and the transmitter can therefore have near perfect knowledge of the ideal transmitter vector. In this case, the optimal function for infinite information fed back is $g^*_{\infty-\text{rate}}(\cdot)$ [44]:

$$g^*_{\infty-\text{rate}}(\mathbf{H}_c) \approx \vec{v}_{max}(\mathbf{H}_c) \tag{4.4}$$

where we have used the notation that the $\vec{v}_{max}(\mathbf{H}_c)$ is the best input eigenmode associated with a particular channel realization $\mathbf{H}_c$. If we have no feedback link, and therefore have no knowledge of the channel state at the transmitter, there will be zero

grid points. In this case, the optimal function for zero rate feedback is $g^*_{0-\text{rate}}$:

$$g^*_{0-\text{rate}}(\mathbf{H}_c) = \kappa \tag{4.5}$$

where $\kappa \sim \text{CN}(0,1)$, CN denotes complex circularly normal. Therefore, allocating random amplitude and phase to each transmit aperture, independent of the channel realization $\mathbf{H}_c$, achieves minimum BER. If we have limited feedback, there are more sophisticated quantization functions to minimize the BER given a feedback rate of R_u.

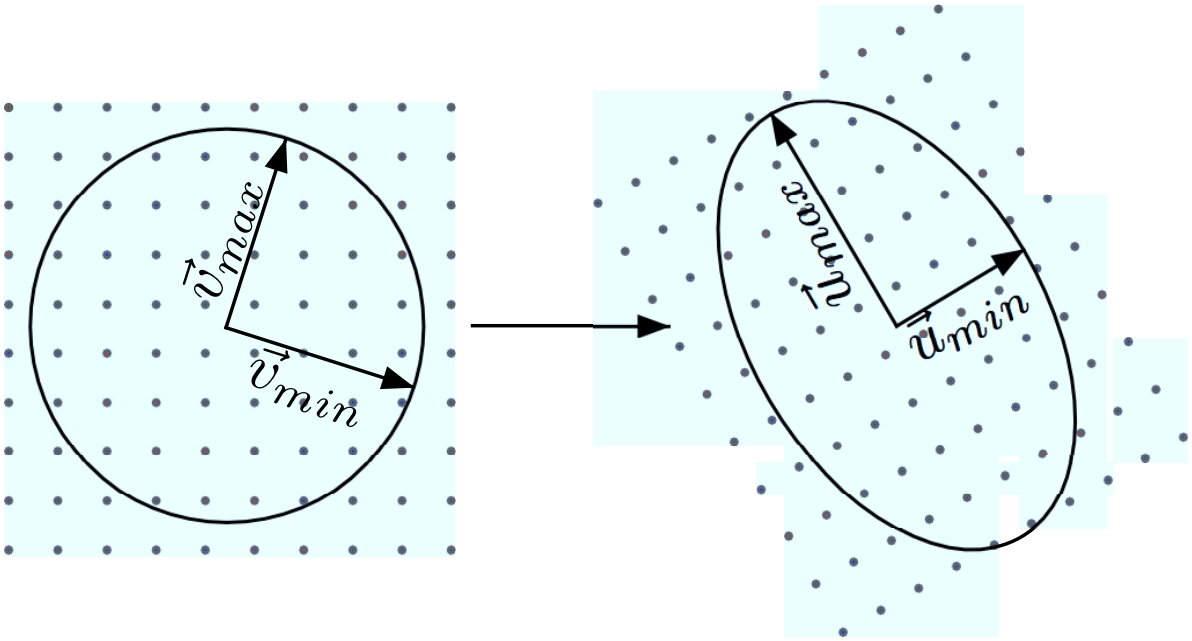

Figure 4-1: Metric space representation of input/output field ($n_{tx} = 2$) with uniform quantization grid overlaid in gray.

Another candidate function $g(\cdot)$ to quantize the ideal transmit vector is a *vector quantizer*, as shown in figure 4-2. Similar to the uniform quantizer, for a particular atmospheric realization the vector quantizer selects the grid point (shown as gray squares in the figure) closest to the ideal transmit vector and feeds back the index associated with the grid point. The quantized transmit vector is then the grid point associated with the fed back index. The vector quantizer is inherently more efficient than the uniform quantizer because it is able to take advantage of the structure of the ideal transmit vector to optimize the quantization regions. A straightforward vector

quantization would simply place grid points equally spaced on the surface of the unit sphere. Is there a better way to place the grid points on the sphere? If there are some regions on the sphere where atmospheric states are more likely to occur, it would increase performance to quantize more finely there, while quantizing more coarsely in regions of the sphere where atmospheric states are less likely to occur. Indeed, we will find that the optimal quantization scheme does just that.

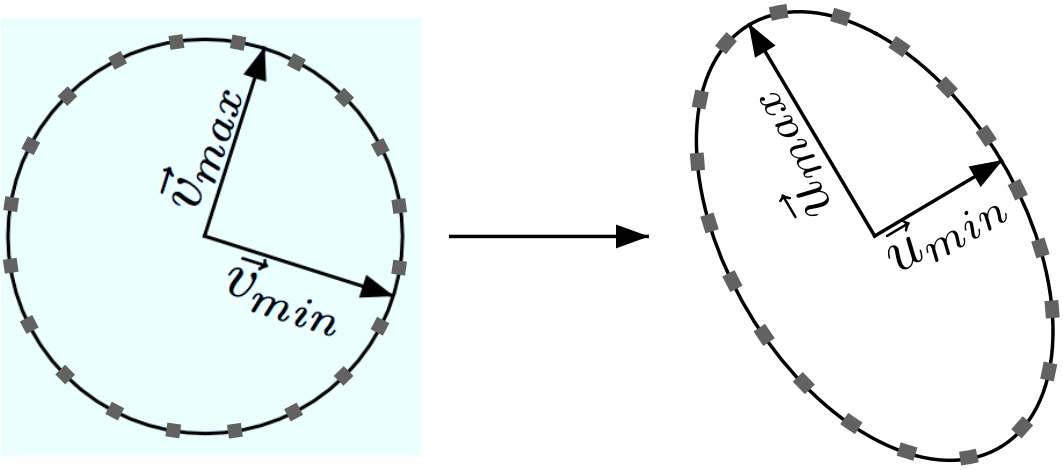

Figure 4-2: Metric space representation of input/output field ($n_{tx} = 2$) with vector quantization grid overlaid in gray.

4.1.1 Asymptotic Analysis of Full Update

In this section, we find the optimal mapping $g^*(\cdot)$ as the number of transmit and receive apertures grows asymptotically large. As the number of transmit and receive apertures grows large, the weak law of large numbers takes effect causing the variation around the expected value to be very small. We therefore focus on minimizing the average BER.

Theorem 12 *For a given rate R_u and an asymptotically large number of transmit and receive apertures, with probability one, the minimum achievable average probability of error is:*

$$\mathbb{E}[\Pr(\text{error})] = Q\left(\sqrt{2\text{SNR}\left[\left(1+\sqrt{\frac{n_{tx^*}}{n_{rx}}}\right)^2\left(1-2^{\frac{-R_u}{n_{tx^*}}}\right)+2^{\frac{-R_u}{n_{tx^*}}}\right]}\right)$$

where $Q(\cdot)$ is the Q-function, n_{rx} is the number of receive apertures and n_{tx^*} is the number of transmit apertures that are allocated a nonzero rate (if a transmit aperture is not allocated rate, it is turned off):

$$n_{tx^*} = \underset{n_{txo}:n_{txo}\leq n_{tx}}{\operatorname{argmax}} \left(1+\sqrt{\frac{n_{txo}}{n_{rx}}}\right)^2 \left(1-2^{\frac{-R_u}{n_{txo}}}\right)+2^{\frac{-R_u}{n_{txo}}}$$

Proof. We start by finding the performance assuming the amount of feedback information is large enough so that allocating bits to all the transmit apertures is optimal. Then we generalize our solution for the case where the amount of information is too small for allocating bits to every transmit aperture to be optimal. We start with the most general expression:

$$\begin{aligned}\mathbb{E}[\Pr(\text{error})] &= \min_{g(\mathbf{H}_c):H(g(\mathbf{H}_c))\leq R_u} \mathbb{E}[\text{BER}] \\ &= \min_{g(\mathbf{H}_c):H(g(\mathbf{H}_c))\leq R_u} \mathbb{E}\left[Q\left(\sqrt{2\text{SNR}\,|\phi_s|^2}\right)\right]\end{aligned} \tag{4.6}$$

where ϕ_s is the signal portion of the sufficient statistic. Assuming an infinite number of receive apertures, the sufficient statistic variance becomes small so that we can move the expectation inside the Q-function:

$$\mathbb{E}[\Pr(\text{error})] = \min_{g(\mathbf{H}_c):H(g(\mathbf{H}_c))\leq R_u} Q\left(\sqrt{2\text{SNR}\cdot\mathbb{E}\left[|\phi_s|^2\right]}\right) \tag{4.7}$$

If we use the optimal spatial matched filter to detect the received field, we can write the sufficient statistic in terms of the transmitted field, $\vec{x'}$, and the square singular values of $\mathbf{H}_c$:

$$\mathbb{E}[\Pr(\text{error})] = \min_{g(\mathbf{H}_c):H(g(\mathbf{H}_c))\leq R_u} Q\left(\sqrt{2\text{SNR}\cdot\mathbb{E}\left[\int_{\gamma_{min}^2}^{\gamma_{max}^2} s\left\langle\vec{x'},\vec{v}(s)\right\rangle ds\right]}\right)$$

where $<\cdot,\cdot>$ is a vector inner product, γ_{min}^2 is the minimum nonzero square singular value of $\mathbf{H}_c$, and γ_{max}^2 is the maximum square singular value of $\mathbf{H}_c$. Asymptotically, the minimum nonzero square singular value converges almost surely to

$\left(1-\sqrt{n_{tx}/n_{rx}}\right)^2$ and the maximum square singular value converges almost surely to $\left(1+\sqrt{n_{tx}/n_{rx}}\right)^2$. Consequently, the expectation can be moved inside the integral:

$$\mathbb{E}[\Pr(\text{error})] = \min_{g(\mathbf{H}_c):g(\mathbf{H}_c)\leq R_u} Q\left(\sqrt{2\text{SNR}\int_{\left(1-\sqrt{\frac{n_{tx}}{n_{rx}}}\right)^2}^{\left(1+\sqrt{\frac{n_{tx}}{n_{rx}}}\right)^2} s\mathbb{E}\left[\left\langle \vec{x'}, \vec{v}(s)\right\rangle\right] ds}\right) \tag{4.8}$$

Physically, assuming the limits on the integral have reached their asymptotic value is the same as assuming that the spatial modes will change but the distribution of square singular values will remain approximately the same. Because we assume the amount feedback information is large enough to support sending information about each transmit aperture, the optimal solution is to allocate all of the feedback information to a n_{tx}-dimensional vector as close, in the L_2-norm sense, to the best input eigenmode as possible. As such, we break the integral into two parts:

$$\begin{aligned}\mathbb{E}[\Pr(\text{error})] = \min_{g(\mathbf{H}_c):g(\mathbf{H}_c)\leq R_u} Q\Bigg(\Bigg[2\text{SNR}\Bigg(\left(1+\sqrt{\frac{n_{tx}}{n_{rx}}}\right)^2 \times \dots \\ \mathbb{E}\left[\left\langle \vec{x'}, \vec{v}\left(\left(1+\sqrt{\frac{n_{tx}}{n_{rx}}}\right)^2\right)\right\rangle\right] + \dots \\ \int_{\left(1-\sqrt{\frac{n_{tx}}{n_{rx}}}\right)^2}^{\left(1+\sqrt{\frac{n_{tx}}{n_{rx}}}\right)^2} s\mathbb{E}\left[\left\langle \vec{x'}, \vec{v}(s)\right\rangle\right] ds\Bigg)\Bigg]^{1/2}\Bigg)\end{aligned} \tag{4.9}$$

Now we define the average distortion D between the transmit vector $\vec{x'}$ and the best input eigenmode $\vec{v}_{max}$ as:

$$D = \mathbb{E}\left[\left(\vec{x'} - \vec{v}_{max}\right)^2\right] \tag{4.10}$$

Because the entries of $\vec{v}_{max}$ are independent complex Gaussian random variables with variance $1/n_{tx}$, rate distortion theory tells us that the minimum distortion is:

$$D = 2^{\frac{-R_u}{n_{tx}}} \tag{4.11}$$

By orthogonality of the distortion error with the estimate, we have:

$$\mathbb{E}\left[\left\|\vec{x'}\right\|^2\right] = D + \mathbb{E}\left[\left\langle \vec{x'}, \vec{v}_{max} \right\rangle\right] = 1 \tag{4.12}$$

Rearranging terms gives:

$$\mathbb{E}\left[\left\langle \vec{x'}, \vec{v}_{max} \right\rangle\right] = 1 - 2^{\frac{-R_u}{n_{tx}}} \tag{4.13}$$

Giving a probability of error of:

$$\begin{aligned}\mathbb{E}[\Pr(\text{error})] = Q\left(\left[2\text{SNR}\left(\left(1+\sqrt{\frac{n_{tx}}{n_{rx}}}\right)^2\left(1-2^{\frac{-R_u}{n_{tx}}}\right)+\ldots\right.\right.\right.\\ \left.\left.\left.\int_{\left(1-\sqrt{\frac{n_{tx}}{n_{rx}}}\right)^2}^{\left(1+\sqrt{\frac{n_{tx}}{n_{rx}}}\right)^2} s\mathbb{E}\left[\left\langle \vec{x'}, \vec{v}(s) \right\rangle\right] ds\right)\right]^{1/2}\right)\end{aligned} \tag{4.14}$$

Because we are using all available bits to provide information about the best input eigenmode, the quantized transmit vector orthogonal to the direction of the best input eigenmode will couple into all other eigenmodes with equal probability. This gives:

$$\begin{aligned}\mathbb{E}[\Pr(\text{error})] = Q\left(\left[2\text{SNR}\left(\left(1+\sqrt{\frac{n_{tx}}{n_{rx}}}\right)^2\left(1-2^{\frac{-R_u}{n_{tx}}}\right)+\ldots\right.\right.\right.\\ \left.\left.\left.2^{\frac{-R_u}{n_{tx}}}\int_{\left(1-\sqrt{\frac{n_{tx}}{n_{rx}}}\right)^2}^{\left(1+\sqrt{\frac{n_{tx}}{n_{rx}}}\right)^2} s f_{\gamma^2}(s) ds\right)\right]^{1/2}\right)\end{aligned}$$

where $f_{\gamma^2}(s)$ is the probability density function of square singular values of $\mathbf{H}_c$, which is almost surely the Marcenko-Pastur density for large n_{tx}, n_{rx}. The mean of the Marcenko-Pastur density is one, so:

$$\mathbb{E}[\Pr(\text{error})] = Q\left(\sqrt{2\text{SNR}\left[\left(1+\sqrt{\frac{n_{tx}}{n_{rx}}}\right)^2\left(1-2^{\frac{-R_u}{n_{tx}}}\right)+2^{\frac{-R_u}{n_{tx}}}\right]}\right)$$

This expression provides the minimum BER under the requirement that the system uses all available transmit apertures. If we allow the system to allocate zero bits to

some transmit apertures (to turn off transmit apertures), then we find the minimum BER:

$$\mathbb{E}[\Pr(\text{error})] = Q\left(\sqrt{2\text{SNR}\left[\left(1+\sqrt{\frac{n_{tx^*}}{n_{rx}}}\right)^2\left(1-2^{\frac{-R_u}{n_{tx^*}}}\right)+2^{\frac{-R_u}{n_{tx^*}}}\right]}\right)$$

where n_{tx^*} is the optimal number of transmit apertures that are allocated some rate:

$$n_{tx^*} = \underset{n_{txo}:n_{txo}\leq n_{tx}}{\text{argmax}}\left(1+\sqrt{\frac{n_{txo}}{n_{rx}}}\right)^2\left(1-2^{\frac{-R_u}{n_{txo}}}\right)+2^{\frac{-R_u}{n_{txo}}} \tag{4.15}$$

It is important to note that for a finite system the BER could be further reduced by selecting the subset of transmit apertures with the largest maximum square singular value. In the asymptotic case, however, the maximum square singular value is determined solely by the number of utilized transmit and receive apertures.

□

Figure 4-3 shows the minimum BER as a function of normalized rate (R_u/n_{tx}) for SNR = 5. The result is only exact asymptotically, but is a very good approximation when the variation of the sufficient statistic ϕ_s is small compared to the rate of change of the Q-function and when the Marcenko-Pastur distribution is applicable. This translates to the following condition for the theorem to be approximately true:

$$n_{tx} \gg \max\left(20, 2\cdot\text{SNR}\right) \tag{4.16}$$

4.1.2 Optimal mapping, channel state description

We derived Theorem 12 without specifying a mapping $g\left(\mathbf{H}_c\right)$. The following describes the mapping:

- *Generation of a codebook.* At system initialization randomly generate a rate distortion codebook C consisting of $|C| = 2^{R_u^0}$ sequences $\vec{x'}$ drawn iid $\sim N(\vec{0}, I)$. Index these code words by $m \in \{1, 2, \cdots, 2^{R_u^0}\}$. Reveal this codebook to the transmitter and receiver.

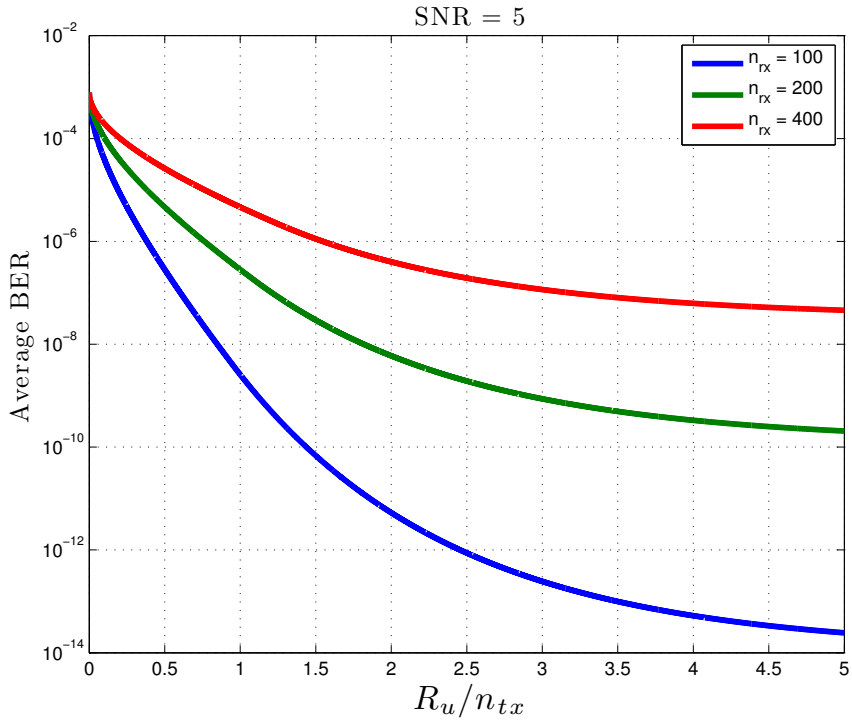

Figure 4-3: Asymptotic BER as a function of normalized rate R_u/n_{tx}

- *Calculate codebook variance.* For each channel state update, calculate the codebook variance: $\left(1 - 2^{-R_u/n_{tx^*}}\right)/n_{tx^*}$. Reveal the variance to both the transmitter and the receiver; the transmitter and receiver should create a scaled codebook.

- *Encoding.* For each full update, find the code word w in the scaled codebook closest to the optimal spatial mode $\vec{v}_{max}(\mathbf{H}_c)$. Make the index w known to both the transmitter and receiver; thus R_u^0 bits suffice to describe the index m of the scaled codebook.

- *Decoding.* The decoded code word is simply $\vec{x'}(m)$.

The physical intuition here is clear: the optimal mapping $g^*(\cdot)$ quantizes more finely in regions of the unit sphere where atmospheric states typically occur while quantizing more coarsely in regions of the sphere where atmospheric states do not typically occur. Figure 4-4 shows an example of such an optimal mapping: for a particular atmospheric realization the quantizer would select the grid point (shown

as gray squares in the figure) closest to the ideal transmit vector and feed back the index associated with grid point. The grid point associated with the index is then the quantized transmit vector. The crucial point for the optimal mapping is that the grid points have been chosen to minimize the average BER.

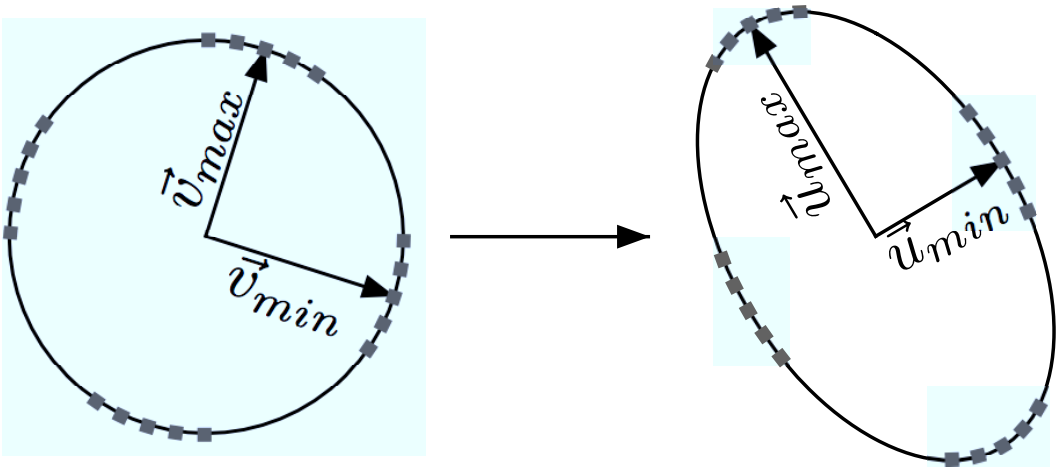

Figure 4-4: Metric space representation of input/output field ($n_{tx} = 2$) with optimal mapping quantization grid overlaid in gray.

4.1.3 Asymptotic Analysis of Incremental Update

A full update is inherently inefficient: there is no mechanism to take advantage of the fact that the transmitter already has some knowledge of the channel state from the previous update. Here we investigate an incremental update strategy that utilizes *a priori* transmitter knowledge. While a full update is required for initialization and periodically to refresh the channel state estimate at the receiver, an incremental update, where the transmitter only receives the change in channel state from the previous state, will have better performance when the update rate is sufficiently fast. Formally, we define an incremental update as the following:

$$\vec{v}_{incremental} = \vec{v}_{max}(\mathbf{H}_c) - \vec{v}_{tx} \tag{4.17}$$

where $\vec{v}_{max}(\mathbf{H}_c)$ is the current channel state and $\vec{v}_{tx}$ is the channel state estimate at the transmitter from the previous update. For this analysis, we still assume we have

some amount of feedback information to describe a fixed atmosphere; the difference is the transmitter already has some information that is correlated with the current fixed atmosphere. The update rate, how often an incremental update is fed back to the transmitter, will control the amount of correlation. This update scheme will have better performance than simply feeding back $\mathbf{H}_c$ at every update provided the update rate is fast enough for $\vec{v}_{incremental}$ to have smaller variance than $\vec{v}(\mathbf{H}_c)$. For the incremental update scheme, Theorem 12 becomes:

$$\mathbb{E}[\Pr(\text{error})] = Q\left(\sqrt{2\text{SNR}\left[\left(1+\sqrt{\frac{n_{tx^*}}{n_{rx}}}\right)^2\left(1-\Psi(\tau)2^{\frac{-R_u}{n_{tx^*}}}\right)+\Psi(\tau)2^{\frac{-R_u}{n_{tx^*}}}\right]}\right) \tag{4.18}$$

where $\Psi(\tau)$ is the average energy of update vector $\vec{v}_{incremental}$ for a given time τ between updates. The number of transmit apertures that are allocated a nonzero rate, n_{tx^*}, is then given by:

$$n_{tx^*} = \underset{n_{txo}:n_{txo}\leq n_{tx}}{\text{argmax}}\left(1+\sqrt{\frac{n_{txo}}{n_{rx}}}\right)^2\left(1-\Psi(\tau)2^{\frac{-R_u}{n_{txo}}}\right)+\Psi(\tau)2^{\frac{-R_u}{n_{txo}}}$$

The average energy of the incremental update vector can be simplified to:

$$\begin{aligned}\Psi(\tau) &= \mathbb{E}\left[\|\vec{v}_{incremental}\|^2\right]\\ &\approx \mathbb{E}\left[\|\vec{v}^{\,\dagger}_{max}(\mathbf{H}_c)-\vec{v}_{tx}\|^2\right]\\ &= 2\left(1-\mathbb{E}\left[\vec{v}^{\,\dagger}_{max}(\mathbf{H}_c)\,\vec{v}_{max}(\mathbf{H}_{tx})\right]\right)+D_0+D_1\\ &= 2\left(1-\mathbb{E}\left[\vec{v}^{\,\dagger}_{max}(\mathbf{H}_c)\,\vec{v}_{max}(\mathbf{H}_{tx})\right]\right)+2^{-R_u^0/n_{tx}}+\Psi(\tau)2^{-R_u/n_{tx}}\end{aligned} \tag{4.19}$$

where D_0 is the distortion of $\vec{v}_{tx}$ because of the finite size of the full-update codebook and D_1 is the distortion of $\vec{v}_{tx}$ because of the size of R_u. We have used that the average energy in $\vec{v}_{max}(\mathbf{H}_c)$ and $\vec{v}_{tx}$ is unity. Solving for $\Psi(\tau)$ yields:

$$\Psi(\tau) = \frac{2\left(1-\mathbb{E}\left[\vec{v}^{\,\dagger}_{max}(\mathbf{H}_c)\,\vec{v}_{max}(\mathbf{H}_0)\right]\right)+2^{-R_u^0/n_{tx}}}{1-2^{-R_u/n_{tx}}} \tag{4.20}$$

This shows that $\Psi(\tau)$ depends on the number of bits used to describe the initial channel state, the number of bits used to describe the channel state update, and the covariance between the current channel state, $\vec{v}_{max}^{\,\dagger}(\mathbf{H}_c)$, and the channel state at the last update, $\vec{v}_{max}(\mathbf{H}_0)$: as $\vec{v}_{max}^{\,\dagger}(\mathbf{H}_c)$ and $\vec{v}_{max}(\mathbf{H}_0)$ become more correlated, the average energy in $\vec{v}_{incremental}$ becomes less and, as a result, fewer bits are needed to describe the channel state. The denominator term $1 - 2^{-R_u/n_{tx}}$ represents a pole in the system; physically, this arises because the energy in each update depends on the distortion of the previous update. If the distortion of the previous update is small, then the current update will require few bits. Conversely, if the distortion of the previous update is large, the current update will require more bits. If the average energy in the incremental update vector is less than the average energy in the full update vector $\Psi(\tau) < 1$, it is better to use the incremental update scheme. If however, the average energy in the incremental update vector is more than the average energy in the full update vector $\Psi(\tau) > 1$, it is better to use the full update scheme. We will more generally refer to $\Psi(\tau)$ as the average energy associated with the best update strategy. As a result, the average energy of the update vector must be less than or equal to one, $\Psi(\tau) \leq 1$.

Using the data processing inequality, in conjunction with our full update result, we find the following bound on $\Psi(\tau)$:

$$\min\left(\frac{2\left(1 - R_{hh}(\tau)\right) + 2^{-R_u^0/n_{tx}}}{1 - 2^{-R_u/n_{tx}}}, 1\right) \leq \Psi(\tau) \leq 1 \tag{4.21}$$

Figure 4-5 shows the upper and lower bounds from equation (4.21) along with a simulation versus atmospheric temporal autocovariance function. Comparing the bounds with the simulation, it is clear the lower bound is too optimistic. As a result, the following approximation was derived to fit the simulation results:

$$\Psi(\tau) \approx \min\left(\frac{2\left(1 - \left(R_{hh}(\tau)\right)^{10}\right) + 2^{-R_u^0/n_{tx}}}{1 - 2^{-R_u/n_{tx}}}, 1\right) \tag{4.22}$$

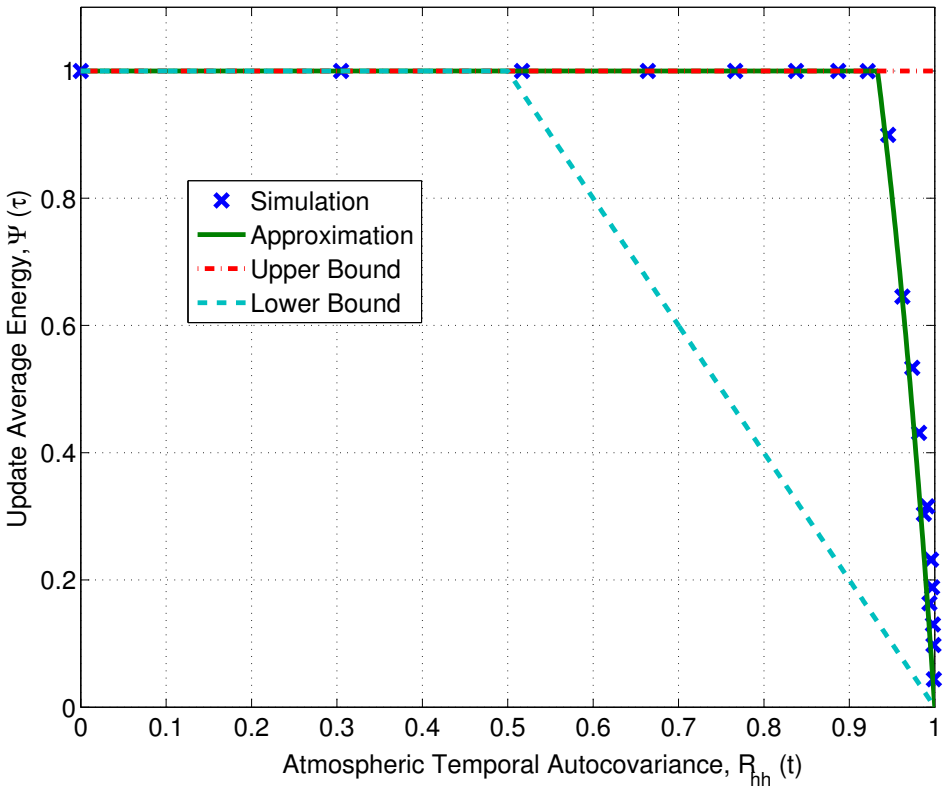

Figure 4-5: Update average energy versus atmospheric temporal autocovariance for $n_{tx} = n_{rx}$.

Equations (4.18) and (4.19) in conjunction with equation (4.22) fully specify the performance for the full update and incremental update schemes. It is optimal to transition from full update to incremental update whenever the update rate is sufficiently fast:

$$t_u \leq \left(\frac{1}{5}\log 2\right)^{3/5} t_0 \approx 0.93 t_0 \tag{4.23}$$

where t_u is the time between updates. Physically, it is intuitively appealing that the transition should be approximately the atmospheric coherence time: if the update rate is much larger than the coherence time, the transmitter's *a priori* information is uncorrelated with the current channel state and we should therefore feed back a full update.

4.1.4 Optimal Mapping, Channel State Description

We derived this theorem without specifying a mapping $g(\mathbf{H}_c)$ for an incremental update. The following describes the mapping for a full update or incremental update:

- *Generation of a codebook.* At system initialization randomly generate a rate distortion codebook C consisting of $2^{R_u^0}$ sequences $\vec{x'}$ drawn iid $\sim N(\vec{0}, I)$. Index these code words by $m \in \{1, 2, \cdots, 2^{R_u^0}\}$. Reveal this codebook to the transmitter and receiver.

- *Calculate codebook variance.* For each channel state update, calculate the codebook variance: $\left(1 - \Psi(\tau)2^{-R_u/n_{tx^*}}\right)/n_{tx^*}$. For a full update, $\Psi(\tau) = 1$ and $R_u = R_u^0$. For an incremental update $\Psi(\tau)$ should be calculated according to equation (4.22) while R_u can be chosen to be any integer smaller than R_u^0. Reveal $\Psi(\tau)$ and R_u to both the transmitter and the receiver; the transmitter and receiver should create a scaled codebook with $\Psi(\tau)$.

- *Encoding.*

  - For a full update, find the code word m in the scaled codebook closest to the optimal spatial mode $\vec{v}_{max}(\mathbf{H}_c)$. Make the index m known to both the transmitter and receiver; thus R_u^0 bits suffice to describe the index w of the scaled code word.

  - For an incremental update, divide the scaled codebook into $\{C_i, \forall i \in 1, \cdots, 2^{(R_u^0 - R_u)}\}$ scaled sub-codebooks each consisting of 2^{R_u} code words. Index these code words $m' \in \{1, 2, \cdots, 2^{R_u}\}$. For the first incremental update, find the code word m' in the first scaled sub-codebook closest to the optimal spatial mode $\vec{v}_{incremental}$. Make the index m' known to the transmitter and receiver; thus R_u bits suffice to describe the index m'. For the second incremental update, use the second scaled sub-codebook and so on. When all of the scaled sub-codebooks have been used, start over at the first scaled sub-codebook.

- *Decoding.* The decoded code word is simply $\vec{x'}(m) \in C$ for a full update or $\vec{x'}(m') \in C_i$ for an incremental update.

4.1.5 Large and Small Rate Limits

In the limit as the rate R_u becomes very large, the minimum BER converges to the minimum BER with perfect state knowledge:

$$\lim_{R_u \to \infty} \mathbb{E}[\Pr(\text{error})] = Q\left(\sqrt{2\text{SNR}\left(1+\sqrt{\frac{n_{tx}}{n_{rx}}}\right)^2}\right) \tag{4.24}$$

Similarly, as the rate R_u tends to zero the minimum BER converges to the minimum BER with no state knowledge:

$$\lim_{R_u \to 0} \mathbb{E}[\Pr(\text{error})] = Q\left(\sqrt{2\text{SNR}}\right) \tag{4.25}$$

It is satisfying that both limits converge to previously known results. It is interesting to look at what happens when the number of transmit apertures is increased without increasing the number of receive apertures or the rate:

$$\lim_{R_u \to \text{small}} \mathbb{E}[\Pr(\text{error})] = Q\left(\sqrt{2\text{SNR}\left(1+\frac{R_u}{n_{rx}}\log(2)\right)}\right)$$

In this rate-starved case, the average power gain is linear in rate R_u.

4.1.6 Optimal Number of Transmit Apertures

While Theorem 12 provides an exact expression, it must be solved for numerically. Figure 4-6 shows the optimal number of transmit apertures versus rate for various numbers of receive apertures. We assumed an unlimited number of transmit apertures for the calculation. Given a desired feedback rate R_u and a number of receive apertures n_{rx}, the figure provides the number of transmit apertures that should be used, n_{tx^*}. If the system has more transmit apertures than n_{tx^*}, then $n_{tx} - n_{tx^*}$,

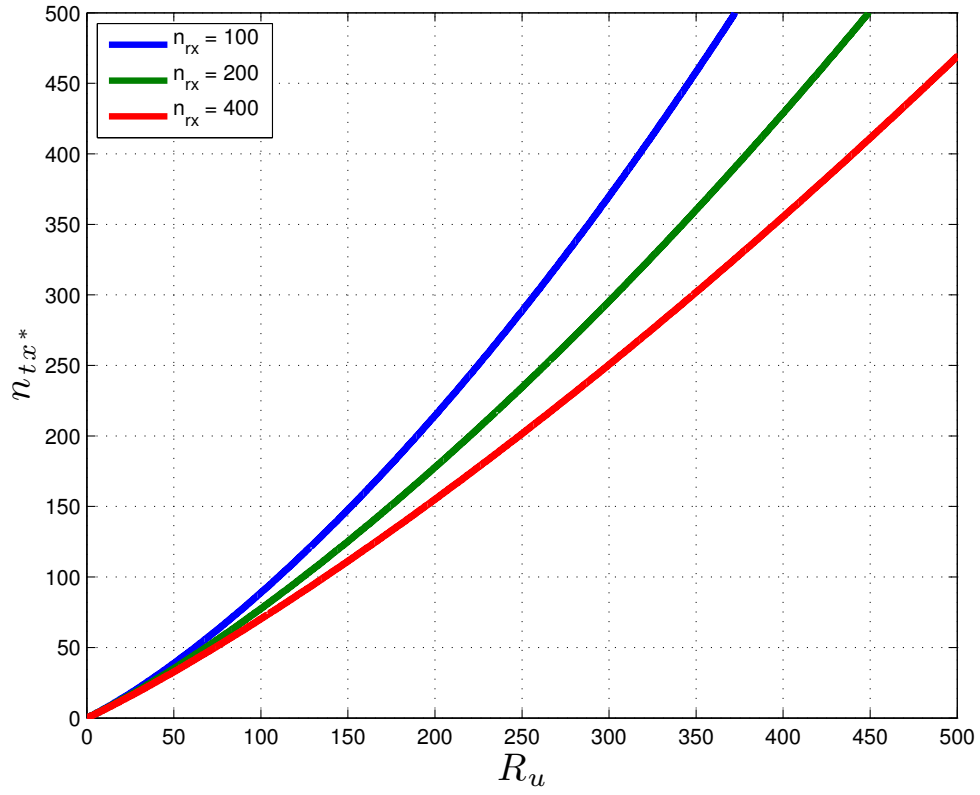

Figure 4-6: Optimal number of transmit apertures as a function of rate R_u

transmit apertures will be unused. While the exact BER solution requires an numeric solution, we can upper bound the minimum performance by requiring that all transmit apertures be used:

$$\mathbb{E}[\Pr(\text{error})] \leq Q\left(\sqrt{2\text{SNR}\left[\left(1+\sqrt{\frac{n_{tx}}{n_{rx}}}\right)^2\left(1-2^{\frac{-R_u}{n_{tx}}}\right)+2^{\frac{-R_u}{n_{tx}}}\right]}\right) \tag{4.26}$$

This upper bound is tight when the normalized rate is large. Figure 4-7 shows the bound and exact expression versus normalized rate. From the figure, it is clear that the bound is tight even in the rate-starved region.

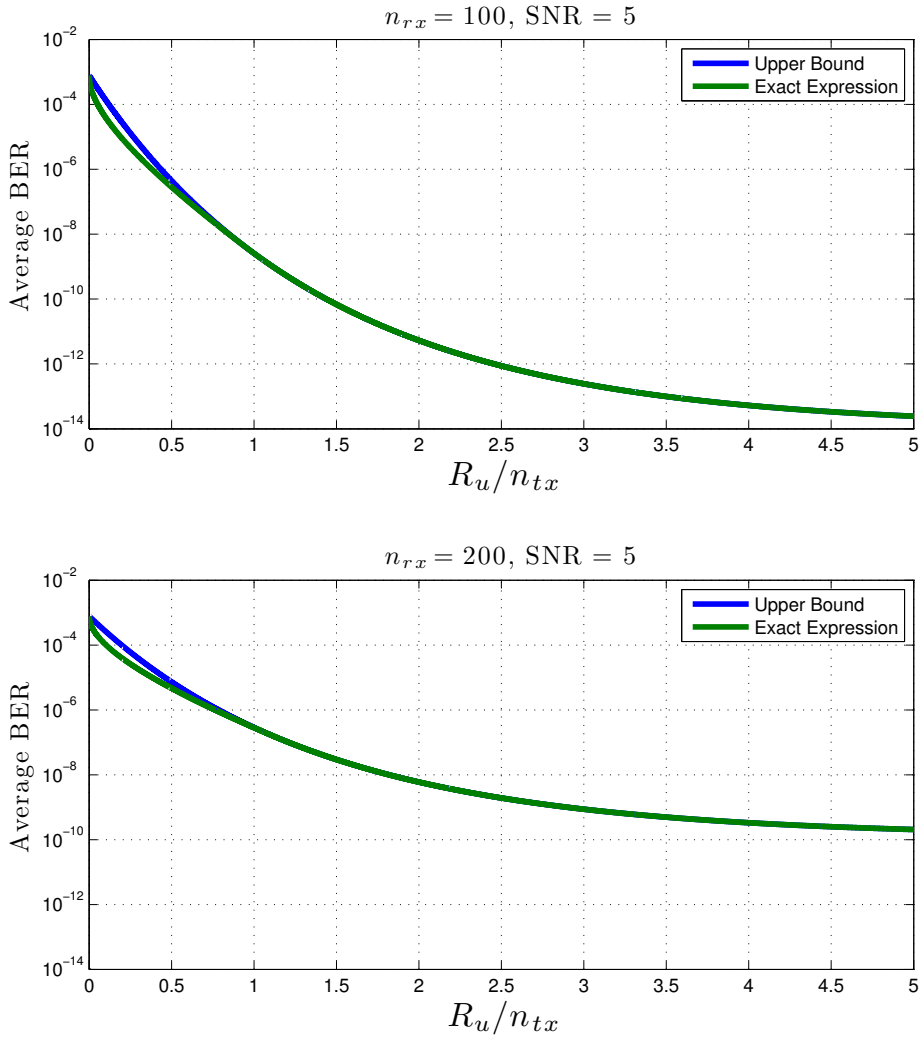

Figure 4-7: Asymptotic BER (exact and bound) as a function of normalized rate R_u/n_{tx}. SNR is dimensionless.

4.2 Atmospheric Time Dynamics

We have described the optimal scheme to describe a fixed atmospheric state given some number of bits in the previous section. In this section, we relax the fixed atmospheric state assumption to study the effects of latency on system performance. We begin by explicitly defining transmitter and receiver knowledge of the channel state at each time: the current channel state is denoted by $\mathbf{H}_c \in \mathbb{C}^{n_{rx} \times n_{tx}}$, the receiver estimate of the channel state is denoted by $\mathbf{H}_{rx} \in \mathbb{C}^{n_{rx} \times n_{tx}}$, and the transmitter

estimate of the optimal propagation mode is $\vec{v}_{tx} \in \mathbb{C}^{n_{tx}}$. The signal portion of the associated sufficient statistic is then:

$$|\phi_s|^2 = \frac{\left|\vec{v}_{tx}^{\dagger}\mathbf{H}_{rx}^{\dagger}\mathbf{H}_c\vec{v}_{tx}\right|^2}{\|\mathbf{H}_{rx}\vec{v}_{tx}\|^2} \tag{4.27}$$

Essentially, the receiver is projecting the measured spatial field distribution onto a unit vector in the direction of the receiver's estimate of the propagated field distribution, thereby ignoring noise and interference components orthogonal to the signal. The performance of the optimal detector is then:

$$\mathbb{E}[\text{BER}] = Q\left(\sqrt{2\text{SNR}\cdot\mathbb{E}[|\phi_s|^2]}\right) \tag{4.28}$$

The system performance is entirely characterized by the statistical distribution of $|\phi_s|^2$. The wavefront predistortion power gain is given by:

$$\Upsilon = \frac{\mathbb{E}\left[|\phi_s|^2\right]}{\mathbb{E}\left[|\phi_{NF}|^2\right]} \tag{4.29}$$

where ϕ_{NF} is the signal portion of the sufficient statistic for the coherent detection diversity system without wavefront predistortion and $|\phi_s|^2$ is the sufficient statistic for the comparison system. The wavefront predistortion power gain is the multiplicative gain resulting from a coherent detection diversity system *with* wavefront predistortion relative to a coherent detection diversity system *without* wavefront predistortion. We now calculate the average BER and wavefront predistortion power gain, Υ, for five cases. First we investigate the degenerate cases of no channel state knowledge at the transmitter and perfect channel state knowledge at the transmitter; we show that these two cases agree with previous results [44] [28]. Next we investigate a more interesting case where the transmitter has delayed channel state knowledge while the receiver has perfect channel state knowledge. This case allows us to find the impact of feedback latency. Next we investigate a case where the transmitter has no channel state knowledge and the receiver has delayed channel state knowledge. This allows us to find the impact of receiver channel state estimation latency for a system without

wavefront predistortion. Finally, we investigate a case where the transmitter and receiver have delayed channel state knowledge. This will allow us to find the impact of receiver channel state estimation latency.

4.2.1 No CSI at Transmitter, Perfect CSI at Receiver

We first consider the case where the feedback link is either down or nonexistent: the receiver has perfect knowledge of the channel state $\mathbf{H}_{rx} = \mathbf{H}_c$, and the transmitter has no channel state knowledge $\vec{v}_{rx} = \vec{r}$, where $\vec{r}$ is any unit average energy vector chosen independently of the channel state. The wavefront predistortion gain is:

$$\mathbb{E}\left[|\phi_s|^2\right] = \mathbb{E}\left[\frac{\left|\vec{r}^{\,\dagger}\mathbf{H}_c^{\dagger}\mathbf{H}_c\vec{r}\right|^2}{\|\mathbf{H}_c\vec{r}\|^2}\right] = 1 \tag{4.30}$$

This result is intuitively satisfying; we expect the sufficient statistic to average to unity because the atmosphere conserves energy. This result agrees with the results in [28]. The wavefront power gain, by definition, is unity for this case, $\Upsilon_{(1)} = 1$.

4.2.2 Perfect CSI at Transmitter, Perfect CSI at Receiver

If the receiver and the transmitter have perfect knowledge of the channel state, then $\mathbf{H}_{rx} = \mathbf{H}_c$, $\frac{1}{\|\mathbf{H}_{rx}\vec{v}_{tx}\|}\left|\vec{v}_{tx}^{\dagger}\mathbf{H}_{rx}^{\dagger}\right| = \vec{u}_{max}\left(\mathbf{H}_c\right)$, and $\vec{v}_{tx} = \vec{v}_{max}\left(\mathbf{H}_c\right)$. We have used the notation that $\vec{v}_{max}\left(\mathbf{H}_c\right)$ and $\vec{u}_{max}\left(\mathbf{H}_c\right)$ are the input and output singular modes of the matrix $\mathbf{H}_c$, respectively. The wavefront predistortion gain is:

$$\begin{aligned}
\Upsilon_{(2)} &= \mathbb{E}\left[\frac{\left|\vec{v}_{max}\left(\mathbf{H}_c\right)^{\dagger}\mathbf{H}_c^{\dagger}\mathbf{H}_c\vec{v}_{max}\left(\mathbf{H}_c\right)\right|^2}{\left\|\mathbf{H}_c\vec{v}_{max}\left(\mathbf{H}_c\right)\right\|^2}\right] \\
&= \mathbb{E}\left[\left\|\mathbf{H}_c\vec{v}_{max}\left(\mathbf{H}_c\right)\right\|^2\right] \\
&= \gamma_{max}^2\left(\mathbf{H}_c\right) \\
&= \left(1+\sqrt{\frac{n_{tx}}{n_{rx}}}\right)^2
\end{aligned} \tag{4.31}$$

where $\gamma^2_{max}(\mathbf{H}_c)$ is the maximum square singular value of the matrix $\mathbf{H}_c$. Physically, the transmitter has perfect knowledge of the instantaneous turbulence state and is therefore able to couple into the optimal propagation mode. Further, the receiver has perfect knowledge of the instantaneous receive wavefront shape and is therefore able to tune the phase and amplitude of each aperture to maximize performance. This result agrees with work in [44], which addressed the idealized performance of the sparse aperture system with wavefront predistortion and feedback.

4.2.3 Delayed CSI at Transmitter, Perfect CSI at Receiver

Here we find the performance for the case where the receiver has perfect knowledge of the channel state while the transmitter has delayed knowledge of the channel state. This would be particularly applicable for systems that experience significant feedback latencies resulting, for example, from a long link or relatively slow feedback data rate.

The transmitter receives a stale channel state estimate, $\mathbf{H}_{tx} = \mathbf{H}_0$, that is τ_{tx} seconds delayed from the current channel state $\mathbf{H}_c$. As a consequence, the transmitter will predistort the transmitted waveform on the basis of the stale channel state estimate $\vec{v}_{tx} = \vec{v}_{max}(\mathbf{H}_0)$. The receiver has perfect knowledge of the channel state so that $\mathbf{H}_{rx} = \mathbf{H}_c$. The wavefront predistortion power gain is then:

$$\begin{aligned}\Upsilon_{(3)} &= \mathbb{E}\left[\frac{\left|\vec{v}^{\,\dagger}_{max}(\mathbf{H}_0)\mathbf{H}_c^{\dagger}\mathbf{H}_c\vec{v}_{max}(\mathbf{H}_0)\right|^2}{\|\mathbf{H}_c\vec{v}_{max}(\mathbf{H}_0)\|^2}\right] \\ &= R_{hh}(\tau_{tx})\gamma^2_{max}(\mathbf{H}_0) + (1 - R_{hh}(\tau_{tx})) \\ &= e^{-\left(\frac{v_\perp \tau_{tx}}{\rho_0}\right)^{5/3}}\left(1 + \sqrt{\frac{n_{tx}}{n_{rx}}}\right)^2 + \left(1 - e^{-\left(\frac{v_\perp \tau_{tx}}{\rho_0}\right)^{5/3}}\right)\end{aligned} \tag{4.32}$$

Physically, this shows that the ability of the transmitter to couple into the optimal propagation mode is degraded as the transmitter's estimate of the atmospheric state becomes decorrelated from current atmosphere state. As we would expect, the delay must be much smaller than the coherence time for good performance. In the limit as the transmitter channel estimate delay approaches zero, the wavefront predistortion power gain approaches that gain found in the case with perfect channel state

knowledge at both the transmitter and receiver:

$$\lim_{\tau_{rx}\to 0} \Upsilon_{(3)} = \Upsilon_{(2)} \tag{4.33}$$

Similarly, as the transmitter channel estimate delay becomes very long, the wavefront power distortion gain approaches that gain found in the case where the transmitter has no channel state knowledge:

$$\lim_{\tau_{rx}\to \infty} \Upsilon_{(3)} = \Upsilon_{(1)} \tag{4.34}$$

These two limits give the intuition that some portion of the predistorted wave is coupled into the optimal propagation mode while the remaining is coupled with equal probability into all other modes. The proportion that is coupled into the optimal propagation mode is governed by the atmospheric autocovariance function.

4.2.4 No CSI at Transmitter, Delayed CSI at Receiver

Here we find the performance for the case where the receiver has delayed knowledge of the channel state while the transmitter has no knowledge of the channel state. This subsection is useful for analyzing coherent detection systems without feedback. Receiver latencies can result from computation delays or delays in the reaction time of the coherent detectors.

The receiver has a stale channel state estimate, $\mathbf{H}_{rx} = \mathbf{H}_0$, that is τ_{rx} seconds delayed from the current channel state $\mathbf{H}_c$. Because the transmitter has no channel state knowledge, $\vec{v}_{rx} = \vec{r}$, where $\vec{r}$ is any unit average energy vector chosen independently of the channel state. The wavefront predistortion power gain is then:

$$\begin{aligned} \Upsilon_{(4)} &= \mathbb{E}\left[\frac{\left|r^\dagger \mathbf{H}_0^\dagger \mathbf{H}_c r^\dagger\right|^2}{\|\mathbf{H}_0 r^\dagger\|^2}\right] \\ &= R_{hh}(\tau_{rx}) \end{aligned} \tag{4.35}$$

Physically this shows that as the receiver's estimate of the received spatial mode becomes stale, the receiver is unable to tune to the right spatial mode. In the limit as the receiver channel estimate delay approaches zero, the wavefront predistortion power gain approaches that gain found in the case with perfect channel state knowledge at the receiver:

$$\lim_{\tau_{rx} \to 0} \Upsilon_{(4)} = \Upsilon_{(1)} \tag{4.36}$$

As the estimate delay becomes large, the power gain approaches zero which implies that systems with long estimate delays should use noncoherent detection techniques.

4.2.5 Delayed CSI at Transmitter, Delayed CSI at Receiver

Here we find the performance for the case where both the transmitter and receiver have delayed knowledge of the channel state. This subsection is useful for analyzing coherent detection systems with wavefront predistortion. Receiver and transmitter estimate latencies are assumed to be the same and, as a result, this analysis is particularly useful for two way communication systems that use reciprocity to measure the channel's state.

The receiver and transmitter have a stale channel state estimate, $\mathbf{H}_{rx} = \mathbf{H}_{tx} = \mathbf{H}_0$, that is τ_{rx} seconds delayed from the current channel state $\mathbf{H}_c$. As a consequence, the transmitter will predistort the transmitted waveform on the basis of the stale channel state estimate $\vec{v}_{tx} = \vec{v}_{max}(\mathbf{H}_0)$. The wavefront predistortion power gain is then:

$$\begin{aligned} \Upsilon_{(5)} &= \mathbb{E}\left[\frac{\left|\vec{v}_{max}^{\dagger}(\mathbf{H}_0)\mathbf{H}_0^{\dagger}\mathbf{H}_c\vec{v}_{max}(\mathbf{H}_0)\right|^2}{\|\mathbf{H}_0\vec{v}_{max}(\mathbf{H}_0)\|^2}\right] \\ &= R_{hh}(\tau_{rx})\gamma_{max}^2(\mathbf{H}_0) \\ &= R_{hh}(\tau_{rx})\left(1+\sqrt{\frac{n_{tx}}{n_{rx}}}\right)^2 \end{aligned} \tag{4.37}$$

Physically this shows that as the system's estimate of the channel state becomes stale, the transmitter is unable to couple into the optimal spatial mode while the receiver

is unable to tune to the right spatial mode. In the limit, as the system channel estimate delay approaches zero, the wavefront predistortion power gain approaches that gain found in the case with perfect channel state knowledge at both the receiver and transmitter:

$$\lim_{\tau_{rx} \to 0} \Upsilon_{(5)} = \Upsilon_{(2)} \tag{4.38}$$

As the estimate delay becomes large, the power gain approaches zero which implies that systems with long estimate delays should use noncoherent detection techniques. □

Figures 4-8 and 4-9 show the wavefront predistortion gain and average BER for each of the five cases versus latency for the special case where $n_{tx} = n_{rx}$.

We see that case two, perfect CSI at the transmitter and receiver, provides an upper bound on the performance of these systems. Similarly, case one, without CSI at the transmitter and perfect CSI at the receiver provides a lower bound on the performance of coherent detection systems with perfect receiver knowledge of the channel state. Case three, with delayed CSI at the transmitter and perfect CSI at the receiver, transitions smoothly from the upper bound to the lower bound as the latency grows. To achieve at least 80% of the wavefront predistortion gain, the transmitter must be updated at least every 0.5 coherence times. If the latency is more than two coherence times, any gain from wavefront predistortion is effectively gone.

Cases four and five both transition to a region with gain of less than one because they both include the effect of imperfect coherent detection. For both cases, as the receiver's knowledge of the incoming spatial mode becomes more stale the performance becomes significantly degraded. A delay of one coherence time causes a 50% reduction in performance. This shows that, if the receiver cannot update its spatial mode knowledge at least once a coherence time, noncoherent communication techniques should be employed.

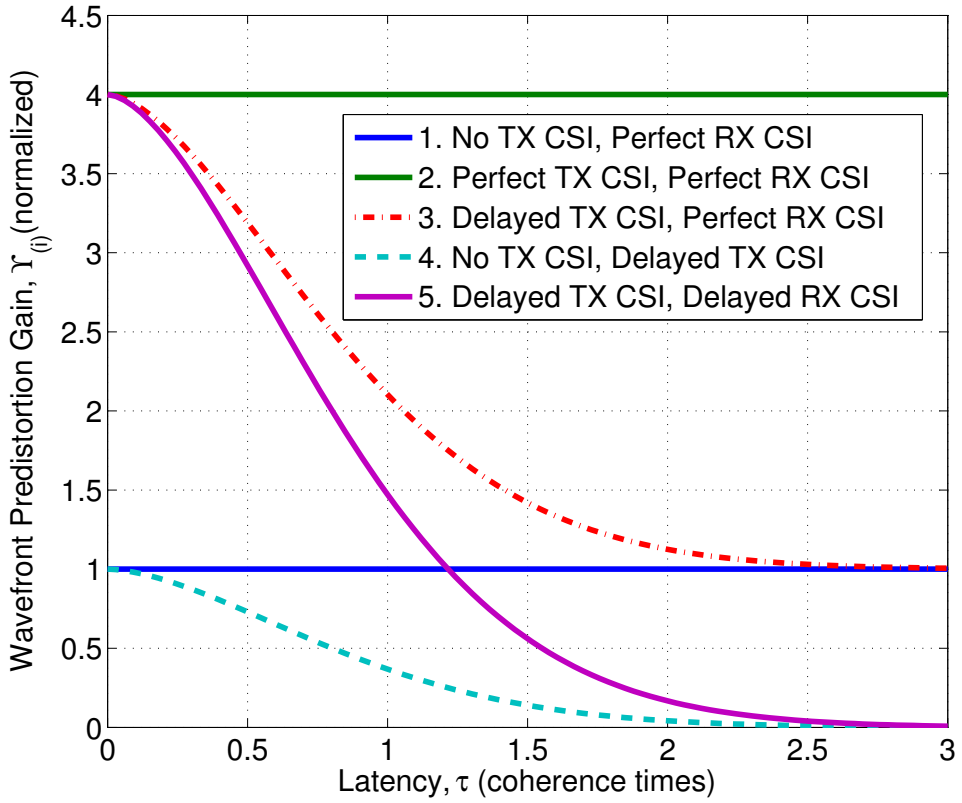

Figure 4-8: Wavefront predistortion gain versus latency for five cases: (1) no transmitter CSI and perfect receiver CSI, (2) perfect transmitter CSI, perfect receiver CSI, (3) transmitter CSI delayed by τ_{tx}, perfect receiver CSI, (4) no transmitter CSI, receiver CSI delayed by τ_{rx}, and (5) transmitter and receiver CSI delayed by τ_{rx}.

4.3 Optimal Feedback Link in the Presence of Atmospheric Time Dynamics

We now investigate the combined effects of latency and feedback rate on the system performance. We assume that the receiver has perfect knowledge of the channel state, $\mathbf{H}_{rx} = \mathbf{H}_c$. The transmitter channel state knowledge is distorted according the scheme described in Section 4.1.4: we represent this distortion as the mapping $f(\cdot) : \mathbb{C}^{n_{tx}} \rightarrow \mathbb{Z}^{2^{R_u}}$. The distorted transmitter knowledge of the channel state is delayed by τ_0 because of receiver processing time and time of flight, among other delays. Additionally, the transmitter does not update its estimate until the entire new estimate is received. This causes an additional delay of R_u/r where R_u is the

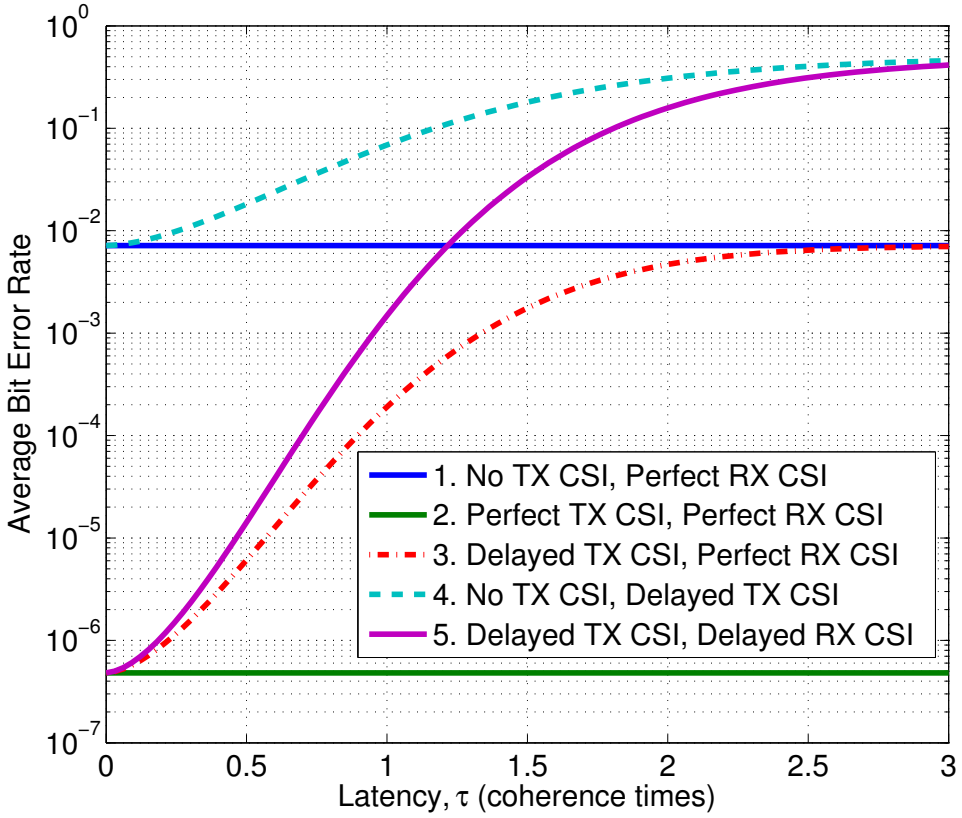

Figure 4-9: Average bit error rate versus latency for five cases: (1) no transmitter CSI and perfect receiver CSI, (2) perfect transmitter CSI, perfect receiver CSI, (3) transmitter CSI delayed by τ_{tx}, perfect receiver CSI, (4) no transmitter CSI, receiver CSI delayed by τ_{rx}, and (5) transmitter and receiver CSI delayed by τ_{rx}.

number of bits per update and r is the feedback link data rate in bits per second; thus $\tau_0 = \tau_{tx} + R_u/r$. Combining the results from sections investigating the feedback link and atmospheric time dynamics—Sections 4.2 and 4.1 respectively—we arrive at the following:

$$
\begin{aligned}
\Upsilon_{(T)} = \mathbb{E}\Bigg[\Bigg\|\Bigg(&\sqrt{R_{hh}\left(\tau_0+\frac{R_u}{r}+t\right)}\mathbf{H}_0\ \ldots \\
&+\ \sqrt{1-R_{hh}\left(\tau_0+\frac{R_u}{r}+t\right)}\mathbf{H}_1\Bigg) f\left(\vec{v}_{\max}(\mathbf{H}_0)\right)\Bigg\|^2\Bigg] \\
= R_{hh}&\left(\tau_0+\frac{R_u}{r}+t\right)\mathbb{E}\left[\|\mathbf{H}_0 f(\vec{v}_{\max}(\mathbf{H}_0))\|^2\right]\ldots \\
&+\left(1-R_{hh}\left(\tau_0+\frac{R_u}{r}+t\right)\right)\mathbb{E}\left[\|\mathbf{H}_1 f(\vec{v}_{\max}(\mathbf{H}_0))\|^2\right] \\
= R_{hh}&\left(\tau_0+\frac{R_u}{r}+t\right)\left(\gamma^2_{max}(\mathbf{H}_0)\left(1-\Psi(R_u/r)2^{-R_u/n_{tx}}\right)+\Psi(R_u/r)2^{-R_u/n_{tx}}\right)\ldots \\
&+\left(1-R_{hh}\left(\tau_0+\frac{R_u}{r}+t\right)\right) \\
= e^{-\left(\frac{\tau_0+R_u/r+t}{t_0}\right)^{5/3}}&\left(1+\sqrt{\frac{n_{tx}}{n_{rx}}}\right)^2\left(1-\Psi(R_u/r)2^{-R_u/n_{tx}}\right)\ldots \\
&+e^{-\left(\frac{\tau_0+R_u/r+t}{t_0}\right)^{5/3}}\Psi(R_u/r)2^{-R_u/n_{tx}}\ldots \\
&+\left(1-e^{-\left(\frac{\tau_0+R_u/r+t}{t_0}\right)^{5/3}}\right)
\end{aligned}
\tag{4.39}
$$

where t is the time since the most recent update arrived at the transmitter. Equation (4.39) relates the fundamental system quantities, the transverse wind velocity, the atmospheric coherence length, the number of transmit and receive apertures, the feedback latency, and the feedback rate to system performance. To maximize the performance, we wish to minimize the distortion of the transmit vector after each update, making R_u large while, at the same time, minimizing the time between updates, R_u/r. These are competing objectives however, decreasing the distortion of the transmit vector increases the time between updates. Evaluating equation (4.39) at

$t = R_u/r$ gives the performance just before a new update, the worst-case performance:

$$\begin{aligned}\Upsilon_{(T)} = & e^{-\left(\frac{\tau_0+2R_u/r}{t_0}\right)^{5/3}} \left(1+\sqrt{\frac{n_{tx}}{n_{rx}}}\right)^2 \ldots \\ & - e^{-\left(\frac{\tau_0+2R_u/r}{t_0}\right)^{5/3}} \left(1+\sqrt{\frac{n_{tx}}{n_{rx}}}\right)^2 \Psi(R_u/r)2^{-R_u/n_{tx}} \ldots \\ & + e^{-\left(\frac{\tau_0+2R_u/r}{t_0}\right)^{5/3}} \Psi(R_u/r)2^{-R_u/n_{tx}} \ldots \\ & + \left(1 - e^{-\left(\frac{\tau_0+2R_u/r}{t_0}\right)^{5/3}}\right)\end{aligned} \tag{4.40}$$

Figure 4-10 shows the worst-case wavefront predistortion gain as a function of the update length, R_u. The full update is shown as a dashed line while the optimal update, either incremental or full depending on which performs better, is shown as the solid line. For the graph, the number of transmit apertures is $n_{tx} = 10$, the number of receive apertures is $n_{rx} = 10$, the atmospheric coherence time is $\rho_0/v_\perp = 1$ second, the feedback latency is $\tau_0 = 0.1$ seconds, the feedback rate is 80 bits per second, and the full update length is $R_u^0 = 10000$ bits.

It is clear from figure 4-10 that an incremental update rate of $R_u = 1$ bits is sometimes optimal. In this region, the additional gain achieved by using a longer description is overwhelmed by the penalty incurred by delaying update to the transmitter and increasing the number of bits required for an incremental update. The rates for which $R_u > 1$ is optimal is the rate-starved region while the rates for which $R_u = 1$ is optimal is the rate-rich region. The transition between the rate-rich and rate-starved regions is given by:

$$r_s \approx \frac{v_\perp}{\rho_0}\left[\frac{1}{5}\log\left(\frac{2}{1+2^{-1/n_{tx}}+2^{-|C|/n_{tx}}}\right)\right]^{-\frac{3}{5}} \tag{4.41}$$

In the rate-starved region, it is optimal to feed back full updates. In the rate-rich region, incremental updates with $R_u = 1$ provide the optimal performance. Using the optimal incremental update length in the rate-rich region gives an expression for the rate required to achieve $(1-\alpha)\times 100\%$ of the infinite rate wavefront predistortion gain, where the infinite rate wavefront predistortion gain is defined to be the wavefront

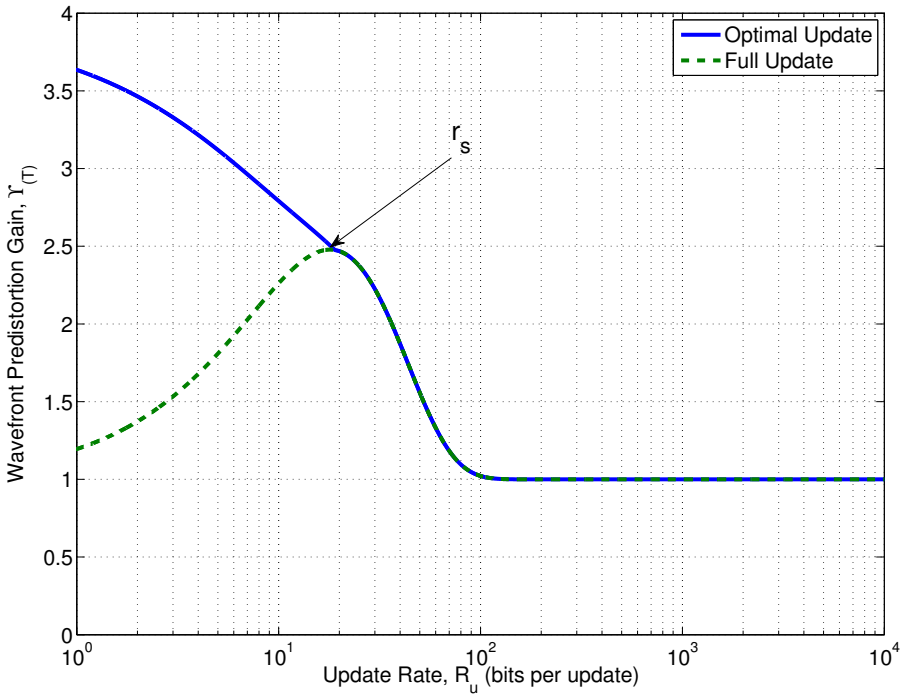

Figure 4-10: Wavefront predistortion gain as a function of the update length, R_u. The full update is shown as a dashed line while the optimal update, either incremental or full depending on which performs better, is shown as the solid line. For the graph, the number of transmit apertures is $n_{tx} = 10$, the number of receive apertures is $n_{rx} = 10$, the atmospheric coherence time is $\rho_0/v_\perp = 1$ second, the feedback latency is $\tau_0 = 0.1$ seconds, the rate is 80 bits per second, and the full update length is $R_u^0 = 10000$ bits. In the figure, r_s is the transition between the rate-starved and the rate-rich region given in equation (4.41).

predistortion gain achievable if the system utilized an infinite rate but finite latency feedback link:

$$r^* \geq \frac{v_\perp}{\rho_0}\left[\frac{1}{5}\log\left(\frac{2}{2-\alpha(1-2^{-1/n_{tx}})+2^{-|C|/n_{tx}}}\right)\right]^{-\frac{3}{5}} \tag{4.42}$$

Figure 4-11 shows the required rate, r^* to achieve $(1-\alpha)\times 100\%$ of the infinite rate gain for various codebook sizes, $|C|$. If the size of the codebook is too small for a given number of transmit apertures, then the number of transmit apertures that can be supported, even with an arbitrarily large rate, is limited. The codebook hard

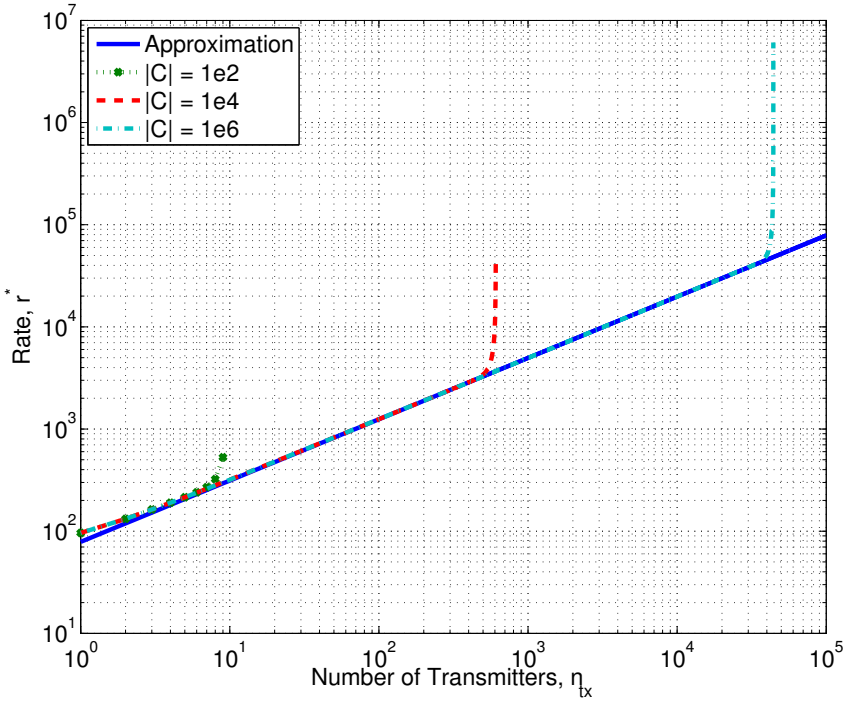

Figure 4-11: Rate required to achieve 99% of the possible gain for various codebook sizes $|C|$.

limit on number of transmit apertures is given by:

$$\begin{aligned} |C| &\geq n_{tx} \log_2 \left(\frac{10^7}{2 - \alpha \left(1 - 2^{-1/n_{tx}}\right)} \right) \\ &\approx 25 n_{tx} \end{aligned} \tag{4.43}$$

Where the approximation is valid for large n_{tx}. Thus if the cardinality of the codebook is larger than $25n_{tx}$, the cardinality of the codebook will not impact system performance. Conversely, if the number of transmit apertures is more than $|C|/25$, the size of the codebook will significantly reduce the system performance. Under the condition that the cardinality of the codebook does not impact the system, equation (4.42) can be approximated for large values of n_{tx} as:

$$r^* \geq \frac{v_\perp}{\rho_0} \left(\frac{10 n_{tx}}{\alpha \log(2)} \right)^{3/5} \tag{4.44}$$

So, the rate necessary to achieve good performance varies sublinearly with the number of transmit apertures and linearly with the coherence time inverse. Physically, the rate varies sublinearly with the number of transmit apertures because of the structure of the atmospheric turbulence. The approximation is shown as a solid line in figure 4-11. Finally, we show the optimal wavefront predistortion gain versus rate for both the full update scheme and the optimal update scheme in figure 4-12. Also shown is the rate-starved to rate-rich transition given in equation (4.41) and the full gain rate given by equation (4.41).

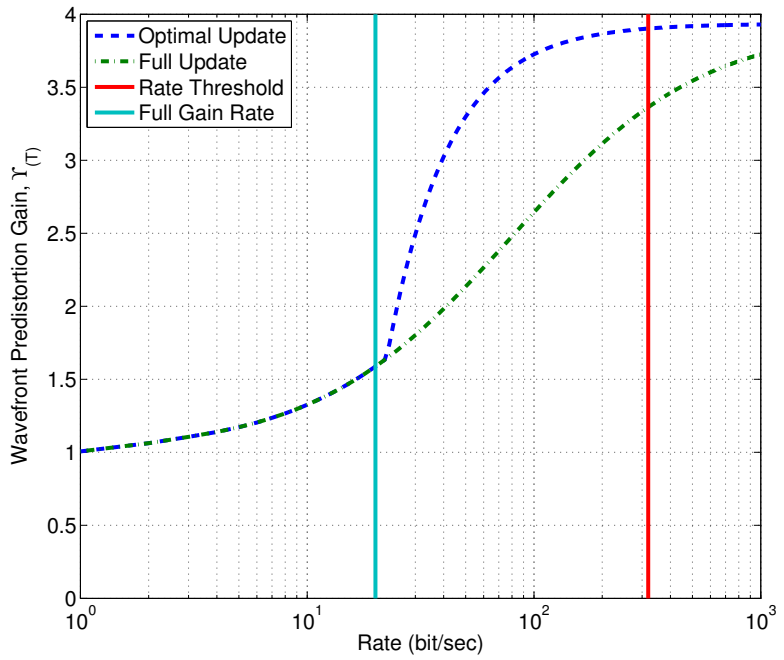

Figure 4-12: Wavefront predistortion gain, $\Upsilon_{(T)}$, as a function of Rate, r, for optimal update length, $n_{tx} = n_{rx} = 10$, coherence time $v_\perp/\rho_0 = 1$ seconds, and feedback latency $\tau_0 = 0.1$ seconds.

Finally, we note that that the feedback latency bounds the system away from idealized performance even if the system is given infinite feedback rate. The reduction in wavefront predistortion gain due to latency for an infinite rate feedback system is:

$$\frac{\Upsilon_{(T)}}{\Upsilon_{(2)}} \leq e^{-\left(\frac{\tau_0}{t_0}\right)^{5/3}} \left(1 + \sqrt{\frac{n_{tx}}{n_{rx}}}\right)^2 + \left(1 - e^{-\left(\frac{\tau_0}{t_0}\right)^{5/3}}\right) \tag{4.45}$$

As a result, a system should not use wavefront predistortion if the latency is a significant fraction of the coherence time. In this case, the performance of a wavefront predistortion system will be no different from a system without the wavefront predistortion.

4.4 Conclusion

Sparse aperture communication with transmitter and receiver diversity has the potential to provide efficient, cost-effective gigabit communication through atmospheric turbulence. To further protect against fading, such a system can employ wavefront predistortion based on channel state information fed back from the receiver. In this section, we characterized the performance of such a wavefront predistortion system in the presences of dynamically evolving turbulence, system latencies, and finite rate feedback. Specifically, we developed a model of the dynamic atmosphere and used it to find the optimal performance of the system in terms of fundamental system and physical parameters, such as latencies, both estimation and feedback, feedback link rate, number of apertures, turbulence strength, link range, etc. We also presented a feedback scheme that achieves optimal performance.

The following describes the asymptotically optimal feedback strategy: a) *initialization* i) create a codebook, known to both the transmitter and receiver; ii) at the receiver, for each update, find the codebook entry closest, in the L_2-sense, to the input spatial mode associated with the largest square singular value; iii) feed back the *index* of the closest codebook entry; b) *steady state operation* i) find the optimal update rate, and make it known to both the transmitter and receiver; ii) calculate the update vector, which is the difference between the current channel state and the current transmitter channel state estimate; iii) find the scaled sub-codebook entry closest, in the L_2-sense, to update vector; iv) feed back the *index* of the closest scaled sub-codebook entry. To prevent the size of the codebook from degrading system performance, a system designer should make a codebook with a cardinality of $25 \times n_{tx}$ known to both the transmitter and receiver. If the cardinality of the codebook is

smaller than $25 \times n_{tx}$, the system's performance will be bounded away from the performance achievable with perfect knowledge regardless of feedback rate and latency. Given a sufficiently large codebook, the feedback rate necessary to take full advantage of the diversity, given in equation (4.44), varies sublinearly with the number of transmit apertures and linearly with the coherence time inverse. Given that there is sufficient feedback rate, the optimal feedback scheme is to create $|C|/2$ sub-codebooks and feed back one-bit updates. Further, the time it takes for an update to reach the transmitter $\tau_0 + 2R_u/r$ should be much smaller than the atmospheric coherence time; the performance degrades roughly exponentially as the time it takes for an update to reach the transmitter increases. In general, the system performance, in terms of wavefront predistortion gain, is given in equation (4.39). If the size of the codebook and rate are sufficient, the performance, given in equation (4.45), is limited only by latency.

While this asymptotic analysis provides insight into the impact of limited rate feedback on wavefront predistortion optical systems, future work should focus on performing an outage analysis for finite systems. This outage analysis would require finding the probability density function of the largest square singular value of optical systems (already known) and finding the probability density function of the distortion distance (unknown). The results describing the feedback information are asymptotically optimal. However, for a finite number of transmit apertures other schemes may converge to the asymptotic result faster than the scheme described. Future work could include developing more efficient schemes for a finite number of transmit apertures.

Chapter 5

Markov Model for the Sparse Aperture System

In this chapter, we analyze experimental data to build a model of the memory properties of the turbulent atmosphere suitable for analyzing the performance of the network Transport Layer. This treatment of outages is especially important when the link is part of a larger network running network protocols because it captures the channels memory. First we analyze data collected by an experimental system with a single laser transmitter located 250 meters from two direct detection receivers. We use the data to validate the use of a two-state continuous-time Markov process to model outage statistics of the diversity system. In the two-state channel model, symbols received during an outage are assumed to be lost, and symbols received during a non-outage are assumed to be received correctly. This channel model can be used to analyze the performance of the Transport Layer.

Next, we use statistical and spectral analysis techniques to show that the log-amplitude fluctuations can be modeled as a Gauss-Markov random process. We create a linear prediction model for signal attenuation for both the single-receiver and diversity systems. The prediction model is an optimal estimator that predicts signal attenuation 1 ms into the future to 1.5 dB accuracy for the single-receiver cases and to 1 dB accuracy for the diversity case. The maximum amount of time the estimator can predict into the future with some confidence is about 5 to 10 ms. This channel

prediction and adaptation can be used to greatly improve the efficiency of free-space optimal communication systems in the atmosphere. Finally we theoretically show that, as a consequence of the log-amplitude Gauss-Markov properties, the outage statistics of systems with many transmitters and many receivers are well modeled as a two-state continuous-time Markov process.

5.1 Atmospheric Markovianity from Experimental Perspective

Work presented in this section was performed in collaboration with Rui Jin as a part of the MIT Undergraduate Research Opportunities Program (UROP). Much of the analysis follows the same path as [8].

5.1.1 Experimental Setup

Etty Lee and Shane Haas collected two receiver, one transmitter free-space optical communication performance data using the setup shown in figure 5-1 [28, 19]. The transmitter directs 0.6 mW of laser light through a telescope. The light then travels through 125 meters of clear air, reflects off a mirror, and travels another 125 meters through clear air to the receiver plane. The field is received by two telescopes, which couple the received power into single mode fibers. Received signals are optically amplified, filtered, and detected every millisecond for a total of six minutes. The received power for each channel was recorded for analysis.

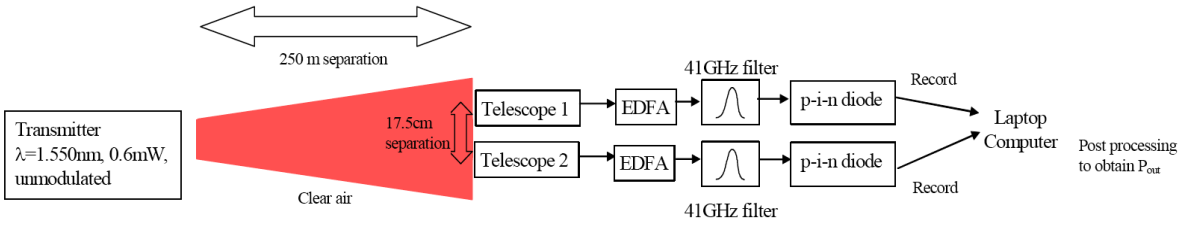

Figure 5-1: Experimental setup: In the figure, EDFA is an erbium doped fiber amplifier [28].

5.1.2 Outage Statistics

In [28], the authors suggested that outage statistics arising from clear-air propagation is well modeled by a two state continuous-time Markov process, in which the two states represent outage and non-outage conditions. Such a two-state representation is depicted in figure 5-2. In the two-state channel model, symbols received during an outage (labeled as state 'Outage') are assumed to be lost, and symbols received during a non-outage (labeled as state 'Non-Outage') are assumed to be received correctly. This channel model keeps memory of the current channel state.

While the authors of [28] calculated expected outage and non-outage duration, we use the data to further validate the use of the Markov outage model. A physical process is well modeled as a two-state Markov process if the frequency distribution of the time spent in a given state is approximately exponential. We can show this by showing the memoryless property of the exponential distribution. Define a random variable X as the time spent in the outage state. Then X is memoryless if and only if:

$$\Pr(X > t + s | X > t) = \Pr(X > s) \tag{5.1}$$

for some non-negative times t and s. We can rewrite this condition as

$$\frac{\Pr(X > t + s | X > t)}{\Pr(X > t)} = \Pr(X > s) \tag{5.2}$$

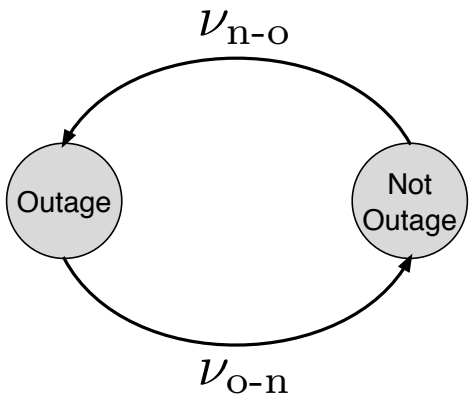

Figure 5-2: Two-state continuous-time Markov channel model.

Now examine the exponential distribution. Let e^{-kt} be the probability that the wait time is greater than t for some positive value k. Then we see that the exponential distribution fits the memoryless property:

$$\frac{e^{-k(t+s)}}{e^{-kt}} = e^{-ks} \tag{5.3}$$

Only the exponential and geometric distributions have such a property. Since a memoryless process is not dependent on the occurrence of previous states (because otherwise the conditional probabilities would not equal the unconditional probabilities), a memoryless process is Markovian. Thus, the duration of time spent in states Outage and Non-Outage, namely the outage and non-outage durations respectively, are exponentially distributed (as a direct consequence of Markov processes). If we let t_{outage} and $t_{\text{nonoutage}}$ be the outage and non-outage durations respectively, their probability density functions are given by:

$$\begin{aligned} f_{t_{\text{outage}}}(t_{\text{outage}}) &= \nu_{o-n} e^{\nu_{o-n} t_{\text{outage}}}, t_{\text{outage}} \geq 0 \\ f_{t_{\text{nonoutage}}}(t_{\text{nonoutage}}) &= \nu_{n-o} e^{\nu_{n-o} t_{\text{nonoutage}}}, t_{\text{nonoutage}} \geq 0 \end{aligned} \tag{5.4}$$

where

$$\nu_{o-n} = \frac{1}{\mathbb{E}[\text{outage duration}]} \tag{5.5}$$

and

$$\nu_{n-o} = \frac{1}{\mathbb{E}[\text{non} - \text{outage duration}]} \tag{5.6}$$

We now show that the outage statistics are well modeled as a two-state continuous-time Markov model by showing that the frequency distribution of the outage and non-outage durations are exponential.

Figure 5-3 shows the cumulative distribution functions (cdfs) of the outage durations of the diversity system and of the two separate channels of the two receivers for the outage threshold power equal to the signal mean. The left figure shows the outage cdfs while the right figure shows the non-outage cdfs. If the cdfs arise from an exponential process, the complementary cumulative distribution function should

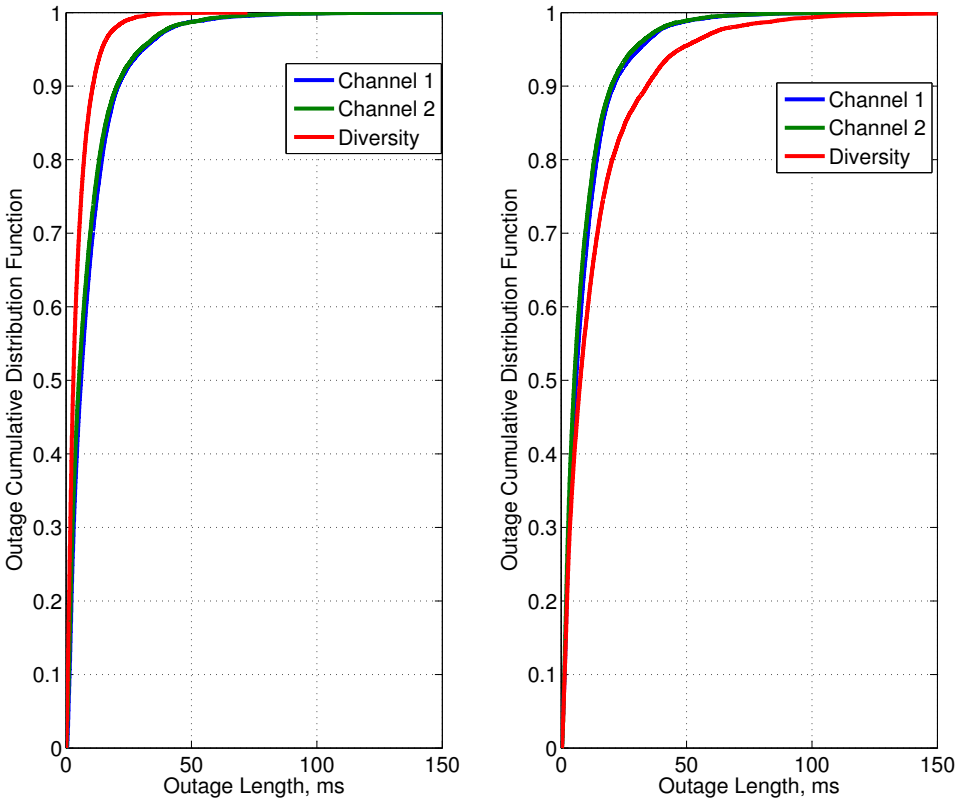

Figure 5-3: Experimental cumulative probability distribution of outage and non-outage duration.

be linear in log-space. Figure 5-4 shows the complementary cdf of the outage and non-outage durations with the y-axis scaled logarithmically. For long outage/non-outage, the data is noisy as evidenced in the figures. This is because long outages become very unlikely; the statistics do not have enough data to converge. More data would reduce the noise, smoothing the curves, for long outages. The linearity of the curves in figure 5-4 suggests an exponential distribution of the outage durations in all cases, and we evaluate this suggestion using statistical tools. We fit the log complementary cdfs of the outage and non-outage durations with a line constrained to pass through the origin $(0, 0)$. The slope of the line was chosen to minimize the mean squared error for outage durations less than 20 ms. Figure 5-5 shows the results of this minimization. Clearly, an exponential distribution approximates the data well for outage/non-outage durations that are most likely. However, the exponential dis-

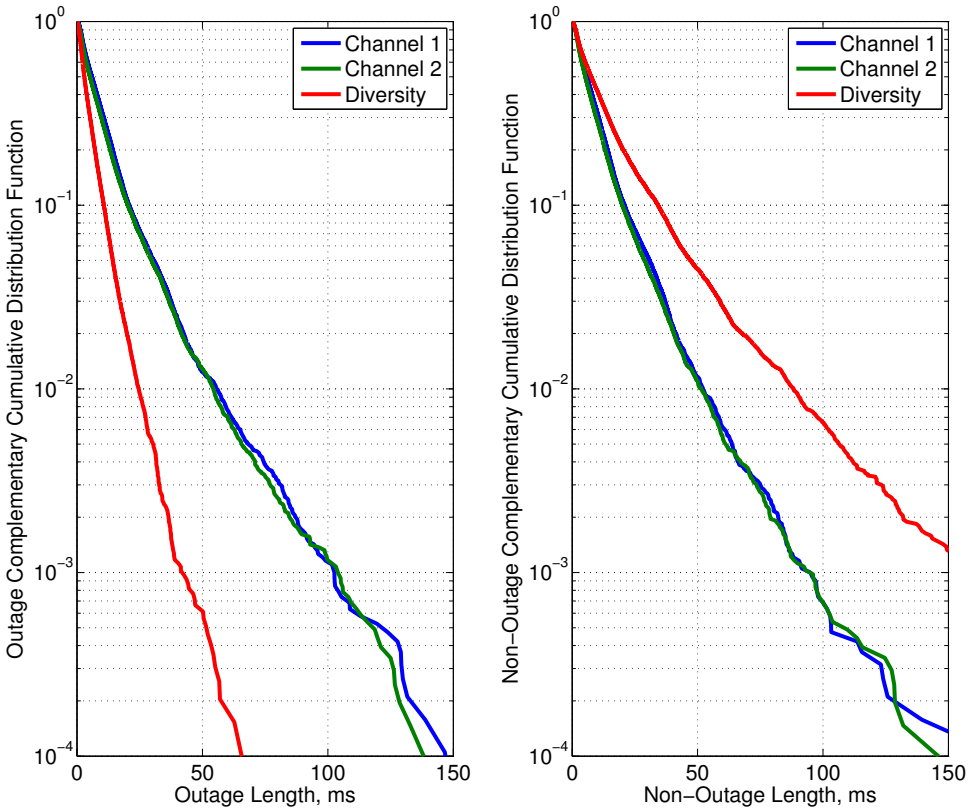

Figure 5-4: Experimental log complementary cumulative probability distribution of outage and non-outage duration.

tribution under-predicts the likelihood of long outage/non-outages. The mean outage duration was 9.5 ms, 8.8 ms, and 4.6 ms for channel 1, channel 2, and diversity respectively. The mean non-outage duration was 9.4 ms, 8.7 ms, and 137.5 ms for channel 1, channel 2, and diversity respectively. As theory predicts, diversity increases the mean non-outage duration and decreases the mean outage duration.

The parameters found by fitting a line to the log complementary cdf were used to generate the cdfs shown in figure 5-6. The results drawn from the cdf are the same as those found from the log complementary cdf: the exponential distribution approximates the data well for short outage durations but is a poor approximation for longer outages.

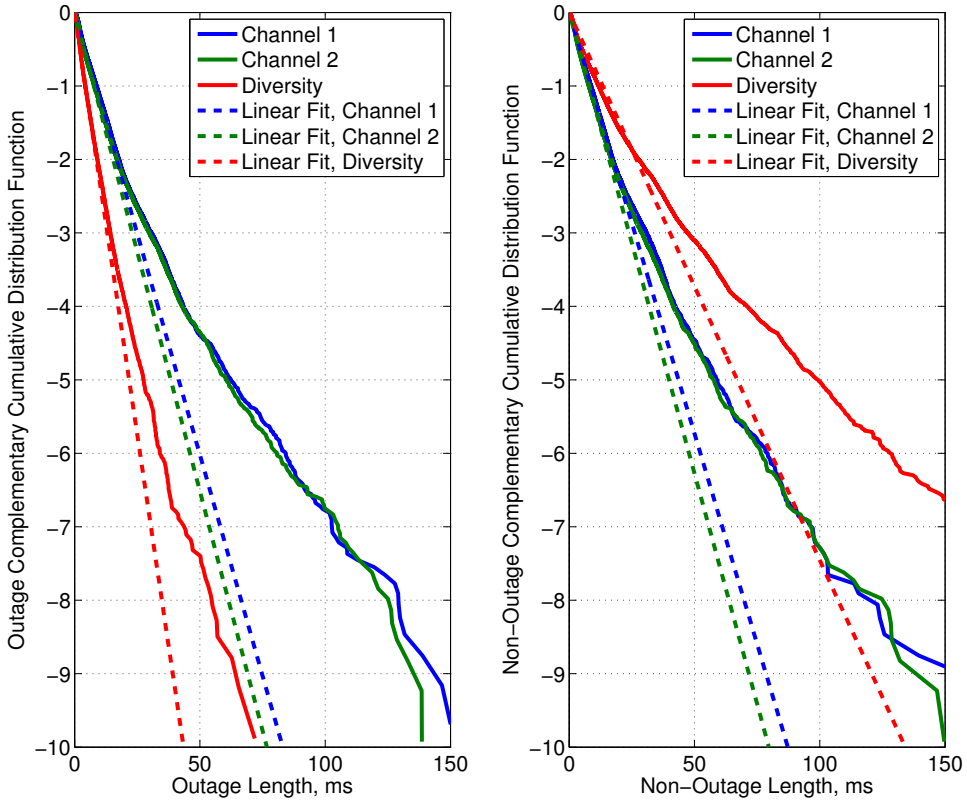

Figure 5-5: Experimental log complementary cumulative probability distribution of outage and non-outage duration with exponential fits.

Next we calculate the log-amplitude power spectral density and autocovariance to determine if the log-amplitude fluctuations are well modeled as a Gauss-Markov random process.

5.1.3 Log-Amplitude Statistics

Proving that the outage statistics are well modeled as a two-state continuous-time Markov does not imply that the log-amplitude fluctuations are Markovian. Thus, we proceed to show that the log-amplitude fluctuations are well modeled as a Gauss-Markov random process. To prove that the log-amplitude fluctuations are well modeled as a Gauss-Markov process, we must:

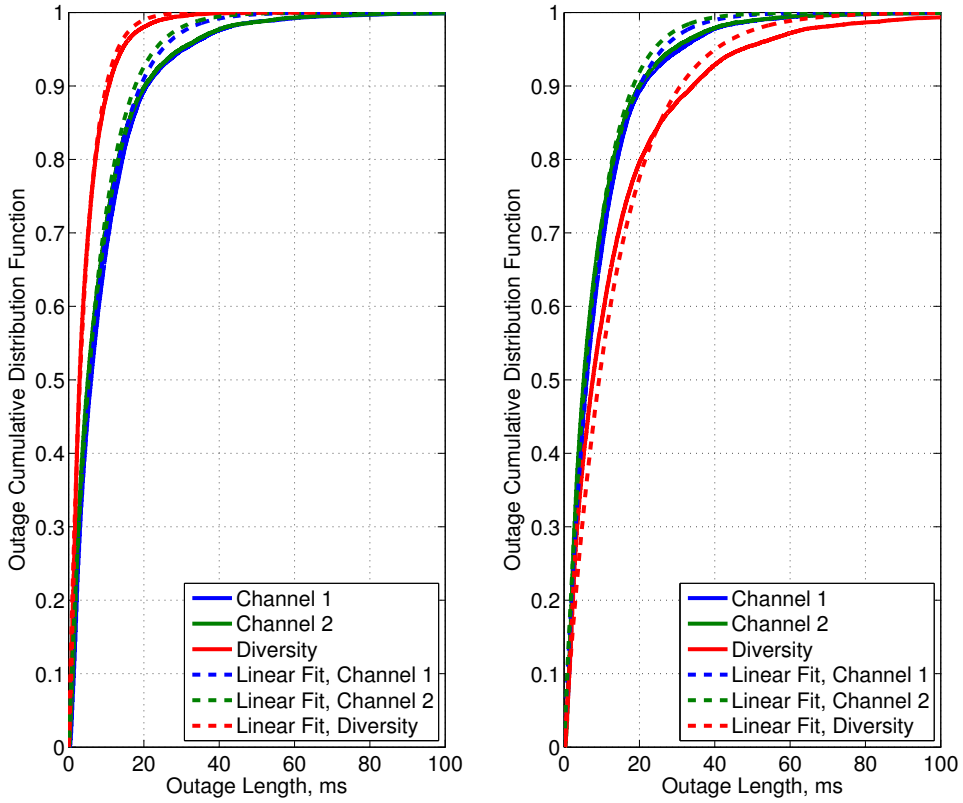

Figure 5-6: Cumulative probability distribution of outage and non-outage duration with exponential fits.

1. Show the log-amplitude fluctuations are well modeled as a Gaussian process and

2. Show that the log-amplitude power spectral density is well modeled as a single pole spectrum.

To address the first issue, we note that Rytov's method predicts that the log-amplitude fluctuations should be normally distributed, specifically that the power fading is modeled by $e^{2\chi}$, where χ is normally distributed. We verify the prediction with the data collected. Figures 5-7 and 5-8 show the cdf of the log-amplitude against the corresponding normal cdf curves with maximum likelihood mean and variance estimates. The figures show a good agreement between Rytov's method prediction of normality and the log-amplitude data.

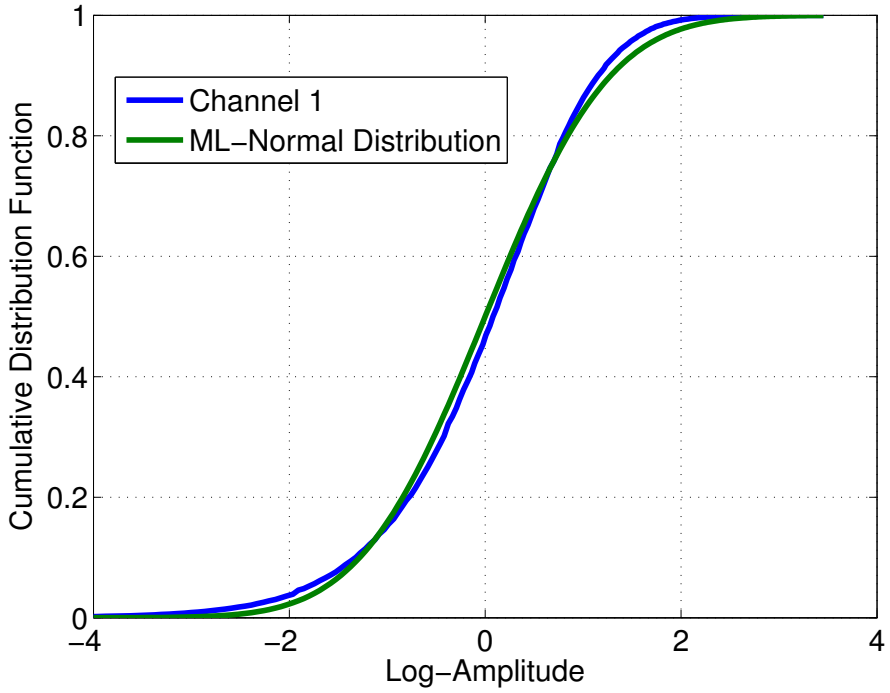

Figure 5-7: Cumulative probability distribution of log-amplitude received with fitted normal curve, channel 1.

While the figures show good qualitative agreement, we quantitatively test that the log-amplitude data is drawn from a normal distribution using the Cramér-von-Mises test. We define the null hypothesis, H_0, as the log-amplitude data was drawn from a Gaussian process while our alternative hypothesis, H_α, where $1-\alpha$ is the confidence level, as log-amplitude data was not drawn from a Gaussian process. For an observed data set, $d_1, d_2, \cdots, d_n$ in increasing order, we cannot reject the null hypothesis with $1-\alpha$ confidence if T is less than the critical value associated with α, where T is defined as [2]:

$$T = \frac{1}{2n} + \sum_{i=1}^{n} \left[\frac{2i-1}{2n} - F(d_i) \right]^2 \tag{5.7}$$

A confidence level of 0.9, $\alpha = 0.1$, corresponds to a critical value of 0.347 [9]. The test statistics are $T = 8.47 \times 10^{-4}$ for channel 1 and $T = 8.71 \times 10^{-4}$ for channel 2. Thus, we cannot reject the null hypothesis in all cases, and we provide evidence that the log-amplitude fluctuations are normally distributed.

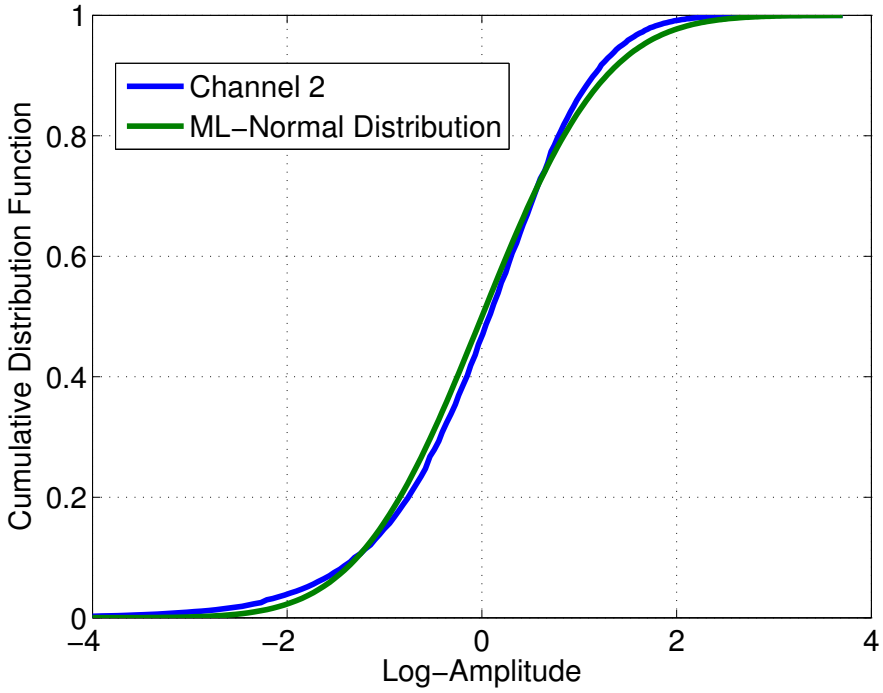

Figure 5-8: Cumulative probability distribution of log-amplitude received with fitted normal curve, channel 2.

Having shown that the log-normal amplitude data is well modeled as a Gaussian process, we now continue to show that it is well modeled as a Gauss-Markov process by demonstrating that the log-amplitude has the temporal statistics characteristic of Markov processes:

1. The power spectral density (PSD) is well modeled as a one pole spectrum and

2. The autocovariance is approximately exponential.

First we examine the power spectral density.

Power Spectral Density Analysis

We use Welch's method of averaged periodograms to estimate the power spectral density (PSD). We then fit these power spectral curves with autoregressive (AR) models of different orders; if the PSD of the log-amplitude fluctuations are well modeled with

a single-pole AR model, then we say the log-amplitude fluctuations are well modeled as a Gauss-Markov random process. By using an AR model, we model the fluctuations as the output of an all-pole filter $H(s)$ driven by zero-mean white noise. AR modeling uses well-known techniques like those described in [8]. If the log-amplitude fluctuations are symmetric Gauss-Markov random processes, then, theoretically, the diversity power fluctuations are Markovian. We also fit the diversity power fluctuation PSD with AR models of various order to determine agreement between theory and experiment.

To calculate the PSD, we must first calculate the magnitude of the signal attenuation of the received power. We used Welch's method to estimate the power spectral density:

1. The data was divided into overlapping 5 second segments.

2. Each segment was weighted with a hamming window.

3. The periodogram of each weighted segment was calculated using the discrete Fourier transform. The result was an estimate of the frequency spectrum with 2 Hz bins from 0 Hz to 500 Hz.

4. The periodograms were then averaged to reduce the variance of each frequency bin.

We fit the PSD with a first order and second order AR model. The AR coefficients are computed by solving the Yule-Walker equations to minimize the mean-squared prediction error. If $y[n]$ is the current output and $x[n]$ is a zero-mean white noise input, then the AR model is given by:

$$\sum_{k=0}^{p} a[k]y[n-k] = x[n] \tag{5.8}$$

where p is the order and $a[k]$ are the AR coefficients. This is a discrete-time system that we would like to find the spectral characteristics for in continuous-time in order to compare to our PSDs. To do this, we first find a discrete-time transfer function for the AR model system by rearranging the above equation:

$$H(z^{-1}) = \frac{1}{\sum_{k=0}^{p} a[k] z^{-k}} \tag{5.9}$$

The PSD of signal attenuation along with first and second order AR model frequency response curves are shown in figures 5-9 through 5-14 for channel 1, channel 2, and diversity.

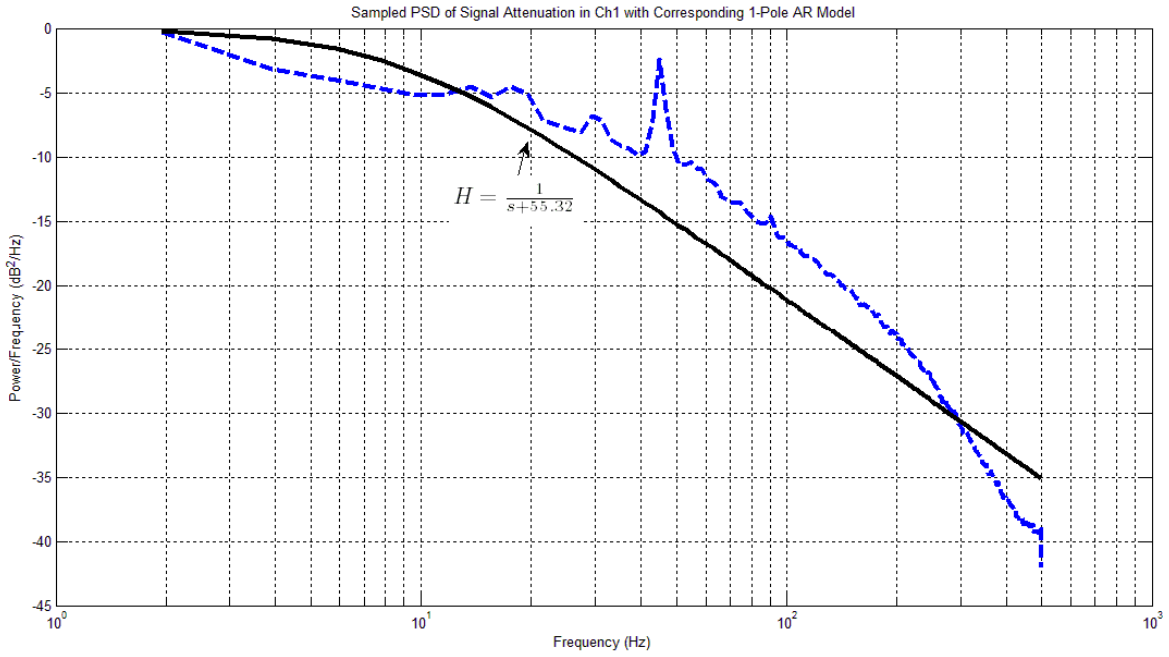

Figure 5-9: Log-amplitude sampled power spectral density and modified 1^{st} order autoregressive models, channel 1.

In all three cases, the first order AR model seems not rich enough to fit the log-normal power spectrum, which rolls off faster, and the second order AR model seems too rich, since the power spectrum rolls off more slowly. The problems in fit are largely due to both tails of the spectrum. The left tail is especially interesting since we observe more power in the lower frequencies than expected.

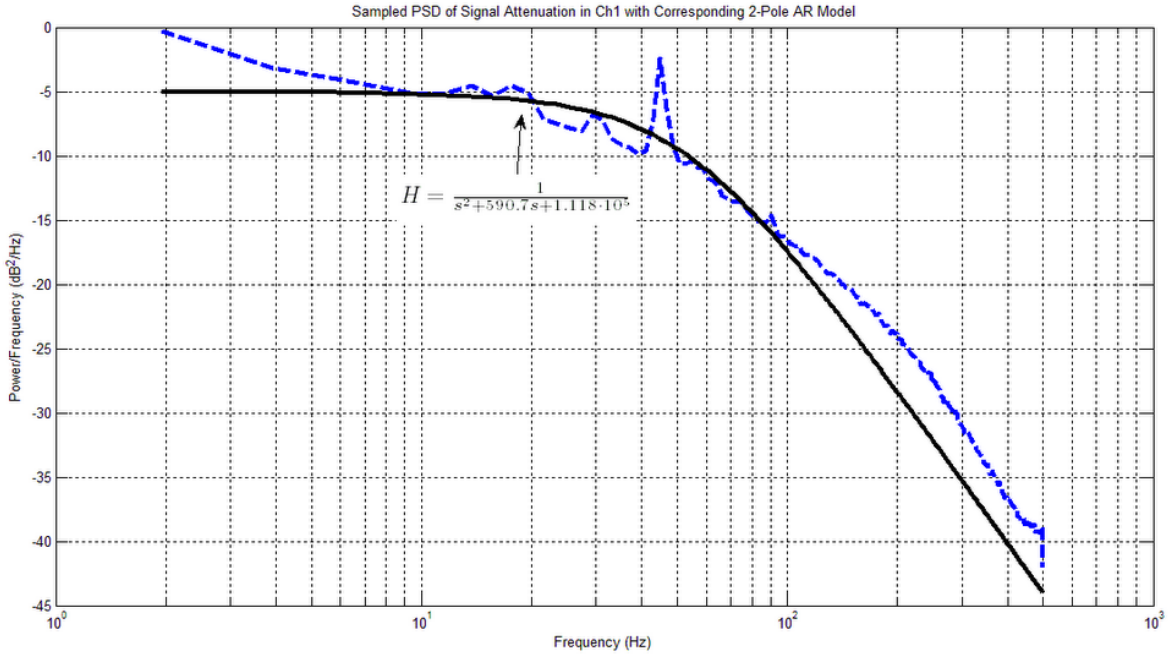

Figure 5-10: Log-amplitude sampled power spectral density and modified 2^{nd} order autoregressive models, channel 1.

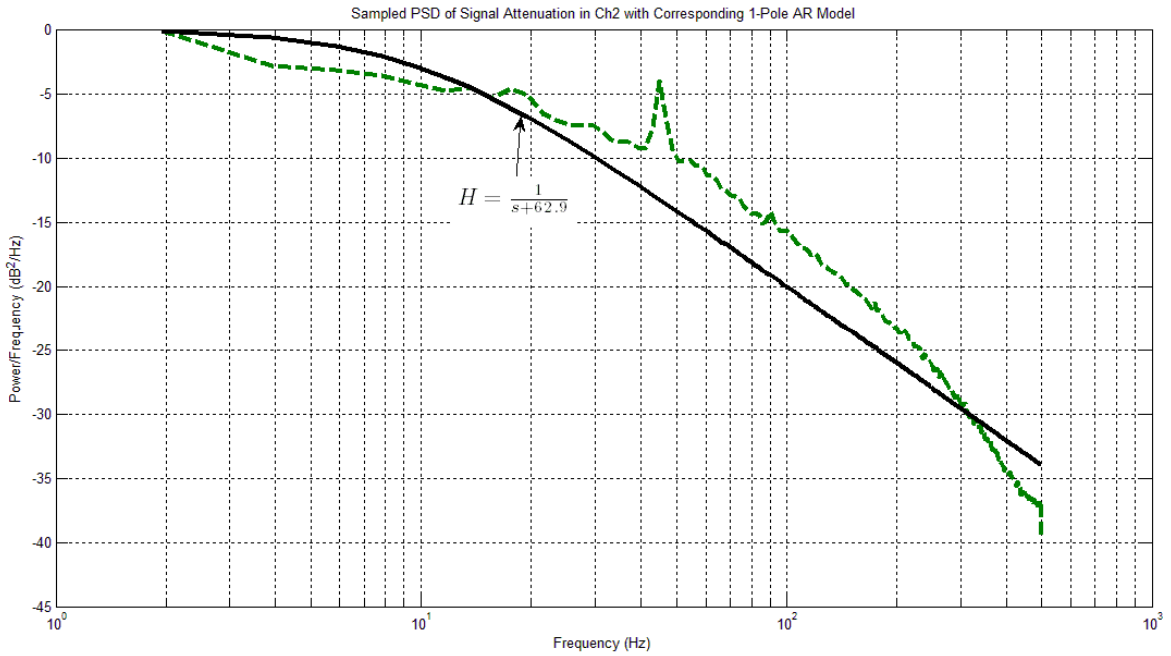

Figure 5-11: Log-amplitude sampled power spectral density and modified 1^{st} order autoregressive models, channel 2.

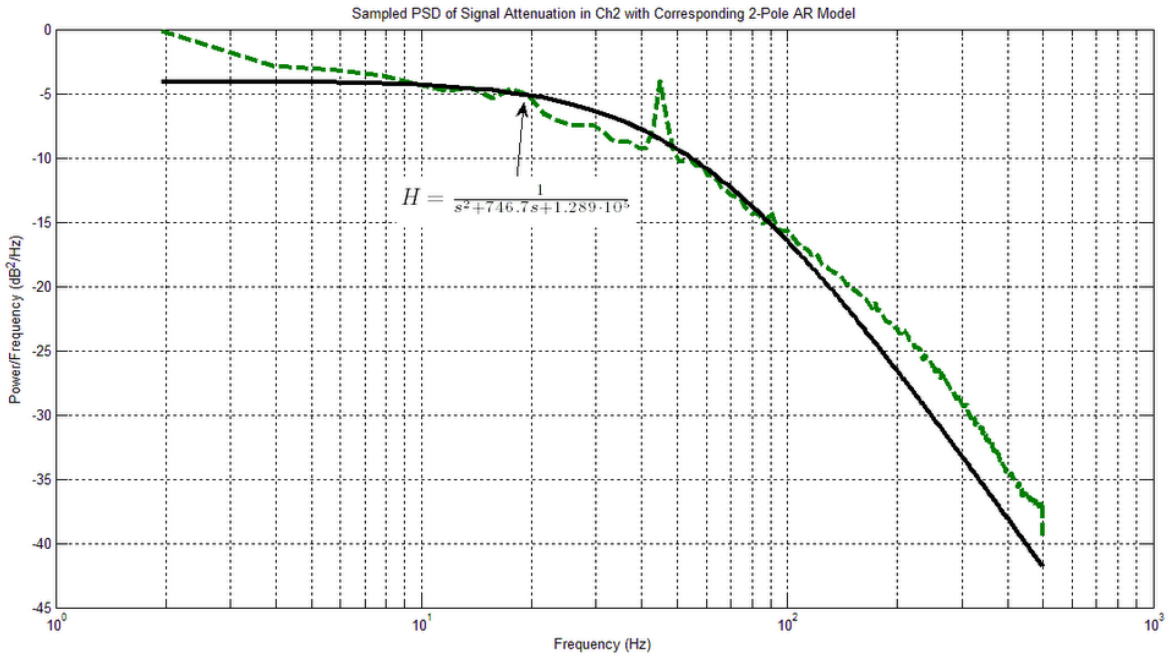

Figure 5-12: Log-amplitude sampled power spectral density and modified 2^{nd} order autoregressive models, channel 2.

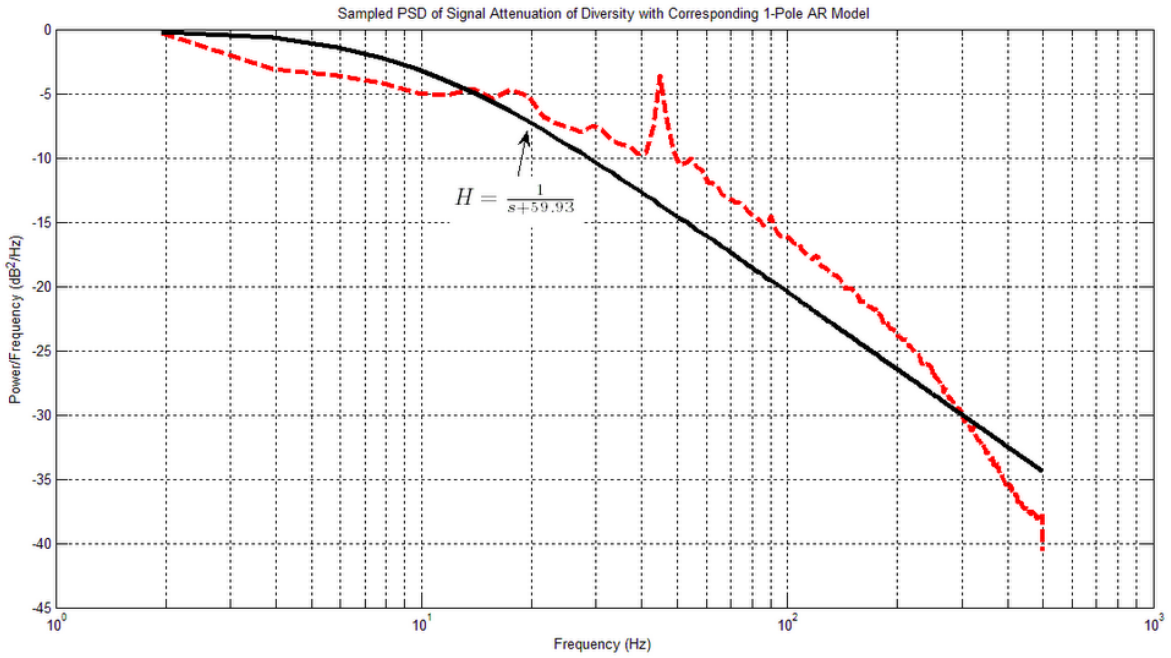

Figure 5-13: Diversity spectral density and modified 1^{st} order autoregressive models, diversity.

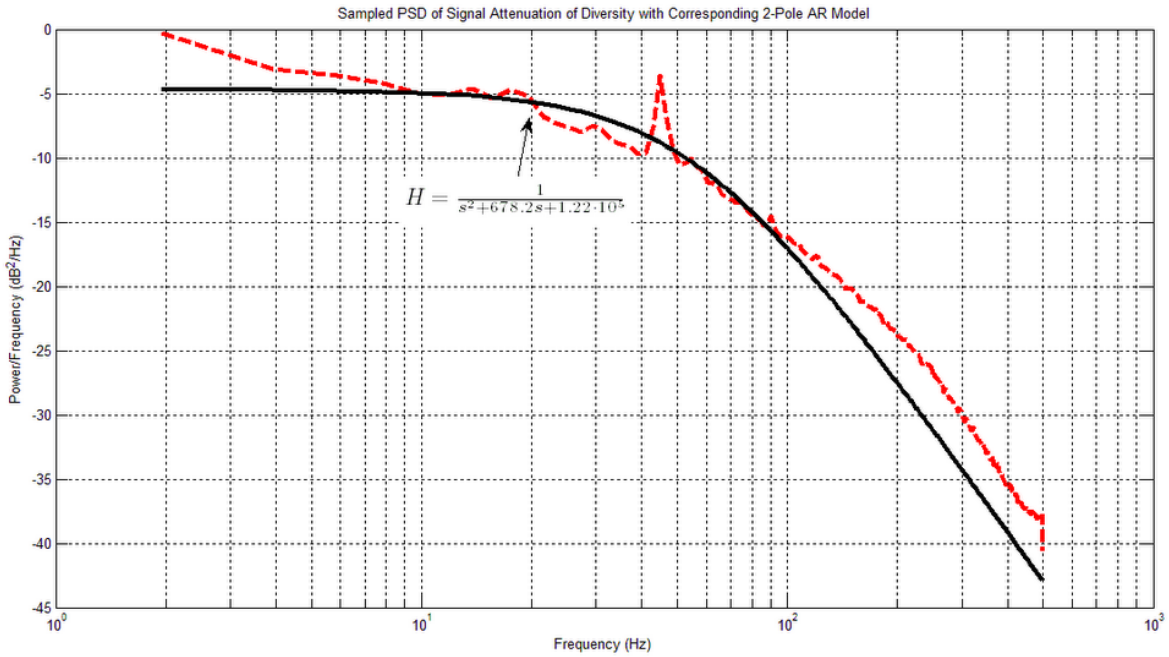

Figure 5-14: Diversity power spectral density and modified 2^{nd} order autoregressive models, diversity.

In figures 5-15 through 5-18 we disregard the tails and fit the mid-frequencies of the spectrums for channel 1, channel 2, and diversity.

Now, it is clear that in all cases the first order AR models fit the power spectrum very well compared to the second order models, which are too rich (e.g., over fit the data) for the power spectral data.

In reality, systems should be designed to operate in the main body of the frequencies, since the spectral characteristics of the tails can change widely given different environmental conditions. Thus, for normally operating systems we can model the signal attenuation at the receiver by a first order AR model. More specifically we can model the fluctuations of the signal attenuation in the channel as the output of a low-pass first order filter driven by white noise. Since a first order AR model represents a system defined by the equation $a[0]y[n] + a[1]y[n-1] = x[n]$ the system represents a one-pole low pass filter. Also, since the current output $y[n]$ depends only on the input and the immediately previous state $y[n-1]$, we may model the channel as Markovian.

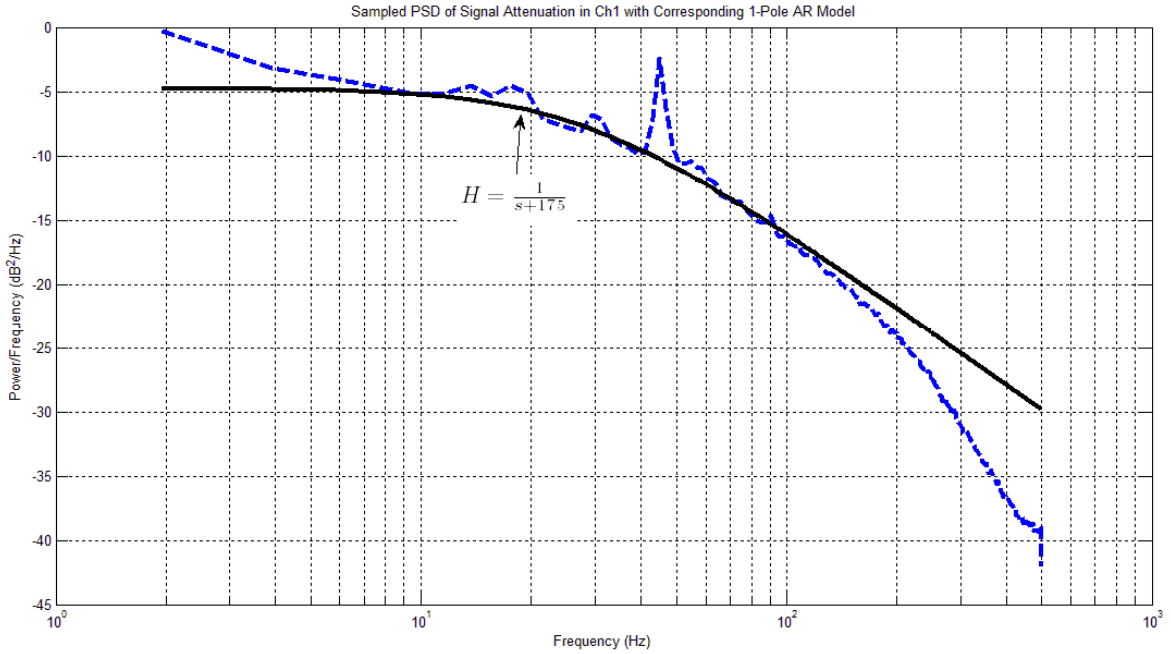

Figure 5-15: Log-amplitude sampled power spectral density and modified 1^{st} order autoregressive models, channel 1.

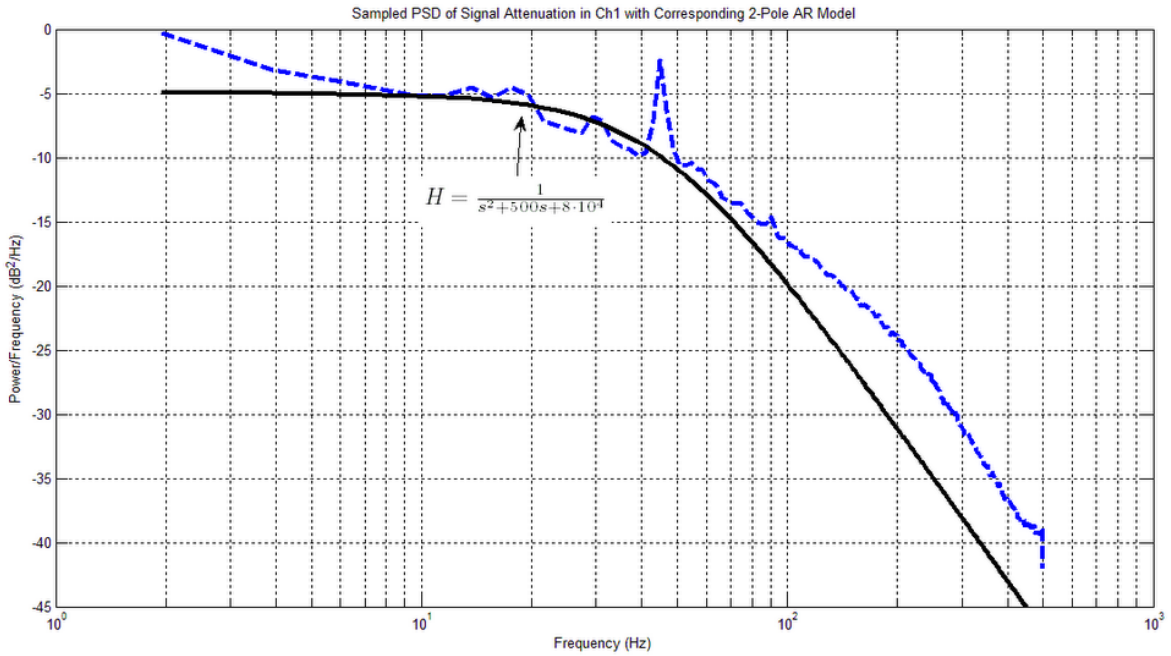

Figure 5-16: Log-amplitude sampled power spectral density and modified 2^{nd} order autoregressive models, channel 1.

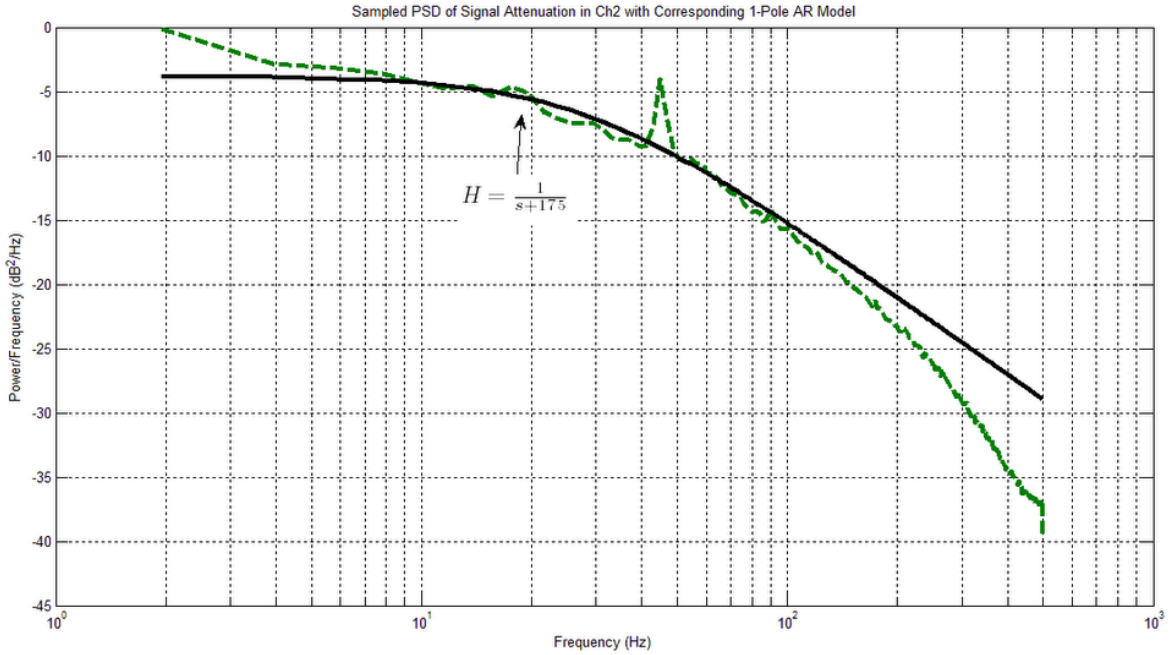

Figure 5-17: Log-amplitude sampled power spectral density and modified 1^{st} order autoregressive models, channel 2.

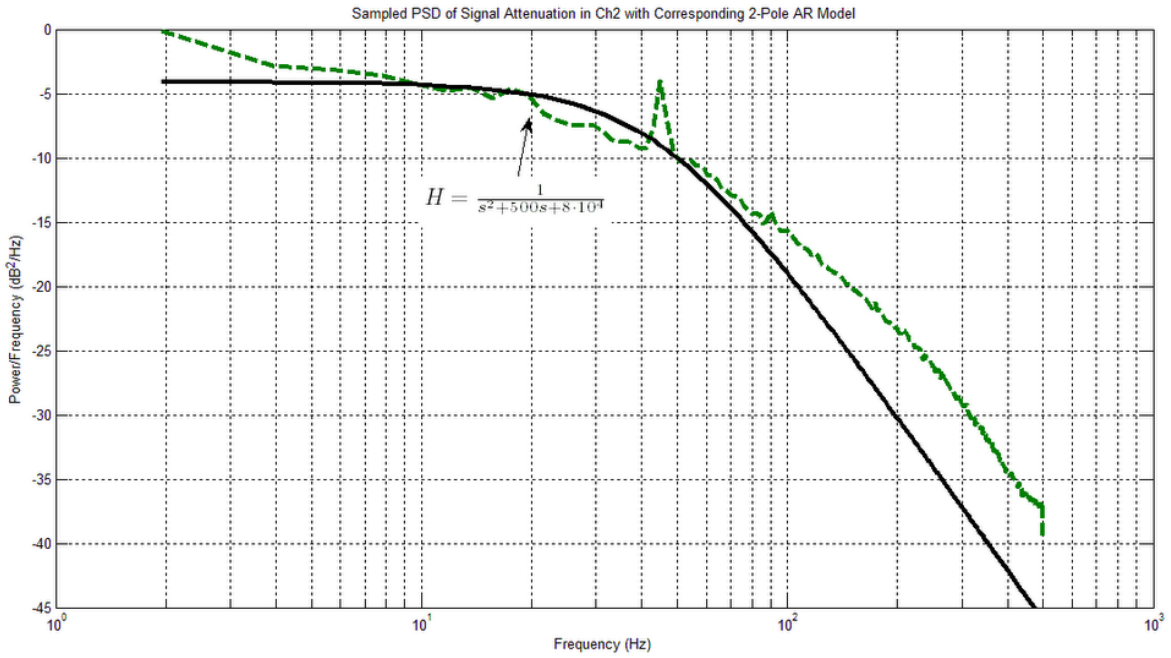

Figure 5-18: Log-amplitude sampled power spectral density and modified 2^{nd} order autoregressive models, channel 2.

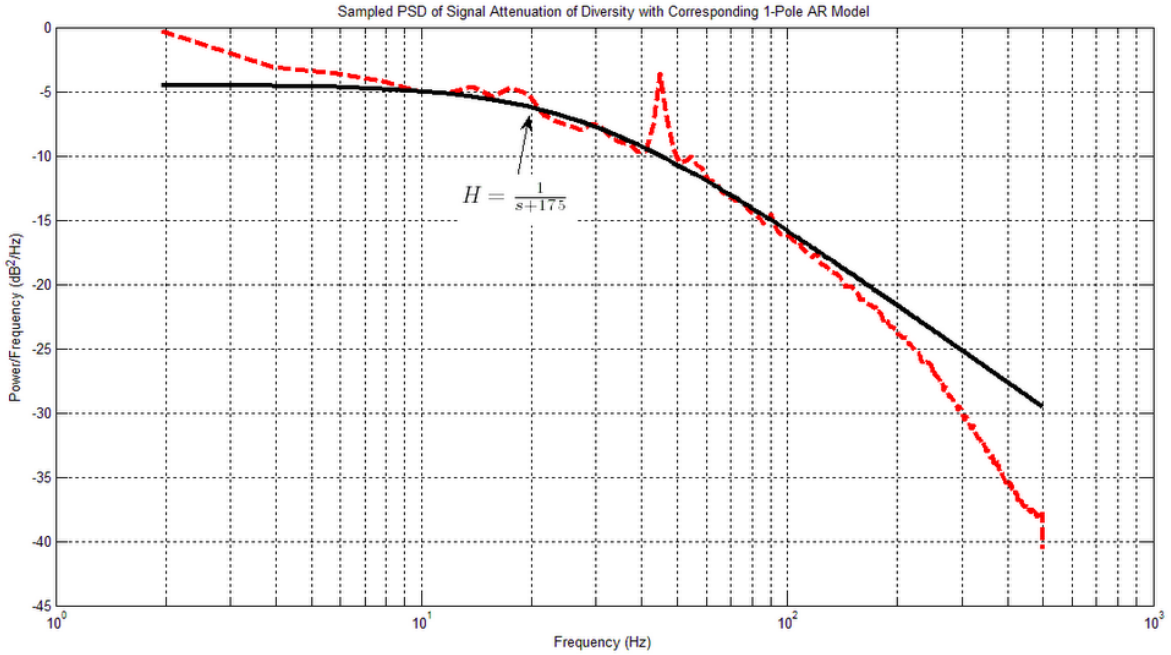

Figure 5-19: Diversity power sampled power spectral density and modified 1^{st} order autoregressive models, diversity.

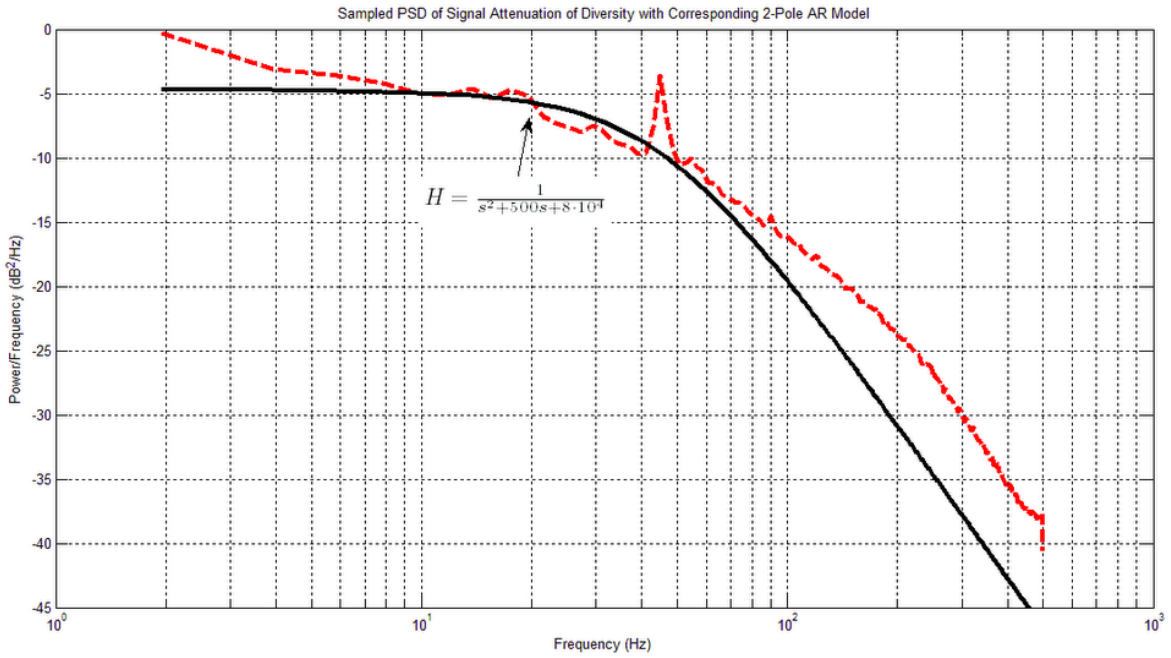

Figure 5-20: Diversity power spectral density and modified 2^{nd} order autoregressive models, diversity.

Autocovariance Analysis

For a wide sense stationary process the Wiener-Khinchin theorem states that the inverse Fourier transform of the PSD provides the autocorrelation function of a random process. As a result, because we showed that the log-amplitude PSD exhibits Markov (i.e. single-pole) structure, we expect the log-amplitude autocovariance to exhibit Markov structure. Thus, on the basis of the PSD analysis, we expect the log-amplitude to have an exponential autocovariance structure.

Figures 5-21 through 5-24 show the estimated log-amplitude covariance for both channel 1 and channel 2. On each figure, we fit a test autocovariance function of the form:

$$f(t) = e^{-|t/t_0|^{\varpi}/2} \tag{5.10}$$

where ϖ is the exponential power and t_0, the atmospheric coherence time, is chosen to fit the data. For figure 5-21, $\varpi = 1$ corresponding to an exponential, or Markov, autocovariance function. Figure 5-22 shows a fit with $\varpi = 1.1$, the value of ϖ that minimizes the mean squared error over all $\varpi > 0$. Figure 5-23 shows a fit with $\varpi = 5/3$ and figure 5-24 shows a fit with $\varpi = 2$.

It is clear from the figures that $\varpi = 1.1$ fits the data the most closely. The Markov fit, $\varpi = 1$, fits the data reasonably well. Thus, we confirm that the log-amplitude fluctuations can be modeled as approximately a Gauss-Markov random process. The fact that the log-amplitude fluctuations are Gauss-Markov implies that the diversity power fluctuations can be modeled as a Markov random process. Additionally, we verified that the diversity power fluctuation data exhibits Markov dynamics. In addition, we may model the fluctuations in the signal attenuation as the output of a one-pole low-pass filter driven by white noise. In the next section we attempt to formulate a prediction model for the signal attenuation based on the first order model we just derived.

Next, we use the single pole spectrum model of the log-amplitude fluctuation to find the optimal channel prediction.

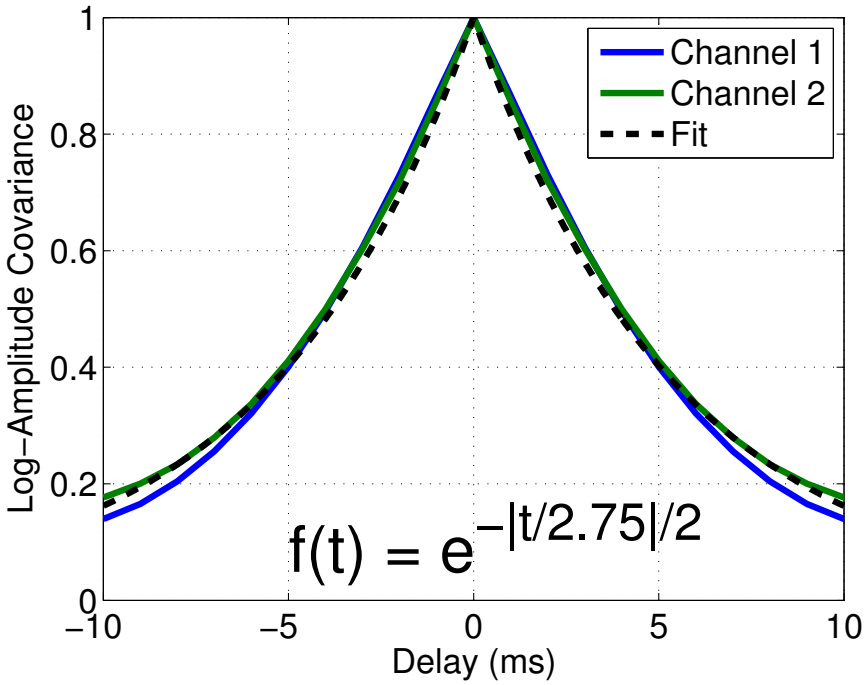

Figure 5-21: Autocovariance of channel 1 and channel 2 with a best fit autocovariance from Gauss-Markov class of processes.

5.1.4 Channel Prediction

We wish to use our knowledge of the channel dynamics to predict the future atmospheric state on the basis of the atmospheric state time history. Because the Markovianity of the atmospheric dynamics, the future state can be optimally predicted based on only the current atmospheric state. Thus, we use the one-pole filter behavior of the log-normal atmosphere fluctuations as a way to predict the signal attenuation in the future given the present turbulence state. If $\chi[n]$ is the log-amplitude state at time n, then we may optimally predict the log-amplitude j time steps later using the equation:

$$\hat{\chi}[n+j] = \mu_\chi[n] + c(\chi[n] - \mu_\chi[n]) \tag{5.11}$$

where we have assumed that the log-amplitude mean μ_χ varies slowly and c is a calculated constant. This is the linear least-squares (LLS) estimator; the Gauss-Markov theorem states that the LLS estimator has the minimum variance of all estimators that are linear combinations of the observations. Further, because the log-

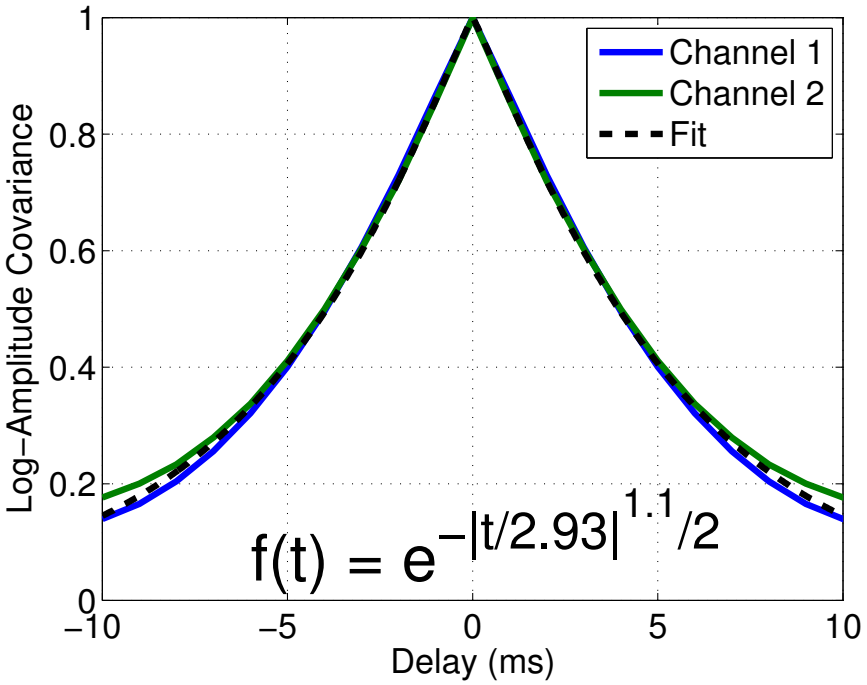

Figure 5-22: Autocovariance of channel 1 and channel 2 with a best fit autocovariance with $\varpi = 1.1$.

amplitude fluctuations are normally distributed, the LLS estimator is simultaneously the optimal Bayes' least square estimator and minimum *a priori* (MAP) estimator [51].

The value of c is calculated from the modified Yule-Walker equation [51]. From the orthogonality principle of LLS estimation, we have:

$$\begin{aligned} \mathbb{E}\left[(\hat{\chi}[n+j] - \chi[n+j])\chi[n]\right] &= 0 \\ \Rightarrow \mathbb{E}\left[(\hat{\chi}[n+j])\chi[n]\right] &= \mathbb{E}\left[\chi[n+j]\chi[n]\right] \end{aligned} \tag{5.12}$$

We define the covariance function of $\chi[n]$ as $K_{\chi\chi}[j] = \mathbb{E}[\chi[n]\chi[n+j]]$ and rewrite the last equation as:

$$\begin{aligned} cK_{\chi\chi}[0] &= K_{\chi\chi}[j] \\ \Rightarrow c &= \frac{K_{\chi\chi}[j]}{K_{\chi\chi}[0]} \end{aligned} \tag{5.13}$$

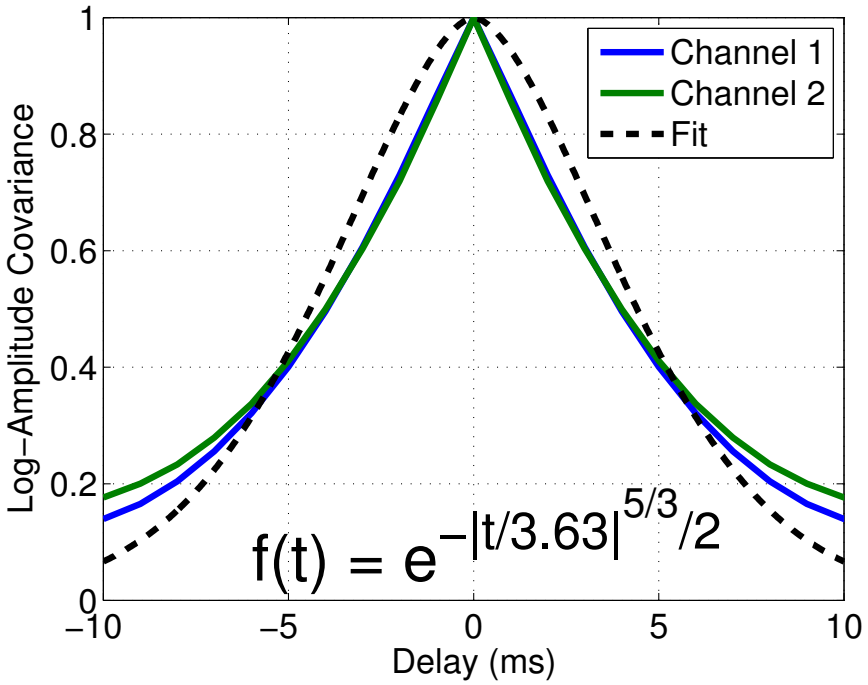

Figure 5-23: Autocovariance of channel 1 and channel 2 with a best fit autocovariance with $\varpi = 5/3$.

Thus, the value of c is the quotient of two covariances. In practice a system would calculate the covariances using the sample correlation function $\hat{K}_{\chi\chi}[j]$ from past data and make the approximation that $K_{\chi\chi}[j] = \hat{K}_{\chi\chi}[j]$. The amount of past data used to estimate the covariance should be around the time for which the process is approximately wide sense stationary, the stationarity time. Because the stationarity time of the atmosphere is on the order of 10^3 to 10^4 seconds, we use around 10^3 seconds of data, or 10^6 data points (since the sampling period is 1 ms), to estimate the correlation function. In practice, significantly fewer than 10^3 data points would yield a sufficient estimate of the correlation function. The sample correlation function at time n using the past N data is defined as

$$\hat{K}_{\chi\chi}[j] = \frac{1}{N - |j|} \sum_{k=n-N+1}^{n-|j|} \chi[k]\chi[k + |j|] \tag{5.14}$$

provided that $|j| \leq N - 1$. Note that the sample correlation function, and thus our values for c, will change at each time step and will therefore be recalculated at each

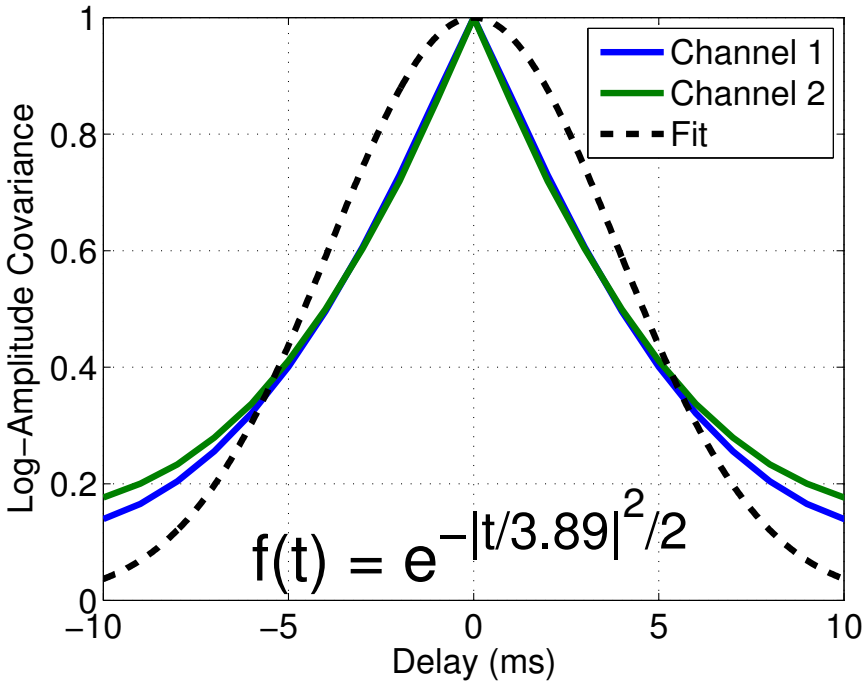

Figure 5-24: Autocovariance of channel 1 and channel 2 with a best fit autocovariance with $\varpi = 2$.

time step. In practice a system would only need to update the covariance estimate at some fraction of the stationarity time, thus significantly reducing the number of calculations required.

For the data, we calculate the covariances and the prediction for the log-amplitude fluctuations for channel 1 and channel 2. To predict the diversity case, we calculate the linear models for each log-amplitude channel individually, then exponentiate and sum the result. This method implicitly assumes the channels are uncorrected.

The predictions are calculated for all time steps starting at $100 + j$ ms (j is the number of ms to predict into the future at time n given data $\chi[n]$). We use this process to predict the signal attenuation for $j = 1, 3, 5$ ms for channel 1, channel 2, and diversity. Figures 5-25, 5-26, and 5-27 show the predicted signal attenuation (dotted lines) and actual signal attenuation values (solid lines) for channel 1, channel 2, and diversity and predictions for times of one, three, and five milliseconds in the future. The graphs show the predictions in a 200 ms window. For channel 1, the estimator is able to predict the signal attenuation to within 1.5 dB for a 1 ms

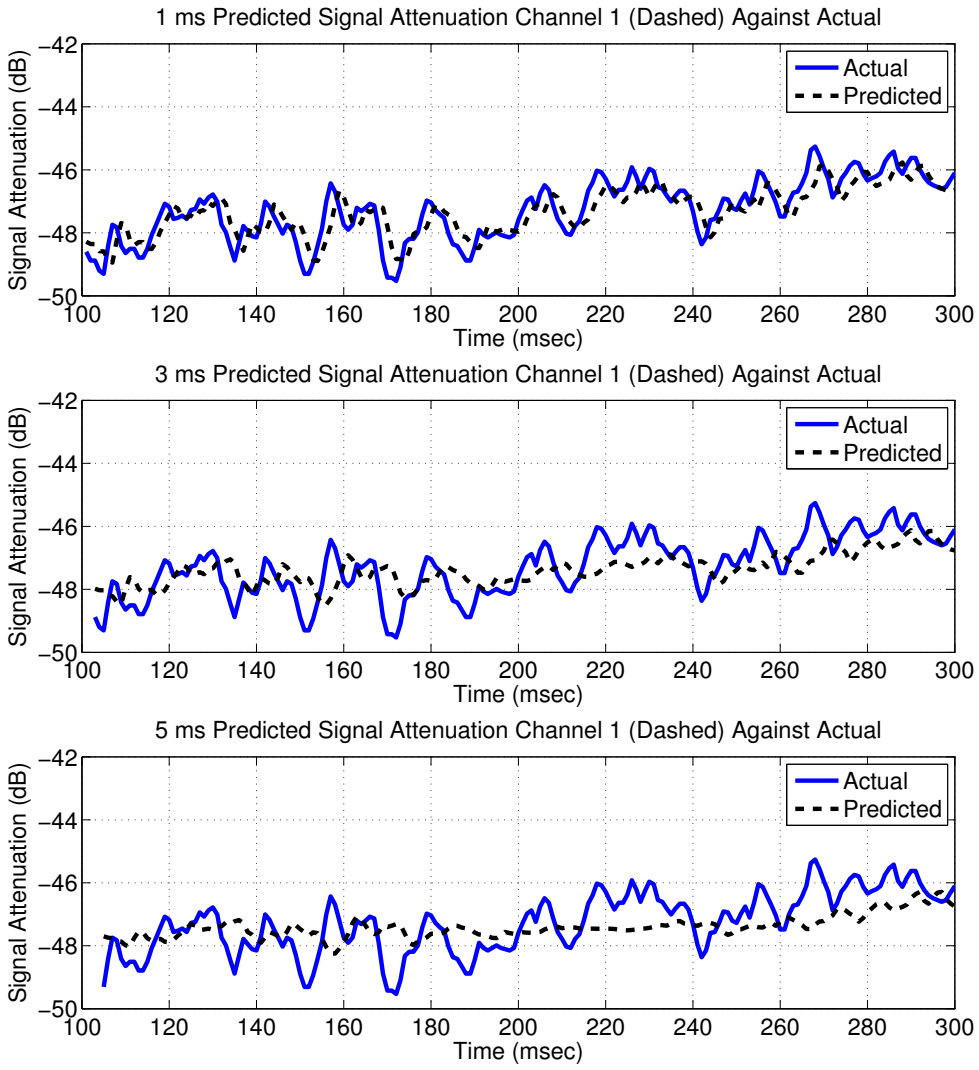

Figure 5-25: Predicted signal attenuation versus actual for 1, 3, and 5 ms prediction times, channel 1.

prediction time (1.5 dB is worst case, typical prediction error is smaller), within 2 dB for a 3 ms prediction time, and within 2.5 dB for a 5 ms prediction time. The range of signal attenuation is 4.5 dB. For channel 2, the estimator is generally able to predict the signal attenuation to within 1.5 dB for a 1 ms prediction time, within 2 dB for a 3 ms prediction time, and within 2 dB for a 5 ms prediction time. The exception is a spike at around 220 ms, at which the error is 2 dB for a 1 ms prediction time and around 4 dB for a 3 ms prediction time and a 5 ms prediction time. The

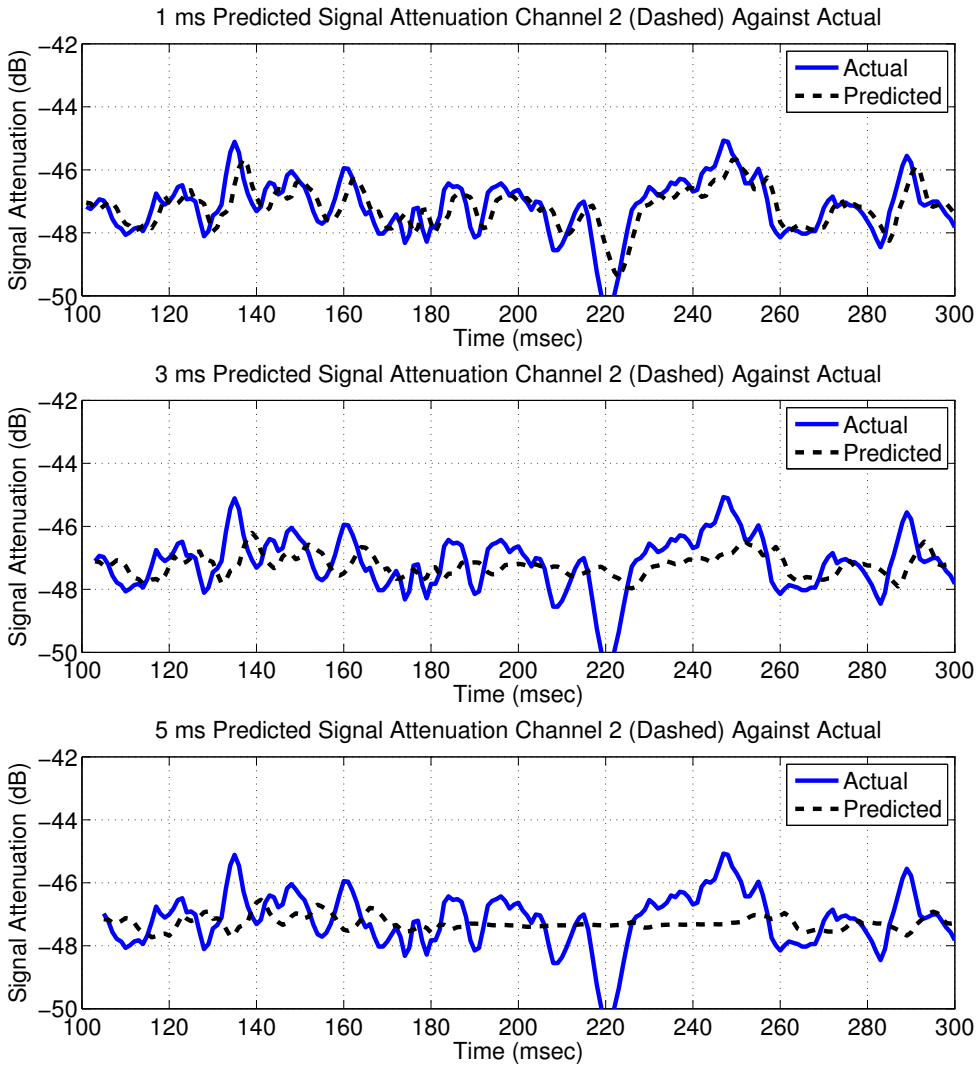

Figure 5-26: Predicted signal attenuation versus actual for 1, 3, and 5 ms prediction times, channel 2.

range of signal attenuation is 3.5 dB (without the spike) or 6 dB (with the spike). For diversity, the estimator is able to predict the signal attenuation to within 1 dB for a 1 ms prediction time, within 1.2 dB for a 3 ms prediction time, and within 1.5 dB for a 5 ms prediction time. The range of signal attenuation is 3 dB.

The error in the diversity case is smaller because the range is tighter. In all cases, as the prediction time increases the error increases because the predicted signal attenuation shows decreasing variation with the variation of the data. In other words,

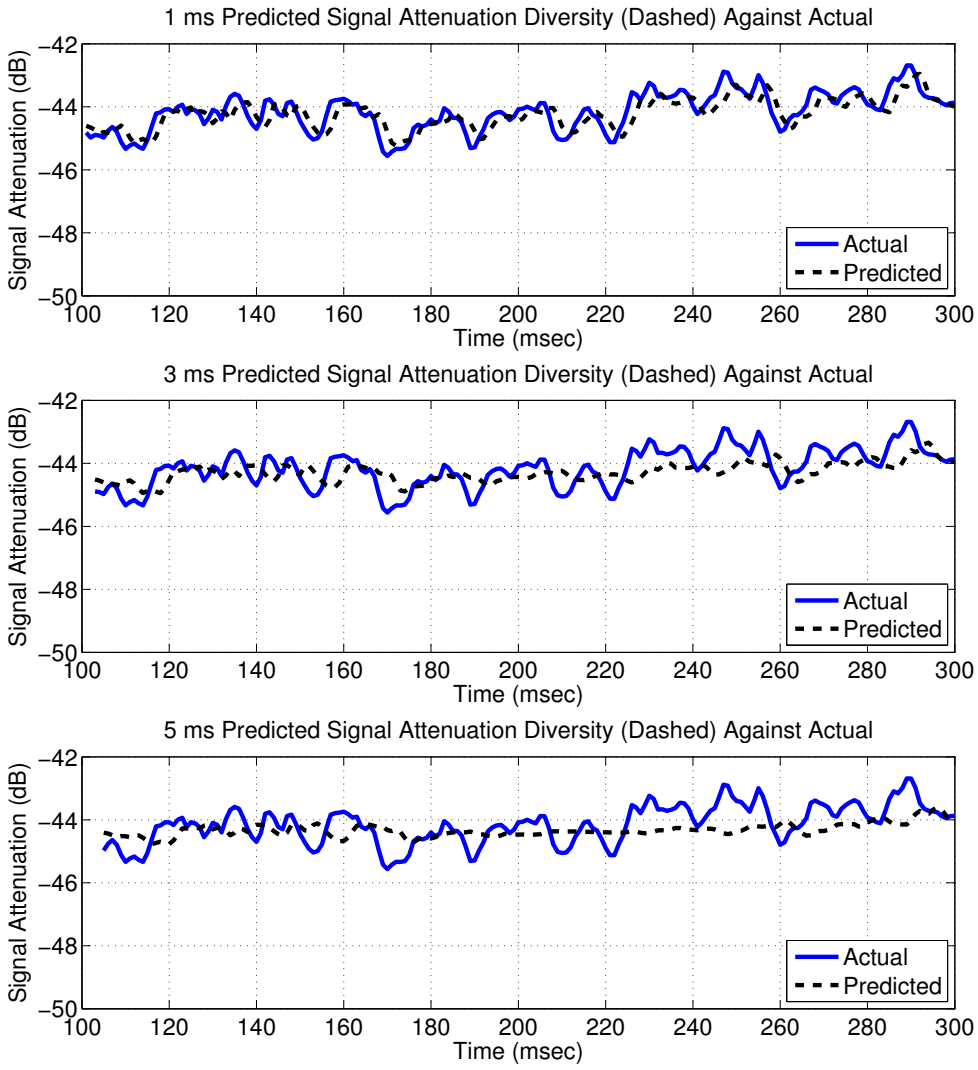

Figure 5-27: Predicted signal attenuation versus actual for 1, 3, and 5 ms prediction times, diversity.

the value calculated for $c = \frac{K_{xx}[j]}{K_{xx}[0]}$ decreases as the prediction time increases. This reflects our decreased confidence in predicting further into the future. We analyze this confidence in the next section.

Channel Prediction Confidence

It is important to learn how far into the future we can predict with high confidence. As we predict further into the future using the equation $\hat{\chi}[n+j] = \mu_\chi[n] + c(\chi[n] - \mu_\chi[n])$, the value of $c = \frac{K_{\chi\chi}[j]}{K_{\chi\chi}[0]}$ decreases, reflecting our decreased ability to predict the future. We plot the value of c as a function of delay, time-averaged over 1000 successive calculations of c (one second of observations) in order to eliminate random variations in the covariance estimate. Figure 5-28 shows the log-amplitude autocovariance for channel 1 and channel 2.

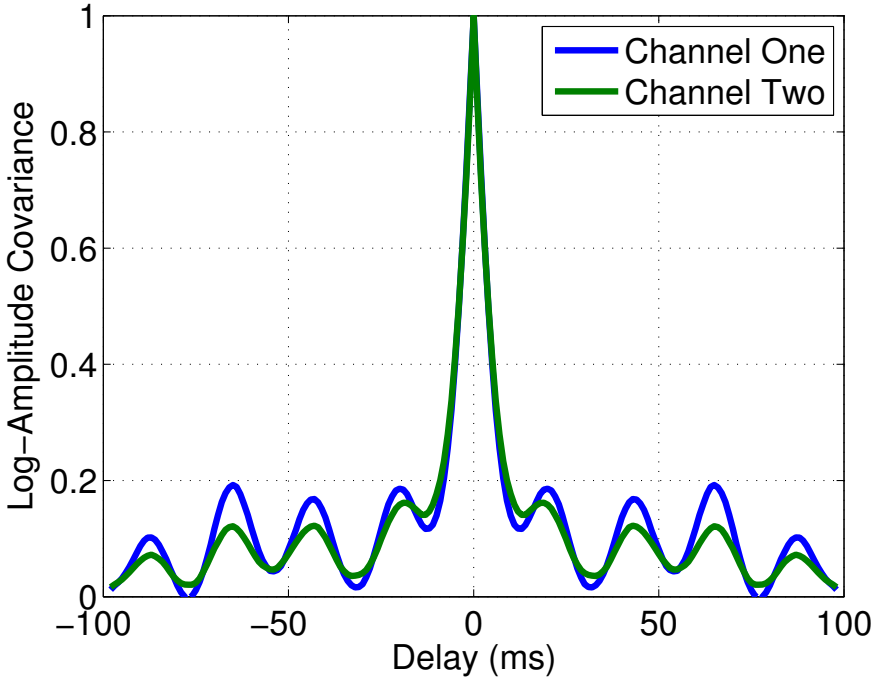

Figure 5-28: Log-amplitude autocovariance, $K_{\chi\chi}[j]$.

In both cases, the value of c drops rapidly so that at $j = 5$ ms, c is only about 0.5. After $j = 10$ ms, the value of c is bound below 0.2. This indicates that the maximum amount of time that we should predict into the future with some confidence is 5 to 10 ms. Beyond that, we are only about as confident as if we simply predicted the mean value. The covariance ripple, which shows up as a resonance peak in the PSD shown in figure 5-28, is interesting and, as of yet, unexplained. The resonance peak could be

due to mirror vibration or some other artifact caused by the particular experimental setup.

The LLS estimator is the optimal estimator for predicting the log-amplitude attenuation in the atmospheric channel. The LLS estimator is not optimal for estimating the power attenuation; nonetheless it is a good estimator. The errors in prediction are substantial — when predicting 1 ms into the future, we make up to a 1.5 dB error in prediction for channel 1 and channel 2 and a 1 dB error in prediction for diversity. Additionally, the maximum time we can predict into the future with any confidence is about 5 to 10 ms. The LLS estimator is not more accurate at predicting the signal attenuation in the diversity channel per se. Relative to the range of the actual signal attenuation data, the predicted signal attenuation values are not more accurate. The fact that the predicted values are closer to the actual values is due to the smaller range of the actual signal attenuation data.

5.2 Atmospheric Markovianity from Theoretic Perspective

In this section, we use the experimentally derived model for the turbulent atmosphere to establish properties of the sparse aperture communication system performance; specifically, we use the property that the log-amplitude fluctuations are approximately a Gauss-Markov process to show that the received signal power, after optimal recombination, of a sparse aperture system without feedback is well modeled as a Gauss-Markov process. We continue to derive the transition rates for the process.

We prove that, under some restricted conditions, the sparse aperture system without feedback can be modeled as a Gauss-Markov process. Next, we find the level crossing rate, a measure of the rapidity of fading, then continue to find the average outage/non-outage duration, and finally find the Markov transition rates.

Theorem 13 *For a sparse aperture system without feedback, optimal recombination, and many transmitters and receivers, the received signal power is a Gauss-Markov*

process. The distribution of the received power at a single time instant is:

$$\|\vec{y}\|^2 \sim \mathcal{N}\left(\mathrm{SNR}, \frac{\mathrm{SNR}^2}{n_{tx}n_{rx}}\left(e^{4\sigma_\chi^2}-1\right)\right) \tag{5.15}$$

and the autocovariance is:

$$R_{\|\vec{y}\|^2\|\vec{y}\|^2}(t) = \frac{\mathrm{SNR}^2}{n_{tx}n_{rx}}\left(e^{4\sigma_\chi^2}-1\right)e^{-\frac{1}{2}\left|\frac{t}{t_o}\right|} \tag{5.16}$$

Proof. If we allocate equal power to each transmitter, the power received at a single receiver is:

$$\begin{aligned}
|y_{\mathsf{j}}|^2 &= \frac{\mathrm{SNR}}{n_{tx}n_{rx}}\left|\sum_{\mathsf{k}=1}^{n_{tx}} h_{\mathsf{kj}}\right|^2 \\
&= \frac{\mathrm{SNR}}{n_{tx}n_{rx}}\left[\sum_{\mathsf{k}=1}^{n_{tx}}|h_{\mathsf{kj}}|^2 + \sum_{\mathsf{k}_1=1}^{n_{tx}}\left(\sum_{\mathsf{k}_2=1,\mathsf{k}_2\neq\mathsf{k}_1}^{n_{tx}} h_{\mathsf{k}_1\mathsf{j}}^\dagger h_{\mathsf{k}_2\mathsf{j}} + h_{\mathsf{k}_1\mathsf{j}}h_{\mathsf{k}_2\mathsf{j}}^\dagger\right)\right] \\
&= \frac{\mathrm{SNR}}{n_{tx}n_{rx}}\left[\sum_{\mathsf{k}=1}^{n_{tx}}|h_{\mathsf{kj}}|^2 + 2\sum_{\mathsf{k}_1=1}^{n_{tx}}\left(\sum_{\mathsf{k}_2=1,\mathsf{k}_2\neq\mathsf{k}_1}^{n_{tx}} Re\left\{h_{\mathsf{k}_1\mathsf{j}}^\dagger h_{\mathsf{k}_2\mathsf{j}}\right\}\right)\right] \\
&= \frac{\mathrm{SNR}}{n_{tx}n_{rx}}\left[\sum_{\mathsf{k}=1}^{n_{tx}}|h_{\mathsf{kj}}|^2 + 2\sum_{\mathsf{k}_1=1}^{n_{tx}}\left(\sum_{\mathsf{k}_2=1,\mathsf{k}_2\neq\mathsf{k}_1}^{n_{tx}} e^{\chi_{\mathsf{k}_1\mathsf{j}}+\chi_{\mathsf{k}_2\mathsf{j}}}\cos\left(\phi_{\mathsf{k}_1\mathsf{j}}-\phi_{\mathsf{k}_2\mathsf{j}}\right)\right)\right]
\end{aligned} \tag{5.17}$$

The $\cos\left(\phi_{\mathsf{k}_1\mathsf{j}}-\phi_{\mathsf{k}_2\mathsf{j}}\right)$ term is a zero mean random variable. As a result, as the number of transmitters becomes very large the second summation approaches zero. Therefore equation (5.17) asymptotically simplifies to:

$$|y_{\mathsf{j}}|^2 = \frac{\mathrm{SNR}}{n_{tx}n_{rx}}\left[\sum_{\mathsf{k}=1}^{n_{tx}}|h_{\mathsf{kj}}|^2\right] \tag{5.18}$$

Assuming optimal recombination, the received power is:

$$\begin{aligned}\|\vec{y}\|^2 &= \frac{\text{SNR}}{n_{tx}n_{rx}}\left[\sum_{\mathsf{j}=1}^{n_{rx}}|y_{\mathsf{j}}|^2\right] \\ &= \frac{\text{SNR}}{n_{tx}n_{rx}}\left[\sum_{\mathsf{j}=1}^{n_{tx}}\sum_{\mathsf{k}=1}^{n_{tx}}|h_{\mathsf{kj}}|^2\right] \\ &= \frac{\text{SNR}}{n_{tx}n_{rx}}\left[\sum_{\mathsf{j}=1}^{n_{tx}}\sum_{\mathsf{k}=1}^{n_{tx}}e^{2\chi_{\mathsf{kj}}}\right]\end{aligned} \tag{5.19}$$

If we wish to perform an analysis for a system with a finite number of transmitters and receivers, we would need measurements of the phase. Because the data analyzed was incoherently detected, phase information is not available. By the central limit theorem, the received power is normally distributed:

$$\|\vec{y}\|^2 \sim \mathcal{N}\left(\text{SNR}, \frac{\text{SNR}^2}{n_{tx}n_{rx}}\left(e^{4\sigma_\chi^2}-1\right)\right) \tag{5.20}$$

Assuming weak turbulence, $\sigma_\chi^2 \leq 0.1$, we apply a Taylor series expansion to the received power to calculate the autocovariance of the optimally recombined received power:

$$R_{\|\vec{y}\|^2\|\vec{y}\|^2}(t) = \frac{\text{SNR}^2}{n_{tx}n_{rx}}\left(e^{4\sigma_\chi^2}-1\right)e^{-\frac{1}{2}\left|\frac{t}{t_o}\right|} \tag{5.21}$$

Since the autocovariance function is exponential, the received power is a Gauss-Markov process. □

Theorem 14 *For a sparse aperture system without feedback, optimal recombination, and many transmitters and receivers, the received signal power level crossing rate is given by:*

$$\text{LCR}(R) = \frac{1}{4\pi t_o}\exp\left(\frac{-n_{tx}n_{rx}}{2\left(e^{4\sigma_\chi^2}-1\right)}\left(\frac{R-\text{SNR}}{\text{SNR}}\right)^2\right)$$

where LCR *is the received signal power level crossing rate and R is the threshold normalized to the root mean squared signal level.*

Proof. The level crossing rate for a normal random variable z with mean μ_z, variance σ_z^2, and autocovariance $g_z(t)$ is given by [36]:

$$\mathrm{LCR}(R) = \frac{1}{2\pi}\sqrt{\frac{g_z''(0)}{g_z(0)}}\exp\left(\frac{-1}{2}\left(\frac{R-\mu_z}{\sigma_z}\right)^2\right) \tag{5.22}$$

Using the statistics of the received signal power given in Theorem 13, we obtain the level crossing rate:

$$\mathrm{LCR}(R) = \frac{1}{4\pi t_o}\exp\left(\frac{-n_{tx}n_{rx}}{2\left(e^{4\sigma_\chi^2}-1\right)}\left(\frac{R-\mathrm{SNR}}{\mathrm{SNR}}\right)^2\right)$$

□

Generally, the LCR is inversely proportional to the coherence time, decreases as the number of transmitters (receivers) increases, and increases as the turbulence becomes stronger. Next we find the average fade duration.

Theorem 15 *For a sparse aperture system without feedback, optimal recombination, and many transmitters and receivers, the average outage duration is given by:*

$$\bar{\tau}_{out}(R) = Q\left(\left[\frac{-(R-\mathrm{SNR})}{\mathrm{SNR}}\right]\sqrt{\frac{n_{tx}n_{rx}}{e^{4\sigma_\chi^2}-1}}\right)4\pi t_o\exp\left(\frac{n_{tx}n_{rx}}{2\left(e^{4\sigma_\chi^2}-1\right)}\left(\frac{R-\mathrm{SNR}}{\mathrm{SNR}}\right)^2\right) \tag{5.23}$$

Similarly, the average non-outage duration is given by:

$$\bar{\tau}_{notout}(R) = Q\left(\left[\frac{R-\mathrm{SNR}}{\mathrm{SNR}}\right]\sqrt{\frac{n_{tx}n_{rx}}{e^{4\sigma_\chi^2}-1}}\right)4\pi t_o\exp\left(\frac{n_{tx}n_{rx}}{2\left(e^{4\sigma_\chi^2}-1\right)}\left(\frac{R-\mathrm{SNR}}{\mathrm{SNR}}\right)^2\right) \tag{5.24}$$

Proof. The average outage duration is given by [22]:

$$\bar{\tau}_{out}(R) = \Pr(r \le R)/\mathrm{LCR}(R) \tag{5.25}$$

Using the statistics given by Theorem 13 and the level crossing rate given by Theorem 14, we obtain the average outage duration of the received signal power:

$$\bar{\tau}_{out}(R) = Q\left(\left[\frac{-(R-\mathrm{SNR})}{\mathrm{SNR}}\right]\sqrt{\frac{n_{tx}n_{rx}}{e^{4\sigma_\chi^2}-1}}\right) 4\pi t_o \exp\left(\frac{n_{tx}n_{rx}}{2\left(e^{4\sigma_\chi^2}-1\right)}\left(\frac{R-\mathrm{SNR}}{\mathrm{SNR}}\right)^2\right) \tag{5.26}$$

By symmetry, the average not-outage duration of the received signal power is:

$$\bar{\tau}_{notout}(R) = Q\left(\left[\frac{R-\mathrm{SNR}}{\mathrm{SNR}}\right]\sqrt{\frac{n_{tx}n_{rx}}{e^{4\sigma_\chi^2}-1}}\right) 4\pi t_o \exp\left(\frac{n_{tx}n_{rx}}{2\left(e^{4\sigma_\chi^2}-1\right)}\left(\frac{R-\mathrm{SNR}}{\mathrm{SNR}}\right)^2\right) \tag{5.27}$$

□

The average outage and non-outage duration as a function of the product of the number of transmitters and receivers for various normalized thresholds is shown in figure 5-29.

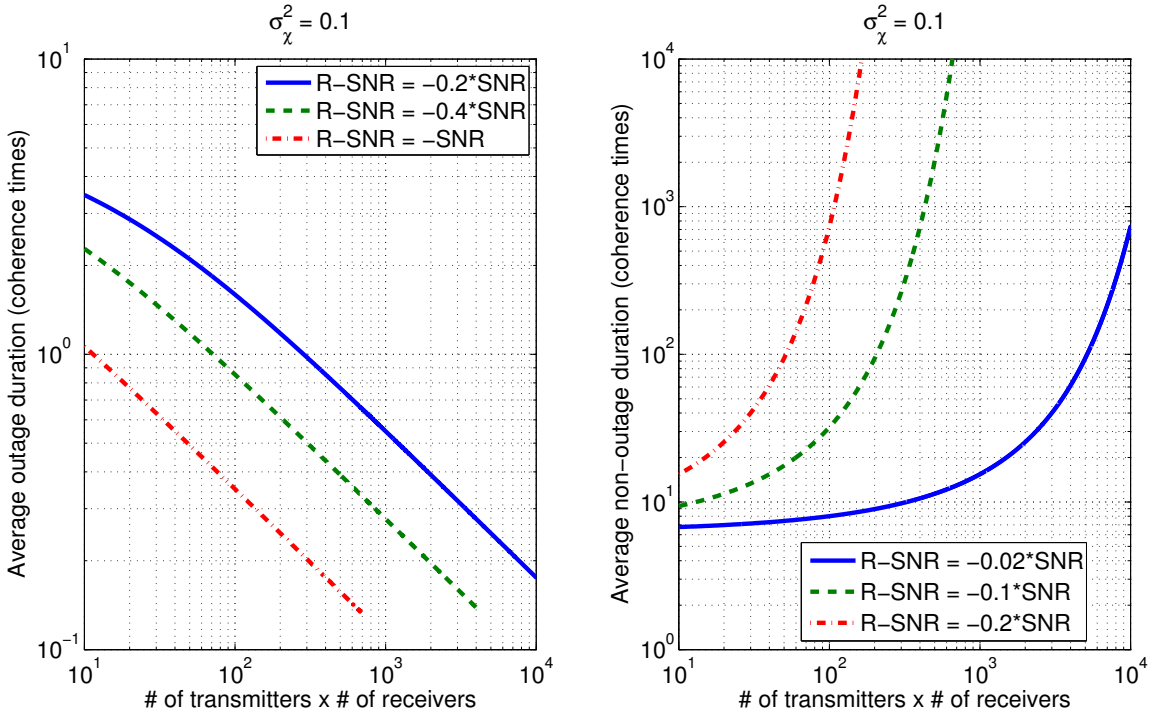

Figure 5-29: Conjectured low probability of outage Markov model for a sparse aperture system without feedback.

The average outage/non-outage durations can be used to find the transition times for the two-state continuous-time Markov channel model:

$$\begin{aligned} \nu_{o-n} &= \frac{1}{\bar{\tau}_{out}(R)} \\ \nu_{n-o} &= \frac{1}{\bar{\tau}_{notout}(R)} \end{aligned} \tag{5.28}$$

Thus we have found the Markov transition rates in terms of fundamental atmospheric parameters and system parameters: the turbulence strength, σ_χ^2, the turbulence coherence time, t_o, the number of transmitters and receivers, n_{tx} and n_{rx}, and the SNR. Figure 5-30 shows the low outage probability Markov model for the sparse aperture system without feedback. If we look at the special case where $R = \text{SNR}$, the transition rates should be equal, indicating that the system will spend an equal amount of time in outage as non-outage. Indeed, the outage and non-outage times are equal:

$$\begin{aligned} \bar{\tau}_{out}(R) = 2\pi t_o \rightarrow \nu_{o-n} &= \frac{1}{2\pi t_o} \\ \bar{\tau}_{notout}(R) = 2\pi t_o \rightarrow \nu_{n-o} &= \frac{1}{2\pi t_o} \end{aligned} \tag{5.29}$$

A typical system will operate in the region where the probability of outage is small, given by $R - \text{SNR} \ll \text{SNR}$. For this special case, we can accurately approximate the Q-function using the well known bound:

$$Q(x) \leq \frac{1}{x\sqrt{2\pi}} e^{-\frac{x^2}{2}} \tag{5.30}$$

This simplifies the average outage and non-outage durations to:

$$\begin{aligned} \bar{\tau}_{out}(R) &= 2t_o \left(\frac{\text{SNR}}{\text{SNR} - R} \right) \sqrt{\frac{2\pi(e^{4\sigma_\chi^2} - 1)}{n_{tx} n_{rx}}} \\ \bar{\tau}_{notout}(R) &= 4\pi t_o \exp\left(\frac{n_{tx} n_{rx}}{2\left(e^{4\sigma_\chi^2} - 1\right)} \left(\frac{R - \text{SNR}}{\text{SNR}} \right)^2 \right) \end{aligned} \tag{5.31}$$

Increasing the product of the number of transmitters and the number of receivers can reduce the average outage duration while increasing the average non-outage duration.

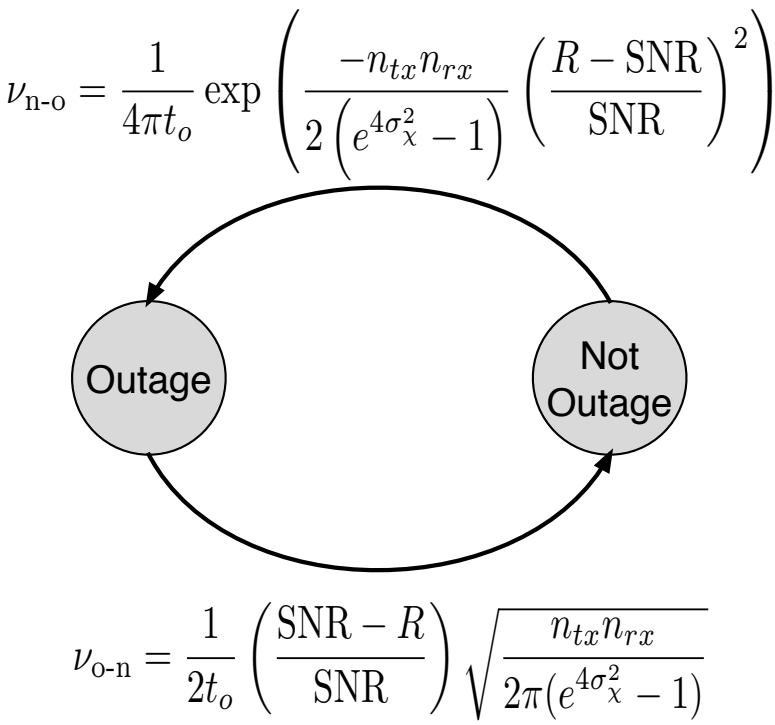

Figure 5-30: Low probability of outage Markov model for a sparse aperture system without feedback.

Both of these performance gains can be realized without bound, provided that the assumptions stated in Chapter 2 continue to hold. Increasing the SNR can reduce the average outage duration while increasing the average non-outage duration. As SNR becomes very large, however, performance gains experience diminishing returns. In the limit as the SNR grows very large, the SNR no longer has an effect of outage and non-outage durations. Stronger turbulence increases the outage duration and decreases the non-outage duration. Finally an increase in the coherence time increases both outage and non-outage durations.

Of importance when designing a Transport Layer protocol, the outage duration varies polynomially with SNR, the number of transmitter and receivers, and turbulence strength while the non-outage duration varies exponential in those same variables. Thus, a system designer cannot substantially reduce the outage duration, but can only increase the time between outages.

5.2.1 Markovianity Discussion

The goals of this section were threefold: first, to show that experimental data supports a Markov model for outage statistics and a Gauss-Markov model for the log-amplitude fluctuations; second, to formulate a linear prediction model for the signal attenuation in the channel; third, to analyze the effect of diversity on the channel model and the prediction model. All goals were satisfactorily investigated.

The outage statistics can be modeled as a Markov process: we can model the channel as a two-state Markov process with the states being outage and non-outage. The system is in outage when the received power is below a threshold. We demonstrated the validity of this model by showing that the distribution of outage times is approximately exponential. The log-amplitude fluctuations can be modeled as a Gauss-Markov process: we can model the log-amplitude fluctuation as Gaussian with a single-pole PSD. We demonstrated the validity of this model by fitting a first order autoregressive model to the power spectral density and by fitting an exponential function to the autocovariance.

We used the Gauss-Markov process behavior of the log-amplitude to create a linear least squares estimator for the signal attenuation in the channel. Such an estimator is optimal for predicting the log-amplitude fluctuations but not for predicting the power fluctuations. The estimator can predict the signal attenuation 1 ms in the future to within 1.5 dB in the single-receiver cases and to within 1 dB in the diversity case. The maximum time the estimator can predict into the future with any confidence is about 5 to 10 ms.

Diversity decreases the probability and duration of outages, from a maximum outage duration of 38 ms in channel 1 to a maximum outage duration of 8 ms for diversity. The model of the channel in the diversity case is still Markovian like the other cases. The linear estimator is approximately as accurate in the diversity case as in the other cases.

We used the Gauss-Markov model of the log-amplitude fluctuations to derive the outage statistics of a sparse aperture system without feedback and many transmitters

and receivers. We further conjectured the transition rates for a Markov outage model of a sparse aperture system with feedback and many transmitters and receivers.

Future research should focus on explaining unexpected results from the data. For example, a few outages are longer than expected. Also, the signal attenuation has higher power at the lowest frequencies and lower power at the highest frequencies than expected. It is likely that other experiments will show different results for these regions. Future research should make sure that protocols and systems avoid these extreme regions, or attempt to model these regions.

The linear least squares estimator is a promising tool for predicting the state of the channel a couple of milliseconds into the future. For wavefront predistortion systems based on feedback, this information can be calculated at the transmitter side and used to improve performance between channel state updates. Future research should investigate exactly how the channel state should be predicted at the transmitter to optimize performance.

Chapter 6

Security of Free Space Optical Communication

Free space optical communication systems are susceptible to eavesdroppers and interferers. An eavesdropper is any user that attempts to receive and decode the information intended for another user. An interferer is a user that (either intentionally or unintentionally) transmits power into a receiver that decreases the ability of that user to receive and decode information from other users. Techniques to mitigate the susceptibility to eavesdroppers and interferes include:

- Polarization diversity
- Spatial diversity
- Temporal diversity
- Frequency diversity

The goal of these techniques is to: 1. increase minimum the eavesdropper's receiver sensitivity required to intercept information intended for other users and 2. increase the minimum interferer transmit power required to degrade the intended receiver's performance. Because the topic of this thesis is the efficient use of spatial diversity, we only address the ability of spatial diversity to mitigate interference and eavesdropping. We compare diversity systems with and without feedback on the basis of the minimum

amount of interferer power required to impair the system. We also compare the systems on the basis of the maximum amount of information that can be transferred to intended receivers while ensuring zero information is transferred to eavesdroppers.

6.1 Sparse Aperture Performance in the Presence of an Interferer

Any deployed system will be affected by interference. In a densely populated urban area, other systems might inadvertently couple power into the receiver. There are other situations where a hacker might couple power into the receiver in an attempt to deny service. We modify the channel transfer equation given in Chapter 2 to include the effects of an interferer:

$$\vec{y} = \sqrt{\frac{\mathrm{SNR}}{n_{rx}}}\mathbf{H}\vec{x} + \sqrt{\mathrm{SIR}}\vec{y}^{\,\mathrm{I}} + \vec{w} \tag{6.1}$$

where $\vec{y}^{\,\mathrm{I}}$ is magnitude and phase of the spatial distribution of the coherently detected interferer field at the interferer receiver plane (normalized to unit energy) and SIR is the interference signal power to noise power ratio.

$$\begin{aligned} &\|\vec{y}^{\,\mathrm{I}}\|^2 = 1 \\ &\mathrm{SIR} = \frac{2(q\eta/hf)^2 P_{lo} P_{\mathrm{I}} A_{rx} T_b}{[(q^2\eta/hf)P_{lo} + (q\eta/hf)^2 P_{lo} N_o + N_{oc}]n_{rx}} \end{aligned} \tag{6.2}$$

where P_{I} is the radiative flux at the intended receiver's aperture, T_b is the bit period of the intended receiver, and P_{lo} is the local oscillator power of the intended receiver. Note that we have placed no restriction on the geometry or capabilities of the interfering transmitter. We have only assumed that it is able to couple P_{I} power into the intended receiver's aperture. Using the SVD to transform the channel into parallel

Gaussian channels, we arrive at:

$$\begin{aligned}
\tilde{y}_1 &= \sqrt{\mathrm{SNR}}\gamma_1\tilde{x}_1 + \sqrt{\mathrm{SIR}}\tilde{y}_1^{\mathrm{I}} + \tilde{w}_1 \\
\tilde{y}_2 &= \sqrt{\mathrm{SNR}}\gamma_2\tilde{x}_2 + \sqrt{\mathrm{SIR}}\tilde{y}_2^{\mathrm{I}} + \tilde{w}_2 \\
&\vdots \qquad\quad \vdots \qquad\quad \vdots \\
\tilde{y}_{n_{\min}} &= \sqrt{\mathrm{SNR}}\gamma_{n_{\min}}\tilde{x}_{n_{\min}} + \sqrt{\mathrm{SIR}}\tilde{y}_{n_{\min}}^{\mathrm{I}} + \tilde{w}_{n_{\min}}
\end{aligned} \tag{6.3}$$

where $\tilde{y}_{\mathsf{i}}^{\mathrm{I}}$ is the projection of the received interference field onto the i^{th} output eigenmode of $\mathbf{H}$, $\tilde{y}_{\mathsf{i}}^{\mathrm{I}} = \vec{u}_{\mathsf{i}}^{\dagger}(\mathbf{H})\vec{y}^{\,\mathrm{I}}$, and $n_{\min} = \min(n_{tx}, n_{rx})$. The vectors $\tilde{\vec{x}}$, $\tilde{\vec{y}}$, and $\tilde{\vec{w}}$ are related to the vectors $\vec{x}$, $\vec{y}$, and $\vec{w}$ through the usual SVD, such as in [48]. Note $\tilde{w}_{\mathsf{i}}$ retains its circularly symmetric complex Gaussian distribution. We denote the variance of $\tilde{w}_{\mathsf{i}}$ as $\sigma^2 = 1$. The constraint that $\mathbb{E}[\|\vec{x}\|^2] = 1$ implies a constraint on the energy allocated to $\tilde{x}_{\mathsf{i}}$ (assuming no energy is allocated to eigenmodes associated with singular values with a value of zero):

$$\mathbb{E}\left[\sum_{\mathsf{i}=1}^{n_{\min}} E_{\mathsf{i}}\right] = 1 \tag{6.4}$$

where E_{i} is the energy in $\tilde{x}_{\mathsf{i}}$, $|\tilde{x}_{\mathsf{i}}|^2 = E_{\mathsf{i}}$. Similarly, the constraint that $\|\vec{y}^{\,\mathrm{I}}\|^2 = 1$ implies a constraint on the energy allocated to $\tilde{y}_{\mathsf{i}}^{\mathrm{I}}$:

$$\mathbb{E}\left[\sum_{\mathsf{i}=1}^{n_{rx}} I_{\mathsf{i}}\right] = 1 \tag{6.5}$$

where I_{i} is the energy in $\tilde{y}_{\mathsf{i}}^{\mathrm{I}}$, $|\tilde{y}_{\mathsf{i}}^{\mathrm{I}}|^2 = I_{\mathsf{i}}$. We now *bound* the impact that an interferer can have on the sparse aperture system by looking at two cases: 1. (lower bound) a *basic interferer* is an interferer that has no ability to predistort its wavefront and no knowledge of the channel state and 2. (upper bound) an *advanced interferer* is an interferer that has knowledge of the power allocation at the receiver arriving from the intended transmitter and the ability to control the spatial distribution of the interference field at the intended receiver. For both cases, we assume that the power coupled into the intended receiver is Gaussian distributed after being integrated over

a bit period. Throughout this chapter, we assume BPSK as the modulation scheme because it provides the best protection against both fading and interference. Based on these results, we provide fuller analysis and insight into the system performance in the presence of interference.

6.1.1 Basic interference

A basic interferer, one that has no knowledge of the turbulence state, will couple power equally into each output eigenmode $\mathbb{E}[I_{\mathrm{i}}] = 1/n_{rx}$. As a result, as the number of receive apertures grows, the average probability of error for a sparse aperture system with perfect turbulence state knowledge (the wavefront predistortion system) in the presence of a basic interferer is:

$$\lim_{n_{tx},n_{rx}\to\infty} \mathbb{E}[\Pr(\text{error})] = Q\left(\sqrt{\frac{2\text{SNR}(1+\sqrt{\beta})^2}{1+\text{SIR}/n_{rx}}}\right) \tag{6.6}$$

As the number of receive apertures grows, the average probability of error for a sparse aperture system without turbulence state knowledge (the open loop system) in the presence of a basic interferer is:

$$\lim_{n_{tx},n_{rx}\to\infty} \mathbb{E}[\Pr(\text{error})] = Q\left(\sqrt{\frac{2\text{SNR}}{1+\text{SIR}/n_{rx}}}\right) \tag{6.7}$$

For both systems, with and without turbulence state knowledge, the interference power must be such that $\text{SIR} > 0.1n_{rx}$ for the interferer to degrade system performance. Wavefront predistortion based on turbulence state knowledge does not affect the interference power needed to impact the system performance. This is because the interferer spreads its power equally among the output eigenmodes. The open loop system can increase SNR or the number of receivers to overcome the effects of the turbulence. The wavefront predistortion system, in contrast to the open loop system, can overcome the effects of the interferer by either increasing the SNR, increasing the number of receive apertures *or* increasing the number of transmitters.

Figure 6-1 shows average performance in the presence of a basic interferer versus interference power, SIR, for a balanced sparse aperture system with SNR = 2. In the figure, the blue line represents the average BER for a sparse aperture system with wavefront predistortion. The green line represents the average BER for a sparse aperture system without wavefront predistortion. The black dashed line represents the minimum interference power necessary to degrade system performance.

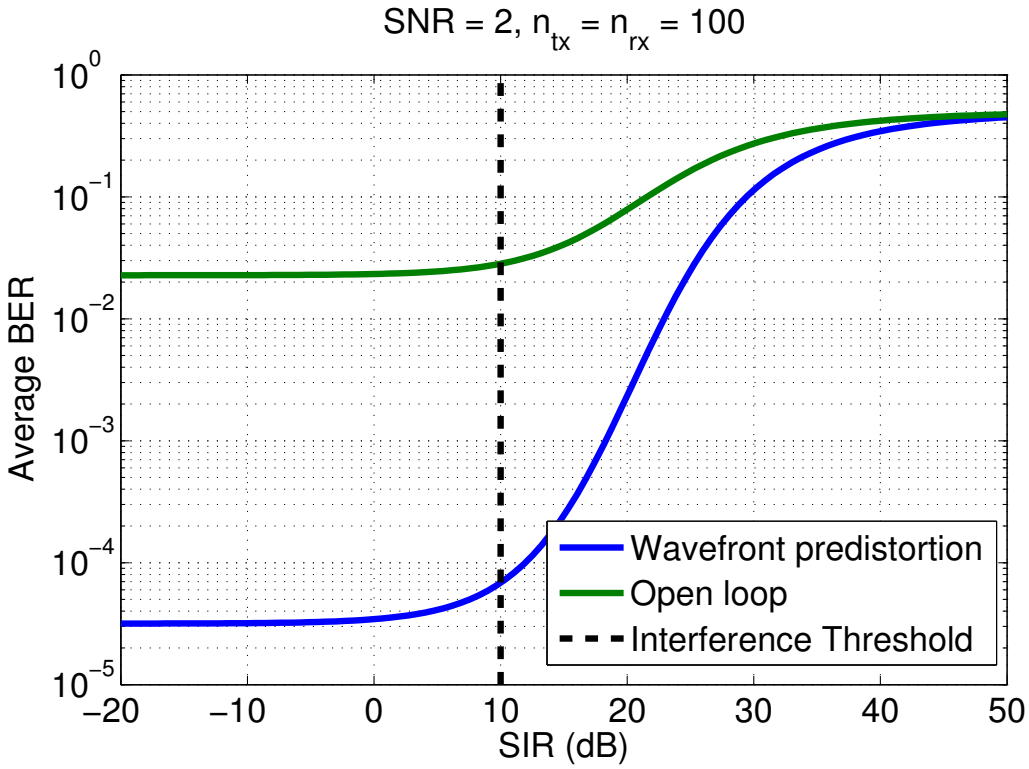

Figure 6-1: Sparse aperture system performance in the presence of a basic interferer: This figure shows average BER versus interference power, SIR, for a balanced sparse aperture system with SNR = 2. In the figure, the blue line represents the average BER for a sparse aperture system with wavefront predistortion. The green line represents the average BER for a sparse aperture system without wavefront predistortion. The black dashed line represents the minimum interference power necessary to degrade system performance.

6.1.2 Advanced interference

In this section we analyze the effects of an advanced interferer: an advanced interferer has knowledge of the power allocation at the receiver arriving from the intended

transmitter and the ability to control the spatial field distribution of the interference at the intended receiver. We first note that, given some interference power allocation, the optimal transmitter allocates all power to the output eigenmode that provides the best performance:

$$E_{\mathsf{i}} = \begin{cases} 1, & \mathsf{i} = \underset{\mathsf{j}}{\text{argmax}} \frac{\gamma_{\mathsf{j}}^2}{1+\text{SIR}I_{\mathsf{j}}} \\ 0, & \text{else} \end{cases} \tag{6.8}$$

The advanced interferer then allocates all power to that same output eigenmode to degrade performance. When the intended receiver detects the degraded channel, the intended transmitter will hop to another eigenmode. As a consequence, the intended transmitter and the interferer both continually hop eigenmodes, with the intended transmitter attempting to minimize BER and the interferer attempting to maximize BER. To find the *steady state* of this eigenmode hopping, we interpret this process in a probabilistic sense by defining $p(E_{\mathsf{i}})$ as the probability that all transmit power is allocated to the i^{th} output eigenmode. For a sparse aperture optical system with wavefront predistortion and eigenmode hopping, transmitting using BPSK, the average worst-case BER is:

$$\mathbb{E}[\Pr(\text{error})] = \mathbb{E}_{\mathbf{H}} \left[\min_{p(E_{\mathsf{i}}):\sum p(E_{\mathsf{i}})=1} \left(\max_{I_{\mathsf{i}}:\sum I_{\mathsf{i}}=1} \sum_{\mathsf{i}=1}^{n_{\min}} p(E_{\mathsf{i}}) Q\left(\sqrt{\frac{2\text{SNR}\gamma_{\mathsf{i}}^2}{1+\text{SIR}I_{\mathsf{i}}}} \right) \right) \right] \tag{6.9}$$

where the expectation $\mathbb{E}_{\mathbf{H}}[\cdot]$ is over the atmospheric turbulence. In this formulation the interferer is able to shape its waveform to couple an arbitrary, but limited, amount of energy into each eigenmode. This formulation implicitly assumes that the transmitter can change its spatial mode much faster than the interferer can measure the transmitter's spatial mode and adapt. This assumption is required for convergence. Thus the optimization can be interpreted as follows. For a given distribution of interference power, I_{i}, the transmitter allocates power to minimize BER. For a given distribution of transmit power $p(E_{\mathsf{i}})$, the interferer allocates power to maximize BER. The solution to the optimization problem in equation (6.9) is presented in Theorem 16.

Theorem 16 *For the problem setup in equation (6.9), the interference power allocation that maximally degrades system performance is:*

$$I_{\mathsf{i}} = \left(\frac{\gamma_{\mathsf{i}}^2}{\mu} - \frac{1}{\mathrm{SIR}} \right)^+ \tag{6.10}$$

where μ is chosen to satisfy the total power constraint:

$$\sum_{\mathsf{i}=1}^{n_{\min}} \left(\frac{\gamma_{\mathsf{i}}^2}{\mu} - \frac{1}{\mathrm{SIR}} \right)^+ = 1 \tag{6.11}$$

The optimal transmitter power allocation is then uniform:

$$\begin{aligned} p(E_{\mathsf{i}}) &= \frac{1}{|\mathcal{S}|}, \ \forall \mathsf{i} \in \mathcal{S} \\ \mathcal{S} &= \left\{ \mathsf{i} \,\middle|\, \mathsf{i} = \underset{\mathsf{j}}{\mathrm{argmax}} \frac{\gamma_{\mathsf{j}}^2}{1 + \mathrm{SIR} I_{\mathsf{j}}} \right\} \end{aligned} \tag{6.12}$$

where $|\mathcal{S}|$ is the cardinality of the set $\mathcal{S}$. The associated BER is then:

$$\mathbb{E}[\Pr(\text{error})] = \mathbb{E}_{\mathbf{H}} \left[Q \left(\sqrt{2\mathrm{SNR} \left(\frac{\sum_{\mathsf{i}=1}^{|\mathcal{S}|} \gamma_{\mathsf{i}}^2}{\mathrm{SIR} + |\mathcal{S}|} \right)} \right) \right] \tag{6.13}$$

Proof. Suppose we are given a transmit power allocation, $p(E_{\mathsf{i}})$. The maximization in equation (6.9) becomes:

$$\mathbb{E}[\Pr(\text{error})] = \mathbb{E}_{\mathbf{H}} \left[\max_{I_{\mathsf{i}}: \sum I_{\mathsf{i}} = 1} \sum_{\mathsf{i}=1}^{n_{\min}} p(E_{\mathsf{i}}) Q \left(\sqrt{\frac{2\mathrm{SNR}\gamma_{\mathsf{i}}^2}{1 + \mathrm{SIR} I_{\mathsf{i}}}} \right) \right] \tag{6.14}$$

The objective function in equation (6.14) is jointly concave in I_{i}. As a result, we solve this problem by the method of Lagrange multipliers. Consider the Lagrangian:

$$\mathcal{L}(\mu, I_1, \ldots, I_{n_{\min}}) = \sum_{\mathsf{i}=1}^{n_{\min}} p(E_{\mathsf{i}}) Q \left(\sqrt{\frac{2\mathrm{SNR}\gamma_{\mathsf{i}}^2}{1 + \mathrm{SIR} I_{\mathsf{i}}}} \right) - \mu \sum_{\mathsf{i}=1}^{n_{\min}} I_{\mathsf{i}} \tag{6.15}$$

where μ is the Lagrange multiplier. The Karush-Kuhn-Tucker (KKT) conditions for the optimal interference power allocation are:

$$\frac{\partial \mathcal{L}}{\partial I_{\mathsf{i}}} \begin{cases} = 0 & \text{if } I_{\mathsf{i}} > 0 \\ \leq 0 & \text{if } I_{\mathsf{i}} = 0 \end{cases} \tag{6.16}$$

The following satisfies the KKT conditions and is therefore the optimal interference power allocation given $p(E_{\mathsf{i}})$:

$$I_{\mathsf{i}} = \left(\frac{P(E_{\mathsf{i}})\gamma_{\mathsf{i}}^2}{\mu} - \frac{1}{\mathrm{SIR}} \right)^+ \tag{6.17}$$

with the Lagrange multiplier as the solution to:

$$\sum_{\mathsf{i}=1}^{n_{\min}} \left(\frac{P(E_{\mathsf{i}})\gamma_{\mathsf{i}}^2}{\mu} - \frac{1}{\mathrm{SIR}} \right)^+ = 1 \tag{6.18}$$

Substituting the optimal interference power into equation (6.9) gives:

$$\mathbb{E}[\Pr(\text{error})] = \ldots$$

$$\mathbb{E}_{\mathbf{H}} \left[\min_{\mu, p(E_{\mathsf{i}}): \sum p(E_{\mathsf{i}})=1, \sum \left(\frac{\gamma_{\mathsf{i}}^2}{\mu} - \frac{1}{\mathrm{SIR}} \right)^+ = 1} \left\{ \sum_{\mathsf{i}=1}^{n_{\min}} p(E_{\mathsf{i}}) Q \left(\sqrt{\frac{2\mathrm{SNR}\gamma_{\mathsf{i}}^2}{1 + \mathrm{SIR}\left(\frac{P(E_{\mathsf{i}})\gamma_{\mathsf{i}}^2}{\mu} - \frac{1}{\mathrm{SIR}} \right)^+}} \right) \right\} \right] \tag{6.19}$$

The objective function is jointly convex in $p(E_{\mathsf{i}})$ and μ. As a result, we solve this problem by the method of Lagrange multipliers. Consider the Lagrangian:

$$\begin{aligned} &\mathcal{L}(\mu, p(E_1), \ldots, p(E_{n_{\min}})) = \ldots \\ &\quad - \sum_{\mathsf{i}=1}^{n_{\min}} p(E_{\mathsf{i}}) Q \left(\sqrt{\frac{2\mathrm{SNR}\gamma_{\mathsf{i}}^2}{1 + \mathrm{SIR}\left(\frac{P(E_{\mathsf{i}})\gamma_{\mathsf{i}}^2}{\mu} - \frac{1}{\mathrm{SIR}} \right)^+}} \right) \\ &\quad - \lambda_1 \sum_{\mathsf{i}=1}^{n_{\min}} p(E_{\mathsf{i}}) - \lambda_2 \sum_{\mathsf{i}=1}^{n_{\min}} \left(\frac{P(E_{\mathsf{i}})\gamma_{\mathsf{i}}^2}{\mu} - \frac{1}{\mathrm{SIR}} \right)^+ \end{aligned} \tag{6.20}$$

where λ_1 and λ_2 are Lagrange multipliers. The Karush-Kuhn-Tucker (KKT) conditions for the optimal power allocation are:

$$\begin{aligned} \frac{\partial \mathcal{L}}{\partial p(E_{\mathsf{i}})} \begin{cases} = 0 & \text{if } p(E_{\mathsf{i}}) > 0 \\ \leq 0 & \text{if } p(E_{\mathsf{i}}) = 0 \end{cases} \\ \frac{\partial \mathcal{L}}{\partial \mu} \begin{cases} = 0 & \text{if } \mu > 0 \\ \leq 0 & \text{if } \mu = 0 \end{cases} \end{aligned} \tag{6.21}$$

The following satisfies the KKT conditions and is therefore the optimal power allocation:

$$\begin{aligned} p(E_{\mathsf{i}}) &= \frac{1}{|\mathcal{S}|}, \ \forall \mathsf{i} \in \mathcal{S} \\ \mathcal{S} &= \left\{ \mathsf{i} \middle| \mathsf{i} = \underset{\mathsf{j}}{\text{argmax}} \frac{\gamma_{\mathsf{j}}^2}{1 + \text{SIR} I_{\mathsf{j}}} \right\} \end{aligned} \tag{6.22}$$

Substituting the optimal power allocation into the expression for optimal interference power allocation proves the theorem. The average BER is then:

$$\mathbb{E}[\Pr(\text{error})] = \mathbb{E}_{\mathbf{H}} \left[\sum_{\mathsf{i}=1}^{n_{\min}} p(E_{\mathsf{i}}) Q \left(\sqrt{\frac{2\text{SNR}\gamma_{\mathsf{i}}^2}{1 + \text{SIR} I_{\mathsf{i}}}} \right) \right] \tag{6.23}$$

Using the optimal transmit and interference power allocation, we have:

$$\begin{aligned} \mathbb{E}[\Pr(\text{error})] &= \mathbb{E}_{\mathbf{H}} \left[Q \left(\sqrt{\frac{2\text{SNR}\gamma_{\mathsf{l}}^2}{\left(1 + \text{SIR}\left(\frac{\gamma_{\mathsf{l}}^2}{\mu} - \frac{1}{\text{SIR}}\right)\right)}} \right) \right] \\ &= \mathbb{E}_{\mathbf{H}} \left[Q \left(\sqrt{\frac{2\text{SNR}\mu}{\text{SIR}}} \right) \right] \end{aligned} \tag{6.24}$$

Substituting the following expression for μ:

$$\mu = \frac{\sum_{\mathsf{i}=1}^{|\mathcal{S}|} \gamma_{\mathsf{i}}^2}{1 + |\mathcal{S}|/\text{SIR}} \tag{6.25}$$

and simplifying proves the average BER portion of the theorem. $\square$

The interference power allocation stated in Theorem 16 is much like water-filling; we plot the values of $1/\gamma_{\mathsf{i}}^2$ versus the square singular value index, i, and imagine the line traced out as a vat which may hold water. Interference power is allocated to eigenmodes such that the water level on the graph (which represents the inverse of the signal-to-interference noise ratio) is SIR/μ. Interference power is first allocated to the eigenmode associated with the largest square singular value. As interference power is increased, it is allocated to weaker and weaker eigenmodes. Thus, as expected, the optimal weak interferer degrades the channel by allocating its total power to the strongest eigenmode. A strong interferer allocates some power to all eigenmodes, effectively creating a channel where all nonzero eigenmodes have equal signal to interference noise ratio. Figure 6-2 shows the effect of a moderate interferer. In the top graph, we show the square singular value distribution (blue histogram) some atmospheric state. The red histogram shows the resulting signal to interference noise ratio after the interferer has optimally selected its interference power allocation according to Theorem 16. We see that the resulting maximum signal to noise interference ratio is constant over many eigenmodes at a level of μ. The optimal transmitter power allocation pdf, shown as the green histogram, is uniform over the eigenmodes with a signal to interference noise ratio of μ/SIR.

The transmit power hops randomly among the eigenmodes with maximum signal to interference noise power $\gamma_{\mathsf{i}}^2/(1+\mathrm{SIR}I_{\mathsf{i}})$. The frequency at which the transmit power hops eigenmodes is governed by the ability of the interferer to measure the transmit waveform. If the interferer can measure the waveform quickly, the transmitter must mode hop faster.

In general, $|\mathcal{S}|$, and consequently average BER, in Theorem 16 must be solved for numerically. By taking the limit, as the number of transmit and receive apertures grow, we can use the Marcenko-Pastur density of square singular values to derive closed form average BER expressions. Next we present the performance of sparse aperture system as the number of apertures grows large for three different interference power regimes, a weak interferer, a moderate interferer, and a strong interferer. These

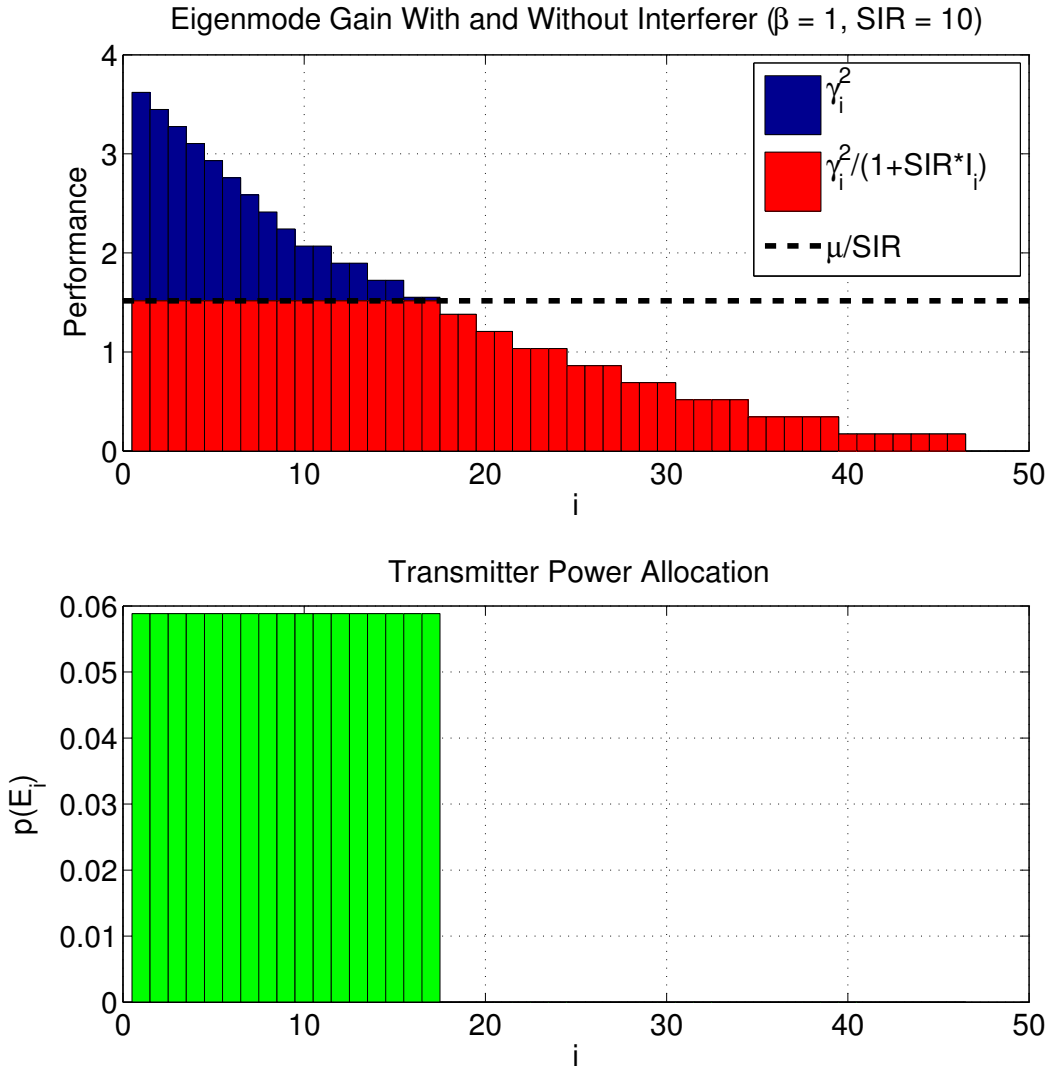

Figure 6-2: Moderate interference: Signal to noise ratio (eigenmode gain without interference) and signal to interference noise (eigenmode gain with interference) ratio versus eigenmode number and optimal transmitter eigenmode hopping pdf.

three regimes cover all possible interference powers. First, we present performance in the presence of a strong interferer.

Theorem 17 *For a sparse aperture system with a large number of apertures, the expected BER in the presence of a strong interferer is:*

$$\lim_{n_{rx},n_{rx}\to\infty} \mathbb{E}[\Pr(\text{error})] = Q\left(\sqrt{2\text{SNR}\left(\frac{\beta n_{min}}{\text{SIR}+n_{min}}\right)}\right) \tag{6.26}$$

Provided the interferer has sufficient total power:

$$\mathrm{SIR} \geq \frac{n_{\min}\left(2\sqrt{\beta}-1\right)}{\left(1-\sqrt{\beta}\right)^2} \tag{6.27}$$

Proof. To prove this theorem, we begin with the optimal interference power allocation given in Theorem 16 and assume the interferer has enough power to interfere with each nonzero eigenmode:

$$\begin{aligned} &\left(\frac{\gamma_{min}^2}{\mu}-\frac{1}{\mathrm{SIR}}\right)=0 \\ &\rightarrow \mu = \mathrm{SIR}(1-\sqrt{\beta})^2 \end{aligned} \tag{6.28}$$

where we have used that the minimum nonzero square singular value is, almost surely, $\left(1-\sqrt{\beta}\right)^2$. Using the power constraint on the optimal interference power allocation, we solve for the condition on interference power for each nonzero eigenmode to be allocated power:

$$\begin{aligned} 1 &= \sum_{\mathsf{i}=1}^{n_{\min}}\left(\frac{\gamma_{\mathsf{i}}^2}{\mu}-\frac{1}{\mathrm{SIR}}\right) \\ &= \frac{\sum_{\mathsf{i}=1}^{n_{\min}}\gamma_{\mathsf{i}}^2}{\mathrm{SIR}(1-\sqrt{\beta})^2}-\frac{n_{\min}}{\mathrm{SIR}} \\ &\rightarrow \mathrm{SIR} \geq \frac{n_{\min}\left(2\sqrt{\beta}-1\right)}{\left(1-\sqrt{\beta}\right)^2} \end{aligned} \tag{6.29}$$

where we have used, for a large number of apertures, that the number of nonzero square singular values converges, almost surely, to $n_{\min}$ and that the average square singular value converges, almost surely, to β. The average BER is then:

$$\begin{aligned} \lim_{n_{rx},n_{rx}\rightarrow\infty}\mathbb{E}[\Pr(\text{error})] &= \mathbb{E}_{\mathbf{H}}\left[Q\left(\sqrt{2\mathrm{SNR}\left(\frac{\sum_{\mathsf{i}=1}^{|\mathcal{S}|}\gamma_{\mathsf{i}}^2}{\mathrm{SIR}+|\mathcal{S}|}\right)}\right)\right] \\ &= \mathbb{E}_{\mathbf{H}}\left[Q\left(\sqrt{2\mathrm{SNR}\left(\frac{\sum_{\mathsf{i}=1}^{n_{\min}}\gamma_{\mathsf{i}}^2}{\mathrm{SIR}+n_{\min}}\right)}\right)\right] \\ &= \mathbb{E}_{\mathbf{H}}\left[Q\left(\sqrt{2\mathrm{SNR}\left(\frac{n_{\min}\beta}{\mathrm{SIR}+n_{\min}}\right)}\right)\right] \end{aligned} \tag{6.30}$$

Thus, we have proven the theorem. $\square$

This result is intuitively satisfying. As the number of system apertures is increased, the interferer must spread its power among more spatial modes thus reducing its impact. Indeed, as the number of apertures becomes large the interferer is completely rejected. Physically, the condition on the interference power guarantees that some interference power is allocated to each nonzero eigenmode. Put into water-filling terms, the interferer has enough water to completely fill the vat.

Figure 6-3 shows the SNR, signal to interference noise ratio, and transmitter power allocation pdf for the case of a strong interferer. In this case, the interferer has enough power to effectively interfere with all nonzero eigenmodes. As a result, the transmitter allocates power equally to all eigenmodes. Next we give the performance for weak interference.

Theorem 18 *For a sparse aperture system with a large number of apertures, the expected BER in the presence of a weak interferer is:*

$$\lim_{n_{rx},n_{rx}\to\infty} \mathbb{E}[\Pr(\text{error})] = Q\left(\sqrt{2\text{SNR}\left(\frac{(1+\sqrt{\beta})^2}{1+\text{SIR}}\right)}\right) \tag{6.31}$$

Provided the interferer's total power is small:

$$\text{SIR} \ll 1 \tag{6.32}$$

Proof. From Theorem 16 the average BER is:

$$\begin{aligned}
\lim_{n_{rx},n_{rx}\to\infty} \mathbb{E}[\Pr(\text{error})] &= \mathbb{E}_{\mathbf{H}}\left[Q\left(\sqrt{2\text{SNR}\left(\frac{\sum_{i=1}^{|\mathcal{S}|}\gamma_i^2}{\text{SIR}+|\mathcal{S}|}\right)}\right)\right] \\
&= \mathbb{E}_{\mathbf{H}}\left[Q\left(\sqrt{2\text{SNR}\left(\frac{\gamma_{\mathsf{max}}^2}{\text{SIR}+1}\right)}\right)\right] \\
&= \mathbb{E}_{\mathbf{H}}\left[Q\left(\sqrt{2\text{SNR}\left(\frac{(1+\sqrt{\beta})^2}{\text{SIR}+1}\right)}\right)\right]
\end{aligned} \tag{6.33}$$

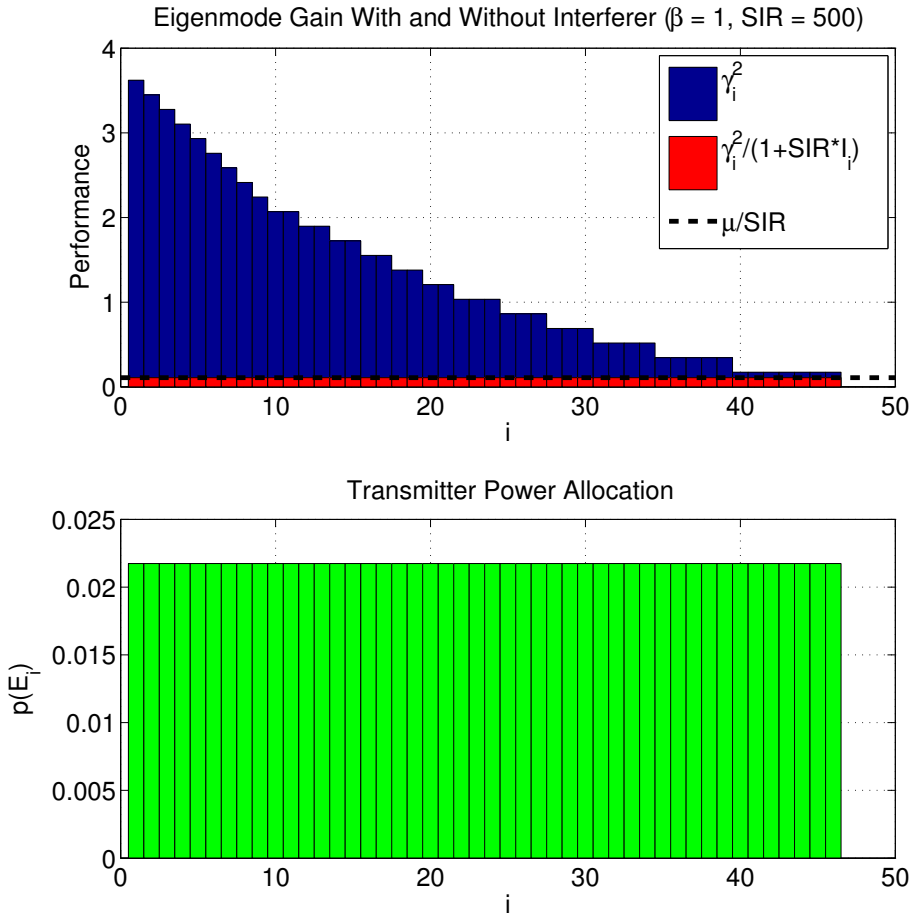

Figure 6-3: Strong interference: Signal to noise ratio (eigenmode gain without interference) and signal to interference noise (eigenmode gain with interference) ratio versus eigenmode number and optimal transmitter eigenmode hopping pdf.

Where we have used that, for weak interference, the only eigenmode that is allocated power is the one associated with the largest square singular value. □

Figure 6-4 shows the system performance in the presence of a weak interferer. As expected, the interferer and transmitter allocate power to only the strongest eigenmode. For a weak advanced interferer, eigenmode hopping is not necessary. Next we give the performance for moderate interference.

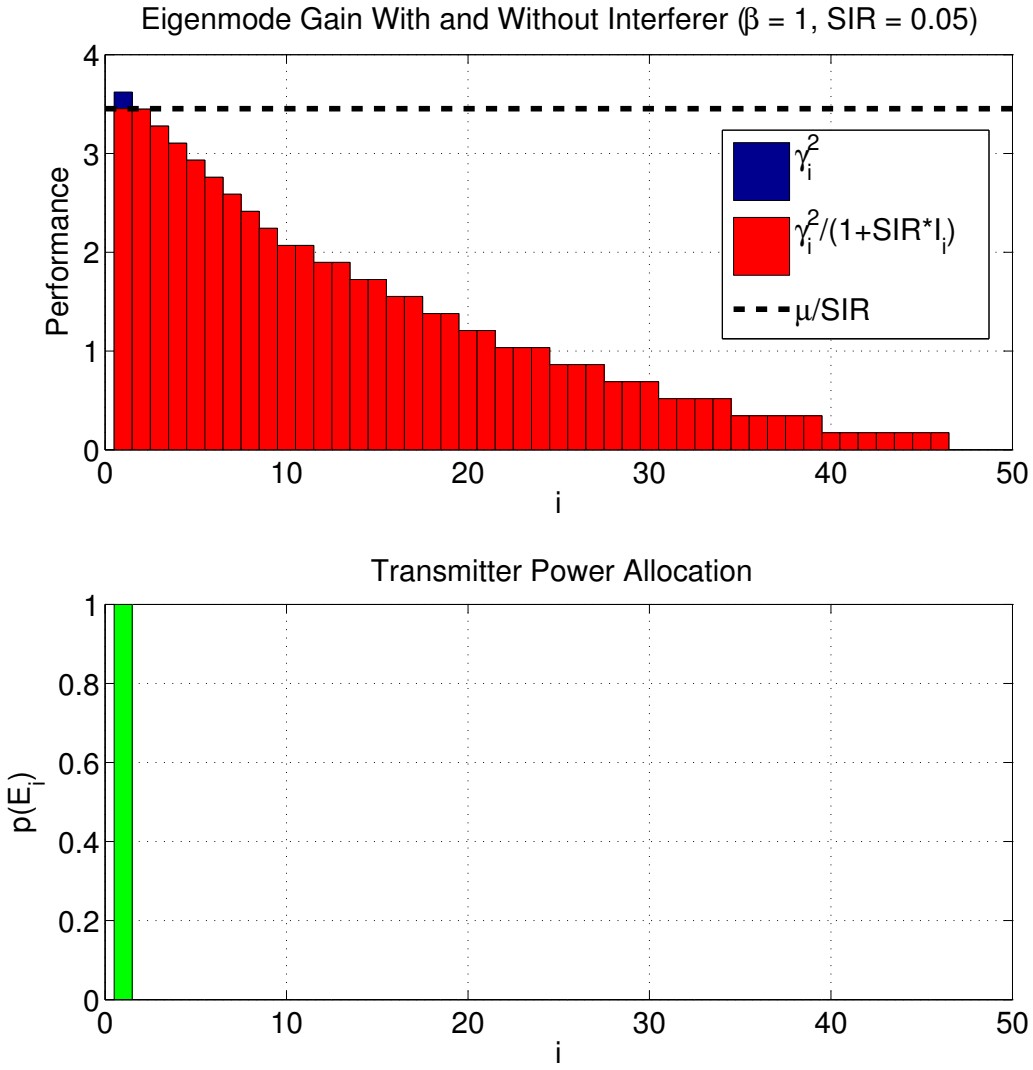

Figure 6-4: Weak interference: Signal to noise ratio (eigenmode gain without interference) and signal to interference noise (eigenmode gain with interference) ratio versus eigenmode number and optimal transmitter eigenmode hopping pdf.

Theorem 19 *For a sparse aperture system with a large number of apertures, the expected BER in the presence of a moderate interferer is:*

$$\lim_{n_{rx},n_{rx}\to\infty} \mathbb{E}[\Pr(\text{error})] = \mathbb{E}_{\mathbf{H}}\left[Q\left(\sqrt{2\text{SNR}\gamma_{\text{eff}}^2}\right)\right] \tag{6.34}$$

where γ_{eff}^2 *is:*

$$\begin{aligned}\gamma_{\text{eff}}^2 = \arg\max_{x^*} \Bigg\{ \text{SIR} &= \frac{\sqrt{(a-x^*)(x^*-b)}(a+b+2x^*)}{8\pi x^*} \\ &- \frac{\left(a^2 - 2(b-2x^*+16)a + 64\sqrt{a} + b^2 + 4bx^* - 8\left(\sqrt{ab}x^* + 4\right)\right)}{32x^*} \\ &+ \frac{((a-b)^2 - 4(a+b)x^*)}{16\pi x^*} \tan^{-1}\left(\frac{a+b-2x^*}{2\sqrt{(a-x^*)(x^*-b)}}\right) \\ &+ \frac{\sqrt{ab}}{2\pi} \tan^{-1}\left(\frac{2ab-(a+b)x^*}{2\sqrt{ab(a-x^*)(x^*-b)}}\right)\Bigg\}\end{aligned} \tag{6.35}$$

where, as before, $a = \left(1-\sqrt{\beta}\right)^2$*, is the minimum square singular value and* $b = \left(1+\sqrt{\beta}\right)^2$ *is the maximum square singular value. Moderate interference power is defined as:*

$$1 < \text{SIR} < \frac{n_{\min}\left(2\sqrt{\beta}-1\right)}{\left(1-\sqrt{\beta}\right)^2} \tag{6.36}$$

Proof. As the number of apertures grows the spacing between square singular values becomes smaller until, in the limit, the square singular values form a continuous distribution. For infinitely many transmit and receive apertures, the optimal interference power allocation given in Theorem 16 becomes:

$$I(\gamma^2) = \left(\frac{\gamma^2}{\mu} - \frac{1}{\text{SIR}}\right)^+ \tag{6.37}$$

with the associated constraint on interference power:

$$\begin{aligned}1 &= \int_0^\infty \left(\frac{\gamma^2}{\mu} - \frac{1}{\text{SIR}}\right)^+ \frac{\sqrt{(\gamma^2-a)^+(b-\gamma^2)^+}}{2\pi\gamma^2} d\gamma^2 \\ &= \frac{1}{\text{SIR}} \int_{x^*}^b \left(\frac{\gamma^2}{x^*} - 1\right)^+ \frac{\sqrt{(\gamma^2-a)^+(b-\gamma^2)^+}}{2\pi\gamma^2} d\gamma^2\end{aligned} \tag{6.38}$$

where x^* is the value of the minimum square singular value that is allocated interference power:

$$\frac{x^*}{\mu} - \frac{1}{\text{SIR}} = 0 \tag{6.39}$$

Evaluating the integral in the last expression in equation (6.38) gives the expression for γ^2_{eff} in the theorem. Finally, we prove the theorem by noting that the largest signal to interference noise power is given by the value of x^* that solves equation (6.38). $\square$

The equation for γ^2_{eff} in equation (6.35) is highly nonlinear and cannot be solved in closed form. Fortunately, the function is monotonically decreasing in x^* and can be efficiently solved with numerical methods.

Finally, we provide the average performance of a sparse aperture system without wavefront predistortion (open loop system) in the presence of an advanced interferer:

$$\mathbb{E}[\Pr(\text{error})] = Q\left(\sqrt{\frac{2\text{SNR}}{1+\text{SIR}}}\right) \tag{6.40}$$

where we have used that the average square singular value is one and that an advanced interferer can couple all power into the information bearing spatial mode. For an open loop sparse aperture system experiencing an advanced interferer, increasing the number of apertures does not improve interference mitigation.

Figure 6-5 shows average performance in the presence of an advanced interferer versus interference power SIR for a balanced sparse aperture system with SNR = 2. In the figure, the red line represents the average BER for a sparse aperture system with wavefront predistortion. The cyan line represents the average BER for a sparse aperture system without wavefront predistortion. For comparison, the dashed lines show average performance in the presence of a basic interferer for sparse aperture system with and without wavefront predistortion.

6.1.3 Interference margin

To compare the effects of the basic and advanced interferer on sparse aperture systems with and without wavefront predistortion, we define *interference margin* as the additional power required to have the same performance as a wavefront predistortion system without interference. The interference margin for a sparse aperture system

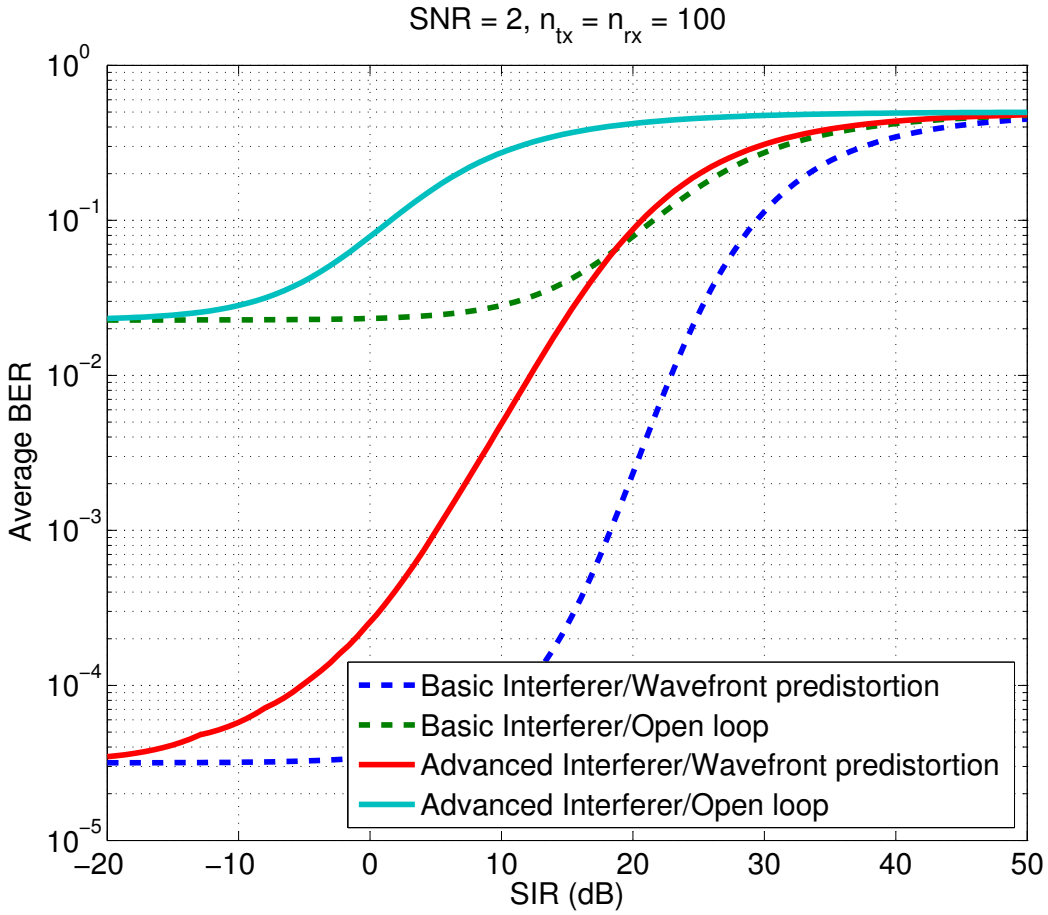

Figure 6-5: Sparse aperture system performance in the presence of a basic and advanced interferer: This figure shows average performance in the presence of an advanced interferer versus interference power SIR for a balanced sparse aperture system with SNR = 2. In the figure, the red line represents the average BER for a sparse aperture system with wavefront predistortion. The cyan line represents the average BER for a sparse aperture system without wavefront predistortion. For comparison, the dashed lines show average performance in the presence of a basic interferer for sparse aperture system with and without wavefront predistortion.

with predistortion in the presence of a basic interferer is:

$$\begin{aligned} m &= \arg\min_{m} \left\{ Q\left(\sqrt{\frac{2m\mathrm{SNR}(1+\sqrt{\beta})^2}{1+\mathrm{SIR}/n_{rx}}} \right) = Q\left(\sqrt{2\mathrm{SNR}(1+\sqrt{\beta})^2} \right) \right\} \\ &= 1 + \frac{\mathrm{SIR}}{n_{rx}} \end{aligned} \tag{6.41}$$

where we have used the average performance of a sparse aperture system with predistortion in the presence of a basic interferer given in equation (6.6). The interference margin for a sparse aperture system without predistortion in the presence of a basic interferer is:

$$\begin{aligned} m &= \arg\limits_{m} \left\{ Q\left(\sqrt{\frac{2m\text{SNR}}{1+\text{SIR}/n_{rx}}} \right) = Q\left(\sqrt{2\text{SNR}(1+\sqrt{\beta})^2} \right) \right\} \\ &= \left(1+\sqrt{\beta}\right)^2 \left(1+\frac{\text{SIR}}{n_{rx}}\right) \end{aligned} \tag{6.42}$$

where we have used the average performance of a sparse aperture system without predistortion in the presence of a basic interferer given in equation (6.7). The interference margin for a sparse aperture system with predistortion in the presence of an advanced interferer is:

$$\begin{aligned} m &= \arg\limits_{m} \left\{ Q\left(\sqrt{2m\text{SNR}\left(\frac{\sum_{\mathsf{i}=1}^{|\mathcal{S}|}\gamma_{\mathsf{i}}^2}{\text{SIR}+|\mathcal{S}|}\right)} \right) = Q\left(\sqrt{2\text{SNR}(1+\sqrt{\beta})^2} \right) \right\} \\ &= \left(1+\sqrt{\beta}\right)^2 \left(\frac{\text{SIR}+|\mathcal{S}|}{\sum_{\mathsf{i}=1}^{|\mathcal{S}|}\gamma_{\mathsf{i}}^2}\right) \end{aligned} \tag{6.43}$$

where $\mathcal{S}$ is defined in Theorem 16. We have used the average performance of a sparse aperture system with predistortion in the presence of an advanced interferer given in Theorem 16. The interference margin for a sparse aperture system without predistortion in the presence of an advanced interferer is:

$$\begin{aligned} m &= \arg\limits_{m} \left\{ Q\left(\sqrt{\frac{2m\text{SNR}}{1+\text{SIR}}} \right) = Q\left(\sqrt{2\text{SNR}(1+\sqrt{\beta})^2} \right) \right\} \\ &= \left(1+\sqrt{\beta}\right)^2 (1+\text{SIR}) \end{aligned} \tag{6.44}$$

where I_{i} is defined in Theorem 16. We have used the average performance of a sparse aperture system without predistortion in the presence of an advanced interferer given in equation (6.40).

Figure 6-6 shows the interference margin versus SIR for sparse aperture systems with SNR = 2 and $n_{tx} = n_{rx} = 100$. The dashed lines represent systems that are experiencing a basic interferer while the solid lines represent systems that are experiencing an advanced interferer. At low SIR, the interference margin is the same for basic and advanced interferers. As the SIR increases, compensating for the advanced interferer requires more power than compensating for the basic interferer. At high SIR, eigenmode hopping provides more than 18 dB of gain relative to an open loop system when being degraded by an advanced interferer. This is because, when eigenmode hopping is used, an advanced interferer must degrade every nonzero eigenmode. In contrast, an interferer must only degrade a single eigenmode when an open loop system is used.

6.2 Eavesdropper

An eavesdropper is any user that attempts to receive and decode the information intended for another user. Khisti and Wornell have performed parallel work on the impact of eavesdroppers for radio frequency systems with multiple antennas [24, 25]. Confidentiality is the ability of the intended receiver to decode source information while ensuring that unintended users are unable to decode source information. Conventional techniques to ensure confidentiality are based on encryption: a transmitter and receiver use a key to encrypt and decrypt source information [34]. Any user with a key can decode source information while any user without a key will be unable to decode source information. The confidentiality is achieved by distributing keys to intended users while ensuring unintended users do not have a key. Traditional key encryption is difficult for free space optical systems because of the lack of a way to pass keys to potential users (especially if the intended users are change rapidly) and the complexity associated with key distribution for a dynamic topology of users. Therefore, we take an information theoretic approach (without the use of encryption keys) to free space optical confidentiality. This approach exploits the inherent randomness of the atmospheric turbulence to ensure confidentiality. As a result, we

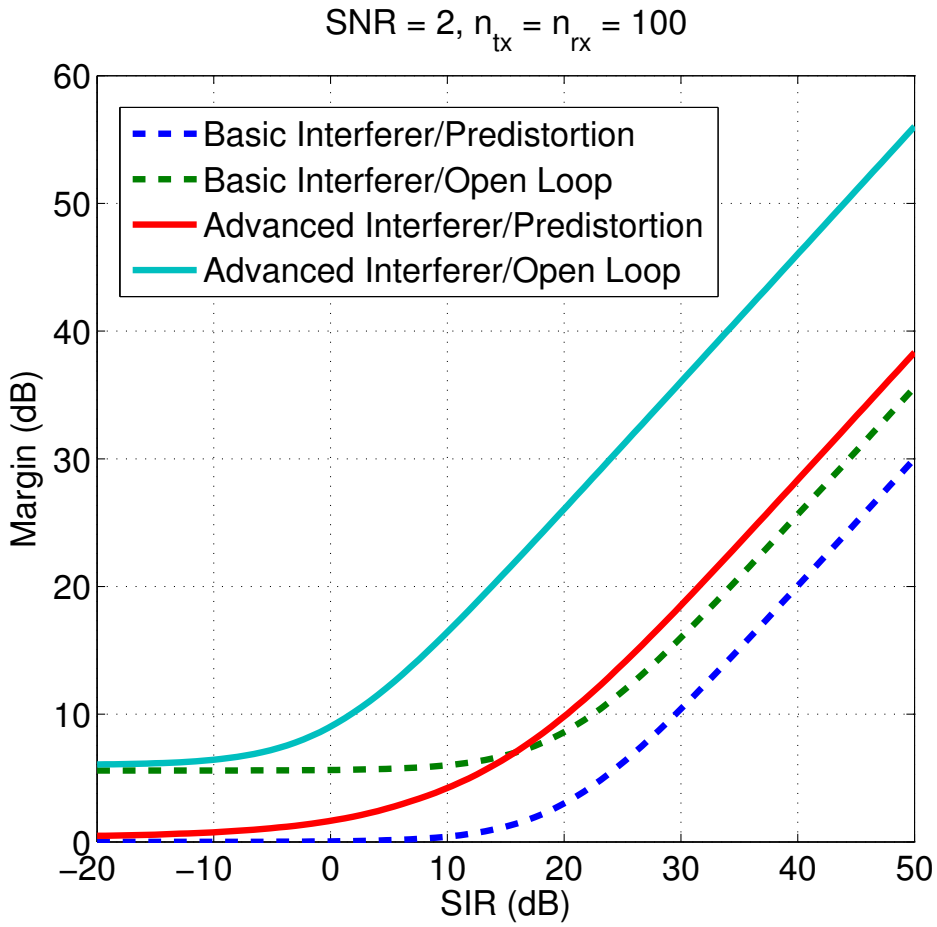

Figure 6-6: Interference margin versus interference power (SIR): The dashed lines represent systems that are experiencing a basic interferer while the solid lines represent systems that are experiencing an advanced interferer.

provide provable security that is robust to eavesdroppers within the main optical beam with unlimited computational resources and knowledge of the communication strategy employed including coding and decoding algorithms [31]. In the section, we address the use of spatial diversity and turbulence to prevent an eavesdropper from intercepting information. We model the eavesdropper as follows:

$$\begin{aligned} \vec{y} &= \sqrt{\frac{\mathrm{SNR}}{n_{rx}}}\mathbf{H}\vec{x} + \vec{w} \\ \vec{y}^{\,E} &= \sqrt{\frac{\mathrm{SER}}{n_{rx}^{E}}}\mathbf{H}^{E}\vec{x} + \vec{w}^{E} \end{aligned} \tag{6.45}$$

where $\vec{y}^{\,E}$ is the field amplitude and phase received by the eavesdropper, SER is the eavesdropper's signal to noise ratio, $\mathbf{H}^E$ is the turbulence channel transfer between the intended transmitter and the eavesdropper, n_{rx}^E is the number of eavesdropper receive apertures, and $\vec{w}^E$ is white noise at the eavesdropper's receiver. If the eavesdropper does not use a sparse aperture system, each element of $\vec{y}^{\,E}$ represents the discrete version of eavesdroppers continuous aperture. We cannot ensure that the eavesdropper will receive zero power from the transmitter, but we can ensure that with proper coding the eavesdropper will not be able to decode any information. Thus, we define *secrecy capacity* as the maximum data transfer rate achievable while ensuring perfect confidentiality. We upper bound and lower bound the amount of information that can be sent to the intended receiver, while ensuring zero information can be intercepted by the eavesdropper, by providing the secrecy capacity for the case where the transmitter has no knowledge of the eavesdropper (lower bound) and the case where the transmitter has perfect knowledge of the eavesdropper (upper bound). We first provide the upper bound.

Theorem 20 *The secrecy capacity rate, the largest rate achievable with perfect confidentiality, when the transmitter has perfect knowledge of the eavesdropper is:*

$$C_s \geq \left(\frac{1}{2}\log\left(1+\gamma_{\max}^2\left(\mathbf{H}\mathbf{K}^E\right)\mathrm{SNR}\right)-\frac{1}{2}\log\left(1+\epsilon\mathrm{SER}\right)\right)^+ \tag{6.46}$$

where $\mathbf{K}^E$ *is the* ϵ*-kernel of* $\mathbf{H}^E$*. The* ϵ*-kernel of* $\mathbf{H}^E$ *is defined in the proof.*

Proof. To prove this theorem, first define the singular value decomposition for the eavesdropper channel:

$$\frac{1}{\sqrt{n_{rx}^E}}\mathbf{H}^E = \mathbf{U}^{\mathbf{E}}\mathbf{\Gamma}^{\mathbf{E}}(\mathbf{V}^{\mathbf{E}})^\dagger \tag{6.47}$$

where the i^{th} column of $\mathbf{U}^E$ is an output eigenmode, the i^{th} row of $\mathbf{V}^E$ is an input eigenmode, and the $(\mathsf{i},\mathsf{i})^{th}$ entry of the diagonal matrix Γ^E is the singular value, or diffraction gain, associated with the i^{th} input/output eigenmode. We define $\vec{v}_{\mathsf{i}}^{\,E}$ to be column i of matrix $\mathbf{V}^E$, $\vec{u}_{\mathsf{i}}^{\,E}$ to be column i of matrix $\mathbf{U}^E$, and γ_{i}^E to be diagonal element (i,i) of matrix $\mathbf{\Gamma}^E$. Using the SVD to transform $\vec{y}^E = \sqrt{\frac{\mathrm{SER}}{n_{rx}^E}}\vec{x} + \vec{w}^E$ into

parallel Gaussian channels, we arrive at:

$$\begin{aligned}
\tilde{y}_1^E &= \sqrt{\text{SER}}\gamma_1^E \tilde{x}_1^E + \tilde{w}_1^E \\
\tilde{y}_2^E &= \sqrt{\text{SER}}\gamma_2^E \tilde{x}_2^E + \tilde{w}_2^E \\
\vdots \quad & \quad \vdots \quad \quad \vdots \\
\tilde{y}_{n_{\min}^E}^E &= \sqrt{\text{SER}}\gamma_{n_{\min}}^E \tilde{x}_{n_{\min}}^E + \tilde{w}_{n_{\min}}^E
\end{aligned} \tag{6.48}$$

where $n_{\min^E} = \min(n_{tx}, n_{rx}^E)$. The vectors $\tilde{\vec{x}}^E$, $\tilde{\vec{y}}^E$, and $\tilde{\vec{w}}^E$ are related to the vectors $\vec{x}^E$, $\vec{y}^E$, and $\vec{w}^E$ through the usual SVD, such as in [48]. Note $\tilde{w}_{\mathsf{i}}^E$ retains its circularly symmetric complex Gaussian distribution. We form an ϵ-kernel (or nullspace) to the eavesdropper channel transfer matrix by selecting only input eigenmodes that are associated with small singular values:

$$\mathbf{K}^E = \begin{bmatrix} | & | & & | \\ \vec{v}_{\mathsf{i}^*}^E & \vec{v}_{\mathsf{i}^*+1}^E & \cdots & \vec{v}_{n_{tx}}^E \\ | & | & & | \end{bmatrix} \tag{6.49}$$

where i^* is given by:

$$\mathsf{i}^* = \min_{\text{s.t.:}\left(\gamma_{\mathsf{i}}^E\right)^2 < \epsilon} \mathsf{i} \tag{6.50}$$

We restrict the transmit vector to be within the nullspace of the eavesdropper:

$$\vec{x} = \frac{\mathbf{K}^E \vec{a}}{\|\mathbf{K}^E \vec{a}\|} \tag{6.51}$$

where $\vec{a} \in \mathbb{C}^{n_{tx} - \mathsf{i}^*}$ is now the information bearing signal. Thus, we transform the system:

$$\begin{aligned}
\vec{y} &= \sqrt{\frac{\text{SNR}}{n_{rx}}}\mathbf{H}\frac{\mathbf{K}^E \vec{a}}{\|\mathbf{K}^E \vec{a}\|} + \vec{w} \\
\vec{y}^{\,E} &= \sqrt{\frac{\text{SER}}{n_{rx}^E}}\mathbf{H}^E\frac{\mathbf{K}^E \vec{a}}{\|\mathbf{K}^E \vec{a}\|} + \vec{w}^E
\end{aligned} \tag{6.52}$$

The spatial field distribution that minimizes instantaneous BER is given by:

$$\vec{a} = b\vec{v}_{\max}\left(\mathbf{HK}^{E}\right) \tag{6.53}$$

where we have used that $\vec{v}_{\max}\left(\mathbf{HK}^{E}\right)$ is the input eigenvector of $\mathbf{HK}^{E}$ associated with the maximum square singular value $\gamma^2_{\max}$ of $\mathbf{HK}^{E}$. Data is encoded by variation of $b \in \mathbb{C}$, which is spatially constant at a particular time. A sufficient statistic for optimum detection is:

$$\phi = Re\left\{\vec{u}^{\,\dagger}_{\max}\left(\mathbf{HK}^{E}\right)\vec{y}\right\} \tag{6.54}$$

where ϕ is the sufficient statistic. The associated received power is normally distributed:

$$|\phi|^2 \sim \mathcal{N}\left(\mathrm{SNR}\gamma^2_{\max}\left(\mathbf{HK}^{E}\right), 1\right) \tag{6.55}$$

A sufficient statistic for eavesdropper optimum detection is:

$$\phi^{E} = Re\left\{\left(\vec{u}^{E}_{\max}\right)^{\dagger}\vec{y}^{E}\right\} \tag{6.56}$$

where ϕ^E is the sufficient statistic for the eavesdropper. The associated eavesdropper received power is normally distributed:

$$|\phi^{E}|^2 \sim \mathcal{N}\left(\mathrm{SER}\sum_{\mathsf{i}=\mathsf{i}^*}^{n_{tx}} a_{\mathsf{i}}(\gamma^{E}_{\mathsf{i}})^2, 1\right) \tag{6.57}$$

This is then a Gaussian wire-tap channel, in which the outputs at the intended receiver and at the eavesdropper are corrupted by additive white Gaussian noise. Using the secrecy capacity from [30], we arrive at:

$$C_s = \left(\frac{1}{2}\log\left(1+\gamma^2_{\max}\left(\mathbf{HK}^{E}\right)\mathrm{SNR}\right) - \frac{1}{2}\log\left(1+\mathrm{SER}\sum_{\mathsf{i}=\mathsf{i}^*}^{n_{tx}} a_{\mathsf{i}}(\gamma^{E}_{\mathsf{i}})^2\right)\right)^{+} \tag{6.58}$$

We can bound the secrecy capacity by noting that $\epsilon \geq \sum_{\mathsf{i}=\mathsf{i}^*}^{n_{tx}} a_{\mathsf{i}}(\gamma_{\mathsf{i}}^E)^2$ for any choice of $\vec{a}$. Thus, a lower bound on the secrecy capacity is:

$$C_s \geq \left(\frac{1}{2}\log\left(1+\gamma_{\max}^2\left(\mathbf{H}\mathbf{K}^E\right)\mathrm{SNR}\right)-\frac{1}{2}\log\left(1+\epsilon\mathrm{SER}\right)\right)^+ \tag{6.59}$$

□

This theorem suggests the following intuition. The system begins with n_{tx} degrees of freedom to control the wavefront. It uses i^* degrees of freedom to null out the receiver and has $n_{tx}-\mathsf{i}^*$ degrees of freedom to provide wavefront predistortion gain.

For a particular atmospheric realization, ϵ should be chosen to maximize the secrecy capacity. Decreasing ϵ decreases the power at the eavesdropper's receiver at the expense of reducing the degrees of freedom for information to be communicated to the intended receiver. Conversely, increasing ϵ increases the power at the eavesdropper's receiver while increasing the degrees of freedom for information to be communicated to the intended receiver. As a result, secrecy capacity is convex in ϵ. As the number of transmit apertures, intended receiver receive apertures, and eavesdropper receive apertures grow, we use the asymptotic square singular value distribution to derive a closed form expression for secrecy capacity.

Corollary 9 *As the number of transmit apertures, intended receiver receive apertures, and eavesdropper receive apertures grow, the secrecy capacity is:*

$$\begin{aligned} C_s &= \left(\frac{1}{2}\log\left(1+\mathrm{SNR}\left(1+\sqrt{\beta F_{\mathbf{H}^E}(\epsilon)}\right)^2\right)-\frac{1}{2}\log\left(1+(\overline{\gamma^2}(\epsilon))\mathrm{SER}\right)\right)^+ \\ &\geq \left(\frac{1}{2}\log\left(1+\mathrm{SNR}\left(1+\sqrt{\beta F_{\mathbf{H}^E}(\epsilon)}\right)^2\right)-\frac{1}{2}\log\left(1+\epsilon\mathrm{SER}\right)\right)^+ \end{aligned} \tag{6.60}$$

where $\overline{\gamma^2}(\epsilon)$ *is the average square singular value of* $\mathbf{H}^E$ *up to* ϵ*:*

$$\overline{\gamma^2}(\epsilon) = \frac{\left(a^E - b^E\right)^2}{32\beta} - \frac{(a^E - b^E)^2 \tan^{-1}\left(\frac{a^E+b^E-2\epsilon}{2\sqrt{(b^E-\epsilon)(\epsilon-a^E)}}\right)}{16\pi\beta} - \frac{\sqrt{(a^E-\epsilon)(\epsilon-b^E)}a^E b^E\sqrt{(a^E-\epsilon)(\epsilon-b^E)} - 2\epsilon\sqrt{(a^E-\epsilon)(\epsilon-b^E)}}{16\pi\beta} \tag{6.61}$$

and $F_{\mathbf{H}^E}(\cdot)$ *is the square singular value distribution of* $\mathbf{H}^E$*:*

$$F_{\mathbf{H}^E}(\epsilon) = 1 - \frac{a^E + b^E - 2\sqrt{a^E b^E}}{8} - \frac{(a^E + b^E)\tan^{-1}\left(\frac{a^E+b^E-2\epsilon}{2\sqrt{(b^E-\epsilon)(\epsilon-a^E)}}\right)}{4\pi} - \frac{\sqrt{a^E b^E}\tan^{-1}\left(\frac{-2a^E b^E+\epsilon b^E+a^E\epsilon}{2\sqrt{a^E b^E(b^E-\epsilon)(\epsilon-a^E)}}\right)}{2\pi} + \frac{\sqrt{(a^E-\epsilon)(\epsilon-b^E)}}{2\pi} \tag{6.62}$$

where $a^E = \left(1+\sqrt{\frac{n_{tx}}{n_{rx}^E}}\right)^2$ *and* $b^E = \left(1-\sqrt{\frac{n_{tx}}{n_{rx}^E}}\right)^2$*. The expressions in equation (6.60) are only satisfied for eavesdroppers using a sparse aperture receiver.*

Proof. From Theorem 20, the secrecy capacity is given by:

$$C_s = \left(\frac{1}{2}\log\left(1+\gamma_{\max}^2\left(\mathbf{H}\mathbf{K}^E\right)\mathrm{SNR}\right) - \frac{1}{2}\log\left(1+\mathrm{SER}\sum_{\mathsf{i}=\mathsf{i}^*}^{n_{tx}} a_{\mathsf{i}}(\gamma_{\mathsf{i}}^E)^2\right)\right)^+ \tag{6.63}$$

As the number of apertures grows, and the spacing between square singular values becomes infinitesimally small, the capacity becomes:

$$C_s = \left(\frac{1}{2}\log\left(1+\gamma_{\max}^2\left(\mathbf{H}\mathbf{K}^E\right)\mathrm{SNR}\right) - \frac{1}{2}\log\left(1+\mathrm{SER}\int_0^{\epsilon}(\gamma^E)^2 f_{(\gamma^E)^2}((\gamma^E)^2)d(\gamma^E)^2\right)\right)^+ \tag{6.64}$$

where $f_{(\gamma^E)^2}(\cdot)$ is the distribution of square singular values of $\mathbf{H}^E$, which is given by:

$$f_{(\gamma^E)^2}(x) = \left(1-\beta^E\right)^+\delta(x) + \frac{\sqrt{\left(x-\left(1-\sqrt{\beta^E}\right)^2\right)^+\left(\left(1+\sqrt{\beta^E}\right)^2 - x\right)^+}}{2\pi x} \tag{6.65}$$

where $\beta^E = n_{tx}/n_{rx}^E$. Thus the average square singular value of $\mathbf{H}^E$ up to ϵ is:

$$\begin{aligned}
\overline{\gamma^2}(\epsilon) &= \int_0^{\epsilon} (\gamma^E)^2 f_{(\gamma^E)^2}((\gamma^E)^2) d(\gamma^E)^2 \\
&= \int_{a^E}^{\epsilon} \frac{\sqrt{\left(x - \left(1-\sqrt{\beta^E}\right)^2\right)^+ \left(\left(1+\sqrt{\beta^E}\right)^2 - x\right)^+}}{2\pi} dx \\
&= \frac{\left(a^E - b^E\right)^2}{32\beta} - \frac{(a^E - b^E)^2 \tan^{-1}\left(\frac{a^E+b^E-2\epsilon}{2\sqrt{(b^E-\epsilon)(\epsilon-a^E)}}\right)}{16\pi\beta} \\
&\quad - \frac{\sqrt{(a^E-\epsilon)(\epsilon-b^E)} a^E b^E \sqrt{(a^E-\epsilon)(\epsilon-b^E)} - 2\epsilon\sqrt{(a^E-\epsilon)(\epsilon-b^E)}}{16\pi\beta}
\end{aligned} \tag{6.66}$$

The term $\gamma^2_{\max}\left(\mathbf{HK}^E\right)$ is related to the degrees of freedom of the transformed system:

$$\gamma^2_{\max}\left(\mathbf{HK}^E\right) = \left(1 + \sqrt{\frac{d}{n_{rx}}}\right)^2 \tag{6.67}$$

where d is the number of degrees of freedom at the transmitter after the eavesdropper's power can be constrained to be less than ϵ. For the finite system, $d = n_{tx} - \mathsf{i}^*$. Asymptotically, $d = n_{tx} F_{\mathbf{H}^E}(\epsilon)$ we have:

$$\gamma^2_{\max}\left(\mathbf{HK}^E\right) = \left(1 + \sqrt{\beta F_{\mathbf{H}^E}(\epsilon)}\right)^2 \tag{6.68}$$

where $F_{\mathbf{H}^E}(\epsilon)$ are the degrees of freedom not being used to ϵ-null the eavesdropper, given by:

$$\begin{aligned}
F_{\mathbf{H}^E}(\epsilon) &= \int_{a^E}^{\epsilon} \frac{\sqrt{\left(x - \left(1-\sqrt{\beta^E}\right)^2\right)^+ \left(\left(1+\sqrt{\beta^E}\right)^2 - x\right)^+}}{2\pi x} dx \\
&= 1 - \frac{a^E + b^E - 2\sqrt{a^E b^E}}{8} - \frac{(a^E + b^E)\tan^{-1}\left(\frac{a^E+b^E-2\epsilon}{2\sqrt{(b^E-\epsilon)(\epsilon-a^E)}}\right)}{4\pi} \\
&\quad - \frac{\sqrt{a^E b^E}\tan^{-1}\left(\frac{-2a^E b^E + \epsilon b^E + a^E \epsilon}{2\sqrt{a^E b^E (b^E-\epsilon)(\epsilon-a^E)}}\right)}{2\pi} + \frac{\sqrt{(a^E-\epsilon)(\epsilon-b^E)}}{2\pi}
\end{aligned} \tag{6.69}$$

Thus the theorem is proven. $\square$

For a particular atmospheric realization, ϵ should be chosen to maximize the secrecy capacity. The optimization problem is convex, one dimensional, and bound. As a result, the maximum secrecy capacity for a particular geometry (n_{tx}, n_{rx} and n_{rx}^{E}) can be efficiently solved for using standard numeric techniques. Figure 6-7 shows the secrecy capacity as a function of ϵ for SNR=SER=2 and various values of β. We have assumed, for the figure, that the number of receive apertures at the intended receiver is equal to the number of receive apertures at the eavesdropper, $n_{rx} = n_{rx}^{E}$. For $\beta = 1$ the optimal ϵ is 0.5. Thus the optimal strategy is to null all eavesdropper eigenmodes associated with square singular values more than 0.5. The remaining degrees of freedom should be used to predistort the wavefront to the intended receiver.

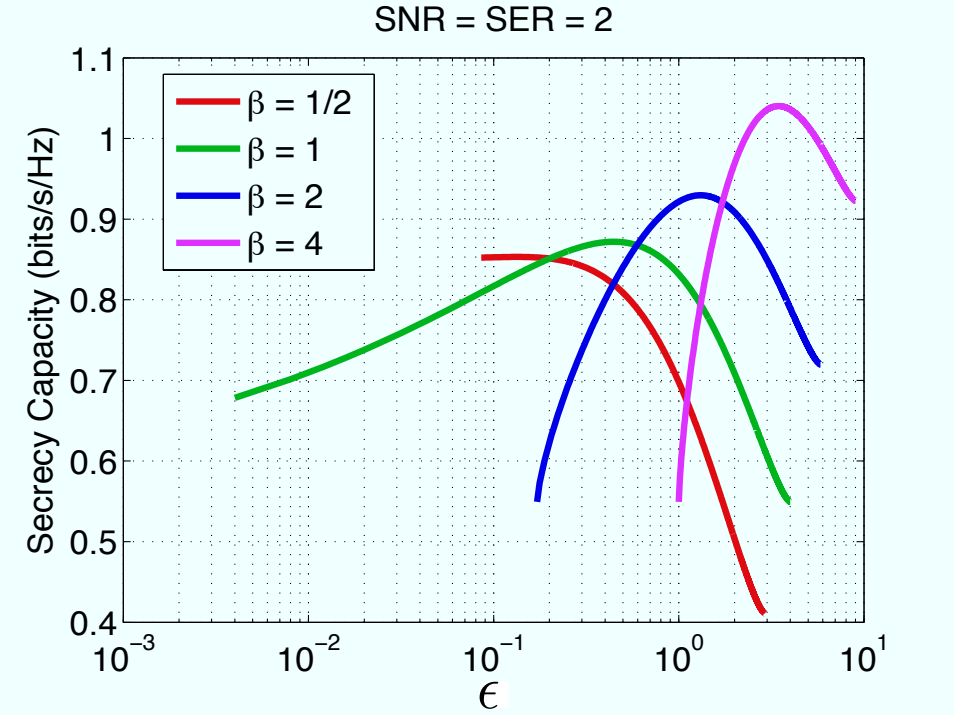

Figure 6-7: Secrecy capacity versus ϵ for SNR=SER=2 and various values of β. We have assumed, for this figure, that the number of receive apertures at the intended receiver is equal to the number of receive apertures at the eavesdropper, $n_{rx} = n_{rx}^{E}$.

We establish the lower bound, when the transmitter has no information about the eavesdropper, on secrecy capacity by allocating zero degrees of freedom to nulling the

eavesdropper:

$$C_s = \left(\frac{1}{2}\log\left(1+\gamma^2_{\max}(\mathbf{H})\text{SNR}\right) - \frac{1}{2}\log\left(1+\overline{\gamma^2}\text{SER}\right)\right)^+ \tag{6.70}$$

where $\overline{\gamma^2}$ is the average square singular value of $\mathbf{H}^E$. For a particular atmospheric realization, the secrecy capacity can be calculated. Asymptotically, we can calculate the secrecy capacity using the Marcenko-Pastur density:

$$C_s = \left(\frac{1}{2}\log\left(1+\left(1+\sqrt{\beta}\right)^2\text{SNR}\right) - \frac{1}{2}\log\left(1+\text{SER}\right)\right)^+ \tag{6.71}$$

where we have used the maximum square singular value of the channel transfer matrix is $\gamma^2_{\max}(\mathbf{H}) = \left(1+\sqrt{\beta}\right)^2$ and the average square singular value of $\mathbf{H}^E$ is one. Figure 6-8 shows the secrecy capacity when the transmitter has no information about the eavesdropper versus β for various values of SNR and SER.

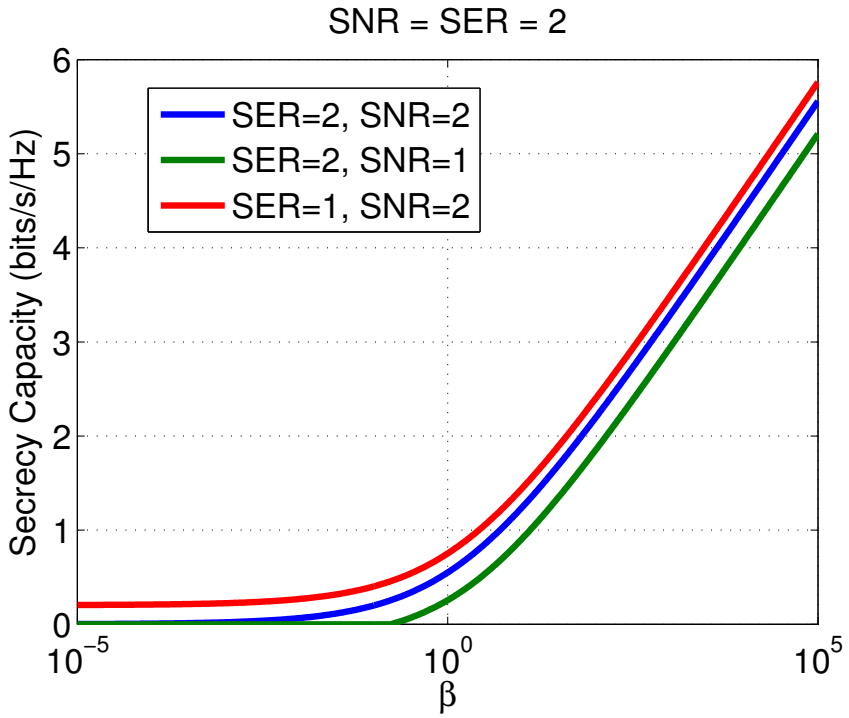

Figure 6-8: Secrecy capacity: This figure shows the secrecy capacity when the transmitter has no information about the eavesdropper versus β for various values of SNR and SER

Figure 6-9 shows the maximum secrecy capacity versus β (optimized over ϵ for each value of β). Also shown for comparison is the channel capacity in the absence of an eavesdropper and the secrecy capacity if the transmitter has no information about the eavesdropper. We have assumed, for the figure, that the number of receive apertures at the intended receiver is equal to the number of receive apertures at the eavesdropper, $n_{rx} = n_{rx}^{E}$. In the figure, we see that increasing the number of transmit apertures relative to the number of receive apertures (both intended and eavesdropper) increases the secrecy capacity. This result is expected: if there are many degrees of freedom (number of transmit apertures) relative to the number of constraints (number of eavesdropper and intended receive apertures) is large, the system can easily null the eavesdropper and predistort the wavefront to the transmitter. We also note that, for a balanced system, knowledge of the eavesdropper only increases capacity by approximately 50%. For a ground to aircraft/spacecraft link, when β is large, knowledge of the eavesdropper does not increase the secrecy capacity. This is because these systems have an excess of degrees of freedom and thus it's not important to allocate them optimally. For the aircraft/spacecraft to ground link, when β is small, knowledge of the eavesdropper is very important. This is because these systems have a dearth of degrees of freedom and thus it's important that they are allocated optimally.

We note that these results can easily be generalized to the case where there are multiple eavesdroppers located in various positions. In closing this chapter, we note that even when the eavesdropper and intended receiver are both in the main beam with equal receiver sensitivity, confidential communication is achievable. Without wavefront predistortion, confidential communication would not be possible.

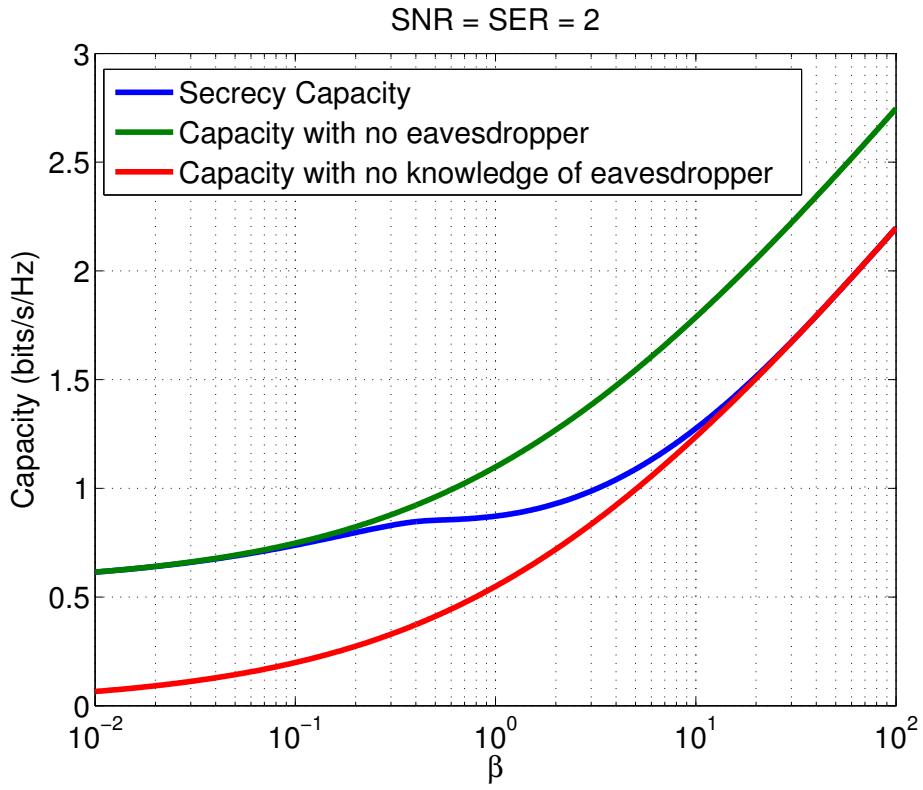

Figure 6-9: The maximum secrecy capacity (optimized over ϵ) versus β. Also shown for comparison is the channel capacity in the absence of an eavesdropper and secrecy capacity when the transmitter does not know about the eavesdropper.

Chapter 7

Conclusion

Optical communication over the turbulent atmosphere has the potential to provide reliable rapidly-reconfigurable multi-gigabit class physical links. Such systems, however, are prone to long (up to 100 ms) and deep (10 to 20 dB) fades. In this thesis, we have shown that for many practical endoatmospheric communication links, a sparse aperture system with spatial wavefront control in homogeneous turbulence provides significant protection against fading: (i) a balanced sparse aperture system with feedback and wavefront control can provide 35 dB of gain compared to a system without diversity and (ii) a balanced sparse aperture system with feedback can provide at least 10 dB of gain compared to a balanced sparse aperture with diversity but without feedback. If the sparse aperture system has more transmit apertures than receive apertures, the gain can be even larger.

Sparse aperture systems are less efficient than filled aperture systems of the same total extent. By using a sparse aperture system, we trade power transfer efficiency for implementation advantages. Sparse aperture systems tend to weigh less than comparable filled aperture systems because there is no need for a deformable mirror at the transmitter and receiver and because the gimbals for sparse aperture systems tend to weigh less (gimbals for sparse aperture systems don't need to be as accurate or support the as large of a load). Further, sparse aperture systems tend to be less complex than a filled aperture system–there is no need for a deformable mirror and tracking can be less accurate. The reduced weight and complexity of the sparse

aperture system means that the sparse aperture system can be field at less expense than comparable systems.

Because today's optical communication systems operate at a very high rate but suffer from deep fades, we focused on schemes that communicate over a single spatial mode instead of communicating on multiple modes simultaneously. Accordingly, our results center on metrics related to communicating on a single spatial mode at any given instant, such as average BER and outage probability in terms of BER. Given BER as the appropriate metric, we showed that coupling all transmit power into the input eigenmode associated with the largest singular value is the optimal predistortion. Further, we showed that a spatial matched filter is the optimal recombination scheme.

In this thesis, we proved that given fairly benign conditions on the placement and size of the system transmit and receive apertures, the square singular value decomposition converges almost surely to the Marcenko-Pastur distribution. We showed the the Marcenko-Pastur distribution approximates the square singular value distribution for as few as 10 transmit and 10 receive apertures. Using the distribution of the square singular values, we derived the asymptotic average BER, outage probability, and diversity power margin (the multiplicative power increase required for the finite sparse aperture system to perform at least as well as the infinite sparse aperture system, at least P_{out} fraction of the time). In contrast with a single aperture system, if average BER needs improvement, the total aperture area (i.e., the sum of the sub-aperture areas) can be increased without saturation. Either adding additional apertures of the same size, or increasing the area of existing apertures, up to the coherence area, can increase the total aperture area. Outage performance can be improved by adding additional apertures. Finally, we showed that the protection against fading in terms of power margin, provided by increasing the number of apertures, diminishes greatly after about 100 apertures. These significant performance gains result from spatial mode control.

For the vertical ground to aircraft/spacecraft link, we showed that wavefront predistortion is much more useful for the ground to aircraft/spacecraft link than the

aircraft/spacecraft to ground link. For the ground to aircraft/spacecraft link, the average wavefront predistortion gain for a balanced system exceeds 10 dB for all example platforms. In contrast, for the aircraft/spacecraft to ground link the average wavefront predistortion gain is approximately 3 dB for the predator drone altitude and is less than 1 dB for all other platforms analyzed. Physically this is because the turbulence is near the transmitter for the ground to aircraft/spacecraft link while the turbulence is very far from the transmitter for the aircraft/spacecraft to ground link. With the transmitter far from the turbulence, it is unable to predistort the wave to undo the turbulence.

In the presence of an interferer, we showed that eigenmode hopping can provide more than 18 dB of gain relative to a system without eigenmode hopping capabilities. This is because, when eigenmode hopping is used, a strong interferer must degrade every nonzero eigenmode. In contrast, an interferer must only degrade a single eigenmode when an eigenmode hopping is not available. We also showed that wavefront predistortion can significantly increase the receiver complexity required for an eavesdropper to intercept information intended for another user.

It may seem strange that we motivated the use of BER as the relevant metric by noting that fading, not data rate, is the main challenge for free space systems, then proceeded to study the asymptotic case where the fading issue is nonexistent. There are two reasons why asymptotic BER is the relevant metric for optical communication. First, asymptotic results are useful only as far as they approximate finite results from practical systems. Because schemes that minimize BER achieve maximal diversity gain, the asymptotic results are applicable for much smaller values of n_{tx}, n_{rx} than a rate maximization scheme. Second, asymptotic analysis allows for an elegant solution that illuminates the relationship of feedback rate, the number of receivers, and the number of transmitters, separated from variation in the square singular values. Finally, we showed an asymptotically optimal mapping from channel state matrix to feedback information, which can be used as guidance for the design of practical systems.

Because of the presence of dynamically evolving turbulence, system latencies, and fsinite rate feedback, the transmitter cannot have perfect knowledge of the turbulence state. As a result, we developed a model of the dynamic atmosphere and used it to find the optimal performance of the system in terms of fundamental system and physical parameters, such as latencies, both estimation and feedback, feedback link rate, number of apertures, turbulence strength, link range, etc. The following describes the asymptotically optimal feedback strategy: (a) *initialization* (i) create a codebook, known to both the transmitter and receiver; (ii) at the receiver, for each update, find the codebook entry closest, in the L_2-sense, to the input spatial mode associated with the largest square singular value; (iii) feed back the *index* of the closest codebook entry; (b) *steady state operation* (i) find the optimal update rate, and make it known to both the transmitter and receiver; (ii) calculate the update vector, which is the difference between the current channel state and the current transmitter channel state estimate; (iii) find the scaled sub-codebook entry closest, in the L_2-sense, to update vector; (iv) feed back the *index* of the closest scaled sub-codebook entry. To prevent the size of the codebook from degrading system performance, a system designer should make a codebook with a cardinality of $25 \times n_{tx}$ known to both the transmitter and receiver. If the cardinality of the codebook is smaller than $25 \times n_{tx}$, the system's performance will be bound away from the performance achievable with perfect knowledge regardless of feedback rate and latency. Given a sufficiently large codebook, the feedback rate necessary to take full advantage of the diversity, given in equation (4.44), varies sublinearly with the number of transmitters and linearly with the coherence time inverse. Given sufficient feedback rate, the optimal feedback scheme is to create $|C|/2$ sub-codebooks and feed back one-bit updates. Further, the time it takes for an update to reach the transmitter $\tau_0 + 2R_u/r$ should be much smaller than the atmospheric coherence time; the performance degrades roughly exponentially as the time it takes for an update to reach the transmitter increases. Occasionally, a new input eigenvector will need to be fed back to the transmitter. In this case, simply feed back a full update. If the feedback rate is not increase, a temporary performance degradation will occure. In general, the system performance,

in terms of wavefront predistortion gain, is given in equation (4.39). If the size of the codebook and rate is sufficient, the performance, given in equation (4.45), is limited only by latency.

While this asymptotic analysis provides insight into the impact of limited rate feedback on wavefront predistortion optical systems, future work could focus on performing an outage analysis for finite systems. This outage analysis requires the probability density function of the largest singular value of optical systems (Section 3.1.1) and the probability density function of the distortion distance (unknown). Additionally, the use of reciprocity to generate turbulence state estimates in bidirectional system should be investigated. As the global Internet becomes increasingly heterogeneous, incorporating both terrestrial fiber and wireless systems, the results from this thesis can be used to study the impact of the free space optical physical layer links. Based on the performance of results for the sparse aperture system with feedback, efficient routing and congestion control algorithms should be designed to maximize resource utilization.

Bibliography

[1] L.C. Andrews and R.L. Phillips, *Laser Beam Propagation through Random Media*, Washington: SPIE Optical Engineering Press, 1998.

[2] T.W. Anderson, "On the Distribution of the Two-Sample Cramer-von Mises Criterion," *The Annals of Mathematical Statistics*, 33 (3): 11481159, 1962.

[3] Z.D. Bai, "Methodologies in spectral analysis of large dimensional random matrices, a review," *Statistica Sinica*, 9(3):611–662, 1999.

[4] M.K. Carson, *Alexander Graham Bell: Giving Voice to the World*, Sterling Publishing Co., New York, 2007.

[5] V.W.S. Chan, "Coherent Optical SPACE Communication System Architecture and Technology Issues," Control and Communication Technology in Laser Systems (Invited), SPIE 295, pp. 10-17, 1981.

[6] V.W.S. Chan, "Space Coherent Optical Communication Systems-An Introduction," *Journal of Lightwave Technology (Invited Paper)*, Volume 5, Issue 4, pp. 633-637, April 1987.

[7] V.W.S. Chan, "Free-Space Optical Communications," *Journal of Lightwave Technology (Invited Paper)*, Volume 24, Issue 12, pp.4750-4762, Dec. 2006.

[8] J.P. Choi, "Channel Prediction and Adaptation over Satellite Channels with Weather-Induced Impairments," *M.S. Thesis*, Massachusetts Institute of Technology, Cambridge, Massachusetts, 2000.

[9] D.S. Cotterill and M. Csörgó, "On the Limiting Distribution of and Critical Values for the Multivariate Cramer-Von Mises Statistic," *The Annals of Statistics*, vol. 10, no. 1, pp. 233-244, November 2004.

[10] D.S. Dean and S.N. Majumdar, "Extreme value statistics of eigenvalues of Gaussian random matrices," *Physical Review E*, vol. 77, pp. 41108, 2008.

[11] I.E. Fang, *A History of Mass Communication: Six Information Revolutions*, Focal Press, Burlington, MA, 1997.

[12] R.M. Gagliardi and S. Karp, "Optical communications," *Wiley series in telecommunications and signal processing*, John Wiley & Sons, New York, 2nd edition, 1995.

[13] J. Galambos, "The Asymptotic Theory Of Extreme Order Statistics [Russian translation]," Nauka, Moscow (1984).

[14] R.G. Gallager, *Information Theory and Reliable Communication*, John Wiley & Sons, New York, 1968.

[15] R.G. Gallager and C. Helstrom, "A bound on the probability that a Gaussian process exceeds a given function (Corresp.)," *IEEE Transactions on Information Theory*, vol.15, no.1, pp. 163- 166, Jan 1969.

[16] J.W. Goodman, *Introduction to Fourier optics*, 3rd Edition, Roberts & Company, Publishers, Englewood, CO, 2005.

[17] J.W. Goodman, *Statistical Optics*, John Wiley & Sons, 1985.

[18] F. Gtze and A.N. Tikhomirov, "Rate of convergence in probability to the Marcenko-Pastur law," Bernoulli, Vol. 10(1), 2004.

[19] S. Haas, "Capacity of and coding for multiple-aperture, wireless, optical communications," Ph.D. Thesis, Massachusetts Institute of Technology, 2003.

[20] G.J. Holzmann and B. Pehrson, *The early history of data networks*, IEEE Computer Society Press, 1995.

[21] E.V. Hoversten, R.O. Harger, and S.J. Halme, "Communication theory for the turbulent atmosphere," *Proc. IEEE*, vol. 58, pp. 1626-1650, Oct. 1970.

[22] W.C. Jakes, *Microwave Mobile Communications*, John Wiley & Sons, 1974.

[23] I.M. Johnstone, "On the distribution of the largest eigenvalue in principal components analysis," *Annals of Statistics*, vol. 29, pp. 295-327, 2001.

[24] A. Khisti and G.W. Wornell, "Secure Transmission with Multiple Antennas I: The MISOME Wiretap Channel," *IEEE Trans. Inform. Theory*, vol. 56, no. 7, pp. 3088-3104, July 2010.

[25] A. Khisti and G.W. Wornell, "Secure Transmission with Multiple Antennas II: The MIMOME Wiretap Channel," *IEEE Trans. Inform. Theory*, vol. 56, no. 11, pp. 5515-5532, Nov. 2010.

[26] Kim et al., "Measurement of scintillation and link margin for the Teralink communication system," Proc. of SPIE, vol. 3232, 1998.

[27] R.S. Lawrence and J.W. Strohbehn, "A Survey of Clear-Air Propagation Effects Relevant to Optical Communications," *Proceedings of the IEEE*, vol. 58, n. 10, pp. 1523-1545, October 1970.

[28] E.J. Lee and V.W.S. Chan, "Part 1: Optical communication over the clear turbulent atmospheric channel using diversity," *IEEE J. Select. Areas Communications*, vol. 22, n. 9, November 2004.

[29] E.J. Lee and V.W.S. Chan, "Diversity Coherent Receivers for Optical Communication over the Clear Turbulent Atmosphere," *IEEE International Conference on Communications*, 2007.

[30] S.K. Leung-Yan-Cheong and M.E. Hellman, "The Gaussian wire-tap channel," IEEE Transactions on Information Theory, vol. 24, pp. 451-456, July 1978.

[31] Y. Liang, H.V. Poor, and S. Shamai, *Information Theoretic Security*, Now. Publishers, Delft, The Netherlands, 2009.

[32] H.S. Lin, "Communication Model for the Turbulent Atmosphere," Ph.D. Thesis, Case Western Reserve Univ., 1973.

[33] R.F. Lutomirski and H.T. Yura, "Wave structure function and mutual coherence function of an optical wave in a turbulent atmosphere," *Journal of the Optical Society of America*, 1971.

[34] A.J. Menezes, P.C. van Oorschot, and S.A. Vanstone, *Handbook of Applied Cryptography*. Boca Raton, FL, USA: CRC Press, 1996.

[35] G.R. Ochs and R.S. Lawrence, NOAA Tech Report, ERL 251-WPL 22, 1972.

[36] S.O. Rice, "Distribution of the duration of fades in radio transmission: Gaussian noise model," *Bell Syst. Tech Journal*, vol. 37, DD. 581-635, 1958.

[37] L.F. Richardson, "Weather Prediction by Numerical Process," *Cambridge University Press*, Cambridge, U.K., 1992.

[38] L. Ritchie, *Scott and Scotland*, Longman, Rees, Orme, Brown, Green and Longman, London, U.K, 1835.

[39] S. Rosenberg and M. C. Teich, "Photocounting array receivers for optical communication through the lognormal atmospheric channel 2: Optimum and suboptimum receiver performance for binary signaling," *Appl. Optics*, vol. 12, pp. 2625-2634, Nov. 1973.

[40] J.W. Strohbehn, ed., *Laser Beam Propagation in the Atmosphere*, New York: Springer-Verlag, 1978.

[41] R.L. Mitchell, "Permanence of the log-normal distribution," *J. Opt. Soc. Amer.*, vol. 58, pp.1267-1272, Sept. 1968.

[42] A.S.Y. Poon, "Use of Spatial Dimension for Spectrum Sharing," *Ph.D. Dissertation*, University of California, Berkeley, May 2004.

[43] A.L. Puryear and V.W.S. Chan, "Optical communication through the turbulent atmosphere with transmitter and receiver diversity, wavefront control, and coherent detection," *SPIE Optical Engineering and Applications* , 2009.

[44] A.L. Puryear and V.W.S. Chan, "Optical Communication Through the Turbulent Atmosphere with Transmitter and Receiver Diversity, Wavefront Predistortion, and Coherent Detection," *IEEE Globecom* Dec., 2009 Honolulu.

[45] J.H. Shapiro and J.W. Strohehn, *Laser Beam Propagation in the Atmosphere*, Eds., Springer-Verlag, New York, 1978, pp. 172-183.

[46] J.H. Shapiro, "Normal-Mode Approach to Wave Propagation in the Turbulent Atmosphere," *Applied Optics*, vol. 13 (11) pp. 2614-2619, 1974.

[47] G.I. Taylor,"The spectrum of turbulence," *Proc. R. Soc. Lond.*, Ser A 164, pp. 476490, 1938.

[48] D. Tse and P. Viswanath, *Fundamentals of Wireless Communication*, New York, NY: Cambridge University Press, 2005.

[49] A. Tulino, A. Lozano, and S. Verdu, "MIMO Capacity with Channel State Information at the Transmitter," *Proc. IEEE Int. Symp. on Spread Spectrum Tech. and Applications (ISSSTA 04)*, Aug. 2004.

[50] S. Verdu and S. Shamai, "Spectral Efficiency of CDMA with Random Spreading," *IEEE Transactions on Information Theory*, Vol. 45, No. 2, March 1999.

[51] A.S. Willsky, G.W. Wornell, and J.H. Shapiro, "6.432 Stochastic Processes, Detection, and Estimation," *Course Notes*, MIT EECS, 1999.

[52] H.P. Yuen and V.W.S. Chan, "Noise in homodyne and heterodyne detection," Opt. Lett., Mar. 1983.

[53] H.T. Yura, "Mutual Coherence Function of a Finite Cross Section Optical Beam Propagating in a Turbulent Medium," *Applied Optics*, Volume 11, Issue 6, pp. 1399-1406, 1972.

[54] X. Zhu and J.M. Kahn, "Markov Chain Model in Maximum-Likelihood Sequence Detection for Free-Space Optical Communication Through Atmospheric Turbulence Channels," *IEEE Transactions on Communications*, vol. 51 (3) pp. 509, 2003.